Quantal calculations on the rotational excitation of NH(_3) and OH in collisions with H(_2)

Alison R. Offer

Quantal Calculations on the Rotational Excitation of NH_3 and OH in collisions with H_2

by

Alison R. Offer

September 1990

An account of the work done at the Department of Physics
submitted to the University of Durham
in accordance with the regulations for admission to the degree of
Doctor of Philosophy

Abstract

Results are presented for quantal close coupled calculations of the rotational excitation of NH_3 and OH in collisions with both ortho and para-H_2. For the latter, these are the first calculations to include the rotational structure of the H_2 molecule, whilst for the former, previous NH_3 – ortho-H_2 calculations have been subject to subsidiary approximations.

The results from the NH_3–H_2 calculation show substantial qualitative changes in the cross-sections when ground state ortho-H_2 ($j = 1$) replaces ground state para-H_2 ($j = 0$) as the collision partner. In particular, cross-sections which were very small for NH_3 – para-H_2 collisions can be of a comparable magnitude with the other rotationally inelastic cross-sections for NH_3 – ortho-H_2 collisions. The changes in cross-sections are discussed in relation to the collisional pumping scheme for an astrophysical maser in the ($jk = 33$) inversion lines.

From the OH–H_2 calculations it is found that the propensities towards preferential excitation of a given component of the Λ doublets are reduced in strength when ortho-H_2 replaces ground state para-H_2 as the collision partner, similarly when ($j = 2$) para-H_2 replaces ground state para-H_2 the propensities are weakened.

In both cases, the results are discussed in the context of crossed beam measurements at energies of 605cm^{-1} (NH_3–H_2) and 680cm^{-1} (OH–H_2). It is found that discrepancies between the experimental results and theoretical calculations for ground state para-H_2 collisions can be explained, at least in part, by the neglect of the ($j > 0$) H_2 rotational states in the latter.

Preface

The work presented in this thesis was carried out between 1987 and 1990 while the author was a research student under the supervision of Dr. D.R.Flower in the Physics Department at the University of Durham.

The research presented is the author's own work. This work has not been submitted for any degree, diploma, or other qualification at any other university.

Certain results have appeared in the following papers:

Offer A. and Flower D.R. (1989) *J.Phys.B:At.Molec.Phys* **22** L439

Offer A. and Flower D.R. (1990) *Faraday Transactions II* **86** 1659

Flower D.R., Offer A. and Schilke P. (1990) *Mon.Notes.Roy.Astron.Soc* **224** 4P

Offer A. and Flower D.R. (1990) *J.Phys.B:At.Molec.Phys* in press

Table of Contents

Appendices:

to my parents

Acknowledgements

I would like to acknowledge the help and guidance of my supervisor, Dr. Flower, and thank Dr. Hutson for his help with using the MOLSCAT computer code, Dr. Valiron for providing the potential data used in the NH_3–H_2 collision calculations, and my fellow students for their support.

Chapter I

Introduction

1.1 Motivation

Over the past few decades a large number of different species of molecule have been observed in the space between the stars, ranging from diatomic molecules to complicated organic molecules. In particular, a large number of molecular radio and microwave lines are observed from dark dense regions of interstellar space. These dark clouds typically have a density of around 10^4 to 10^7 Hydrogen atoms per cubic centimetre, and, in the absence of any internal heating sources, temperatures of 30K or less. In such regions molecule–molecule and atom–molecule collisions play an important role in determining the energy distribution within the cloud, and at such low temperatures vibrational transitions are highly unlikely, thus most collisionally induced transitions are purely rotational.

The observed molecular spectra can be interpreted to yield information on the physical conditions (temperature and density) within the clouds (eg Walmsley, 1987). If collisions dominate the energy transfer within the cloud, the populations of the molecular energy levels will be in thermodynamic equilibrium with the surroundings and the relative level populations will be related to the local kinetic temperature, T, by the Boltzmann formula:

$$\frac{n_i}{n_j} = \frac{g_i}{g_j} \exp\left(-\frac{(E_i - E_j)}{k_B T}\right) \qquad 1.1.1$$

where g_i, g_j are the statistical weights of the levels with energies E_i, E_j respectively, and k_B is Boltzmanns constant. However, in many cases the molecular spectra show significant departures from local thermodynamic equilibrium. In such cases the energy distribution is determined by the balance between collisional and radiative processes, and in order to model the energy transfer, and to interpret the observed spectra, a knowledge of the collisional and radiative rates is required.

The collisional rates are obtained by averaging the collisional cross-sections over a velocity distribution, and the need for reliable astrophysical rates has lead to much interest in the low energy collisional cross-sections for inelastic rotational and rovibrational transitions. The most abundant elements are hydrogen and helium, with the former being about ten times more abundant than the latter. In the dark clouds, from which many observed molecular lines originate, it is thought likely that most of the hydrogen will be in its molecular form, thus the rates for inelastic collisions with H_2 are important parameters.

In this thesis, quantal calculations to determine cross-sections for the rotational excitation of two astrophysically important molecules, ammonia (NH_3) and OH in collisions with H_2 are reported. Both OH and NH_3 have been widely observed in the interstellar medium, and NH_3 has been proposed as an interstellar thermometer (Walmsley and Ungerechts, 1983). NH_3 level populations are often far from thermodynamic equilibrium with their surroundings but Walmsley and Ungerechts have shown that corrections can be made, if the collisional rates are known, to allow a determination of the kinetic temperature from the observed line intensities. Kinetic temperatures obtained in this way agree well with those derived from CO observations (Takano, 1986, Danby et al, 1988).

In addition, cross-sections for both NH_3 and OH in collisions with the spherically symmetric ground state para-H_2 molecule show strong propensities towards certain transitions, and these 'propensity rules' have been proposed as possible pumping mechanisms leading to maser emission in some transitions for both NH_3 (Walmsley and Ungerechts, 1983, Guilloteau et al, 1983, Johnston et al, 1989) and for the OH molecule.

Previous fully quantal calculations on both NH_3 – H_2 and OH – H_2 collisions have neglected the rotational motion of the hydrogen molecule, and treated collisions with ground state para-H_2 only, but the change in the symmetry properties of the collision when ($j > 0$) H_2 is the collision partner, along with the non-zero quadrupole moment of rotationally excited H_2, could make a qualitative difference to the results.

The reasons for investigating this are two-fold. The existing NH_3 – H_2 and OH – H_2 quantal collisional rates are strictly only applicable if all the molecular

hydrogen is in its ($j = 0$) rotational ground state. Whilst this will be essentially true for para-H_2 at the temperatures of the dark clouds, molecular hydrogen is believed to form on grains in a 3:1 ortho:para-H_2 ratio, and under normal circumstances radiative ortho to para conversion is strongly forbidden. The conversion can take place via proton exchange reactions, but the ortho:para-H_2 ratio within the clouds is uncertain (Flower and Watt, 1984). At higher temperatures the influence of ortho-H_2 could become significant, and the way in which this may effect the collisional rates could be important.

The most detailed experimental information on the cross-sections for rotationally inelastic NH_3 – H_2 and OH – H_2 collisions comes from the molecular beam experiments of Seelemann et al (1988) and Ebel et al (1990) for NH_3, and Andresen et al (1984) for OH. Both sets of experiments used normal (3:1 ortho:para-H_2) as the collision partner, and both found significant differences between the experimental results and those predicted by theory for ground state para-H_2 collisions.

The aim of the work reported in this thesis was to answer the questions:

- Do the collisional cross-sections change appreciably when ($j > 0$)-H_2 is considered as the collision partner, and if so, how ?
- Can this explain the discrepancies between theory and experiment?

In the following sections the methods for obtaining collisional cross-sections and rate coefficients are reviewed. In chapter two the quantal calculations are discussed in more detail, and the algebra extended to that needed to treat the rotational motion of the hydrogen molecule. The results of the calculations are presented and discussed in chapters three and five, whilst chapter four considers a possible astrophysical application of the results. The work is summarised in chapter six along with suggestions for future work.

1.2 Definition of Cross-Sections and Rate Coefficients

The cross-section for a process ($i \rightarrow j$) is defined as the transition probability per unit time, per unit scatterer, per unit flux of incident particles with respect to the scatterer. It has the (classical) physical interpretation as an area centred on the

scatterer through which an incident particle must pass for the process $(i \rightarrow j)$ to occur.

Quantum mechanically, the cross-section for single channel scattering is derived by considering an incoming plane wave, ψ_{inc} and a scattered spherical wave, ψ_{sc}. In the limit of large r, where r is the distance from the scatterer, assuming the plane wave is incident along the z-axis, the total wave function can be written:

$$\begin{aligned} \Psi &= \psi_{inc} + \psi_{sc} \\ &= e^{i\kappa z} + f(\theta,\phi)\frac{e^{i\kappa r}}{r} \end{aligned} \tag{1.2.1}$$

where $f(\theta,\phi)$ is the scattering amplitude, and the wave number κ is related to the energy, E, and the reduced mass, μ, through $\kappa^2 = 2\mu E/\hbar^2$. Under these conditions the incident flux is $(\hbar\kappa/\mu)$, and the scattered flux per unit solid angle is $(\hbar\kappa/\mu)|f|^2$. The differential cross-section, $\frac{d\sigma}{d\Omega}$, is the ratio of the scattered flux per unit solid angle to the incident flux:

$$\frac{d\sigma}{d\Omega} = |f(\theta,\phi)|^2 \tag{1.2.2}$$

The total cross-section can be obtained by integrating over all angles:

$$\sigma = \int \frac{d\sigma}{d\Omega}\, d\Omega \tag{1.2.3}$$

In reality, the situation is complicated by the possibility of scattering into many different states (or channels). In many channel scattering, the wavefunction Ψ_i describing a particle incident in channel i can be written as:

$$\Psi_i \sim \sum_j \frac{1}{r(4\pi v_j)^{1/2}}(e^{-i\kappa_j r}\delta_{ij} - S_{ij}e^{i\kappa_j r}) \tag{1.2.4}$$

where the sum runs over all possible channels, j. For N channels, N constants, S_{ij}, are required to describe asymptotic behaviour of Ψ_i. To describe the wavefunction of the whole system N $\times$ N constants are needed for all possible i's, and these constants constitute the scattering matrix of system at an energy, E. The scattering matrix determines the asymptotic behaviour of the wavefunction completely, and

the cross-sections for a given process can be derived from the scattering matrix (or S-matrix) elements.

The cross-section, $\sigma_{i\rightarrow j}(E)$ gives the probability of the process $(i \rightarrow j)$ occurring for a mono-energetic beam. In the real world, however, interacting particles will have a range of energies depending on the conditions. The rate coefficient, $\alpha_{ij}(T)$, for a given process is obtained by averaging the cross-section over a range of energies, $F(E,T)$ (or equivalently a velocity distribution $F(v,T)$):

$$\alpha_{ij}(T) = \langle E\sigma_{ij}(E)\rangle = \int \sigma_{ij}(E)\, E\, F(E,T)\, dE \qquad 1.2.5$$

1.3 Experimental Determination

In principle, experimental methods provide the most accurate measure of the cross-sections or rate coefficients, and experiments are often used to probe the intermolecular potentials. However, experiments are often carried out at room temperature and extrapolation of the results to give collisional rates at low temperatures is unreliable. The experimental measurements complement the theoretical calculations, providing tests for the theory that can then be extended to interstellar conditions.

The most detailed information comes from the molecular beam experiments, which have been reviewed by Toennies (1976) and Buck (1988). The experimental set up consists of two molecular beams which intersect in the scattering region. The pressure is low, and multiple collisions are very rare, so provided the initial and final states distributions can be established, the measurements can give direct information on the state-to-state cross sections for inelastic scattering.

The initial state can be selected by a variety of methods (Buck, 1988) but the simplest is to use supersonic nozzle beams. The nozzle beams are prepared by allowing the incident beam to expand supersonically from a high pressure source to a low pressure region, which can yield rotationally cold beams with essentially all the molecules in their ground rotational state.

The final state distribution can be probed either by an energy change method, in which the final states are deduced indirectly from the change in relative velocity of the scattered beam (Buck, 1988), or by optical methods in which laser radiation

is used to probe the final population distribution through a variety of techniques (Dagdigian, 1988). The former relies on the principle of the conservation of energy, and can, in theory, be applied to any system, but it is limited in practice by the requirement of a high velocity resolution. The latter is not limited by velocity resolution but is only suited to molecules with relevant transitions at accessible frequencies.

In addition to the state-resolved molecular beam measurements, a number of other experimental techniques have been useful in providing information on the cross-sections. Most other methods measure only an average over many transitions, and a range of energies, so give only indirect information on the collisional rates, however, they can provide useful checks on theoretical results. One indirect experimental method that has provided useful information on the collisional selection rules governing rotational transitions, is that of the double resonance experiments (Oka, 1973). In these experiments strong infrared or microwave radiation at a pumping frequency, ν_p, is used to saturate a given transition (level 1 to level 2). The non-Boltzmann population is the redistributed through transitions, and the change in population is monitored via a second transition (level 3 to level 4) using weak radiation at the signal frequency, ν_s. The method is particularly suited to molecules with symmetrically split doublets as the equations relating the changes in intensity to the collisional rates simplify considerably if ν_s and ν_p correspond to intradoublet transitions. Information on the relative sizes of the collisional rates between the levels can be extracted, which provide a good test of the theory.

1.4 Theoretical determination: The Interaction Potential

Whether treated classically, semi-classically or quantally, the collision calculation is essentially the solution of the equation of motion of the molecular nuclei moving on a predetermined potential surface. In general, the potential surface is a function of the co-ordinates describing the intermolecular vector, $\mathbf{R}$, and the internal molecular co-ordinates giving the relative positions of the nuclei.

The interaction potential, V, is defined within the bounds of the Born – Oppenheimer separation of the electronic and nuclear motion. The Born–Oppenheimer approximation rests on the assumption that the electronic motion is very fast compared with the nuclear motion. Then the electronic motion is treated as if

the nuclei are fixed at some internuclear distance, R, and the nuclei move in the averaged field due to the electronic motion.

The Schrödinger equation for the system of nuclei and electrons is:

$$\left[-\sum_{\alpha}\frac{\hbar^2}{2M_\alpha}\nabla^2_{R_\alpha}-\sum_{i}\frac{\hbar^2}{2m_i}\nabla^2_{r_i}+V(R_\alpha,r_i)\right]\Psi(R_\alpha,r_i)=E\Psi(R_\alpha,r_i) \qquad 1.4.1$$

where M_α is the mass of the αth nuclei with co-ordinates R_α, and m_i is the mass of the ith electron with co-ordinates r_i. Expressing the dependence on the electronic and nuclear motion explicitly, the wavefunction can be written as a product of the electronic wavefunction, $U_n(R_\alpha,r_i)$, and a nuclear term, $\phi_n(R_\alpha)$:

$$\Psi(R_\alpha,r_i)=\sum_{n}\phi_n(R_\alpha)U_n(R_\alpha,r_i) \qquad 1.4.2$$

If we then assume that R_α is fixed, or equivalently, that M_α is infinitely large, we obtain the Schrödinger equation for the motion of the electrons with fixed nuclei:

$$\left[-\sum_{i}\frac{\hbar^2}{2m_i}\nabla^2_{r_i}+V(R_\alpha,r_i)\right]U_n(R_\alpha,r_i)=\varepsilon(R_\alpha)U_n(R_\alpha,r_i) \qquad 1.4.3$$

Here $\varepsilon(R_\alpha)$ is an effective electronic energy depending on the relative positions of the nuclei.

Substituting equation 1.4.2 into the full Schrödinger equation gives:

$$-\sum_{\alpha}\frac{\hbar^2}{2M_\alpha}\nabla^2_{R_\alpha}(\phi_n(R_\alpha)U_n(R_\alpha,r_i))+ \left\{\left(-\sum_{i}\frac{\hbar^2}{2m_i}\nabla^2_{r_i}+V(R_\alpha,r_i)\right)\phi_n(R_\alpha)U_n(R_\alpha,r_i)\right\}=E\phi_n(R_\alpha)U_n(R_\alpha,r_i) \qquad 1.4.4$$

where the term in the curly brackets is equal to $\varepsilon(R_\alpha)U_n\phi_n$.

Using the product rule the first term can be rewritten as:

$$\nabla^2_{R_\alpha}(\phi_n(R_\alpha)U_n(R_\alpha,r_i))=\phi_n(R_\alpha)\nabla^2_{R_\alpha}U_n(R_\alpha,r_i)+2\nabla_{R_\alpha}\phi_n(R_\alpha)\nabla_{R_\alpha}U_n(R_\alpha,r_i) + U_n(R_\alpha,r_i)\nabla^2_{R_\alpha}\phi_n(R_\alpha) \qquad 1.4.5$$

The Born – Oppenheimer approximation is obtained by assuming that the electronic part of the wavefunction, $U_n(R_\alpha, r_i)$, is a slowly varying function of R_α. With this assumption the Schrödinger equation becomes:

$$\left[-\sum_\alpha \frac{\hbar^2}{2M_\alpha} + \varepsilon(R_\alpha)\right] \phi_n(R_\alpha) = E\phi_n(R_\alpha) \qquad 1.4.6$$

Thus the Schrödinger equation has separated into two parts describing the electronic motion at fixed nuclear positions, and the nuclear motion in an effective potential given by $\varepsilon(R_\alpha)$.

The interaction potential between two molecules is just the difference between the electronic energy at some intermolecular distance, R, and the electronic energy of the separated molecules ($R \rightarrow \infty$).

The methods of obtaining the potential surface range from completely *ab initio* theoretical treatments, through varying degrees of semi-empirical treatments, to direct inversion of experimental measurements.

In principle, direct inversion of experimental data should give the most accurate description of the potential surface, however, such procedures are hampered by the fact that any measurement of the surface is indirect. What is in fact measured is the effect of the potential surface, and a theoretical model of the surface is usually needed. Inversion of experimental data is most suited to the isotropic part of the potential, but it is the anisotropic part that drives rotationally inelastic transitions.

The most rigorous methods of obtaining theoretical potential surfaces is from *ab initio* calculations. The precise method used for *ab initio* calculations depend on the region of the interaction that is of interest and is convenient to divide the interaction into short range and long range contributions.

Short range forces fall off exponentially with R, and are responsible for the strongly repulsive behaviour at very small distances. Long range forces fall off as R^{-n}, where n is a positive integer. The main contributors to the long range behaviour are the electrostatic, induction and dispersion energies (eg Buckingham 1978).

The electrostatic energy is the interaction energy between the permanent electronic charge distributions of the molecules, and can be expressed in a multipolar expansion in terms of dipole–dipole, dipole–quadrupole, quadrupole–quadrupole interactions etc. The induction energy is the interaction between the induced electronic moment of one molecule with the permanent charge distribution of the other (eg induced dipole – quadrupole interactions), and the dispersion energy is the energy due to a correlation in the fluctuations of the electronic co-ordinates of the interacting molecules.

In the long range regime, where the probability of electron exchange between the two molecules is negligible, the molecules can be treated as non-overlapping charge distributions. In this limit, standard perturbation theory is applicable. Following Buckingham (1978), the Hamiltonian of a pair of molecules can be written:

$$H = H^a + H^b + H' \qquad 1.4.7$$

where H^a, H^b are the Hamiltonians of the separated molecules and H' is the interaction:

$$H' = (4\pi\epsilon_o)^{-1} \sum_{ij} e_i^a e_j^b (r_{ij})^{-1} \qquad 1.4.8$$

with r_{ij} being the distance between the charges e_i associated with molecule a and e_j associated with molecule b.

With H' treated as a perturbation, the unperturbed wavefunction is an eigenfunction of $H^a + H^b$, and can be expressed as a product of the separated molecule wavefunctions. Using perturbation theory, the perturbed wavefunction can be written as:

$$|\psi_{m_a m_b}\rangle = |m_a m_b\rangle + \sum_{p_a p_b \neq m_a m_b} \frac{\langle p_a p_b | H' | m_a m_b \rangle}{E_{m_a} + E_{m_b} - E_{p_a} - E_{p_b}} |p_a p_b\rangle + \ldots \qquad 1.4.9$$

where p_a, p_b are a complete set of normalised unperturbed states, and the sum runs over all states p_a, p_b, such that $p_a p_b \neq m_a m_b$. The energy of the perturbed system

is then (Buckingham, 1978):

$$\begin{aligned} E_{m_a m_b} &= \frac{\langle \psi_{m_a m_b} | H | \psi_{m_a m_b} \rangle}{\langle \psi_{m_a m_b} | \psi_{m_a m_b} \rangle} \\ &= E_{m_a} + E_{m_b} + \langle m_a m_b | H' | m_a m_b \rangle \\ &\quad - \sum_{p_a p_b \neq m_a m_b} \frac{|\langle p_a p_b | H' | m_a m_b \rangle|^2}{E_{p_a} + E_{p_b} - E_{m_a} - E_{m_b}} + \cdots \end{aligned} \qquad 1.4.10$$

The first order term, $\langle m_a m_b | H' | m_a m_b \rangle$, is identified with the electrostatic energy, whilst the second order term comprises of the induction contribution, ($p_a \neq m_a$, $p_b = m_b$ or $p_a = m_a$, $p_b \neq m_b$), and the dispersion contribution ($p_a \neq m_a$, $p_b \neq m_b$). The above expression for the interaction energy can be related to the properties of the individual molecules by expanding the interaction term, H', in a multipolar series. Algebraic expressions for the long range interaction potential have been given in a cartesian form by Buckingham (1967), and in a spherical tensor form by Leavitt (1980) and Stone and Tough (1984).

In the short range region there is significant overlap between the electron clouds, and an electron can no longer be assigned to any particular molecule. In this region a molecular orbital approach is more applicable. The collection of electrons and nuclei of the two molecules are treated as one 'supermolecule', and the interaction energy is the defined as the difference between the electronic energy of the supermolecule, and the combined electronic energies of the separated molecules.

A commonly used approach is the Hartree Fock – self consistent field (SCF) method. The Hartree Fock – SCF method is a variational method based on the variational principle which states that, for any approximate wavefunction, Φ_{approx}, the quantity:

$$E_{approx} = \frac{\int d\tau \, \Phi^*_{approx} H \Phi_{approx}}{\int d\tau \, \Phi^*_{approx} \Phi_{approx}}, \qquad 1.4.11$$

(where H is the true Hamiltonian) is always greater than the lowest true eigenvalue. Variational methods are based on choosing an initial wavefunction, Φ_{approx}, with variable parameters, and minimising the quantity E_{approx}, with respect to these parameters.

The true electronic Hamiltonian can be written as:

$$H_{el} = -\sum_i \frac{\hbar^2}{2m_i}\nabla^2_{r_i} - \sum_{\alpha,i} \frac{Z_\alpha e^2}{|R_\alpha - r_i|} + \sum_{\alpha>\beta} \frac{Z_\alpha Z_\beta e^2}{|R_\alpha - R_\beta|} + \sum_{i>j} \frac{e^2}{|r_i - r_j|} \qquad 1.4.12$$

with the Schrödinger equation being:

$$H_{el}\Phi = E\Phi \qquad 1.4.13$$

In the Hartree Foch method, Φ is expanded as an antisymmetric product of single electron spin orbitals ($\phi_i^{so} = \psi_i\alpha_i$ or $\psi_i\beta_i$ where α and β represent spin wavefunctions for opposite spin electrons, and ψ_i are the parameterized molecular orbitals). The antisymmeterized wavefunction for a n electron system can be expressed (for even n) as a Slater determinant:

$$\Phi = (n!)^{-1/2} \times \begin{vmatrix} \psi_1(1)\alpha(1) & \psi_1(1)\beta(1) & \psi_2(1)\alpha(1) & \dots & \psi_{\frac{n}{2}}(1)\beta(1) \\ \psi_1(2)\alpha(2) & \psi_1(2)\beta(2) & \psi_2(2)\alpha(2) & \dots & \psi_{\frac{n}{2}}(2)\beta(2) \\ \vdots & \vdots & \vdots & & \vdots \\ \psi_1(n)\alpha(n) & \psi_1(n)\beta(n) & \psi_2(n)\alpha(n) & \dots & \psi_{\frac{n}{2}}(n)\beta(n) \end{vmatrix} \qquad 1.4.14$$

The energy is minimised with respect to the Φ, and the condition imposed on Φ by requiring that E should be a minimum is embodied in the Hartree Fock equations (Roothaan, 1951).

The 'best' Φ leading to a minimum energy can be calculated by solving the Hartree – Fock equations iteratively, and once the optimum Φ has been established, the Schrödinger equation can be solved to yield an upper bound to the electronic energy.

For open shell molecules the method must be modified slightly. Two possibilities are the spin-restricted Hartree Fock method where some orbitals are doubly occupied, and some are only singly occupied with an electron of α spin, and the spin-unrestricted Hartree Fock method where different spatial orbitals, ψ, are assigned to electrons of α and β spin. The optimum Φ is calculated from the variational principle as before, and an upper bound to the electronic energy may be derived in the same way.

The energy obtained thus is commonly called the SCF energy, the true Hartree Fock energy being obtained in the limit $n \rightarrow \infty$ where n is the number of molecular orbitals included.

The disadvantage of the SCF method is that, since it uses only a single determinant wavefunction, it cannot correctly treat the correlation between the electronic wavefunctions, and does not, therefore, contain the dispersion energy.

An improvement on the single determinant methods is obtained using a configuration interaction calculation. The true wavefunction can be approached if the single determinant wavefunction of the Hartree Fock treatment is replaced by a linear sum of Slater orbitals of the form:

$$\Phi = c_0\Phi_0 + \sum_{s>0} c_s\Phi_s \qquad 1.4.15$$

The first determinant , Φ_0, is just the Hartree Foch determinant, and further terms in the sum are obtained by replacing successive numbers of occupied orbitals in the determinant by virtual (unoccupied) orbitals (Hehre et al, 1986), The value of the coefficients, c_s, in equation 1.4.15 can be determined by a variational calculation.

Because of the successive substitution of virtual orbitals, a full configuration interaction calculation can account for the dispersion energy, and indeed, in the limit $n \rightarrow \infty$, $s \rightarrow \infty$ the true wavefunction is approached. In addition, a full configuration interaction calculation does not break down at intermediate distances where the assumptions of overlapping charge distributions at short range and completely non-overlapping charge distributions at long range fail. However, such calculations are very large, and impractical for most systems.

An alternative method to deal with the short range dispersion contribution is to use a variant on perturbation theory and a number of such approaches have been developed (eg Hehre et al, 1986). These perturbation approaches treat the correlation effects as a perturbation to the first order (Hartree Fock) Hamiltonian. All the potential surfaces that have been used in the present study (Danby et al, 1986, Billing and Diercksen, 1985, 1986, Kochanski and Flower, 1981) have been obtained with an SCF calculation supplemented by a dispersion contribution calculated from a variant on perturbation theory.

The data from potential calculations is obtained as the potential energy at a series of separations and relative orientations of the molecules. To convert this into a useful form the data is fitted to some angular function, and the angular coefficients fitted to some radial function allowing the potential to be evaluated at any point. The form of these fitting functions will be discussed in more detail later.

1.5 Theoretical Determination: The Scattering Calculation

Once the interaction potential has been established the problem reduces to solving the equation of motion of the molecular nuclei on the resulting potential surface. In the case of low energy rotational excitation it is usually adequate to neglect the vibrational degrees of freedom, and solve the equations of motion for two rigid rotors (spherical perturbers, linear rotors, symmetric tops or asymmetric tops).

In low energy molecular collisions the collision energy is not much greater than the energy level splitting, so a classical treatment of the collision is not applicable, and some method of treating quantal effects is required.

The most rigorous treatment of the collision problem is a direct solution of the Schrödinger equation which, in the case of two rigid molecules moving in a potential $V(\mathbf{R}, \hat{\Omega}_1, \hat{\Omega}_2)$ can be written:

$$\left[-\frac{\hbar^2}{2\mu}\nabla_R^2 + H_1^{rot} + H_2^{rot} + V(\mathbf{R}, \hat{\Omega}_1, \hat{\Omega}_2)\right] \Psi(\mathbf{R}, \hat{\Omega}_1, \hat{\Omega}_2) = E\Psi(\mathbf{R}, \hat{\Omega}_1, \hat{\Omega}_2), \quad 1.5.1$$

where H_i^{rot} is the rotational Hamiltonian for molecule i, μ is the reduced mass related to the masses of the two molecules through $\mu = \frac{m_1 m_2}{m_1+m_2}$, $\hat{\Omega}_i$ is the set of Euler angles specifying the orientation of molecule i with respect to some co-ordinate axes and E is the total kinetic energy (translational and rotational) of the system.

However, there are practical problems with fully quantal methods which stem from the large number of molecular rotational states that need to be included in the calculation to correctly describe the system. The molecular rotation couples to the orbital angular momentum associated with the relative motion of the molecules, and this can lead to a very large number of coupled equations. The size of the

problem is reduced considerably if some part of the motion is treated classically so a number of semi-classical methods have been developed (eg Child, 1976, Dickinson and Richards, 1982).

Two common semi-classical methods are the semi-classical S-matrix method and the classical path approximation.

The semi-classical S-matrix method (Miller, 1974) treats both the relative and the molecular internal motion classically using exact classical trajectories to obtain the classical limit of the S-matrix elements (or transition amplitudes), which contain all the dynamical information. Quantal effects are introduced through the principle of superposition, thus, with a phase associated with each trajectory the transition probability is related to the S-matrix elements through (Miller, 1974,1975):

$$P(i \rightarrow j) = |S_{ij}|^2 \qquad 1.5.2$$

The classical equivalent of equation 1.5.2 would be a simple sum of the squares of the S-matrix elements, and in a purely classical approach it is customary to calculate the transition probability directly, and the principle of superposition is not included. As quantal effects such as interference are a direct result of the principle of superposition they are qualitatively included in the semi-classical S-matrix approach.

Whilst semi-classical S-matrix calculations have shown reasonable agreement with quantal calculations for atom – linear rotor collisions (Miller, 1971, Kreek et al, 1975), the method becomes increasingly less tractable with added degrees of freedom (Dickinson and Richards, 1982).

The alternative approach which predates the S-matrix method and has been widely used in studies of rotational excitation is the classical path approximation (eg Child, 1976). In the classical path approximation the relative motion is calculated classically whilst the internal motion is treated quantally. The relative motion of the molecules is solved using standard classical trajectory methods to calculate the motion in some effective potential, V_{eff}. In the simplest case the trajectory is a straight line (constant potential). Alternatively the isotropic part of the potential can be used, or, more correctly, the expectation value of the full

interaction potential in the time dependant internal states. The latter method has been widely used by Billing (1975).

The calculated classical trajectory gives rise to a time dependant perturbation, $V(R(t))$, which is then used for solving the time dependant Schrödinger equation for the molecules internal motion.:

$$i\hbar\frac{\partial U(t,t_0)}{\partial t} = [H_{int} + V(R(t))]\,U(t,t_0) \qquad 1.5.3$$

where $U(t,t_0)$ is the time development operator, and H_{int} is the Hamiltonian for the internal motion. The probability of a given transition can then be obtained from:

$$P(i \rightarrow f) = |\langle i|U(+\infty,-\infty)|f\rangle|^2 \qquad 1.5.4$$

Equation 1.5.3 must be solved numerically and the calculations can be quite substantial. A subsidiary approximation is to treat the system in a body fixed frame that rotates with the intermolecular axis, and neglect transitions that change the projection of the angular momenta on the body fixed z'-axis (the intermolecular axis). This approximation has been called the 'semi-classical coupled-states' approximation by Billing (1976), and is the analogue of the quantal coupled states approximation (McGuire and Kouri, 1974, Pack, 1974). The latter has been very successful in quantal treatments and will be discussed further in chapter two.

A number of calculations of rotationally inelastic molecular collisions have been reported using the classical path approximation, and, in general, the results are in reasonable qualitative agreement with the quantal results. In particular, calculations using this method have been reported for NH_3 – He collisions (Davis and Boggs, 1978, Billing et al, 1984, 1985) and NH_3 – H_2 collisions (Billing and Diercksen, 1985, 1986, 1987, 1988).

Semi-classical methods are most applicable where the intermolecular interaction is not too strong, and can provide useful insights into the physics, however, at the low temperatures found in the interstellar clouds, quantal effects become more important, and a semiclassical treatment is not always adequate. This is particularly true for transitions between states which are not directly coupled by

the potential and can only proceed via an intermediate state. For such transitions resonance structures can be important at low energies and such behaviour is not correctly treated by semi-classical methods (Danby et al, 1987). In addition, quantal calculations are required to assess the accuracy of computationally cheaper methods. For these reasons, the calculations reported in this thesis are quantal close coupled calculations. The close coupling method of solving the Schrödinger equation is reviewed in the following chapter.

Chapter II

The Quantal Close Coupled Equations

2.1 Introduction

The quantal formulation of rotational excitation of a linear rigid rotor in collision with a spherically symmetric atom was first given by Arthurs and Dalgarno in 1960. Although the atom – linear rigid rotor represents the simplest molecular collision problem, the method remains essentially the same for any quantal study of rotational and vibrational excitation. The molecules are treated in the Born – Oppenheimer approximation in which the coupling between the nuclear and electronic motion has been neglected, and the problem reduced to the motion of the molecular nuclei on a predetermined electronic potential surface, V.

The most accurate treatment of the problem is solution of the quantal close coupled or coupled channel (CC) equations. In principle, solution of the CC equations amounts to a full numerical solution of the Schrödinger equation for the nuclear motion, with the accuracy being limited only by the accuracy of the potential surface used, and the amount of available computing resources. It is the CC equations that have been used in the present study, and the form of these equations is derived in the following section.

In practice, the system of close coupled equations is often too large to be computationally tractable for anything but the simplest molecular systems, and a number of decoupling approximations have been developed. Foremost amongst these is the coupled states (CS) approximation of McGuire and Kouri (1974). In section three this is briefly reviewed. Numerical methods for the solution of the coupled equations are discussed in section four.

The principal approximation in the treatment of rotational excitation by the CC method is the truncation of the rotational basis set to some finite number of states. A similar approximation is the assumption that the molecules behave as rigid rotors, and the vibrational degrees of freedom can be ignored. This is

equivalent to truncating the vibrational basis set to just one state and the effects of these approximations are discussed in section five.

Finally, in section six, the theory is applied to the specific case of the rotational excitation of symmetric top molecules in collisions with linear rigid rotor molecules.

2.2 The Close Coupled Equations

The close coupled equations can be derived either in a space fixed frame (Arthurs and Dalgarno, 1960, Blatt and Biedenharn, 1952, Takayanagi, 1965) or in a body fixed frame that rotates with the collision system (Pack, 1974, Launay, 1976).

The body fixed frame is the natural system of reference in which to describe the interaction potential, and as a result the potential terms that appear in the equations are much simpler than their space fixed analogues. However, the body fixed frame rotates with time and the non-inertial nature of the body fixed frame leads to Coriolis effects that appear as off diagonal terms in the centrifugal potential. The centrifugal potential behaves as R^{-2} at large R and the off diagonal terms can persist after the interaction potential, V, has become very small. As a result, the space fixed frame is often preferred for full CC calculations, and the equations will be derived in this frame.

The Schrödinger equation for the relative motion of two molecules in an arbitrary space fixed frame is:

$$\left[-\frac{1}{2\mu}\nabla_R^2 + H_1 + H_2 + V(\mathbf{R},\hat{\Omega}_1,\hat{\Omega}_2)\right]\Psi(\mathbf{R},\hat{\Omega}_1,\hat{\Omega}_2) = E\Psi(\mathbf{R},\hat{\Omega}_1,\hat{\Omega}_2) \qquad 2.2.1$$

(from hence forth, atomic units will be used throughout; $\hbar = m_e = e = 1$.)

In the general case the molecules have both vibrational and rotational degrees of freedom, but here they are treated as rigid rotors. The interaction potential is then $V(\mathbf{R},\hat{\Omega}_1,\hat{\Omega}_2)$ where $\mathbf{R}$ is the intermolecular vector and $\hat{\Omega}_i$ ($\equiv \alpha,\beta,\gamma$) are the Euler angles describing the orientation of molecule i with respect to the space fixed frame. The interaction potential is defined as the difference between the total electronic energy of the system at $(\mathbf{R},\hat{\Omega}_1,\hat{\Omega}_2)$ and the total electronic energy as

$|\mathbf{R}| \rightarrow \infty$. The energy E in equation 2.2.1 is the incident energy of the system and is equal to the total translational kinetic energy plus the initial rotational energy of the two molecules, and H_i is the rotational Hamiltonian of molecule i. The reduced mass of the system is μ.

The kinetic energy operator, $(\nabla_R{}^2/2\mu)$ can be separated into angular and radial parts giving:

$$\left[-\frac{1}{2\mu R}\frac{d^2}{dR^2}R + \frac{\mathbf{l}^2}{2\mu R} + H_1 + H_2 + V(\mathbf{R},\hat{\Omega}_1,\hat{\Omega}_2) - E\right]\Psi(\mathbf{R},\hat{\Omega}_1,\hat{\Omega}_2) = 0 \quad 2.2.2$$

where $\mathbf{l}$ is the orbital angular momentum operator.

The coupled equations are formed by expanding the total wavefunction in some basis set complete in the possible states of the separated molecules. Following Arthurs and Dalgarno (1960), the basis set is chosen as a complete set of eigenfunctions of the total angular momentum $\mathbf{J}$ and its projection on the space fixed axis $\mathbf{J}_z$. The potential cannot couple states of different total angular momentum so, with this choice of basis functions, the system of coupled equations that results decomposes into smaller blocks of equations that can be solved separately for each value of J.

For two arbitrary molecules with angular momentum j_1 and j_2, and relative orbital angular momentum, l, eigenfunctions of total angular momentum can be formed from:

$$Z^{JM}_{j_1 k_1 j_2 k_2 j_{12} l}(\hat{R},\hat{\Omega}_1,\hat{\Omega}_2) = \sum_{\substack{m_1 m_2 \\ m_{12} m_l}} C^{j_1\ j_2\ j_{12}}_{m_1 m_2 m_{12}} C^{j_{12}\ l\ J}_{m_{12} m_l M}\, \chi^{j_1}_{k_1 m_1}(\hat{\Omega}_1)\chi^{j_2}_{k_2 m_2}(\hat{\Omega}_2)Y^l_{m_l}(\hat{R}) \quad 2.2.3$$

Here k_1, k_2 are the projections of j_1, j_2 on the molecules symmetry axis, m_1, m_2 and m_l are the projections of j_1, j_2 and l on the space fixed axis, the $C^{j_1\ j_2\ j}_{m_1 m_2 m}$ are the Clebsch Gordan coefficients (eg Edmonds, 1960), and $\chi^{j_i}_{k_i,m_i}(\hat{\Omega}_i)$ is the normalised rotational eigenfunction of molecule (i). $Y^l_{m_l}(\hat{R})$ is a normalised spherical harmonic.

The total wavefunction may be expanded as:

$$\Psi_{\gamma}^{JM}(\mathbf{R},\hat{\Omega}_1,\hat{\Omega}_2) = \sum_{\gamma''} \frac{G_{\gamma''}^{J\gamma}(R)}{R} Z_{\gamma''}^{JM}(\hat{R},\hat{\Omega}_1,\hat{\Omega}_2) \qquad 2.2.4$$

where

$$\gamma \equiv (j_1, k_1, j_2, k_2, j_{12}, l).$$

Substituting into the Schrödinger equation gives:

$$\begin{aligned}\sum_{\gamma''} Z_{\gamma''}^{JM}(\hat{R},\hat{\Omega}_1,\hat{\Omega}_2) \left[\frac{d^2}{dR^2} - \frac{l''(l''+1)}{R^2} + \kappa_{\alpha''}^2\right] G_{\gamma''}^{J\gamma}(R) \\ = -2\mu V \sum_{\gamma''} G_{\gamma''}^{J\gamma}(R) Z_{\gamma''}^{JM}(\hat{R},\hat{\Omega}_1,\hat{\Omega}_2)\end{aligned} \qquad 2.2.5$$

Here we have introduced the wave number κ_α,

$$\kappa_\alpha^2 = 2\mu(E - E_{j_1 k_1} - E_{j_2 k_2}) \qquad 2.2.6$$

$$\alpha \equiv (j_1, k_1, j_2, k_2)$$

and used the fact that:

$$\mathbf{l}^2 Z_{\gamma}^{JM}(\hat{R},\hat{\Omega}_1,\hat{\Omega}_2) = l(l+1) Z_{\gamma}^{JM}(\hat{R},\hat{\Omega}_1,\hat{\Omega}_2) \qquad 2.2.7$$

Channels with $\kappa_\alpha^2 \geq 0$ are energetically accessible and are known as open channels. Channels with $\kappa_\alpha^2 < 0$ are known as closed channels and are classically inaccessible at the energy E.

Multiplying equation 2.2.5 from the left by $Z_{\gamma'}^{JM\,*}(\hat{R},\hat{\Omega}_1,\hat{\Omega}_2)$, integrating over all angles, and making use of the orthonormality properties of the Z's gives:

$$\left[\frac{d^2}{dR^2} - \frac{l'(l'+1)}{R^2} + \kappa_{\alpha'}^2\right] G_{\gamma'}^{J\gamma}(R) = 2\mu \sum_{\gamma''} \langle\gamma'|V|\gamma''\rangle G_{\gamma''}^{J\gamma}(R) \qquad 2.2.8$$

All the angular and rotational information on the problem is contained within the coupling matrix, $\langle\gamma'|V|\gamma''\rangle$. This quantity can be evaluated by expanding the

potential as a linear combination of angular functions. In the most general case this is a product of rotation matrices (eg Secrest 1979). The angular integration can be done by standard methods (Edmonds 1960), and the coupling matrix elements reduce to algebraic expressions.

The set of coupled equations (2.2.8) are the close coupled equations. Information on the observable properties of the system can be obtained by integrating the equations numerically, starting in the classically forbidden region where $V > E$, and propagating the solution out to the asymptotic region, $V \rightarrow 0$.

In the limit $\langle \gamma' | V | \gamma'' \rangle \rightarrow 0$, the general solution of equation 2.2.8 can be written as a linear contribution of spherical Bessel functions of the first and second kind (Abramowitz and Stegun, 1965). The scattering matrix, $\mathbf{S}$, can be derived in the asymptotic region by fitting the solutions to the long range form :

$$\begin{aligned} \mathbf{G}^J(R) &= \mathbf{j}(R)\mathbf{A} - \mathbf{n}(R)\mathbf{B} \\ \mathbf{G}^{J'}(R) &= \mathbf{j}'(R)\mathbf{A} - \mathbf{n}'(R)\mathbf{B} \end{aligned} \qquad 2.2.9a$$

where:

$$\begin{aligned} j_{ij}(R) &= \delta_{ij} \kappa_j^{1/2} R\, j_l(\kappa_j R) \\ n_{ij}(R) &= \delta_{ij} \kappa_j^{1/2} R\, n_l(\kappa_j R) \end{aligned} \qquad \text{for } \kappa_j^2 \geq 0 \qquad 2.2.9b$$

and:

$$\begin{aligned} j_{ij}(R) &= \delta_{ij} (-1)^{l+2} \left(\frac{\kappa_j}{2}\right)^{1/2} R\, h_l^{(2)}(\kappa_j R) \\ n_{ij}(R) &= \delta_{ij}\, i^{l+2} \left(\frac{\kappa_j}{2}\right)^{1/2} R\, h_l^{(1)}(\kappa_j R) \end{aligned} \qquad \text{for } \kappa_j^2 < 0 \qquad 2.2.9c$$

Here $j_l(\kappa R)$ and $n_l(\kappa R)$ are spherical Bessel functions of the first and second kind, and $h_l^{(1,2)}(\kappa R)$ are Hankel functions.

The scattering matrix may be obtained from:

$$\mathbf{S}^J = (\mathbf{I} + i\mathbf{K}^J)(\mathbf{I} - i\mathbf{K}^J)^{-1} \qquad 2.2.10$$

where $\mathbf{I}$ is the unit matrix and $\mathbf{K}$ is the reactance matrix:

$$\mathbf{K} = \mathbf{B}\mathbf{A}^{-1} \qquad 2.2.11$$

The relationship between the integral cross-sections and the scattering matrix is derived in appendix A, and is merely stated here as:

$$\sigma(\alpha \rightarrow \alpha') = \sum_J \sigma^J(\alpha \rightarrow \alpha') = \frac{\pi}{(2j_1+1)(2j_2+1)\kappa_\alpha^2} \sum_J \sum_{\substack{ll' \\ j_{12}j_{12}'}} (2J+1)|T^J_{\gamma\gamma'}|^2 \qquad 2.2.12$$

where $\mathbf{T}^J$ is the transmission matrix defined by:

$$\mathbf{T}^J = \mathbf{I} - \mathbf{S}^J \qquad 2.2.13$$

The matrices $\mathbf{S}^J$, $\mathbf{K}^J$ and $\mathbf{T}^J$ are all symmetric and a consequence of this is the detailed balance relation :

$$g_i\,\kappa_i^2\,\sigma(i \rightarrow j) = g_j\,\kappa_j^2\,\sigma(j \rightarrow i) \qquad 2.2.14$$

where g_i, g_j are the statistical weight factors. This reflects the invariance of the dynamics of the system under time reversal.

In theory, the system of CC equations is unbounded, and any required accuracy can be obtained by increasing the number of states in the basis set (equation 2.2.3). In reality, the coupling of the angular momentum results in a large number of coupled equations for even a modestly small number of states. As the CPU time required for any calculation increases by around N^2 to N^3, where N is the number of coupled equations, the size of the calculation can rapidly become prohibitive. CC calculations remain feasible, however, for systems with relatively widely spaced energy levels or at a collision energy at which only a small number of states are energetically accessible. The CC approach remains by far the most accurate approach to the solution of the coupled equations, and reliable CC calculations are important in evaluating the adequacy of the various approximate methods that have been developed. In addition, the region in which the CC calculations are easiest, low energies, is that region in which the decoupling approximations tend to fail.

2.3 Decoupling Approximations

The most successful of the decoupling approximations in the regime of low energy collisions is the coupled states approximation of McGuire and Kouri (1974) and Pack (1974). The derivation of the coupled states (CS) approximation makes use of the fact that when the CC equations are formulated in the body fixed frame, the distinction between coupling due to l and coupling due to the interaction potential is made explicit. The body fixed frame is defined so that the z'-axis lies along the intermolecular vector (figure 2.1).

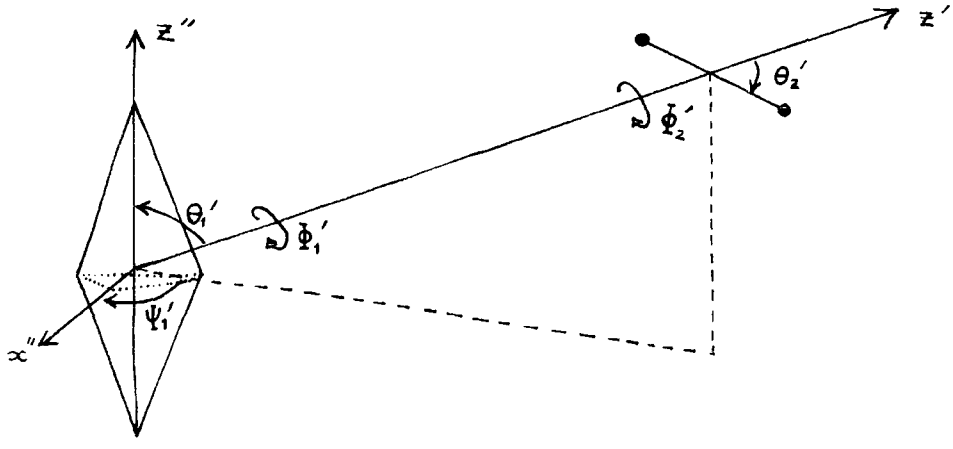

Figure 2.1: The Body Fixed Co-ordinate System

The Hamiltonian in the space fixed frame can be rewritten:

$$H_{SF}\Psi_{\beta l}^{JM}(\mathbf{R},\hat{\Omega}_1,\hat{\Omega}_2) = E\Psi_{\beta l}^{JM}(\mathbf{R},\hat{\Omega}_1,\hat{\Omega}_2) \qquad 2.3.1$$

where β indicates the set of indices $(j_1, k_1, j_2, k_2, j_{12})$ but not l. M is the projection of $\mathbf{J}$ on the space fixed z-axis.

The space fixed wavefunction, Ψ, and body fixed wavefunction, Φ, are related through the transformation:

$$\Psi_{\beta l}^{JM}(\mathbf{R},\hat{\Omega}_1,\hat{\Omega}_2) = \sum_{\Omega} D_{\Omega M}^{J}(\alpha,\beta,\gamma)\Phi_{\beta l}^{J\Omega}(R,\hat{\Omega}_1',\hat{\Omega}_2') \qquad 2.3.2$$

where Ω is the projection of $\mathbf{J}$ on the body fixed z'-axis, $\hat{\Omega}'_i$ are the Euler angles describing the orientation of molecule i in the space fixed frame and (α, β, γ) are the Euler angles taking the body fixed frame into the space fixed frame.

We may choose to expand the body fixed wavefunction in eigenfunctions of $\mathbf{J}, \mathbf{J}_z, \mathbf{j}_{12}$ and $\mathbf{j}_{12,z'}$ given by (Launay 1976):

$$\Upsilon^{J\Omega}_{\beta}(\hat{\Omega}'_1, \hat{\Omega}'_2) = \sum_{\Omega_1 \Omega_2} C^{j_1\ j_2\ j_{12}}_{\Omega_1 \Omega_2 \Omega} \times \chi^{j_1}_{k_1 \Omega_1}(\hat{\Omega}'_1) \chi^{j_2}_{k_2 \Omega_2}(\hat{\Omega}'_2) \qquad 2.3.3$$

where $\mathbf{j}_{12} = \mathbf{j}_1 + \mathbf{j}_2$ and $\mathbf{J} = \mathbf{j}_{12} + \mathbf{l}$. Note that in the body fixed frame the component of l along the body fixed z'-axis is zero because:

$$\mathbf{l} = \mu(\mathbf{R} \times \mathbf{v}) \qquad 2.3.4$$

where $\mathbf{v}$ is the relative velocity. As a result, the component of $\mathbf{j}_{12}$ along the body fixed z'-axis is just Ω , the component of $\mathbf{J}$ along z'.

Expanding the body fixed wavefunction as:

$$\Phi^{J\Omega}_{\beta l}(R, \hat{\Omega}'_1, \hat{\Omega}'_2) = \sum_{\beta'' \Omega''} \frac{F^{J\Omega\beta l}_{\beta'' \Omega''}(R)}{R} \Upsilon^{J\Omega''}_{\beta''}(\hat{\Omega}'_1, \hat{\Omega}'_2) \qquad 2.3.5$$

where $\alpha \equiv j_1, k_1, j_2, k_2$, the body fixed CC equations can be obtained as before, multiplying the Schrödinger equation from the left by $\Upsilon^{J\Omega'}_{\beta'}{}^*(\hat{\Omega}'_1, \hat{\Omega}'_2)$ and integrating over $\hat{\Omega}'_1, \hat{\Omega}'_2$ to give:

$$\left[\frac{d^2}{dR^2} + \kappa^2_{\alpha'}\right] F^{J\Omega\beta l}_{\beta'\Omega'}(R) = 2\mu \sum_{\beta''\Omega''} \langle \beta'\Omega' | V(R, \hat{\Omega}'_1, \hat{\Omega}'_2) - \mathbf{l}^2/2\mu | \beta''\Omega'' \rangle F^{J\Omega\beta l}_{\beta''\Omega''}(R) \qquad 2.3.6$$

Equation 2.3.6 is exact, and is of the same dimensionality as the space fixed equivalent. It can be shown (eg Rabitz 1976) that $\langle \beta'\Omega' | V | \beta''\Omega'' \rangle$ is zero unless $\Omega' = \Omega''$. This is a consequence of the invariance of the interaction potential under rotations of the whole system about the intermolecular axis; V cannot change the projection of $\mathbf{J}$ (or $\mathbf{j}_{12}$) along that axis.

However, unlike the space fixed equations, the centrifugal barrier operator, $\mathbf{l}^2$ is no longer diagonal in Ω'. Following Rabitz (1976), $\mathbf{l}$ can be expanded as:

$$\mathbf{l}^2 = \mathbf{J}^2 + \mathbf{j}_{12}^2 - 2\mathbf{J}_{z'}^2 - \mathbf{J}_+\mathbf{j}_{12,-} - \mathbf{J}_-\mathbf{j}_{12,+} \qquad 2.3.7$$

Here $\mathbf{J}_\pm, \mathbf{j}_{12\pm}$ are the raising and lowering operators, and their presence leads to non-vanishing coupling between Ω' and $\Omega'' = \Omega' \pm 1$.

The essence of the CS method (also known as the centrifugal decoupling method) is to ignore the $\Omega' \neq \Omega''$ coupling. In this approximation the CS equations become:

$$\begin{aligned}&\left[\frac{d^2}{dR^2} - \frac{1}{R^2}[J(J+1) + j'_{12}(j'_{12}+1) - 2\Omega'^2] + \kappa_{\alpha'}^2\right] F^{J\Omega\beta l}_{\Omega'\beta'}(R) \\ &= 2\mu \sum_{\beta''} \langle \beta'\Omega'|V(R,\hat{\Omega}'_1,\hat{\Omega}'_2)|\beta''\Omega'\rangle F^{J\Omega\beta l}_{\Omega'\beta''}(R)\end{aligned} \qquad 2.3.8$$

As the interaction potential, V, does not couple states of different Ω, the coupled equations separate into blocks that can be solved separately for each value of Ω, with a subsequent saving in computer time.

The CS equations can be solved in the same way as the CC equations and are subject to the same boundary conditions. The adequacy of the CS approximation is usually gauged by direct comparison with CC calculations. In general, the CS approximation is expected to give the best results in collisions dominated by short range forces, and at low values of total angular momentum. This is because the centrifugal potential terms fall off like R^{-2} at large R whilst the interaction potential between two neutral molecules decreases as R^{-6}, and the CS approximation will give the best results in regions where the interaction potential dominates the anisotropic terms.

2.4 Numerical Solution of the Coupled Equations

The close coupled equations (2.2.8) can be written in matrix form as:

$$\left[\mathbf{I}\frac{d^2}{dR^2} + \mathbf{W}(R)\right]\mathbf{G}(R) = 0 \qquad 2.4.1$$

where:

$$\mathbf{W}(R) = \mathbf{k}^2 - \mathbf{l}^2 - \mathbf{V}(R). \qquad 2.4.2$$

Here $\mathbf{V}(R)$ is the potential coupling matrix, and $\mathbf{k}^2(R)$ is the wavevector matrix. Both $\mathbf{k}^2(R)$ and $\mathbf{l}^2(R)$ are diagonal matrices, and $\mathbf{G}(R)$ is an $N \times N$ matrix where N is the number of channels.

The equations are solved subject to the boundary conditions (appendix A):

$$G^{J\gamma}_{\gamma'}(R) = 0 \quad \text{at} \quad R = 0 \qquad 2.4.3a$$

and

$$G^{J\gamma}_{\gamma'}(R) \rightarrow \kappa^{-1/2}_{\alpha'}\left[\sin\left(\kappa_\alpha R - \frac{l\pi}{2}\right)\delta_{\gamma\gamma'} + K^J_{\gamma\gamma'}\cos\left(\kappa_{\alpha'}R - \frac{l'\pi}{2}\right)\right] \qquad 2.4.3b$$

as $R \rightarrow \infty$.

The scattering matrix, $\mathbf{S}$, can be obtained from the reactance matrix $\mathbf{K}$ through the relationship 2.2.10.

There are many different methods for integrating the coupled equations but the underlying principles behind the methods are similar. The integration is started in the classically forbidden region, where the potential energy is larger than the collision energy, at some minimum value of the intermolecular distance, $R_{\min}$. $R_{\min}$ should be sufficiently far into the classically forbidden region that the final cross-sections are independent of its choice, but as far from the origin as the first condition allows. The reasons for this are twofold. Firstly, one does not want to waste time on unnecessary integration in the nonclassical region, and secondly, the solutions are all exponentially growing in the classically forbidden region. Strongly growing channels can dominate the solution matrix and lead to a loss of linear

independence of the solutions, and stabilisation problems for some integration methods (Secrest, 1979).

The solution is propagated out to the asymptotic region where $V \rightarrow 0$ and fitted to boundary conditions of the form 2.4.3. In this region open channels give oscillating solutions, whilst closed channels decay exponentially. The period of oscillation and rate of decay is dependent on the collision energy (through $\kappa_{\alpha'}$). For the open channels, the rate of oscillation increases with increasing energy, and consequently more integration steps are required as the energy increases. In addition, more partial waves, and more channels are required for convergence and the problem grows rapidly.

The methods of integration have been discussed in a recent review (Allison, 1988), and can be divided into two classes; approximate solution techniques and approximate potential techniques (Secrest, 1979).

The approximate solution techniques use the exact potential coupling matrix and employ numerical techniques to solve the resulting Schrödinger equation approximately. In their simplest form $\mathbf{G}$ is propagated out from $R_{\min}$ using some step routine to solve the equations in either their integral or differential forms. One such method is the DeVogelaere method (Lester, 1971), which integrates from R_n to R_{n+1} using an intermediate step, $R_{n+1/2}$. If we define the step size as $h = R_{n+1} - R_n$, the integration proceeds via the equations:

$$\begin{aligned}
\mathbf{G}_{n+1/2} &= \mathbf{G}_n + \frac{h}{2}\mathbf{G}'_n - \frac{h^2}{24}(4\mathbf{W}_n\mathbf{G}_n - \mathbf{W}_{n-1/2}\mathbf{G}_{n-1/2}) \\
\mathbf{G}_{n+1} &= \mathbf{G}_n + h\mathbf{G}'_n - \frac{h^2}{6}(\mathbf{W}_n\mathbf{G}_n + 2\mathbf{W}_{n+1/2}\mathbf{G}_{n+1/2}) \\
\mathbf{G}'_{n+1} &= \mathbf{G}'_n - \frac{h}{6}(\mathbf{W}_n\mathbf{G}_n + 4\mathbf{W}_{n+1/2}\mathbf{G}_{n+1/2} + \mathbf{W}_{n+1}\mathbf{G}_{n+1})
\end{aligned} \qquad 2.4.4$$

with the initial conditions:

$$\mathbf{G}_0(R_{\min}) = 0$$

$$\mathbf{G}_{-1/2} = -h\mathbf{G}_0{}'(R_{\min}) \qquad 2.4.5$$

$\mathbf{G_0}'$ is an arbitrary non-singular matrix, usually taken as the identity matrix:

$$\mathbf{G_0}' = \mathbf{I} \qquad 2.4.6$$

The solution following approximate solution methods such as this are inherently unstable, particularly in the classically forbidden region where $\mathbf{G}$ grows exponentially, and stabilisation routines are required for all such techniques.

The problem of stability can be overcome if the derivative of the natural logarithm of $\mathbf{G}$ is propagated instead, that is:

$$\frac{d}{dR}(\ln \mathbf{G}) = \mathbf{G}'\mathbf{G}^{-1} \qquad 2.4.7$$

Such log-derivative methods were first developed by Johnson (1973). They are very stable, and have been found to be particularly useful at short range where other methods are less satisfactory (Thomas et al, 1981).

The alternative approach, embodied in the approximate potential methods, is to break the integration region down into small intervals, and approximate the potential within an interval by an analytic function, taking it as zero outside the interval. The Schrödinger equation is then solved analytically for each interval, with the step size been estimated from perturbation theory. The method requires the potential to be diagonalised at the centre point of each interval being considered, and the solutions must be transformed into the appropriate space for each interval. As a result there is more work per step than for the approximate solution methods, but larger steps can be taken. The advantage of large step sizes is lost, however, if high accuracy is required, or in regions of rapidly changing potentials and consequently, the approximate potential methods are most applicable in the long range, slowly varying region of the potential.

In addition to the methods outlined above, hybrid methods have been developed that take advantage of the relatively good behaviour of the log-derivative methods at small R, and the economy of the approximate potential methods at large R (Thomas et al, 1981, Secrest, 1983, Allison, 1988).

The integration used in the bulk of the work reported in this thesis was the diabatic modified log-derivative method of Manolopoulos (1986), as implemented in the MOLSCAT computer code (Hutson and Green, 1986).

2.5 Effect of Basis Set Truncation

2.5.1 Rotational basis set truncation

The space fixed close coupled equations were derived by expanding the total wavefunction in the form:

$$\Psi_\gamma^{JM}(\mathbf{R},\hat{\Omega}_1\hat{\Omega}_2) = \sum_{\gamma'} \frac{G_{\gamma'}^{J\gamma}(R)}{R} \sum_{\substack{m_1' m_2' \\ m_{12}' m_l'}} C^{j_1' \; j_2' \; j_{12}'}_{m_1' m_2' m_{12}'} C^{j_{12}' \; l' \; J}_{m_{12}' m_l' M} \times \chi^{j_1'}_{k_1' m_1'}(\hat{\Omega}_1)\chi^{j_2'}_{k_2' m_2'}(\hat{\Omega}_2) Y^{l'}_{m_l'}(\hat{R}) \qquad 2.5.1$$

In the general case, the vibrational wavefunctions of the molecules should also be included on the right hand side. For the equality to be exact, the sum over γ' should run over all possible states, leading to an infinite set of coupled equations. Clearly, some truncation is needed. The truncation of the basis set is the major approximation of the CC approach to the collision problem, and the effect of this truncation has to be considered.

At any given collision energy, E, only those states with $\kappa_{\alpha'}^2 > 0$ are classically accessible. States with $\kappa_{\alpha'}^2 < 0$ have radial wavefunctions that are exponentially decaying with R, and the cross-sections for transitions to these states are identically zero. However, these closed channels can still play an important role in the collision, especially in regions where the potential is strongly anisotropic. Indirect collisions proceeding through an intermediate state become increasingly important as the anisotropy increases.

Even where cross-sections between the low j levels only are required, more anisotropic potentials require a larger basis set (eg Green and Thaddeus, 1976). This can be seen by considering the form of the potential expansion. For simplicity,

consider the simplest atom – linear rotor collision system. The potential can be expanded as a series of Legendre polynomials:

$$V(R,\theta') = \sum_{\lambda} v_{\lambda}(R) P_{\lambda}(\cos\theta') \qquad 2.5.2$$

where θ' is the angle between the linear rotor internuclear axis and the intermolecular axis. A true isotropic potential would have a non-zero contribution from the $(\lambda = 0)$ term only. Progressively more anisotropic potentials would have significant contributions to the sum over λ from progressively larger values of λ. Any term in the potential can couple states such that:

$$|j - j'| \leq \lambda \leq (j + j') \qquad 2.5.3$$

thus strongly anisotropic potentials will directly couple states with larger Δj than less anisotropic potentials.

The effect of basis set truncation in calculations is usually investigated non-rigorously by comparing **S**-matrix elements or cross-sections from calculations with successively larger basis sets and examining how well the results converge.

The results suggest that whilst it is necessary to include states that are directly coupled to the states of interest by strong anisotropies (Green and Thaddeus, 1976), it is not even always necessary to include all the open channels if only transitions between the lower j transitions are of interest.

In general, basis set truncation does not seem to be too critical, provided the basis is chosen carefully with an eye to which cross-sections are of interest. Thus whilst it is usually necessary to include closed channels when all cross-sections are of interest, a certain amount of economy in basis set size can be obtained if only some of the cross-sections are required. The adequacy of the basis set chosen for any particular collision calculation is usually assessed by performing basis set convergence tests for the first few partial waves.

2.5.2 Vibrational basis set truncation

The assumption of a rigid rotor is equivalent to truncating the vibrational basis set to one state only. The empirical argument usually given to justify this

assumption is that the vibrational energy spacing is generally very much larger than the rotational energy spacing, so that the probability of the excited vibrational states intervening in a collision is very much smaller than the probability of the rotational states intervening. This assumption is harder to test than the truncation of the rotational basis, but tests have been carried out for rotational excitation of the H_2 molecule (eg Eastes and Secrest, 1972, Choi, Poe and Tang, 1977). Eastes and Secrest found that the first excited vibrational state, a closed channel, did have an effect on the results, even when open rotational channels were neglected. However, Choi et al (1977) found the opposite, and suggested that the discrepancy could have been due to the fact that Eastes and Secrest compared **S**-matrix elements at low values of total angular momentum, whereas Choi et al compared converged cross-sections, by which time differences evident at low values of total angular momentum could have been rendered insignificant. It should be remembered that the H_2 molecule is very light and therefore has a much smaller ratio of vibrational energy level spacing to rotational energy level spacing. It is expected that the rigid rotor approximation will generally be good at low collision energies.

2.6 Formulation for Linear Rotor – Symmetric Top Collisions

The closed coupled equations in their space fixed form are given by equation 2.2.8 as:

$$\left[\frac{d^2}{dR^2} - \frac{l'(l'+1)}{R^2} + \kappa_{\alpha'}^2\right] G_{\gamma'}^{J\gamma}(R) = 2\mu \sum_{\gamma''} \langle \gamma' | V | \gamma'' \rangle G_{\gamma''}^{J\gamma}(R) \qquad 2.6.1$$

Apart from the wavenumber, κ_α, the left hand side of the equation is independent of the collision system. All information on the rotational properties of the particular collision system under consideration is contained in the coupling matrix:

$$\langle \alpha' j_{12}' l' | V | \alpha j_{12} l \rangle = \int\int\int C^{j_1\ j_2\ j_{12}}_{m_1\ m_2\ m_{12}} C^{j_{12}\ l\ J}_{m_{12}\ m_l\ M} C^{j_1'\ j_2'\ j_{12}'}_{m_1'\ m_2'\ m_{12}'} C^{j_{12}'\ l'\ J}_{m_{12}'\ m_l'\ M}$$
$$\chi^{j_1'^*}_{k_1' m_1'}(\hat{\Omega}_1) \chi^{j_2'^*}_{k_2' m_2'}(\hat{\Omega}_2) Y^{l'^*}_{m_l'}(\hat{R}) V\ \chi^{j_1}_{k_1 m_1}(\hat{\Omega}_1) \chi^{j_2}_{k_2 m_2}(\hat{\Omega}_2) Y^{l}_{m_l}(\hat{R})\, d\hat{\Omega}_1\, d\hat{\Omega}_2\, d\hat{R} \qquad 2.6.2$$

The problem of formulating the equations for any particular collision system reduces to evaluating this integral. The form of the coupling matrix elements

for the atom – linear rotor, linear rotor – linear rotor, atom – symmetric top and atom – asymmetric top have been presented and discussed in the literature (AT–LR: Arthurs and Dalgarno, 1960, LR–LR: Green, 1975, AT–ST: Green, 1976, AT-aST: Garrison et al, 1976). Here the form of the coupling matrix element for the linear rotor – symmetric top collision problem is explicitly derived.

2.6.1 Rotational Eigenfunctions

A symmetric top molecule has equal moment of inertia about two of its principal axes, and a non-zero moment of inertia about the third, the symmetry axis, ie.

$$I_{x''} = I_{y''} \qquad I_{z''} > 0 \tag{2.6.3}$$

where $I_{z''}$ is the moment of inertia about the symmetry axis.

For a symmetric top the total angular momentum, $\mathbf{j}$, and its projection on the space fixed z-axis, $\mathbf{j}_z$, are constants of the motion, as always, and in addition the projection of the angular momentum on the molecular symmetry axis, $\mathbf{j}_{z''}$, is also a constant of the motion. The rotational eigenfunctions are therefore labelled by $|jkm\rangle$, where j, k and m are all good quantum numbers and:

$$\begin{aligned} \mathbf{j}^2|jkm\rangle &= j(j+1)\,|jkm\rangle \\ \mathbf{j}_z|jkm\rangle &= m\,|jkm\rangle \\ \mathbf{j}_{z''}|jkm\rangle &= k\,|jkm\rangle \end{aligned} \tag{2.6.4}$$

It can be shown (Edmonds 1960) that the rotational eigenfunctions of a symmetric top are given by:

$$|jkm\rangle = \left(\frac{2j+1}{8\pi}\right)^{1/2} D^j_{km}(\alpha,\beta,\gamma) \tag{2.6.5}$$

where $D^j_{km}(\alpha,\beta,\gamma)$ is a rotation matrix and (α,β,γ) are the Euler angles describing the rotation taking the space fixed axes into the internal molecule fixed axes. Edmonds definitions of the rotations matrices are used throughout:

$$D^j_{km}(\alpha,\beta,\gamma) = e^{ik\gamma}\, d^j_{km}(\beta)\, e^{im\alpha} \tag{2.6.6}$$

The rotational Hamiltonian of the symmetric top is given by:

$$\begin{aligned} H_{rot} &= \frac{I_{x''}}{2\mu}\mathbf{j}_{x''}^2 + \frac{I_{y''}}{2\mu}\mathbf{j}_{y''}^2 + \frac{I_{z''}}{2\mu}\mathbf{j}_{z''}^2 \\ &= A\,\mathbf{j}_{x''}^2 + B\,\mathbf{j}_{y''}^2 + C\,\mathbf{j}_{z''}^2 \end{aligned} \qquad 2.6.7$$

With $\mathbf{j}^2 = \mathbf{j}_{x''}^2 + \mathbf{j}_{y''}^2 + \mathbf{j}_{z''}^2$, the energy levels of the symmetric top follow from:

$$H_{rot}|jkm\rangle = \left(Bj(j+1) + (C-B)\,k^2\right)|jkm\rangle = E|jkm\rangle \qquad 2.6.8$$

The eigenfunctions, $|jkm\rangle$ are the primitive symmetric top eigenfunctions. For the description of a symmetric top molecule such as ammonia it is necessary to use symmetry adapted rotational eigenfunctions of the form (Green, 1980):

$$|jkm\epsilon\rangle = \frac{1}{(2\,(1+\delta_{k0}))^{1/2}}(|jkm\rangle + \epsilon|j\ -km\rangle) \qquad 2.6.9$$

where $k \geq 0$ and $\epsilon = \pm 1$ if $k > 0$, $\epsilon = +1$ only if $k = 0$.

The linear rotor molecule is equivalent to a symmetric top molecule with zero angular momentum about the molecule fixed z''-axis ($I_{z''} = 0$). The rotational properties of the linear rotor can be obtained from the symmetric top properties, to within a normalisation factor, by setting $C = k = 0$, thus:

$$\begin{aligned} \mathbf{j}^2|jm\rangle &= j(j+1)|jm\rangle, \\ \mathbf{j}_z|jm\rangle &= m\,|jm\rangle, \\ H_{rot}|jm\rangle &= Bj(j+1)|jm\rangle \\ &= E|jm\rangle. \end{aligned} \qquad 2.6.10$$

The rotational eigenfunction for the linear rotor is given by:

$$|jm\rangle = Y_m^j(\beta,\alpha) \qquad 2.6.11$$

where $Y^j_m(\beta,\alpha)$ is a normalised spherical harmonic (Edmonds, 1960). The spherical harmonics are related to the rotation matrices by:

$$D^j_{0m}(\alpha,\beta,\gamma) = \left(\frac{4\pi}{2j+1}\right)^{1/2} Y^j_m(\beta,\alpha) \qquad 2.6.12$$

The close coupled equations were derived by expanding the total wavefunction in eigenfunctions of total angular momentum, **J**, and its projection on the space fixed z-axis. In the case of the linear rotor – symmetric top collision system the eigenfunctions are given by:

$$Z^{JM}_{j_1 k_1 j_2 j_{12} \epsilon l}(\hat{R},\hat{\Omega}_1,\hat{\Omega}_2) = \sum_{\substack{m_1 m_2 \\ m_{12} m_l}} C^{j_1\ j_2\ j_{12}}_{m_1\ m_2\ m_{12}} C^{j_{12}\ l\ J}_{m_{12}\ m_l\ M} \left(\frac{2j_1+1}{4\pi}\right)^{1/2} \qquad 2.6.13$$
$$[\, D^{j_1}_{km_1}(\hat{\Omega}_1) + \epsilon\, D^{j_1}_{-km_1}(\hat{\Omega}_1)\,] Y^{j_2}_{m_2}(\hat{R}_2)\, Y^l_{m_l}(\hat{R})$$

From henceforth, the subscript '1' refers to the symmetric top molecule, and the subscript '2' to the linear rotor.

2.6.2 The Potential Expansion

The form of the potential expansion has been discussed explicitly for atom – symmetric top scattering ($j_2 = 0$) (Green 1976) and for linear rotor – linear rotor scattering ($k = 0$) Green, 1975) in both the body fixed and space fixed frames. These are all special cases of the most general invariant expansion for two polyatomic molecules (eg Stone and Tough, 1984, Leavitt, 1980). In this section the potential expansion for the specific case of linear rotor – symmetric top scattering is discussed.

Body Fixed Frame

It is most natural to express the potential in the body fixed co-ordinate system introduced in section 2.2 where the z'-axis is taken to be the intermolecular axis. *Ab initio* potential data are usually derived in this frame.

The body fixed co-ordinates were defined in figure 2.1. Here z' is the intermolecular axis, $(\phi'_1,\theta'_1,\psi'_1)$ are the Euler angles of the symmetric tops internal axes

with respect to the body fixed axes, and (θ_2', ϕ_2') are the polar angles describing the orientation of the linear rotor.

From the figure several symmetries of the system are immediately obvious, and these should be echoed in the potential expansion. Namely,

- the potential in invariant to rotations of both molecules around the z'-axis, and depends only on the difference $(\phi_1' - \phi_2')$.
- if the symmetric-top molecule has an n-fold axis of symmetry under rotations about the molecule fixed z''-axis, the potential is left unchanged by rotations of the molecule through $\psi_1' = 2\pi p/n$ radians $(p = 0, 1, 2...)$.
- if the linear rotor is a homonuclear diatomic molecule, the potential is left unchanged by rotations of the molecule through $\theta_2' = \pi$.

In addition, for an isolated system, the potential will be unchanged by inversion of all co-ordinates in the origin, and by rotation of the entire system through any angle (i.e. the space fixed potential expansion should be rotationally invariant, and unchanged by inversion).

The potential expansion in the body fixed frame may be taken as:

$$V(R, \hat{\Omega}_1', \hat{R}_2') = \sum_{\substack{\lambda_1 \lambda_2 \\ \mu\nu}} v_{\lambda_1 \mu \lambda_2 \nu}(R) D^{\lambda_1}_{\mu\nu}(\hat{\Omega}_1') Y^{\lambda_2}_{-\nu}(\hat{R}_2') \qquad 2.6.14$$

where $\hat{\Omega}_1' \equiv (\phi_1', \theta_1', \psi_1')$, $\hat{R}_2' \equiv (\theta_2', \phi_2')$ and R is the intermolecular distance.

If we use equations 2.6.6 and 2.6.12 to express the potential expansion in terms of the reduced rotation matrices and exponential functions (Edmonds, 1960) we obtain:

$$V(R, \hat{\Omega}_1', \hat{R}_2') = \sum_{\substack{\lambda_1 \lambda_2 \\ \mu\nu}} v_{\lambda_1 \mu \lambda_2 \nu}(R) \left(\frac{2\lambda_2 + 1}{4\pi}\right)^{1/2} e^{i\mu\psi_1'} d^{\lambda_1}_{\mu\nu}(\theta_1') e^{i\nu\phi_1'} e^{-i\nu\phi_2'} d^{\lambda_1}_{0-\nu}(\theta_2') \qquad 2.6.15$$

Note that the $\pm\nu$ index ensures that the potential depends only on the difference $(\phi_1' - \phi_2')$ as required, and we may set ϕ_1' (say) equal to zero.

The requirement that the potential must be invariant to rotations of the symmetric top molecule through $2\pi p/n$ for a molecule with an n-fold axis of symmetry is met if μ is an integer multiple of n.

Similarly, if the collision partner is a homonuclear molecule the requirement that the potential should be invariant to rotations of the molecule through an angle of π imposes the constraint that λ_2 must be even, as:

$$d^{\lambda_2}_{0\,-\nu}(\theta_2) = (-1)^{\lambda_2} d^{\lambda_2}_{0\,-\nu}(\theta_2 + \pi) \qquad 2.6.16$$

An important property of the body fixed v's may be derived from the requirement that the potential is real. Rewriting the body fixed expansion, we have:

$$V(R, \hat{\Omega}'_1, \hat{\Omega}'_2) = \sum_{\substack{\lambda_1 \lambda_2 \\ \mu \geq 0 \\ \nu \geq 0}} \left(v_{\mu\nu} \Upsilon_{\mu\nu} + v_{\mu -\nu} \Upsilon_{\mu -\nu} + v_{-\mu -\nu} \Upsilon_{-\mu -\nu} + v_{-\mu\nu} \Upsilon_{-\mu\nu} \right) \qquad 2.6.17a$$

where:

$$\Upsilon_{\mu\nu} \propto d^{\lambda_1}_{\mu\nu}(\theta'_1)\, d^{\lambda_2}_{0\,-\nu}(\theta'_2)\, \exp(i\mu\psi'_1 - i\nu\phi'_2) \qquad 2.6.17b$$

Here we have dropped the λ subscripts for clarity.

Since all the terms in the expansion should be independent, the imaginary part of this expression should vanish:

$$\begin{aligned} & d^{\lambda_2}_{0\,-\nu}(\theta'_2) \{ d^{\lambda_1}_{\mu\nu}(\theta'_1)\, v_{\mu\nu}(R) \sin(\mu\psi'_1 - \nu\phi'_2) \\ & + (-1)^{\nu} d^{\lambda_1}_{\mu\,-\nu}(\theta'_1)\, v_{\mu\,-\nu}(R) \sin(\mu\psi'_1 + \nu\phi'_2) \\ & - (-1)^{\nu} d^{\lambda_1}_{-\mu\,-\nu}(\theta'_1)\, v_{-\mu\,-\nu}(R) \sin(\mu\psi'_1 - \nu\phi'_2) \\ & - d^{\lambda_1}_{-\mu\nu}(\theta'_1)\, v_{-\mu\nu}(R) \sin(\mu\psi'_1 + \nu\phi'_2) \} = 0 \end{aligned} \qquad 2.6.18$$

making use of the property (Edmonds, 1960):

$$d^{\lambda}_{\mu\nu}(\theta) = (-1)^{\mu-\nu}\, d^{\lambda}_{-\mu\,-\nu}(\theta) \qquad 2.6.19$$

we have:

$$\begin{aligned} & d^{\lambda_1}_{\mu\nu}(\theta_1')\sin(\mu\psi_1' - \nu\phi_2')\{\, v_{\mu\nu} - (-1)^{\mu} v_{-\mu\,-\nu}\,\} \\ & + d^{\lambda_1}_{-\mu\nu}(\theta_1')\sin(\mu\psi_1' + \nu\phi_2')\{\, v_{-\mu\nu} - (-1)^{\mu} v_{\mu\,-\nu}\,\} = 0 \end{aligned} \qquad 2.6.20$$

As this must be true for all angles we obtain:

$$\begin{aligned} v_{\mu\nu}(R) &= (-1)^{\mu} v_{-\mu\,-\nu}(R) \\ v_{-\mu\nu}(R) &= (-1)^{\mu} v_{\mu\,-\nu}(R) \end{aligned} \qquad 2.6.21$$

but we have no relation between $v_{\mu\nu}$ and $v_{-\mu\nu}$ in the general case.

Space Fixed Frame

The potential expansion has been given in the body fixed frame. However, as was discussed in section 2.2, the fact that the body fixed z'-axis is rotating in space leads to off diagonal terms in the centrifugal potential. The coupled equations can be solved in both frames, but we choose to tackle the problem in the space fixed frame, sacrificing the relative simplicity of the body fixed coupling matrix elements in favour of a diagonal centrifugal contribution.

As we wish to perform the integrals over angular functions to obtain the coupling matrix elements,

$$\langle j_1' k' j_2' j_{12}' l'; JM | V | j_1 k j_2 j_{12} l; JM \rangle$$

the potential expansion should be expressed in the space fixed frame. The body fixed potential expansion can be transformed into the space fixed frame using the transformation:

$$D^{j}_{mm'}(\angle\text{s of c wrt a}) = \sum_{m''} D^{j\,*}_{m'm''}(\angle\text{s of a wrt b})\, D^{j}_{mm''}(\angle\text{s of c wrt b}) \qquad 2.6.22$$

Transforming each term in equation 2.6.14 we have:

$$\begin{aligned} D^{\lambda_1}_{\mu\nu}(\hat{\Omega}_1') &= \sum_{n_1} D^{\lambda_1\,*}_{\nu n_1}(\hat{\Omega}) D^{\lambda_1}_{\mu n_1}(\hat{\Omega}_1) \\ Y^{\lambda_2}_{-\nu}(\hat{R}_2') &= \sum_{n_2} D^{\lambda_2\,*}_{-\nu n_2}(\hat{\Omega}) Y^{\lambda_2}_{n_2}(\hat{R}_2) \end{aligned} \qquad 2.6.23$$

where Ω are the Euler angles that take the space fixed axes into the body fixed axes.

The rotation matrices may be combined to give (Edmonds 1960):

$$D^{\lambda_1 *}_{\nu n_1}(\hat{\Omega}) D^{\lambda_2 *}_{-\nu n_2}(\hat{\Omega}) = \sum_{\lambda} C^{\lambda_1 \lambda_2 \lambda}_{\nu \; -\nu 0} C^{\lambda_1 \lambda_2 \lambda}_{n_1 n_2 n} \left(\frac{4\pi}{2\lambda + 1} \right)^{1/2} Y^{\lambda *}_{n}(\hat{R}) \qquad 2.6.24$$

Substituting equations 2.6.23 and 2.6.24 into the body fixed expansion (equation 2.6.14) we obtain the space fixed potential expansion:

$$V(\mathbf{R}, \hat{\Omega}_1, \hat{\Omega}_2) = \sum_{\substack{\lambda_1 \lambda_2 \\ \lambda \mu}} v_{\lambda_1 \lambda_2 \lambda \mu}(R) \sum_{n_1 n_2} C^{\lambda_1 \lambda_2 \lambda}_{n_1 n_2 n} D^{\lambda_1}_{\mu n_1}(\hat{\Omega}_1) Y^{\lambda_2}_{n_2}(\hat{R}_2) Y^{\lambda *}_{n}(\hat{R}) \qquad 2.6.25$$

where:

$$v_{\lambda_1 \lambda_2 \lambda \mu}(R) = \sum_{\nu = -\lambda_{\min}}^{+\lambda_{\min}} v_{\lambda_1 \mu \lambda_2 \nu}(R) C^{\lambda_1 \lambda_2 \lambda}_{\nu \; -\nu 0} \left(\frac{4\pi}{2\lambda + 1} \right)^{1/2} \qquad 2.6.26$$

and $\lambda_{\min}$ is the minimum of λ_1 and λ_2.

Using the symmetry properties of the Clebsch Gordan coefficients, the relationship between the space fixed and body fixed potential expansion coefficients can be rewritten with the sum running over positive values of ν only:

$$v_{\lambda_1 \lambda_2 \lambda \mu}(R) = \sum_{\nu \geq 0} \frac{C^{\lambda_1 \lambda_2 \lambda}_{\nu \; -\nu 0}}{(1 + \delta_{\nu 0})} \left(\frac{4\pi}{2\lambda + 1} \right)^{1/2} \left(v_{\lambda_1 \mu \lambda_2 \nu}(R) + (-1)^{\lambda_1 + \lambda_2 + \lambda} v_{\lambda_1 \mu \lambda_2 \; -\nu}(R) \right) \qquad 2.6.27$$

From equation 2.6.27 and the relationship 2.6.21, it can be seen that if $\mu = 0$ (linear rotor – linear rotor scattering), then the sum, $(\lambda_1 + \lambda_2 + \lambda)$ must be even for a non-vanishing space fixed coefficient. Similarly, there is no $\nu = 0$ contribution to the space fixed coefficient if the sum is odd. If μ and ν are both non-zero, however, the sum can be either even or odd, and this has important consequences for the propensity rules governing linear rotor – symmetric top collisions.

The requirement for $(\lambda_1 + \lambda_2 + \lambda)$ to be even for linear rotor – linear rotor scattering, and for atom – symmetric top scattering, may be more rigorously derived by invoking the requirement that the potential is unchanged by reflection of

all co-ordinates in the origin. In the case of the linear rotor - symmetric top space fixed potential expansion given by equation 2.6.25 the same operation yields the symmetry properties of the space fixed potential expansion coefficients. Inversion of the co-ordinates in the origin is equivalent to the transformation:

$$\alpha \rightarrow \alpha + \pi, \qquad \beta \rightarrow \pi - \beta, \qquad \gamma \rightarrow \pi - \gamma. \tag{2.6.28}$$

where α, β and γ are the Euler angles. Under this transformation:

$$\begin{aligned} D^{\lambda_1}_{\mu n_1}(\hat{\Omega}_1) &\rightarrow (-1)^{\lambda_1+\mu} D^{\lambda_1}_{-\mu n_1}(\hat{\Omega}_1) \\ Y^{\lambda_2}_{n_2}(\hat{R}_2) &\rightarrow (-1)^{\lambda_2}\, Y^{\lambda_2}_{n_2}(\hat{R}_2) \\ Y^{\lambda}_{n}(\hat{R}) &\rightarrow (-1)^{\lambda}\, Y^{\lambda}_{n}(\hat{R}) \end{aligned} \tag{2.6.29}$$

thus inversion in the origin has the effect of changing μ to $-\mu$ and introducing a factor, $(-1)^{\lambda_1+\lambda_2+\lambda+\mu}$. The requirement that the potential remains unchanged thus imposes the restriction that:

$$v_{\lambda_1\lambda_2\lambda\mu}(R) = (-1)^{\lambda_1+\lambda_2+\lambda+\mu} v_{\lambda_1\lambda_2\lambda-\mu}(R) \tag{2.6.30}$$

Using this relation it is useful to rewrite the space-fixed expansion (2.6.25) as:

$$V(\mathbf{R}, \hat{\Omega}_1, \hat{\Omega}_2) = \sum_{\substack{\lambda_1\lambda_2\lambda \\ \mu\geq 0}} \frac{v_{\lambda_1\lambda_2\lambda\mu}(R)}{1+\delta_{\mu 0}} [\Upsilon_{\lambda_1\lambda_2\lambda\mu} + (-1)^{\lambda_1+\lambda_2+\lambda+\mu} \Upsilon_{\lambda_1\lambda_2\lambda-\mu}] \tag{2.6.31a}$$

where:

$$\Upsilon_{\lambda_1\lambda_2\lambda\mu} \equiv \sum_{n_1 n_2} C^{\lambda_1\lambda_2\lambda}_{n_1 n_2 n} D^{\lambda_1}_{\mu n_1}(\hat{\Omega}_1) Y^{\lambda_2}_{n_2}(\hat{R}_2) Y^{\lambda\,*}_{n}(\hat{R}) \tag{2.6.31b}$$

2.6.3 Coupling Matrix Elements

Armed with the space fixed potential expansion, and form of the wavefunction, we are now in the position to derive the form of the coupling matrix elements. The projection of the tops angular momentum on its symmetry axis, k, takes a spectator role in the angular momentum coupling (Green 1976), and so it is

sufficient at this stage to perform the angular integration using only the primitive symmetric top functions $|jkm\rangle$ (eqn. 2.6.5). The angular integral then becomes:

$$\langle j_1' k' j_2' j_{12}' l'; JM|V|j_1 k j_2 j_{12} l; JM\rangle = \int\int\int \frac{((2j_1+1)(2j_1'+1))^{1/2}}{8\pi}$$
$$\times \sum_{\substack{m_1 m_2 \\ m_{12} m_l}} \sum_{\substack{m_1' m_2' \\ m_{12}' m_l'}} \sum_{\substack{\lambda_1 \lambda_2 \\ \lambda \mu}} \sum_{n_1 n_2} C^{j_1\ j_2\ j_{12}}_{m_1 m_2 m_{12}} C^{j_{12}\ l\ J}_{m_{12} m_l M} C^{j_1'\ j_2'\ j_{12}'}_{m_1' m_2' m_{12}'} C^{j_{12}'\ l'\ J}_{m_{12}' m_l' M} C^{\lambda_1 \lambda_2 \lambda}_{n_1 n_2 n}$$
$$\times D^{j_1'\,*}_{k_1' m_1'}(\hat{\Omega}_1) Y^{j_2'\,*}_{m_2'}(\hat{R}_2) Y^{l'\,*}_{m_l'}(\hat{R})\, D^{\lambda_1}_{\mu n_1}(\hat{\Omega}_1) Y^{\lambda_2}_{n_2}(\hat{R}_2) Y^{\lambda\,*}_{n}(\hat{R})$$
$$\times D^{j_1}_{k_1 m_1}(\hat{\Omega}_1) Y^{j_2}_{m_2}(\hat{R}_2) Y^{l}_{m_l}(\hat{R})\, d\hat{\Omega}_1\, d\hat{R}_2\, d\hat{R} \qquad 2.6.32$$

Equation 2.6.32 can be evaluated by applying standard methods to perform the angular integrals (Edmonds, 1960) and summing the resultant Clebsch Gordan coefficients or equivalently, the 3-j symbols to give 6-j and 9-j symbols. Integration over $d\hat{R}$ gives:

$$\int d\hat{R}\, Y^{l'\,*}_{m_l'}(\hat{R}) Y^{\lambda\,*}_{n}(\hat{R}) Y^{l}_{m_l}(\hat{R}) = \left(\frac{(2l'+1)(2\lambda+1)}{4\pi(2l+1)}\right)^{1/2} C^{l'\ \lambda\ l}_{m_l n m_l} C^{l'\lambda l}_{0\,0\,0} \qquad 2.6.33a$$

Integration over dR_2 gives:

$$\int d\hat{R}_2\, Y^{j_2}_{m_2}(\hat{R}_2) Y^{\lambda_2}_{n_2}(\hat{R}_2) Y^{j_2'\,*}_{m_2'}(\hat{R}_2) = \left(\frac{(2j_2+1)(2\lambda_2+1)}{4\pi(2j_2'+1)}\right)^{1/2} C^{j_2\ \lambda_2 j_2'}_{m_2 n_2 m_2'} C^{j_2 \lambda_2 j_2'}_{0\ 0\ 0} \qquad 2.6.33b$$

Integration over $d\hat{\Omega}_1$ gives:

$$\int d\hat{\Omega}_1\, D^{j_1}_{k m_1}(\hat{\Omega}_1) D^{\lambda_1}_{\mu n_1}(\hat{\Omega}_1) D^{j_1'\,*}_{k' m_1'}(\hat{\Omega}_1)$$
$$= 8\pi^2 (-1)^{m_1' - k'} \begin{pmatrix} j_1 & j_1' & \lambda_1 \\ k & -k' & \mu \end{pmatrix} \begin{pmatrix} j_1 & j_1' & \lambda_1 \\ m_1 & -m_1' & n_1 \end{pmatrix} \qquad 2.6.33c$$

where (:::) are the 3-j symbols and are related to the Clebsch Gordan coefficients by:

$$C^{j_1\ j_2\ j}_{m_1 m_2 m} = (-1)^{j_2 - j_1 - m} (2j+1)^{1/2} \begin{pmatrix} j_1 & j_2 & j \\ m_1 & m_2 & -m \end{pmatrix} \qquad 2.6.34$$

Combining the three integrals and using the relation 2.6.34 to convert the Clebsch Gordan coefficients to 3-j symbols gives:

$$
\begin{aligned}
V_{\gamma'}^{J\gamma} &= \sum \frac{v_{\lambda_1\lambda_2\lambda\mu}(R)}{(4\pi)} \\
&\times (-1)^{-j_1-j_2-j_1'+j_2'-j_{12}-j_{12}'+\lambda_2-\lambda_1-k'+l'+l-\nu-m_{12}-m_{12}'-m_l-m_l'-M} \\
&\times [(2j_1+1)(2j_2+1)(2j_{12}+1)(2l+1)(2J+1)(2j_1'+1) \\
&\times (2j_2'+1)(2j_{12}'+1)(2l'+1)(2J+1)(2\lambda_2+1)(2\lambda+1)^2]^{1/2} \\
&\times \begin{pmatrix} j_1 & j_2 & j_{12} \\ m_1 & m_2 & -m_{12} \end{pmatrix} \begin{pmatrix} j_{12} & l & J \\ m_{12} & m_l & -M \end{pmatrix} \begin{pmatrix} j_1' & j_2' & j_{12}' \\ m_1' & m_2' & -m_{12}' \end{pmatrix} \\
&\times \begin{pmatrix} j_{12}' & l' & J \\ m_{12}' & m_l' & -M' \end{pmatrix} \begin{pmatrix} \lambda_1 & \lambda_2 & \lambda \\ n_1 & n_2 & -n \end{pmatrix} \begin{pmatrix} l' & \lambda & l \\ -m_l' & n & m_l \end{pmatrix} \\
&\times \begin{pmatrix} l' & \lambda & l \\ 0 & 0 & 0 \end{pmatrix} \begin{pmatrix} j_2' & \lambda_2 & j_2 \\ -m_2' & n_2 & m_2 \end{pmatrix} \begin{pmatrix} j_2' & \lambda_2 & j_2 \\ 0 & 0 & 0 \end{pmatrix} \\
&\times \begin{pmatrix} j_1' & \lambda_1 & j_1 \\ -m_1' & n_1 & m_1 \end{pmatrix} \begin{pmatrix} j_1' & \lambda_1 & j_1 \\ -k' & \mu & k \end{pmatrix}
\end{aligned}
\qquad 2.6.35
$$

where the summation is over $m_1, m_2, m_{12}, m_l, \lambda_1, \lambda_2, \lambda, \mu, n_1, n_2, m_1', m_2', m_{12}', m_l'$. The 3-j symbols can be combined to yield 6-j and 9-j symbols giving as the final coupling matrix element:

$$
\begin{aligned}
V_{\gamma'}^{J\gamma} &= \sum_{\substack{\lambda_1\lambda_2 \\ \lambda\mu}} \left(\frac{2\lambda+1}{4\pi}\right) v_{\lambda_1\lambda_2\lambda\mu}(R)\,(-1)^{j_1'+j_2'-j_{12}-k'-J} \\
&\times [(2j_1+1)(2j_2+1)(2j_{12}+1)(2l+1) \\
&\times (2j_1'+1)(2j_2'+1)(2j_{12}'+1)(2l'+1)(2\lambda_2+1)]^{1/2} \\
&\times \begin{pmatrix} l' & \lambda & l \\ 0 & 0 & 0 \end{pmatrix} \begin{pmatrix} j_2' & \lambda_2 & j_2 \\ 0 & 0 & 0 \end{pmatrix} \begin{pmatrix} j_1' & \lambda_1 & j_1 \\ -k' & \mu & k \end{pmatrix} \\
&\times \begin{Bmatrix} l' & l & \lambda \\ j_{12} & j_{12}' & J \end{Bmatrix} \begin{Bmatrix} j_{12} & j_2 & j_1 \\ j_{12}' & j_2' & j_1' \\ \lambda & \lambda_2 & \lambda_1 \end{Bmatrix}
\end{aligned}
\qquad 2.6.36
$$

where $(:::)$ are the Wigner 3-j symbols, $\{:::\}$ are the 6-j symbols, and $\{\vdots\vdots\vdots\}$ is a 9-j symbol. The sum over μ runs from $-\lambda_1$ to $+\lambda_1$.

It can easily be verified that when $k = 0$ this reduces to the linear rotor – linear rotor expression (Green, 1975) and when $j_2 = 0, j_{12} = j_1$ the expression reduces to the atom – symmetric top expression (Green, 1976).

The 3-j symbols impose the conditions that the sums, $(l'+l+\lambda)$ and $(j_2+j_2'+\lambda_2)$ must both be even for a nonvanishing coupling matrix element, and whilst the latter must be true if the linear rotor is a homonuclear diatomic molecule, the restriction is independent of any external constraints on j_2, j_2' and λ_2.

2.6.4 Symmetry Adapted Coupling Matrix Elements

Further 'selection rules' may be obtained by recalling that the symmetry adapted symmetric top wavefunction is given by equation 2.6.9. The coupling matrix elements discussed above were derived using the primitive symmetric top eigenfunctions, $|jkm\epsilon\rangle$ but, as noted by Green (1976), k plays a spectator role in the angular momentum coupling, and the symmetry adapted coupling matrix element can be formed from a linear combination of terms of the form given by equation 2.6.36.

Following Green (1976) we rewrite the potential as:

$$V(\mathbf{R}, \hat{\Omega}_1, \hat{\Omega}_2) = \sum_{\substack{\lambda_1\lambda_2 \\ \lambda}} \sum_{\mu\geq 0} \frac{v_{\lambda_1\lambda_2\lambda\mu}(R)}{1+\delta_{\mu 0}} \left[\Upsilon_{\lambda_1\lambda_2\lambda\mu} + (-1)^{\lambda_1+\lambda_2+\lambda+\mu}\Upsilon_{\lambda_1\lambda_2\lambda-\mu}\right] \quad 2.6.37$$

where $\Upsilon_{\lambda_1,\lambda_2,\lambda,\mu}$ is given by equation 2.6.31b. With the 'true' symmetry adjusted symmetric top wavefunction:

$$|jkm\epsilon\rangle = \frac{1}{(2\,(1+\delta_{k0}))^{1/2}}\,(|jkm\rangle + \epsilon|j-km\rangle), \quad 2.6.38$$

the coupling matrix elements can be rewritten as:

$$V_{\gamma'}^{J\gamma} = \sum_{\substack{\lambda_1\lambda_1 \\ \lambda}} \sum_{\mu\geq 0} \frac{v_{\lambda_1\lambda_2\lambda\mu}(R)}{2(1+\delta_{\mu 0})[(1+\delta_{k0})(1+\delta_{k'0})]^{1/2}} (\langle j'k'm'| + \epsilon'\langle j'-k'm'|)$$
$$\times\,(\Upsilon_{\lambda_1\lambda_2\lambda\mu} + (-1)^{\lambda_1+\lambda_2+\lambda+\mu}\Upsilon_{\lambda_1\lambda_2\lambda-\mu})(|jkm\rangle + \epsilon|j-km\rangle) \quad 2.6.39$$

The terms in equation 2.6.39 can be simplified by applying the symmetry properties of the coupling matrix elements (eq. 2.6.36) and of the potential itself (eq. 2.6.31).

Using the short-hand notation, $|k\rangle \Rightarrow |j_1 k j_2 j_{12} l \epsilon; JM\rangle$ and $\Upsilon_\mu \Rightarrow \Upsilon_{\lambda_1,\lambda_2,\lambda,\mu}$ we have:

$$\langle -k'|\Upsilon_\mu|-k\rangle = (-1)^{j_1+{j_1}'-2k'+\lambda_1}\langle k'|\Upsilon_{-\mu}|k\rangle \qquad 2.6.40$$

thus:

$$\begin{aligned}&\langle -k'|\Upsilon_\mu + (-1)^{\lambda_1+\lambda_2+\lambda+\mu}\Upsilon_{-\mu}|-k\rangle \\ &\quad = (-1)^{j_1+{j_1}'-2k'+\lambda_2+\lambda+\mu}\langle k'|\Upsilon_\mu + (-1)^{\lambda_1+\lambda_2+\lambda+\mu}\Upsilon_{-\mu}|k\rangle\end{aligned} \qquad 2.6.41$$

For any value of k and k', the properties of the 3-j symbols imply that there is only a non-zero contribution to the coupling matrix element if:

$$k' - k = \mu \qquad 2.6.42$$

thus for any given k, k', only one of the $\langle k|\Upsilon_{\pm\mu}|k'\rangle$ terms is non-zero, and it enters with a phase of $(-1)^{\lambda_1+\lambda_2+\lambda+\mu}$ if $(k'-k) = -\mu$, or $(+1)$ if $(k'-k) = \mu$.

Similarly, we can write:

$$\begin{aligned}&\langle -k'|\Upsilon_\mu + (-1)^{\lambda_1+\lambda_2+\lambda+\mu}\Upsilon_{-\mu}|k\rangle \\ &\quad = (-1)^{j_1'+j_1-2k'+\lambda_2+\lambda+\mu}\langle k'|\Upsilon_\mu + (-1)^{\lambda_1+\lambda_2+\lambda+\mu}\Upsilon_{-\mu}|-k\rangle\end{aligned} \qquad 2.6.43$$

Here,as k, k' and μ are all greater than zero, only the $\langle k|\Upsilon_{+\mu}|-k\rangle$ term can contribute to the coupling matrix element.

Substituting 2.6.42 and 2.6.43 into equation 2.6.39, the symmetry adapted coupling matrix elements become:

$$\begin{aligned}\langle j_1' k' j_2' j_{12}' l' \epsilon'; JM|V|j_1 k j_2 j_{12} l; JM\rangle &= \sum_{\substack{\lambda_1\lambda_2 \\ \lambda}}\sum_{\mu\geq 0}\frac{v_{\lambda_1\lambda_2\lambda\mu}(R)}{2[(1+\delta_{k0})(1+\delta_{k'0})]^{1/2}} \\ &\times (1+\epsilon\epsilon'(-1)^{j_1+j_1'-2k'+\lambda+\lambda_2+\mu})\,(\langle j_1' k' j_2' j_{12}' l'; JM|\Upsilon_{\pm\mu}|j_1 k j_2 j_{12} l; JM\rangle \times \omega \\ &+ \epsilon\langle j_1' k' j_2' j_{12}' l'; JM|\Upsilon_{+\mu}|j_1 k j_2 j_{12} l; JM\rangle)\end{aligned} \qquad 2.6.44$$

where:

$$\omega = (-1)^{\lambda_1+\lambda_2+\lambda+\mu} \text{ if } (k'-k) < 0$$
$$\omega = (+1) \qquad\qquad \text{if } (k'-k) \geq 0 \qquad 2.6.45$$

2.6.5 Separation into two non-interacting parity blocks

From the symmetry properties of equation 2.6.44 it can be seen that the coupling matrix element vanishes unless:

$$\epsilon\epsilon'(-1)^{j_1+j_1'+\lambda+\lambda_2+\mu} = (+1)$$
$$(-1)^{\lambda_2+j_2+j_2'} = (+1) \qquad 2.6.46$$
$$(-1)^{\lambda+l+l'} = (+1).$$

Eliminating λ and λ_2 from the above equations gives the condition for a non-vanishing coupling matrix element as:

$$\epsilon\epsilon'(-1)^{j_1+j_1'-j_2-j_2'-l-l'+\mu} = (+1) \qquad 2.6.47$$

This can be simplified using the properties of the collision partners involved. If all the angular momenta are integer, then using the property $\mu = (k'-k)$, the condition for a non-vanishing coupling matrix element becomes:

$$\epsilon(-1)^{j_1+k-j_2-l} = \epsilon'(-1)^{j_1'+k'-j_2'-l'} \qquad 2.6.48$$

The problem therefore partitions out into two non-interacting parity blocks that can be solved separately, reducing the computational effort required for the calculation.

2.6.6 Body-fixed coupling matrix elements

Although the CC equations will be solved in the space fixed frame, it is instructive to investigate the coupling matrix element in the body fixed frame, where the form of the angular momentum coupling is more transparent. As this is the natural

frame in which to describe the interaction potential, the form of the potential matrix element is simpler.

The potential in the body fixed frame (eq. 2.6.14) is given by:

$$V(R,\hat{\Omega}_1',\hat{R}_2') = \sum_{\substack{\lambda_1\lambda_2\\ \mu\nu}} v_{\lambda_1\mu\lambda_2\nu}(R) D^{\lambda_1}_{\mu\nu}(\hat{\Omega}_1') Y^{\lambda_2}_{-\nu}(\hat{R}_2') \qquad 2.6.49$$

The total wavefunction can be expanded in the form:

$$\Upsilon^{J\Omega}_{\beta}(\hat{\Omega}_1',\hat{R}_2') = \left(\frac{2j_1+1}{8\pi}\right)^{1/2} \sum_{\Omega_1\Omega_2} C^{j_1\ j_2\ j_{12}}_{\Omega_1\Omega_2\Omega}(D^{j_1}_{k\Omega_1}(\hat{\Omega}_1') + \epsilon\, D^{j_1}_{-k\Omega_1}(\hat{\Omega}_1'))Y^{j_2}_{\Omega_2}(\hat{R}'). \qquad 2.6.50$$

Using the primitive symmetric top functions, $|j_1 k\Omega_1\rangle$, the integral to be evaluated becomes:

$$\int\int \sum_{\substack{\Omega_1\Omega_2\\ \Omega_1'\Omega_2'}} \sum_{\substack{\lambda_1\lambda_2\\ \mu\nu}} \frac{((2j_1+1)(2j_1'+1))^{1/2}}{8\pi} C^{j_1\ j_2\ j_{12}}_{\Omega_1\Omega_2\Omega} C^{j_1'\ j_2'\ j_{12}'}_{\Omega_1'\Omega_2'\Omega'} D^{j_1'*}_{k'\Omega_1'}(\hat{\Omega}_1') Y^{j_2'*}_{\Omega_2'}(\hat{R}')$$
$$D^{\lambda_1}_{\mu\nu}(\hat{\Omega}_1') Y^{\lambda_2}_{-\nu}(\hat{R}') D^{j_1}_{k\Omega_1}(\hat{\Omega}_1') Y^{j_2}_{\Omega_2}(\hat{R}')\, d\hat{\Omega}_1'\, d\hat{R}_2' \qquad 2.6.51$$

Integrating over $d\hat{\Omega}_1', d\hat{R}_2'$ and using equation 2.6.34 to convert the Clebsch Gordan equations into 3-j symbols gives the result:

$$\begin{aligned} V^{J\gamma}_{\gamma'} = & \sum_{\substack{\lambda_1\lambda_2\\ \mu\nu\\ \Omega_1\Omega_2\Omega_1'\Omega_2'}} v_{\lambda_1\mu\lambda_2\nu}\,(4\pi)^{-1/2}(-1)^{j_1-j_2+j_1'-j_2'-k'-\Omega'} \\ & \times [(2j_1+1)(2j_2+1)(2j_{12}+1)(2j_1'+1)(2j_2'+1)(2j_{12}'+1)(2\lambda_2+1)]^{1/2} \\ & \times \begin{pmatrix} j_1' & \lambda_1 & j_1 \\ -k' & \mu & k \end{pmatrix} \begin{pmatrix} j_1' & \lambda_1 & j_1 \\ -\Omega_1' & \nu & \Omega_1 \end{pmatrix} \begin{pmatrix} j_2' & \lambda_2 & j_2 \\ 0 & 0 & 0 \end{pmatrix} \\ & \times \begin{pmatrix} j_2' & \lambda_2 & j_2 \\ -\Omega_2' & -\nu & \Omega_2 \end{pmatrix} \begin{pmatrix} j_1 & j_2 & j_{12} \\ \Omega_1 & \Omega_2 & -\Omega \end{pmatrix} \begin{pmatrix} j_1' & j_2' & j_{12}' \\ \Omega_1' & \Omega_2' & -\Omega' \end{pmatrix} \end{aligned} \qquad 2.6.52$$

From here it can be seen that the $|\nu| > 0$ terms in the potential drive the change in the projection of the angular momenta j_1 and j_2 on the intermolecular axis. The value of $\Omega\,(=\Omega_1+\Omega_2)$ is unchanged by the body fixed interaction potential, but will be coupled to $\Omega' = \Omega \pm 1$ by the off diagonal centrifugal terms.

2.6.7 Extension to linear rotor – asymmetric top collisions

Garrison et al (1976, 1977) have shown how the atom – symmetric top treatment can be extended to give the atom – asymmetric top coupling matrix elements, with regard to rotational excitation of H_2CO by He. The ease of the extension is a consequence of the fact that the asymmetric top rotational functions can be expressed as a linear combination of symmetric top functions.

The rotational Hamiltonian for an asymmetric top is

$$H_{rot} = A\mathbf{j}^2 + (B - A)\mathbf{j}_{y''}^2 + (C - A)\mathbf{j}_{z''}^2 \qquad 2.6.53$$

where none of the moments of inertia in the principal axes frame are equal.

The asymmetric top differs from the symmetric top in that the projection of the total angular momentum on the molecule fixed z''- axis is no longer a constant of the motion. However, it is convenient to expand the asymmetric top wavefunctions in a basis of symmetric top wavefunctions which form a complete set in the space of the rotation of a rigid body:

$$|j\tau m\rangle = \sum_{k=-j}^{j} a_{jk\tau}|jkm\rangle^{(ST)}. \qquad 2.6.54$$

The fact that k is no longer a good quantum number leads to a mixing of the $(2j + 1)$ asymmetric top states labelled by τ. Consideration of the symmetries of the system (Garrison et al, 1976) lead to 'symmetry adapted wave functions' in the same form as those found in the case of the symmetric top molecule. Thus we may rewrite the asymmetric top wavefunction as:

$$|j\tau m\rangle = \sum_{k\geq 0} \frac{b_{jk\tau}}{(2(1+\delta_{k0}))^{1/2}}[|jkm\rangle^{(ST)} + \epsilon\,|j-km\rangle^{(ST)}] \qquad 2.6.55$$

The $b_{jk\tau}$ coefficients may be obtained by diagonalising the Hamiltonian in this basis.

We have already noted that k plays a spectator role in the angular momentum coupling, and as a result of this, the asymmetric top coupling matrix elements

may be obtained from the linear rotor – symmetric top coupling matrix elements simply by taking the appropriate linear combinations of the latter:

$$\langle j_1'\tau' j_2' j_{12}' l'\epsilon'; JM|V|j_1\tau j_2 j_{12} l\epsilon; JM\rangle$$
$$= \sum_{k=-j}^{j} b_{jk\tau}^{2} \langle j_1' k' j_2' j_{12}' l'\epsilon'; JM|V|j_1 k j_2 j_{12} l\epsilon; JM\rangle \qquad 2.6.56$$

Chapter III

Rotational Excitation of NH_3 in collisions with ortho and para-H_2

3.1 Introduction

The ammonia (NH_3) molecule was the first polyatomic molecule to be observed in the interstellar medium (Cheung 1968), and since then has been extensively observed in the microwave, radio and infrared regions (Ho and Townes, 1983). Its wide range of transitions have made it a valuable tool for deriving information on the physical conditions that prevail within the interstellar clouds. In particular, rotational–inversion transitions of para-NH_3 have been used to obtain estimates of the temperature in the clouds (Walmsley and Ungerechts 1983, Danby et al 1988), information on the density can also be deduced. In addition there have been observations of maser emission in both non-metastable, and metastable states (Mauersberger et al 1987, 1988, Guilloteau et al 1983, Johnston et al 1989). The latter will be discussed further in the next chapter.

Molecular hydrogen is thought to be the major collision partner in regions of interest, and reliable information on the collisional rates are required to interpret the observations.

Experimental work on this system is generally performed at room temperatures, and extrapolation to the low energies is very unreliable, especially as the low energy collisions sample different regions of the interaction potential than do high energy collisions. In addition, most experimental measurements give some average or ratio of the collision rates, and interpretation can be difficult. The experimental measurements do, however, provide some useful insights into the propensity rules governing the rotational transitions, and provide an important measure of the accuracy of the theoretical calculations.

In order to gain a deeper understanding of the propensity rules, and to attempt to calculate reliable rates for the astrophysicists, there have been a number

of theoretical studies of the rotational excitation of NH_3 in collisions with both H_2 and He. To date, the quantal calculations have only treated collisions with He or para-H_2 constrained to its rotational ground state, both of which act as spherically symmetric collision partners. Although there have been some limited semi–classical calculations considering rotational excitation of NH_3 by ortho-H_2, the effect of replacing ground state para-H_2 by rotationally excited H_2 has not been fully investigated.

Information on NH_3 ortho-H_2 collisions is also relevant to the astrophysical studies where, although it seems fair to assume most para-H_2 is in the ($j = 0$) rotational ground state at molecular cloud temperatures of 10 to 30K, the ortho:para H_2 ratio is not known, and could be anything up to 3:1 (Flower and Watt 1984).

3.2 Introducing the NH_3 Molecule

The NH_3 molecule (figure 3.1) is a typical example of a symmetric top molecule, with a three-fold axis of symmetry under rotation about the molecule fixed z''-axis. Its rotational wavefunction can be characterized by $|jkm\rangle$ (section 2.6.1), and, ignoring small corrections, the rotational energy levels are given by:

$$E_{rot} = Bj(j+1) + (C - B)\,k^2. \qquad 3.2.1$$

The energy is therefore dependent on j and $|k|$ (through k^2), giving jk levels which are degenerate, at least in so far as the rigid rotor approximation holds.

Ammonia separates into two distinct species, depending on the direction of the spins of the H nuclei. Ortho-NH_3 has all spins parallel whilst para-NH_3 has two spins parallel and one anti-parallel. It can be shown by consideration of the symmetry under interchange of two hydrogen nuclei (Townes and Schawlow, 1955) that ortho-NH_3 has allowed rotational states with $k = 3n$ (n = 0,1,2,3...) whilst para-NH_3 has allowed rotational states with $k \neq 3n$. In the absence of a magnetic field, collisional and radiative transitions cannot change the direction of the hydrogen spins, so transitions between ortho- and para-NH_3 are forbidden.

If the NH_3 has no vibration perpendicular to the z''-axis, the dipole moment of the molecule lies entirely along this axis, thus radiative transitions obey the

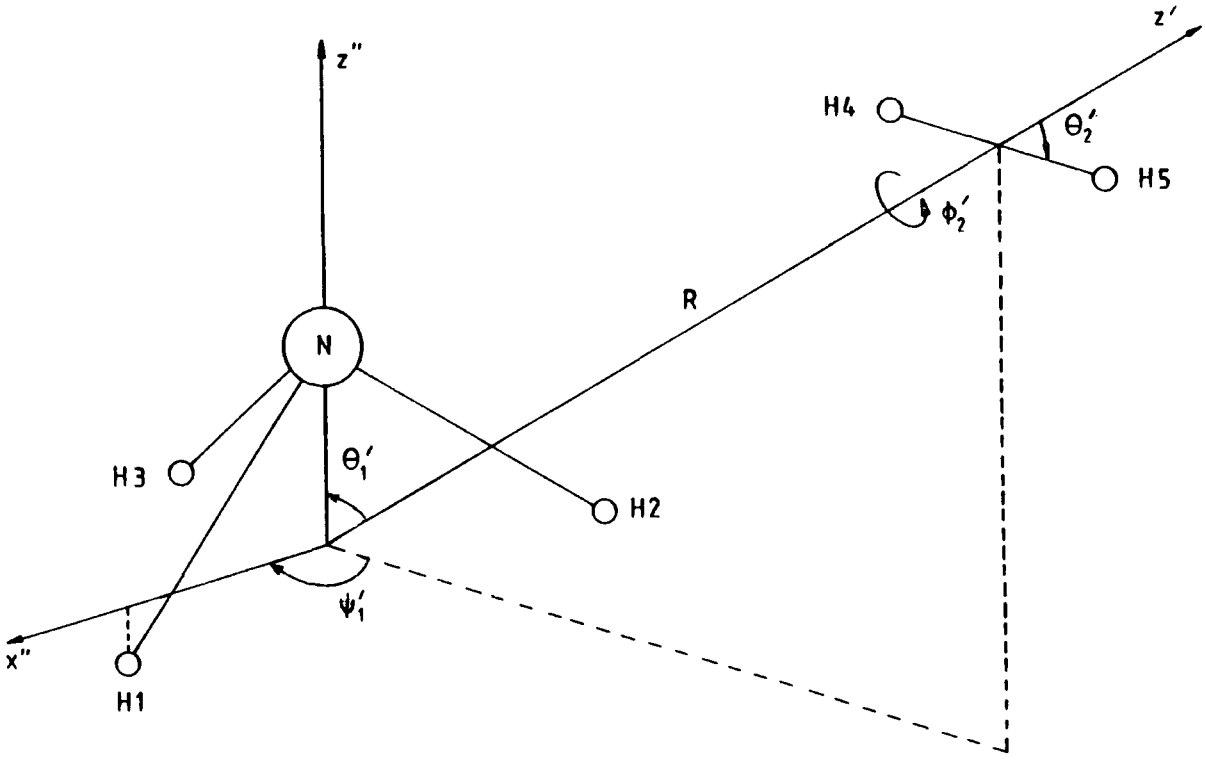

Figure 3.1: The NH_3 – H_2 Collision Co-ordinates

selection rules $\Delta k = 0$ and $\Delta j = \pm 1$. The energy levels form k-ladders (same k, different j). The lowest level in each ladder ($j = k$) is a metastable state, whilst the other states ($j > k$) decay rapidly via the $\Delta j = \pm 1$ radiative transitions.

For collisions the presence of the three-fold axis of symmetry about the z''-axis leads to the collisional selection rule $\Delta k = 3n$ where n is an integer. This is a consequence of the constraints on the potential discussed in section 2.6.2 ($\mu = 3n$). Collisions can therefore lead to transitions within a k-ladder and between k-ladders. It is collisions that are largely responsible for the latter although a slight coupling between the rotation and vibration can lead to slow radiative $\Delta k = 3$ transitions even in the vibrational ground state (Oka et al, 1971).

Implicit in this discussion is the assumption that NH_3 is a 'rigid rotor' with no vibrational motion. In fact, the nitrogen nucleus can tunnel quantum-mechanically

through the plane of the hydrogen nuclei in a large amplitude inversion motion. This inversion motion splits the normally degenerate k doublets by $\sim 1\text{cm}^{-1}$. The rotational wavefunction can be written as:

$$|jkm\epsilon\rangle = \frac{1}{(2(1+\delta_{k0}))^{1/2}}(|jkm\rangle + \epsilon|j-km\rangle) \qquad 3.2.2$$

and the k doublets are split into a symmetric (lower) and antisymmetric (upper) state such that (Green 1980);

$$\epsilon = \pm(-1)^j \qquad 3.2.3$$

where the upper sign applies to the upper (a) state and the lower sign applies to the lower (s) state.

For para-NH_3 the potential matrix element is invariant to simultaneous changes of the symmetry of the levels ($a \leftrightarrow s$), but this is not true for ortho-NH_3 where only one of the inversion doublets exists for $k = 0$.

The effect of neglecting the inversion motion of NH_3 in the theoretical calculations has been discussed by Green (1976) and by Davis and Boggs (1978). Green argued that the period of the inversion motion ($\sim$50ns) is very much larger than the typical collision time at thermal energies ($\sim$1ns). Davis and Boggs gave the conditions under which the rigid-rotor approximation may be expected to be valid. If it is assumed that the inversion barrier is sufficiently high that the upper and lower inversion state wavefunctions may be represented as symmetric and antisymmetric combination of some normalised function, f, then the wavefunction can be written as:

$$|\pm\rangle = 2^{-1/2}\,(f(h_e - h) \pm f(h_e + h)) \qquad 3.2.4$$

where h is the distance of the N nucleus from the plane of the H nuclei, and h_e is the equilibrium distance.

Davis and Boggs showed that if f is sharply peaked , and the potential expansion coefficients (section 2.6.2) are slowly varying functions of h, then the rigid rotor approximation can be justified. Effectively, the rigid rotor approximation assumes f can be modelled as a linear combination of delta-functions centred at the equilibrium positions of the nitrogen.

3.3 The Story So Far

Because of the astrophysical importance of the NH_3 molecule, there have been many experimental and theoretical studies of the rotational excitation of NH_3 in collisions with H_2 and He. The experimental studies of NH_3 - H_2 collisions include pressure broadening (Broquier et al, 1985, 1987, 1988), microwave double resonance experiments (Daly and Oka, 1970, Fabris and Oka, 1972, Oka, 1973), double resonance microwave beam maser studies (Klaasen et al, 1982, 1983) and molecular crossed beam measurements (Seelemann et al, 1988, Ebel et al, 1990).

Ideally, to provide a stringent test of theory, direct measurements of state-to-state collision cross-sections are needed. Many experimental measurements give information only on the sums of state-to-state cross-sections for many transitions, and the averaging can destroy much of the detailed information needed to fully test the theoretical results.

The earliest experiments to approach this ideal were the microwave double resonance experiments of Oka et al (1970, 1972, 1973). In these experiments a mixture of NH_3 and its collision partner were pumped by strong microwave radiation at a pumping frequency, f_p. The frequency was chosen so as to produce virtual saturation of one of the NH_3 inversion doublets ($j'k'$). The non-Boltzmann distribution was transferred to other levels by collisions and a second level, the signal level (j,k), was monitored by weak microwave radiation at the signal frequency, f_s. Oka has shown that to first order, the change in intensity of absorption at the signal frequency is related to the collisional rates by:

$$\frac{\Delta I}{I} = -\frac{f_p}{f_s}\left(\frac{\alpha(jks \rightarrow j'k'a) - \alpha(jks \rightarrow j'k's)}{\alpha_{tot}}\right) \qquad 3.3.1$$

where $\alpha(jks \rightarrow j'k's(a))$ are the rate constants for the symmetry preserving (changing) transitions, and α_{tot} is the total rate for transitions out of both the signal doublet lines plus the interdoublet rate (counted twice).

Thus the microwave double resonance technique provides a measure of the difference between parity changing and parity preserving transitions. The non zero values of $\frac{\Delta I}{I}$ found in the experiments yields information on the 'propensity rules' governing the transitions.

Collisions of NH_3 with a number of collision partners were studied, including collisions with He, para-H_2 and normal H_2 and the experiments were performed at 300K. The results may be split into two cases.

Firstly, $\Delta k = 0$ transitions. For all collisions with H_2, as for collisions with all polar and non-polar molecules, the dipole allowed transitions dominated when $\Delta j = 1$ (i.e. $\frac{\Delta I}{I}$ was positive, parity changing transitions were preferred). For all $\Delta j = 2$, quadrupole allowed transitions dominated, and $\frac{\Delta I}{I}$ was negative. However, for collisions with rare gas atoms (He, Xe, Ar...), no clear propensity rule was found. This was explained by the fact that rare gas atoms have zero electric multipole moment, and only short-range forces were contributing, whereas for molecules, the long-range dipole quadrupole interactions were drowning out all other information.

The relevance of this discussion to the current work becomes obvious, when it is recalled that ground state para-H_2 ($j = 0$) is expected to act like He in collisions (Green, 1980), as its average electric multipole moment vanishes. Thus the behaviour of cross-sections for collisions of NH_3 with ground state para-H_2 might be expected to be very different from that for collisions with rotationally excited Hydrogen.

For $\Delta k = 3$ transitions (Fabris and Oka, 1972), a close parallelism was found for collisions with H_2 and collisions with He. This was explained by proposing that $\Delta k = 3$ transitions were driven by short range forces which were similar in both cases.

The microwave double resonance results of Oka et al have been widely used to probe the accuracy of the theoretical potential used in quantal and semi-classical calculations for both NH_3–He collisions (Davis and Boggs, 1978, Green, 1979, 1980, Billing, Poulsen and Diercksen, 1985) and NH_3–H_2 collisions (Billing and Diercksen, 1986, Danby et al, 1987, Danby and Valiron, 1989).

For the NH_3–He collisions it was found that, whilst all potentials gave reasonable agreement with the experimental data for $\Delta k = 0$ transitions, only the most sophisticated of the potentials (Billing, Poulsen and Diercksen, 1985) could predict the correct $\frac{\Delta I}{I}$ for $\Delta k = 0$ transitions.

The most rigorous experimental test of the theory is provided by the recent crossed molecular beam measurements of Seelemann et al (1988) and Ebel at al (1990), which were the first to give direct information on state-to-state cross-sections for $\Delta j > 1, \Delta k > 1$ transitions. The molecular beams were rotationally cooled giving an initial NH_3 beam consisting almost entirely of ground state ortho-NH_3 ($jk\epsilon = 00+$) or ground state para-NH_3 ($jk\epsilon = 11\pm$). They studied collisions with normal H_2 (3:1 ortho:para-H_2 ratio) and helium, and were able to detect the excited states with complete state sensitivity. The results obtained were interpreted as *relative* state-to-state integral cross-sections. No absolute measurement could be made, but detailed information on collisional propensities could be extracted.

There have been a number of theoretical studies of NH_3–H_2 collisions using both quantal methods (Danby et al, 1986, 1987) and semi-classical approaches (Billing and Diercksen, 1985, 1986, 1987, 1988). Much of the theoretical work has treated collisions of NH_3 with para-H_2 constrained to its rotational ground-state ($j_2 = 0$). In this limit the problem reduces to the collision of a symmetric top molecule with a spherically symmetric perturber. This is formally the same as collisions between NH_3 and helium which have been widely studied, and the theory for treating such a system has been presented by Green (1976).

Quantal calculation of NH_3-H_2 collisions have been presented by Danby et al (1986, 1987) who treated collisions of NH_3 with ($j_2 = 0$) para-H_2 only. They employed a potential consisting of an SCF part complemented by a dispersion contribution calculated from second order perturbation theory. Using full CC calculations they treated collisions with both ortho (1986) and para-NH_3 (1987). They compared their para-NH_3 rates with the results of Oka et al, and found reasonable agreement for $\Delta k = 0, \Delta j = 0$ transitions where theory correctly predicted that dipole allowed ($s \rightarrow a$) transitions are preferred. The $\Delta k = 3$ theoretical results were found to agree well with the NH_3-He double resonance data, as would be expected if ground state para-H_2 behaves in a similar way to He as a collision partner.

Billing and Diercksen (1985, 1986, 1988) have performed semi-classical calculations with both para-H_2 ($j_2 = 0, (2)$) and ortho-H_2 ($j_2 = 1$). They used a

potential consisting again of an SCF contribution but with the dispersion terms coming from a many body perturbation theory (MBPT) treatment, and solved the coupled equations using the semi-classical classical path method where the rotation of the target molecule is treated quantally, whilst the relative motion of the molecules is treated classically. At higher energies, where this became impractical, they used a form of the semi-classical coupled-states approximation, formulated by neglecting changes in the projection of j_2 on the intermolecular axis. These calculations were more complete than the quantal calculations in that they took some account of the rotational structure of the H_2 molecule and Billing and Diercksen were able to demonstrate the importance of including some ($j_2 = 2$) terms in the para-H_2 basis set. However, they employed a number of approximations in addition to that of using semi-classical physics. In particular, they expanded the interaction potential in the form (Billing and Diercksen, 1986):

$$V(R, \hat{R}_1, \hat{R}_2) = \sum_{\substack{\lambda_1 \lambda_2 \\ \eta_1 \eta_2}} v_{\lambda_1 \eta_1 \lambda_2 \eta_2}(R) Y_{\eta_1}^{\lambda_1}(\hat{R}_1) Y_{\eta_2}^{\lambda_2}(\hat{R}_2) \qquad 3.3.2$$

where $\hat{R}_{1(2)}$ are the polar angles of NH_3 (H_2) with respect to the body fixed frame. They interpreted the role of η_1 as coupling k and k', whilst η_2 couples Ω_2 and Ω_1', the projection of the H_2 angular momentum on the intermolecular axis. Comparison of the above potential expansion with the body fixed potential expansion derived in chapter two (eq 2.6.15) shows that the two only correspond when $\eta_2 = \nu = 0$. The significance of this difference will be discussed further in section 3.5.

Very recently, Ebel et al (1990) have presented results using a quantal coupled states approximation derived from the potential expansion of Billing and Diercksen (1985), for the rotational excitation of para-H_2 ($j = 0$) and ($j = 2$) and ortho-H_2 ($j = 1$).

Throughout all these calculations a consistent feature found for NH_3 collisions was the propensity rules :

$$\sigma(11\pm \rightarrow 22\mp) >> \sigma(11\pm \rightarrow 22\pm) \qquad 3.3.3a$$

for para-NH_3 and:

$$\sigma(00+ \rightarrow j3-) >> \sigma(00+ \rightarrow j3+) \qquad 3.3.3b$$

for ortho-NH_3, where $\sigma(jk\epsilon \rightarrow j'k'\epsilon')$ is the cross-section for transitions from the NH_3 rotational states labelled by j, k and ϵ to the state labelled by j', k' and ϵ'. However, this is at variance with the results of the experimental crossed beam measurements of Seelemann et al and Ebel et al. In the experiments, although there is a slight propensity in favour of $(00+ \rightarrow 33-)$ transition for ortho- NH_3, the cross-sections for $(00+ \rightarrow 33+)$ and $(00+ \rightarrow 33-)$ are of similar magnitude. For para-NH_3 such a comparison is not possible, because both the $11+$ and $11-$ rotational levels are present in the initial beam.

Although some account has been taken of the rotational structure of the H_2 molecule in more recent calculations it has not previously been treated fully. The question arises, would a proper treatment of the rotational structure of H_2 solve the discrepancy between theory and experiment?

3.4 Numerical Calculations

3.4.1 The Interaction Potential

An important element of any scattering calculation is the form of the potential used. The present calculations employed two separate *ab initio* potentials. Both potential surfaces contained the same SCF contribution, but differed in the dispersion terms. Long range terms were calculated from the analytic formulae discussed in section 1.3.

As discussed in chapter one, the SCF analysis treats the molecules as two overlapping charge distributions and is therefore applicable at short range. It includes the short range overlap, electrostatic and induction terms, but not the dispersion which is due to correlation effects and must be added in separately.

The potential is then fitted to the body fixed potential expansion discussed in chapter two:

$$V(R,\hat{\Omega}_1',\hat{R}_2') = \sum_{\substack{\lambda_1\lambda_2\\ \mu\nu}} v_{\lambda_1\mu\lambda_2\nu}(R) D^{\lambda_1}_{\mu\nu}(\hat{\Omega}_1') Y^{\lambda_2}_{-\nu}(\hat{R}_2') \qquad 3.4.1$$

In the present calculation the SCF part of the potential has been taken from the *ab initio* large basis set SCF calculation of Diercksen (Billing and Diercksen, 1985, 1986). The *ab initio* data has been given for angles of $\theta_1' = 0(22.5)180$, $\psi_1' = 0(20)60$ and $\theta_2', \phi_2' = (0,0),(90,0),(90,90)$.

The first few spherical harmonics that enter the body-fixed potential expansion (eq 3.4.1) are:

$$\begin{aligned} Y_0^0(\theta,\phi) &= \left(\frac{1}{4\pi}\right)^{1/2} \\ Y_0^2(\theta,\phi) &= \left(\frac{5}{16\pi}\right)^{1/2} 3\cos^2\theta \\ Y_{\pm1}^2(\theta,\phi) &= \mp\left(\frac{15}{8\pi}\right)^{1/2} \sin\theta\cos\theta\exp(\pm i\phi) \\ Y_{\pm2}^2(\theta,\phi) &= \left(\frac{15}{32\pi}\right)^{1/2} \sin^2\theta\exp(\pm 2i\phi) \end{aligned} \qquad 3.4.2$$

thus with $\theta_2', \phi_2' = (0,0),(90,0)$ and $(90,90)$, there is only sufficient angular data to obtain terms with $\nu = 0, \pm 2$. Previous calculations have only considered collisions with ground state para-H_2 ($j_2 = j_2' = \lambda_2 = \nu_2 = 0$), and have averaged the potential over the three hydrogen orientations (eg Danby et al, 1986), so the fact that the $\nu = \pm 1$ terms cannot be obtained was unimportant. However, the physical significance of the $\nu = \pm 1$ terms to the linear rotor - symmetric top case can be seen by reference to figure 3.2.

In the absence of the $Y_1^2(\theta_2', \phi_2')$ term in the expansion:

$$V(\theta_2') = V(\pi - \theta_2') \qquad 3.4.3$$

(which is not true for the general case of a symmetric top - linear rotor in an arbitrary orientation) it is clear that in order to give a reasonable representation of the behaviour of the potential with θ_2, additional terms are needed.

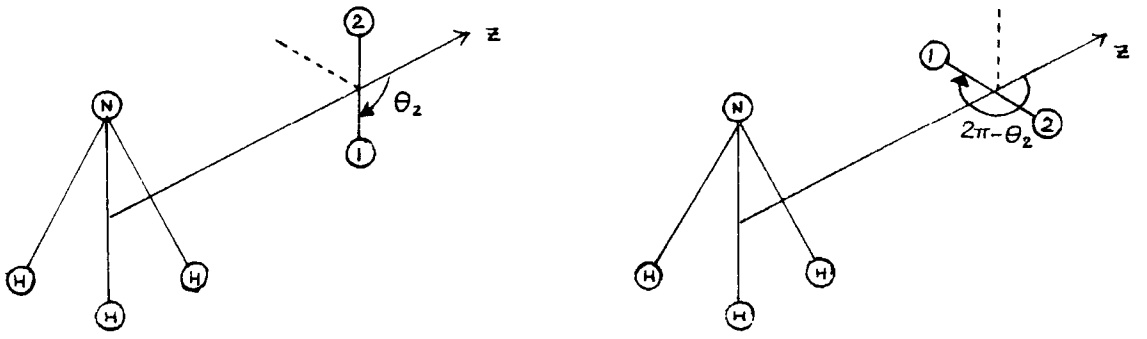

Figure 3.2: Significance of the $\nu = \pm 1$ terms

The additional terms have been taken from computations with $\cos\theta_2' = \pm 3^{-\frac{1}{2}}$, and $\phi_2' = \pm\pi/4$ (Valiron, 1988), enabling $\nu = \pm 1$ terms to be evaluated. A smaller basis set was used in these calculations and they are not strictly compatible with the large basis set SCF data, so when the potential was fitted to obtain the expansion coefficients, the two sets of data were treated separately so as not to degrade the accuracy of the large basis set calculations.

Most of the calculations have been performed with a dispersion contribution taken from the second order perturbation theory calculations discussed by Danby et al (1986). The data has been supplemented by additional terms enabling the $\nu = \pm 1$ terms to be evaluated (Valiron 1988). The additional data points are fully compatible with the earlier data points. Following the notation adopted by Danby and Valiron (1989) this potential will be refered to as the SCF+EK potential.

To complement these calculations, additional calculations were performed using the fourth order many body perturbation theory (MBPT) dispersion potential of Billing and Diercksen (1985). The difference between the two potentials has been discussed in detail by Danby and Valiron (1989). In principle the SCF+MBPT potential is more accurate than the SCF+EK potential used for most of the current work, however, there is insufficient angular information to obtain the $\nu = \pm 1$ terms from the MBPT data. The MBPT potential coefficients were therefore supplemented by the relevant terms taken from the second order perturbation theory (EK) dispersion data.

In fitting the potential, the SCF part is forced to fall off exponentially, and the information about the long range electrostatic and induction terms tends to

3.1: Leading long range terms when $\mu = 0$

λ_1	μ	λ_2	ν	electrostatic	induction
0	0	0	0		$-(4\pi)^{1/2}\alpha_2\mu_1^2R^{-6}$
0	0	2	0		$-(4\pi/45)^{1/2}\Delta\alpha_2\mu_1^2R^{-6}$
1	0	0	0		$\sim R^{-7}$
1	0	2	0	$-(36\pi/5)^{1/2}\Theta_2\mu_1R^{-4}$	
1	0	2	1	$-(12\pi/5)^{1/2}\Theta_2\mu_1R^{-4}$	
2	0	0	0		$-(4\pi)^{1/2}\alpha_2\mu_1^2R^{-6}$
2	0	2	0	$+(24\pi)^{1/2}\Theta_2\Theta_1R^{-5}$	$-(4\pi/5)^{1/2}\Delta\alpha_2\mu_1^2R^{-6}$
2	0	2	1	$+(64\pi/5)^{1/2}\Theta_2\Theta_1R^{-5}$	$-(16\pi/45)^{1/2}\Delta\alpha_2\mu_1^2R^{-6}$
2	0	2	2	$+(4\pi/5)^{1/2}\Theta_2\Theta_1R^{-5}$	$-(4\pi/45)^{1/2}\Delta\alpha_2\mu_1^2R^{-6}$

Here:

μ_1: dipole moment of NH_3 = 0.589au (Diercksen and Sadlej, 1986)

Θ_1: quadrupole moment of NH_3 = −2.210au (Diercksen and Sadlej, 1986)

α_2: polarizability of H_2 = 5.18au (Kolos and Wolniewicz, 1967)

Θ_2: quadrupole moment of NH_3 = 0.478au (Karl, Poll, Wolniewicz, 1975)

$\Delta\alpha_2$: quadrupole polarisability of the H_2 molecule.

get lost in the numerical manipulation. In particular, long range terms due to the interaction of the molecular multipole moments are not included in the expansion.

At large values of the intermolecular distance, R, where the molecules can be treated as non-overlapping charge distributions, analytical expressions for the long range electrostatic and induction terms may be obtained from perturbation theory (Buckingham, 1967, Leavitt, 1980). When $\mu = 0$, the linear rotor - symmetric

top potential terms reduce (to within a factor) to that found for linear rotor – linear rotor collisions, and the form of the long range terms for the latter have been discussed by Flower et al (1979). The linear rotor – linear rotor analysis uses the body fixed potential expansion :

$$\sum_{\substack{\lambda_1\lambda_2\\ \nu\geq 0}} \frac{v_{\lambda_1\lambda_2\nu}}{2(1+\delta_{\nu 0})^{1/2}} \quad 4\pi \quad (Y_\nu^{\lambda_1}(\hat{R}_1')Y_{-\nu}^{\lambda_2}(\hat{R}_2') + Y_{-\nu}^{\lambda_1}(\hat{R}_1')Y_\nu^{\lambda_2}(\hat{R}_2')) \qquad 3.4.4$$

This is equivalent to the linear rotor – symmetric top body fixed potential expansion (3.4.1) when $\mu = 0$ if:

$$v_{\lambda_1 0\lambda_2\nu}^{LR-ST} = ((1+\delta_{\nu 0})(2\lambda_1+1)(2\pi))^{1/2} v_{\lambda_1\lambda_2\nu}^{LR-LR} \qquad 3.4.5$$

Thus the leading $\mu = 0$ terms in the linear rotor – symmetric top perturbation expansion are just the leading terms in the linear rotor – linear rotor expansion multiplied by the factor $((1+\delta_{\nu 0})(2\lambda_1+1)(2\pi))^{1/2}$. The leading long range terms are given in table 3.1.

3.4.2 Fitting of the Potential

SCF:

The *ab initio* data has been calculated at intermolecular distances of R = 4 to 9 atomic units in steps of one atomic unit, with a few selected terms at 10, 11 and 12 atomic units. To obtain the potential at intermediate R, and to extrapolate beyond R=9au, a fitting routine must be used. Following Danby et al (1986), we use the fact that the SCF contribution is expected to fall off exponentially with R, and scale the energies by a scaling function $A\exp(\alpha(R - R_0))$ where A is the potential at R_0. This reduces the rapid variation with R at small intermolecular distances and renders the data more amenable to spline fitting.

In the present work the value of α was optimized by taking an initial value from the first two data points, and varying α until a trial fit agreed, to within some given tolerance, with the value of the nth data point $V(R)$, where $R >$ 5au.

A spline was fitted to the scaled function using the NAG routine E02BAF. To allow extrapolation beyond the maximum value of R it was necessary to set $V = 0$ at some appropriately large value of R. Extrapolation beyond $R_{\max}$ will not, of course, be reliable, but the fitted SCF potential is rapidly killed off by the exponential scaling in this region.

A rough check on the reliability of the fitting function can be obtained by fitting to, say, all but two of the data points for a given angular configuration, and checking the extrapolated points against the known data points. The results of two such tests are shown in table 3.2. It can be seen that the fit is adequate at intermediate values of R but, as expected, it falls off too rapidly beyond $R_{\max}$ and all long range information is lost.

As suggested earlier, this problem can be largely overcome by including the long range induction and electrostatic terms explicitly. It was decided to include those terms falling off as R^{-n} where $n \leq 5$, plus the isotropic R^{-6} term.

The following algorithm was used to introduce these terms:

i: A quantity $f(R)$ equal to the numerical value of the induction and electrostatic long range expressions evaluated at R was subtracted from the data terms

ii: The modified data points were fitted as before

iii: The quantity subtracted in (i) was added back to all values of R.

The leading long range induction and electrostatic terms are thus included explicitly, and are no longer 'killed off' by the exponential scaling procedure. The results of tests on this fitting method are shown in table 3.2. The behaviour of the interaction potential with R appears to be satisfactory.

3.2:SCF fit with and without explicit long range terms

The potential at $(R, \theta_1', \psi_1', \theta_2', \phi_2')$ is given in units of inverse centimetres.

$\theta_1' = 22.5, \psi_1' = 20.0, \theta_2', \phi_2' = 0.0$				$\theta_1' = 112.5, \psi_1' = 40.0, \theta_2', \phi_2' = 0.0$			
R	data points	SCF fit without LR terms	SCF fit with LR terms	R	data points	SCF fit without LR terms	SCF fit with LR terms
9.0	**-51.893**	**-51.893**	**-51.893**	8.0	**29.805**	**29.805**	**29.805**
9.2		-47.407	-47.201	8.2		25.477	25.645
9.4		-43.273	-42.927	8.4		22.024	22.404
9.6		-39.417	-39.047	8.6		19.198	19.823
9.8		-35.804	-35.534	8.8		16.830	17.721
10.0	**-32.414**	**-32.414**	-32.361	9.0	**15.534**	14.807	15.974
11.0	**-20.696**	-17.554	-20.617	10.0	**9.896**	7.837	10.223
12.0	**-13.724**	- 8.392	-13.628	15.0		0.150	1.881
15.0		- 0.591	- 4.909	20.0		0.001	0.561
20.0		- 0.004	- 1.418				
Bold face entries indicate the given data points							

Dispersion Energy:

Bearing in mind that the dispersion energy can be expressed as a sum of terms falling off as R^{-n} with $n \geq 6$, the dispersion energy was fitted to the functional form :

$$V_{disp}(R, \hat{\Omega}_1', \hat{R}_2') = \sum_{n=6}^{11} \frac{C_n(\hat{\Omega}_1', \hat{R}_2')}{R^n} \qquad 3.4.6$$

(Danby et al, 1986) ~~it was performed~~ using the NAG routine F04ATF. The calculated dispersion data again covers R = 4 → 9au, with a few additional long range terms at 25, 40 and 80au which can be used to provide a check on the fit.

Fitting the function to the 4 → 9au data points introduced an error of a factor of two at 25au, and three at 80au. However, it was found that the fit could be greatly improved by setting E = 10^{-12}cm^{-1} (or zero) at R=1000au. With this modification the results agreed to around 2% at 25au, and 25% at 40au (table 3.3).

3.3:Dispersion fit for the long range values

The potential at $(R, \theta_1', \psi_1', \theta_2', \phi_2')$ is given in units of inverse centimetres.

V(R)=4,5,6,7 and 9 are given				
	$\theta_1, \psi_1, \theta_2, \phi_2 = (90, 0, 90, 0)$		$\theta_1, \psi_1, \theta_2, \phi_2 = (180, 0, 0, 0)$	
R	data	fit	data	fit
8.0	**-36.888**	-36.914	**-39.846**	-39.937
8.2		-31.326		-33.960
8.4		-26.700		-28.999
8.6		-22.855		-24.864
8.8		-19.644		-21.404
9.0	**-16.953**	**-16.953**	**-18.496**	**-18.496**
10.0		- 8.571		- 9.391
15.0	**- 6.760**	- 6.964	**- 0.753**	- 0.755
25.0	**- 0.030**	- 0.030	**- 0.032**	- 0.034
40.0	**- 0.0018**	- 0.0015	**- 0.0015**	- 0.0020
bold face entries indicate given data points				

3.4.3 Fitting to the body fixed potential coefficients.

The body fixed potential expansion (eqn 2.6.14) can be rewritten as:

$$V(R,\hat{\Omega}'_1,\hat{R}'_2) = \sum_{\lambda_1\lambda_2\nu}\sum_{\mu\geq 0} v_{\lambda_1\mu\lambda_2\nu}(R)$$

$$\times \quad (D^{\lambda_1}_{\mu\nu}(\hat{\Omega}'_1)Y^{\lambda_2}_{-\nu}(\hat{R}'_2) + (-1)^{\mu}D^{\lambda_1}_{-\mu-\nu}(\hat{\Omega}'_1)Y^{\lambda_2}_{\nu}(\hat{R}'_2)) \qquad 3.4.7$$

$$= \sum_{\lambda_1\lambda_1\nu}\sum_{\mu\geq 0} \frac{v_{\lambda_1\mu\lambda_2\nu}(R)}{(1+\delta_{\mu 0})}\left(\frac{2\lambda_2+1}{4\pi}\right)^{1/2}$$

$$\times \quad d^{\lambda_1}_{\mu\nu}(\theta'_1)d^{\lambda_2}_{0-\nu}(\theta'_2)(2\cos(\mu\psi'_1 - \nu\phi'_2))$$

Thus for each value of R there is a set of I simultaneous equations, where I is the number of angles for which data is available. The set of simultaneous equations can be solved using standard methods to yield the expansion coefficients, $v_{\lambda_1\mu\lambda_2\nu}$. In the current work the expansion coefficients were evaluated using the NAG routine F04JAF.

For the SCF potential, the data for the geometries $\theta'_2 = \pm\cos^{-1}(3^{-1/2})$, $\phi'_2 = \pm\pi/4$ was fitted separately to the $\theta'_2,\phi'_2 = (0,0)$, $(90,0)$, $(90,90)$ data (Billing and Diercksen, 1985) so as not to degrade the accuracy of the latter. Thus the $\nu = 0,\pm 2$ terms were taken from a fit to the large basis set data, and these were then supplemented by a fit to the additional geometries from which only the $\nu = \pm 1$ terms were retained.

There was no such problem with the second order perturbation theory (EK) dispersion data where the number of geometries was sufficient to give all four H_2 spherical harmonics with $\lambda_2 \leq 2$, but the MBPT fit yielded only those with $\nu = 0,\pm 2$. The $\nu = \pm 1$ terms used in the MBPT calculation were taken directly from the EK dispersion energy fit.

Having obtained the body fixed potential expansion coefficients, it remains only to convert them to the space fixed frame. This may be done using the conversion already derived (eqn 2.6.27). The space fixed $v_{\lambda_1\lambda_2\lambda\mu}(R)$ are given in appendix D. The number of angles at which data was available was sufficient to yield all $v_{\lambda_1\lambda_2\lambda\mu}(R)$ with $\lambda_1 \leq 6$, and $\lambda_2 = 0, 2$, giving 55 non-vanishing space fixed coefficients.

3.4.4 Integration of the Coupled Equations

The coupled equations for NH_3 – H_2 collisions take the form:

$$\left[\frac{d^2}{dR^2} - \frac{l'(l'+1)}{R^2} + \kappa_{\alpha'}^2\right] G_{\gamma'}^{J\gamma}(R) = 2\mu \sum_{\gamma''} \langle\gamma'|V|\gamma''\rangle G_{\gamma''}^{J\gamma}(R) \qquad 3.4.8$$

where $\gamma \equiv j_1, k, j_2, j_{12}, l$, and $\langle\gamma'|V|\gamma''\rangle$ is given by equation 2.6.36.

The coupling of j_1 and j_2 to form j_{12} increases the number of coupled equations, the size of arrays and the CPU time needed dramatically in comparison with the atom – symmetric top problem, and the calculation can become very unwieldy at all but the lowest energies.

The coupled equations were solved using the MOLSCAT computer code (Hutson and Green, 1986), once the necessary modifications had been made to treat linear rotor – symmetric top collisions. These changes are detailed in appendix B. The calculations were done partly on the Amdahl 5860 at Durham, and partly on the CRAY XMP at Rutherford. Typical CPU time per partial wave was 830 Cray CPU seconds for the low energy ortho-NH_3 – H_2 collision which used a maximum of 2176312 eight-byte words of storage with the basis set used. This was largely due to the size of the array that stores the individual terms in the coupling matrix element sum. This is of dimension $N^2 \times Mxlam$, where N is the number of channels considered, and $Mxlam$ is the number of potential expansion coefficients (55 here). The wavevector array is smaller due to the summation over $\lambda_1, \lambda_2, \lambda$ and μ.

The potential expansion coefficients were fed into Molscat using the VSTAR mechanism. The program requires the value of $v_{\lambda_1\lambda_2\lambda\mu}(R)$ at a given R. To this end a spline was fitted to the $v_{\lambda_1\lambda_2\lambda\mu}$'s from which $v_{\lambda_1\lambda_2\lambda\mu}(R)$ could be obtained for any R such that $2.1\text{Å} \leq R \leq 52.92\text{Å}$.

The changes made to Molscat were checked by running the program with $j_2 = 0$ and comparing with the para-H_2 ($j_2 = 0$) results of Danby et al (1985, 1986). The only difference between the analysis of Danby et al and that used here when $j_2 = 0$ only is the method of averaging over the H_2 orientations. In the former this was done by giving each H_2 orientation a weight of 1/3 and simply adding the weighted values, in the latter it was done by the fitting the potential to an expansion that explicitly takes account of the H_2 orientations.

Table 3.4:

Using potential of Danby et al, for the first two partial waves, $J_{tot} = 0, 1$ only, at an energy of 200cm^{-1} above the respective ground state, and with a NH_3 basis consisting of the first six rotational levels of ortho-NH_3. Units are 10^{-16}cm^2.

i f	$\sigma^{j_2=0}$	$\sigma^{j_2=1}$
10+ 00+	0.747 E-1	0.621 E-1
20+ 00+	0.886 E-2	0.737 E-2
30+ 00+	0.117 E-1	0.970 E-2
33+ 00+	0.159 E-6	0.229 E-6
33- 00+	0.437 E-1	0.363 E-1

At this point a further test was done. Using the potential with $\lambda_2 = 0$ terms only, collisional calculations were done using both ortho ($j_2 = 1$) and para ($j_2 = 0$) H_2 and ortho-NH_3. These were performed with a small NH_3 basis set ($j, k \leq 3$), and only considering the first three partial waves. Some results are shown in table 3.4. It can readily be seen that the two cases exhibit very similar behaviour, which would be expected given that the only terms in the potential are those with no dependence on the H_2 orientation , but, when taken in conjunction with the later results, they underline the importance of proper treatment of the H_2 rotation in these collisions.

3.5 Ortho-NH_3 – H_2 Collisions.

3.5.1 Low Energy Calculations: $125cm^{-1}$

It has already been mentioned that calculations for the linear rotor – symmetric top type problem rapidly become very large as the energy increases, so the energy was chosen to be as low as possible whilst still high enough to illustrate the basic differences between excitation by ground state H_2 ($j = 0$) and H_2 with $j > 0$.

The energies of the first few rotational levels of NH_3 (calculated using the symmetric top formula with $B = 9.9402$, $C = 9.3044$ (Green, 1976)) are:

j	k	ϵ	Energy
0	0	+	$0.0000cm^{-1}$
1	0	+	$19.8805cm^{-1}$
2	0	+	$59.6414cm^{-1}$
3	0	+	$119.2828cm^{-1}$
3	3	±	$86.5601cm^{-1}$
4	0	+	$198.8046cm^{-1}$
4	3	±	$166.0819cm^{-1}$
5	0	+	$298.2068cm^{-1}$
5	3	±	$265.4841cm^{-1}$
6	0	+	$417.4895cm^{-1}$
6	3	±	$384.7668cm^{-1}$
6	6	±	$286.5989cm^{-1}$

It was decided to choose an energy of $125cm^{-1}$ (0.0155 eV) as this includes the first of the k-doublet levels, but the calculation has no yet become too unmanageable. The collision energy of $125cm^{-1}$ is with respect to the ground state of both molecules.

The major approximation in the use of the close coupled equations is the truncation of the basis set. For NH_3 – H_2 collisions there are two basis sets to

consider, that on the NH_3 and that on the H_2. In the calculations of rotational excitation NH_3 by ground state para - H_2 it is implicitly assumed that one rotational state in the H_2 basis is adequate. The argument for this is that the molecular Hydrogen rotational levels are widely spaced with respect to the energy ($E_{j=2} - E_{j=0} = 354\text{cm}^{-1}$).

For the low energy H_2 - NH_3 collision, calculations were performed using para-H_2 basis sets of both ($j_2 = 0$) and ($j_2 = 0, 2$). The ortho-H_2 calculations used only a basis of ($j_2 = 1$). Tests were done to assess the effect of neglecting the ($j_2 = 3$) level, and it was found to be small (table 3.5).

The rotational spacing between the first two ortho-H_2 levels is larger than for the first two para-H_2 levels ($E_3 - E_1 = 587\text{cm}^{-1}$), and in addition, the ($j_2 = 3$) state of ortho-H_2 might be expected to behave in a similar way to the ($j_2 = 1$) state. It therefore seems likely that the neglect of ($j_2 = 3$) collisions can be justified, especially when the great increase in computer time which would result from the inclusion of the ($j_2 = 3$) level is taken into account.

The basis set on the NH_3 is more critical. Basis set convergence tests were performed for NH_3 - para-H_2 ($j_2 = 0$) collisions and the results are given in table 3.6. A B14 basis set was chosen for the calculations, including the fourteen energetically lowest states ($E_{jk} \leq E_{66}$). In these calculations no account was taken of the energy splitting between the inversion doublets, as this has been shown to have only a negligible effect on the results (Green, 1980, Billing and Diercksen, 1985).

The calculations were performed using both the potentials (SCF+MBPT, SCF+EK), and with H_2 basis sets of ($j_2 = 0$), ($j_2 = 0, 2$) and ($j_2 = 1$). Twenty-one partial waves were included to give convergence with respect to total angular momentum of three significant figures.The results are given in table 3.7.

3.5:The effect of neglecting the first excited levels of ortho and para-H_2

Calculations used a B9 basis for ortho-H_2 and a B12 basis for para-H_2. The calculations were for an energy of 125cm^{-1}, and considered the first two partial waves ($J_{tot} = 0, 1$), cross-sections are given in units of 10^{-16}cm^2.

$jk\epsilon \rightarrow j'k'\epsilon'$	$\sigma^{j_2=1}$	$\sigma^{j_2=1.3}$	$\sigma^{j_2=0}$	$\sigma^{j_2=0.2}$
00+ → 00+	1.26	1.20	1.80	1.14
00+ → 10+	0.14	0.09	0.30	0.61
00+ → 20+	0.13	0.15	0.05	0.03
00+ → 33+	0.085	0.078	0.000	0.000
00+ → 33−	0.055	0.057	0.24	0.19
00+ → 30+	0.025	0.030	0.043	0.049
10+ → 20+	0.11	0.10	0.17	0.35
10+ → 33+	0.042	0.044	0.16	0.13
10+ → 33−	0.075	0.068	0.016	0.034
10+ → 30+	0.051	0.059	0.020	0.040
20+ → 33+	0.058	0.056	0.013	0.022
20+ → 33−	0.050	0.053	0.049	0.056
20+ → 30+	0.13	0.13	0.089	0.32
33+ → 33−	0.43	0.40	0.051	0.13
33+ → 30+	0.025	0.027	0.028	0.042
33− → 30+	0.041	0.045	0.006	.017

3.6:Ortho-NH_3 – H_2 convergence tests

Convergence tests were performed at 125cm^{-1}, using a ($j_2 = 0$) H_2 basis set, and considering the first two partial waves ($J_{tot} = 0 \rightarrow 2$), cross-sections are given in units of 10^{-16}cm^2.

Transition	NH_3 basis					
$jk\epsilon \rightarrow j'k'\epsilon'$	B6	B9	B12	B14	B16	B17
00+ → 10+	0.640	0.663	0.663	0.658	0.658	0.658
00+ → 20+	0.119	0.115	0.119	0.119	0.119	0.119
00+ → 33+	0.000	0.000	0.000	0.000	0.000	0.000
00+ → 33−	0.502	0.526	0.525	0.549	0.551	0.551
00+ → 30+	0.069	0.082	0.082	0.081	0.082	0.083
10+ → 20+	0.439	0.436	0.446	0.442	0.442	0.442
10+ → 33+	0.397	0.419	0.420	0.440	0.440	0.440
10+ → 33−	0.049	0.038	0.039	0.040	0.040	0.040
10+ → 30+	0.017	0.042	0.043	0.042	0.043	0.043
20+ → 33+	0.072	0.061	0.062	0.065	0.065	0.065
20+ → 33−	0.217	0.257	0.261	0.272	0.272	0.272
20+ → 30+	0.382	0.361	0.368	0.366	0.368	0.369
33+ → 33−	0.458	0.410	0.413	0.407	0.408	0.408
33+ → 30+	0.072	0.081	0.085	0.089	0.088	0.089
33− → 30+	0.044	0.040	0.040	0.042	0.042	0.042

3.7: Ortho-NH_3 – H_2 converged cross-sections at 125cm^{-1}

Cross-sections are given in units of 10^{-16}cm^2. The calculations were done using the Manolopoulos integrator and a basis set consisting of the energetically lowest 14 rotational states of NH_3.

Transition	SCF+EK potential			SCF+MBPT potential		
$jk\epsilon \rightarrow j'k'\epsilon'$	$j_2 = 1$	$j_2 = 0$	$j_2 = 0,2$	$j_2 = 1$	$j_2 = 0$	$j_2 = 0,2$
00+ → 10+	36.8	10.3	25.5	40.5	4.13	13.0
00+ → 20+	10.9	2.90	2.30	9.93	7.59	4.91
00+ → 30+	0.444	0.588	0.357	0.478	0.406	0.511
00+ → 33+	3.05	0.118	0.0465	3.15	0.0237	0.0570
00+ → 33−	1.77	5.57	4.71	1.50	4.98	5.04
10+ → 20+	17.7	6.23	15.6	17.6	3.75	9.99
10+ → 30+	0.993	0.363	0.361	0.972	0.694	0.533
10+ → 33+	2.33	4.82	3.93	1.96	3.76	3.62
10+ → 33−	3.06	0.351	0.602	3.00	0.114	0.300
20+ → 30+	3.81	3.30	4.58	3.81	1.29	3.57
20+ → 33+	3.31	1.59	1.48	3.20	0.241	0.496
20+ → 33−	3.20	3.18	2.95	2.95	2.24	2.32
30+ → 33+	10.9	8.27	5.03	6.62	2.32	2.39
30+ → 33−	9.33	2.74	3.09	7.40	0.686	1.33
33+ → 33−	43.7	16.1	37.3	49.4	4.37	19.7

3.5.2 Discussions:

Para-H_2 (j = 0) versus Para-H_2 (j = 0, 2)

We first discuss the comparison between the results for collisions with para-H_2 confined to its rotational ground state ($j_2 = 0$ only) and the results for calculations using a ($j_2 = 0, 2$) basis set.

It can be seen from table 3.7 that the inclusion of ($j_2 = 2$) in the basis set has an appreciable effect on the cross sections, even at energies well below the threshold energy of the ($j_2 = 2$) H_2 state. In particular, the dipole allowed transitions, $\Delta j = 1$, $\Delta k = 0$, are enhanced when ($j_2 = 2$) is included in the basis set.

It should be noted that the basis convergence tests indicated that the inclusion of the ($j_2 = 3$) rotational state in the ortho-H_2 basis set had a far smaller effect than the inclusion of the ($j_2 = 2$) state in the para-H_2 basis set. Although the difference could be explained by the fact that the energy spacing of the rotational levels is greater for ortho-H_2 than for para-H_2, it may also be partly due to the fact that rotationally excited hydrogen molecules have nonvanishing quadrupole moments whereas ground state para-H_2 molecules are spherically symmetric. Thus the first excited state of para-H_2 may be needed to obtain a good convergence with respect to basis set size because it enables the H_2 and NH_3 molecules to interact via potential terms that are not available if spherically symmetric collisions partners ($j_2 = 0$) are considered. In contrast, the first two rotational levels of ortho-H_2, ($j_2 = 1$) and ($j_2 = 3$) will behave similarly as collision partners.

The conclusion that the ($j_2 = 2$) level should be included in the basis set is in agreement with the conclusions drawn by Billing and Diercksen (1985) from a semi-classical study of the NH_3 - H_2 collision system, and contrasts with the findings of Brechignac et al (1980) for the CO - H_2 collision system. The CO molecule has a weak dipole moment, and the latter reported that for the CO - H_2 system the inclusion of the ($j_2 = 2$) level had less than a 10% effect on the rotational cross-sections.

Ortho-H_2 versus Para-H_2

From table 3.7 it can be seen that, in general, the ortho-H_2 cross-sections are larger than the corresponding para-H_2 cross sections. In particular, the dipole allowed transitions are very much larger for transitions with ($j_2 = 1$) ortho-H_2. This is particularly clear in the comparison between the results for the ($j = 0$) H_2 and ($j = 1$) H_2 calculations using the SCF+MBPT potential. The $jk\epsilon = (00+ \rightarrow 10+)$ cross-section increases by a factor of ten for the ($j_2 = 1$) calculations, and the $jk\epsilon = (10+ \rightarrow 20+)$ cross-section increases by a factor of six. The enhancement of the dipole allowed transitions is less marked in calculations using the SCF+EK potential, but it remains substantial. It should be noted here that the SCF+MBPT potential is probably the most reliable of the two potentials used, although the SCF+EK is more complete, in so far as all the dispersion expansion coefficients were obtained from the same data set.

When the ($j_2 = 2$) rotational level is included in the para-H_2 basis set there is still an appreciable enhancement of the dipole allowed cross-sections for collisions with ortho ($j = 1$) H_2 when compared with the para ($j = 0, 2$) H_2 results.

The physical reason for this enhancement can be seen by dividing the results into $\Delta k = 0$ and $\Delta k = 3$ transitions. In the limit $k \rightarrow 0$ the linear rotor – symmetric top problem reduces formally to the linear rotor – linear rotor problem and comparisons can be drawn with previous work on H_2 – linear rotor collisions. Table 3.8 gives the ratio of cross-sections for excitation with ($j = 1$) H_2 to cross-sections for excitation with ($j = 0$) H_2 for both HCl – H_2 collisions (Green, 1977) and NH_3 – H_2 collisions (this work).

Both the HCl – H_2 collisions and the NH_3 – H_2 collisions show ortho-H_2 cross-sections that are appreciably larger than the para-H_2 results. The model HCl – H_2 potential used by Green (1977) explicitly included long range dipole – quadrupole type interactions, but did not include any long range quadrupole – quadrupole type interactions, and the enhancement of the $\Delta j = 2$ transitions is correspondingly smaller.

3.8: Comparison between the ratios $\sigma(j_2 = 1)/\sigma(j_2 = 0)$ for NH_3 – H_2 collisions and HCl – H_2 collisions (Green, 1977)

Transition	HCl – H_2		NH_3 – H_2	
$j \rightarrow j'$	200cm^{-1}	300cm^{-1}	125cm^{-1}	
			SCF+MBPT	SCF+EK
$0 \rightarrow 1$	3.5	2.6	9.8	3.6
$0 \rightarrow 2$	1.2	1.1	1.3	3.8
$0 \rightarrow 3$	1.0	1.0	1.2	0.8
$1 \rightarrow 2$	3.0	2.6	4.7	2.8
$1 \rightarrow 3$	1.1	1.0	1.4	2.7
$2 \rightarrow 3$	1.9	2.1	3.0	1.2

In the NH_3 – H_2 potential, both long range dipole – quadrupole and quadrupole – quadrupole type interactions were included. For the SCF+MBPT potential the behaviour is qualitatively similar to that of the HCl – H_2 results, in that the dipole allowed transitions ($\Delta j = 1$) are much enhanced, and the enhancement falls off rapidly with increasing Δj. For the SCF+EK potential there is a much larger enhancement of the quadrupole allowed transitions ($\Delta j = 2$). The difference between the SCF+MBPT and SCF+EK potentials here can be explained by the fact that the latter has a smaller v_{2020} term so the boost given to the $\Delta j = 2$ transitions is relatively larger than was the case for the former.

The most striking difference between the ortho and para-H_2 results is for the $\Delta k = 3$ transitions, in particular the behaviour of the $jk\epsilon = (00+ \rightarrow 33\pm)$ cross-section. The para-H_2 results clearly show the propensity rule:

$$\sigma(00+ \rightarrow 33+) << \sigma(00+ \rightarrow 33-)$$

However, for collisions with ortho-H_2 this is no longer case, and there is a slight propensity in the opposite direction.

The reason for this change can be seen by examination of the form of the coupling matrix elements.

We have:

$$\langle\gamma'|V_{\lambda_1\lambda_2\lambda\mu}|\gamma\rangle \sim (1+\epsilon\epsilon'(-1)^{j_1+j_1'+\lambda_2+\lambda+\mu}) \begin{pmatrix} j_2' & \lambda_2 & j_2 \\ 0 & 0 & 0 \end{pmatrix} \begin{pmatrix} j_1' & \lambda_1 & j_1 \\ -k' & \mu & k \end{pmatrix} \quad 3.5.1$$

Consider the transition $(jk\pm \leftrightarrow 00+)$. For collisions with ground state para-H_2, j_2 and j_2' are both zero. If we consider transitions out of the ortho-NH_3 ground state, the 3-j symbols give:

$$\left.\begin{aligned} \lambda_2 &= 0 \\ \lambda_1 &= j_1' \end{aligned}\right\} \quad \Rightarrow \quad \lambda = j_1' \quad \text{only.} \qquad 3.5.2$$

Thus, with $\mu = 3$, the coupling matrix element is proportional to:

$$\begin{aligned} &(1+\epsilon\epsilon'(-1)^{j_1+j_1'+k}) \\ &= (1+\epsilon\epsilon'(-1)^{k}) \end{aligned} \qquad 3.5.3$$

For $k = 3$ the coupling matrix element vanishes if $\epsilon = \epsilon'$. Thus the transition $(j3+ \rightarrow 00+)$ can only take place through indirect coupling. The transition $(j3- \rightarrow 00+)$ proceeds through direct coupling.

For transitions with ortho-H_2 $(j = 1)$ we have:

$$\left.\begin{aligned} \lambda_2 &= 0 \\ \lambda &= j_1 \end{aligned}\right\} \quad \text{or} \quad \left\{\begin{aligned} \lambda_2 &= 2 \\ \lambda &= (j_1 \pm 2), (j_1 \pm 1), j \end{aligned}\right. \qquad 3.5.4$$

We now have non-zero contributions for both $\epsilon\epsilon' = +1$ and $\epsilon\epsilon' = -1$.

The difference in propensities for the $(00+ \rightarrow 33\pm)$ transition found here between the results for collisions with ground state para-H_2, and the results for

collisions with ground state ortho-H_2 is at variance with the results of Billing and Diercksen (1988) and Ebel et al (1990) for the same system. Their calculations predict qualitatively similar behaviour in this transition for collisions with both ortho-H_2 and ground state para-H_2. The physical reason for this discrepancy can be most clearly seen with reference to the body-fixed formulation (section 2.6.6).

In the body fixed frame, the potential expansion can be written as:

$$V(R,\hat{\Omega}_1',\hat{R}_2') = \sum_{\substack{\lambda_1\lambda_2\\ \mu\nu}} v_{\lambda_1\mu\lambda_2\nu}(R)(D^{\lambda_1}_{\mu\nu}(\hat{\Omega}_1')Y^{\lambda_2}_{-\nu}(\hat{R}_2')). \qquad 3.5.5$$

Working in the coupled states approximation for simplicity, the coupling matrix elements take the form:

$$\text{CME} \propto \begin{pmatrix} j_1' & \lambda_1 & j_1 \\ -k' & \mu & k \end{pmatrix}\begin{pmatrix} j_1' & \lambda_1 & j_1 \\ -\Omega_1' & \nu & \Omega_1 \end{pmatrix}\begin{pmatrix} j_2' & \lambda_2 & j_2 \\ 0 & 0 & 0 \end{pmatrix}$$
$$\times \begin{pmatrix} j_2' & \lambda_2 & j_2 \\ -\Omega_2' & -\nu & \Omega_2 \end{pmatrix}\begin{pmatrix} j_1 & j_2 & j_{12} \\ \Omega_1 & \Omega_2 & -\Omega \end{pmatrix}\begin{pmatrix} j_1' & j_2' & j_{12}' \\ \Omega_1' & \Omega_2' & -\Omega' \end{pmatrix} \qquad 3.5.6$$

where Ω_1 is the projection of j_1 on the intermolecular axis, and Ω_2 is the projection of j_2. In the coupled states approximation, $\Omega(=\Omega_1+\Omega_2)$, is assumed constant, although Ω_1 and Ω_2 may change within this constraint,

$$\Omega_1' - \Omega_1 = \Omega_2 - \Omega_2' = \nu \qquad 3.5.7$$

In a full close coupled calculation, Ω is coupled to $\Omega' = \pm 1$ through the Coriolis term (Rabitz, 1976):

$$\langle\Omega|l^2/R^2|\Omega\pm 1\rangle = -\frac{1}{R^2}\left((J\pm\Omega+1)(J\mp\Omega)(j_{12}\mp\Omega)(j_{12}\pm\Omega+1)\right)^{1/2}$$
$$\times\left((1+\delta_{\Omega 0})(1+\delta_{\Omega\pm 1,0})\right)^{1/2} \qquad 3.5.8$$

but if $j_2 = 0$, then Ω must be conserved if $j_1(=j_{12})$ and Ω_1 are zero.

Billing and Diercksen (1986) introduce a potential expansion of the form:

$$V(R,\hat{R}_1',\hat{R}_2') = \sum_{\substack{\lambda_1\lambda_2\\ \mu\eta}} v_{\lambda_1\mu\lambda_2\eta}(R)(Y_\mu^{\lambda_1}(\hat{R}_1')Y_\eta^{\lambda_2}(\hat{R}_2')). \qquad 3.5.9$$

The equivalent of equation 3.5.6 is then:

$$\text{CME} \propto \begin{pmatrix} j_1' & \lambda_1 & j_1 \\ -k' & \mu & k \end{pmatrix} \begin{pmatrix} j_1' & \lambda_1 & j_1 \\ -\Omega_1' & 0 & \Omega_1 \end{pmatrix} \begin{pmatrix} j_2' & \lambda_2 & j_2 \\ 0 & 0 & 0 \end{pmatrix}$$

$$\times \begin{pmatrix} j_2' & \lambda_2 & j_2 \\ -\Omega_2' & \eta & \Omega_2 \end{pmatrix} \begin{pmatrix} j_1 & j_2 & j_{12} \\ \Omega_1 & \Omega_2 & -\Omega \end{pmatrix} \begin{pmatrix} j_1' & j_2' & j_{12}' \\ \Omega_1' & \Omega_2' & -\Omega' \end{pmatrix} \qquad 3.5.10$$

With the potential expansion, 3.5.9, the value of Ω_1 cannot change, as there is no term in the potential to affect such transitions (although note that now Ω is not fixed if $\eta > 0$). In the version of the coupled states approximation used by Billing and Diercksen, and by Ebel et al, the average over ϕ_2 is taken, setting $\eta = 0$, so that Ω_2 (and Ω) are conserved. In this limit the potential expansion, 3.5.9, is the same, to within a constant, as the expansion 3.5.6 with $\nu = 0$ only.

Returning to equation 3.5.6, we see that with the potential expansion (eq 3.5.5), the principal difference between ($j_2 = 0$) and ($j_2 > 0$) collisions, is that in the latter Ω_1 and Ω_2 may change, as $\lambda_2 > 0$, $\nu > 0$ are allowed. From the body fixed to space fixed conversion (eq 2.6.27):

$$v_{\lambda_1\lambda_2\lambda\mu}(R) = \sum_\nu \frac{C_{\nu\,-\nu 0}^{\lambda_1\lambda_2\,\lambda}}{(1+\delta_{\nu 0})} \left(\frac{4\pi}{2\lambda+1}\right)^{1/2}$$

$$\times \left(v_{\lambda_1\mu\lambda_2\nu}(R) + (-1)^{\lambda_1+\lambda_2+\lambda} v_{\lambda_1-\mu\lambda_2\nu}(R)\right) \qquad 3.5.11$$

along with the relation:

$$v_{\lambda_1\mu\lambda_2\nu}(R) = (-1)^\mu v_{\lambda_1-\mu\lambda_2-\nu}(R) \qquad 3.5.12$$

it can be seen that if the sum, $(\lambda_1+\lambda_2+\lambda+\mu)$, is odd, only $\nu > 0$ terms contribute to $v_{\lambda_1\lambda_2\lambda\mu}$. Space fixed expansion terms with $(\lambda_1 + \lambda_2 + \lambda + \mu)$ odd are the very

terms which drive the ortho-NH_3 transitions that are 'forbidden' by symmetry when $j_2 = 0$, thus ortho-NH_3 transitions such as $(00+ \rightarrow j3+)$ are driven only by body fixed terms with $\nu > 0$.

The body fixed terms with $\nu > 0$ in the potential expansion 3.5.5 are the terms that change the projection of j_1 and j_2 on the intermolecular axis, and are present regardless of whether or not the coupled state approximation is used.

In contrast the potential expansion 3.5.9 does not contain these terms, and the behaviour of the NH_3 cannot be not fully represented with this expansion.

SCF+MBPT versus SCF+EK

The para-H_2 results are noticeably affected by the change in the potential. In particular, transitions with $\Delta j = 1, \Delta k = 0$ are smaller with the MBPT potential, whilst terms with $\Delta j = 2, \Delta k = 0$ are larger. The former transitions are driven by the v_{1010} term in the space fixed potential expansion whilst the latter are driven by the v_{2020} term. The differences between the two potentials have been discussed by Danby and Valiron (1989). They conclude, after comparison of the theoretical results with the double-resonance data, that the v_{2020} term could have been underestimated by the SCF+EK potential.

The ortho-H_2 results are far less affected by the change in potential. This may be due to the effect of the number of additional terms contributing to the coupling matrix element for each transition. It may also be due in part to the fact that the $\nu = \pm 1$ terms in the body fixed expansion could not be obtained from the MBPT data and had to be taken from the EK potential surface with which comparison is now been made.

3.5.3 Experimental Energy: 605cm^{-1}

In view of the change in the $(00+ \rightarrow 33\pm)$ propensity rules found for collisions with ortho-H_2 $(j = 1)$ it is interesting to run calculations at the energy of the cross-beam measurements of Seelemann et al (1989) and Ebel et al (1990), to see if the inclusion of rotationally excited H_2 states could explain the discrepancy between the theoretical and experimental results.

The major problem for such a calculation is the size of the basis set that would be required to treat the system fully. At an energy of 605cm^{-1} seventeen NH_3 rotational states are energetically accessible. In addition, the ($j_2 = 2$) rotational state of para-H_2 is also energetically allowed. The CPU time per partial wave increases as $E^{1/2}$, as does the number of partial waves needed for convergence, so even with the same basis sets as previously, the calculation takes five times as long at 605cm^{-1} than at 125cm^{-1}. If we wish only to make a comparison with the experiment and if we are, therefore, only interested in the relative behaviour of the cross-sections, it seems reasonable to truncate the basis set to a manageable size, and look only at the transitions between the energetically lower states, making the assumption that for these states the convergence is adequate (eg the discussion in section 2.5.1).

For this reason it was decided to use the same B14 basis set on the NH_3 as had been used for he lower energy calculation. For collisions with ortho-H_2, $j_2 = 1$ only was included. Tests including the $|j_1 k j_2 \epsilon\rangle = |003+\rangle$ and $|103+\rangle$ states in the basis showed that their inclusion made very little difference to the relevant cross-sections ($<$ 10% for the first three partial waves). For para-H_2 an incomplete basis set was used, including $j_2 = 2$ for the $|002+\rangle$ and $|102+\rangle$ states only. This will not give excellent convergence with respect to basis set size, but, for comparison with the experiment, the cross-sections are weighted to allow for the 3:1 ortho:para-H_2 ratio. Thus the final results are dominated by the ortho-H_2 results, and the reduced para-H_2 basis set should be adequate.

The calculations were performed on the CRAY XMP at Rutherford using the Manolopoulos method for integrating the coupled equations. Thirty-eight partial waves were necessary to give convergence of the relevant cross-sections.

The experimental results are quoted as relative cross-sections, and are normalised with respect to previous theoretical cross-sections. Results for the present calculation are presented in table 3.9.

The crossed-beam experiments of Seelemann et al and Ebel et al yielded information on the relative sizes of the inelastic cross-sections for rotational transitions out of the rotational ground state for collisions of NH_3 with normal (3:1 ortho:para) H_2. In table 3.10 the experimental and current theoretical results are compared.

3.9: Ortho-NH_3 results at 605cm^{-1}

Cross-sections in units of 10^{-16}cm^2 for the rotational excitation of ortho-NH_3 from its $jk\epsilon = 00+$ ground state in collisions with ortho and para-H_2 at 605cm^{-1}.

Final state	Ortho-H_2	Para-H_2
10+	16.4	14.4
20+	6.97	0.314
30+	1.59	0.586
40+	0.738	0.211
33+	2.39	0.0165
33−	3.07	5.29
43+	1.12	0.0018
43−	1.65	3.65

The results are normalised so that the sum of the inelastic cross-sections given in table 3.9 is one.

The experiment studied collisions of rotationally cooled NH_3 with a beam of normal H_2, so for comparison with the experiment the results were weighted in a 3:1 ortho:para ratio. The 3:1 ratio is appropriate if the hydrogen molecules are exclusively in their respective rotational ground states. For a room temperature distribution approximately half the para-H_2 is in excited rotational states, and under such conditions it might be more appropriate to assume the ($j > 1$) H_2 behaves more like ($j = 1$) H_2 than ($j = 0$) H_2, and weight the results in a 7:1 ortho:para ratio.

From table 3.10 it can be seen that, despite the inadequacy of the basis set used, the agreement between the experimental and theoretical results is very satisfactory. The potential used for the calculation was the SCF+EK potential and, following

3.10: Comparison with experiment

Relative cross-sections for excitation from the 00+ ground state into the final state, $j'k'\epsilon'$. All results are normalised so that the sums of the given cross-sections are one.

Final state	experiment		theory		
$j'k'\epsilon'$	Seelemann et al	Ebel et al	Current work	Ebel et al	Billing
10+	0.38	0.44	0.50	0.44	0.70
20+	0.23	0.21	0.17	0.13	0.05
30+	0.05	0.05	0.04	0.06	0.02
40+	0.03	0.02	0.02	0.01	0.02
33+	0.09	0.08	0.06	0.00	0.00
33−	0.14	0.12	0.12	0.24	0.08
43+	0.04	0.04	0.03	0.00	0.00
43−	0.05	0.04	0.07	0.13	0.13

the discussion of Danby and Valiron (1989), it is thought that the v_{2020} term could have been underestimated by the SCF+EK potential. In line with the 125cm^{-1} results, one might expect that $\sigma(00+ \rightarrow 10+)$ would be smaller and $\sigma(10+ \rightarrow 20+)$ would be larger if a more reliable potential surface was used.

Thus it appears that the discrepancy between the experimental results and earlier theoretical calculations can be explained by the neglect of the hydrogen rotation in the latter.

A cautionary note might be added here. Whilst the above explains the discrepancy between the ortho-NH_3 - H_2 results, a similar discrepancy remains between the NH_3 - He results (Seelemann et al 1989).

For the NH_3 - H_2 collisions, we note in passing that for the higher energy calculations the cross-sections for the $jk\epsilon = (00+ \rightarrow 10+)$ transitions are of a similar magnitude for collisions with both ortho ($j_2 = 1$) H_2 and para ($j_2 = 0$) H_2, whereas there were substantial differences between these cross-sections at 125cm^{-1}. At high energies the collisions sample small impact parameters, and probe further into the short range region of the interaction. As small impact parameters the short range forces dominate the interaction, and they may be much the same for ($j_2 = 0$) and ($j_2 = 1$) H_2. In this region the effects of the long range interactions are drowned out, and the effects of the different multipole interactions are less prominent.

3.6 Para-NH_3 Collisions

3.6.1 Details of the Calculations

The energy of the first few rotational levels of para-NH_3 are:

$jk\pm$	Energy (cm^{-1})
11±	0.000
21±	36.532
22±	28.765
31±	99.402
32±	88.495

Again, no account has been taken of the inversion splitting of the (otherwise) degenerate k-doublets.

An energy of 60cm^{-1} was chosen to give the basic features of the behaviour of the cross-sections. At this energy there are six energetically accessible levels. Basis set convergence tests were performed with respect to the NH_3 basis set (table 3.11a), and the H_2 basis set (table 3.11b) for both ortho and para-H_2. It can be seen that the inclusion of the ($j_2 = 3$) state in the ortho-H_2 basis had a

less than 10% effect on the cross-sections for the first three partial waves, whilst the inclusion of the para-H_2 ($j = 2$) state introduces a factor of two or more.

A basis consisting of the lowest ten rotational levels was chosen for the NH_3, with H_2 basis sets of $(j_2 = 0), (j_2 = 0, 2)$ and $(j_2 = 1)$. For the bulk of the calculation the Manolopoulos method was used to solve the coupled equations. However, for $J_{tot} = 2$ the integrator became unstable and failed to produce results with the correct symmetry or even reproducible results. No satisfactory explanation was found for this, and the gaps were filled in using the R-matrix propagator. The problem might have gone unnoticed if there were no parity symmetry. The results are presented in table 3.12.

3.6.2 Discussion

Para-H_2 (j = 0) versus para-H_2 (j = 0, 2)

The para-H_2 ($j = 0, 2$) inelastic rates are larger than those obtained using the ($j_2 = 0$) only basis set. The difference is more pronounced here than it was for ortho-NH_3 despite the fact that a lower relative collision energy is being considered. In addition, the magnitude of the change seems to depend on the inversion symmetry of the two states.

For example, labelling the states by j, k and symmetry, where the symmetry is related to ϵ by equation 3.2.3, we see:

$$\frac{\sigma^{j=0,2}(11s \rightarrow 21a)}{\sigma^{j=0}(11s \rightarrow 21a)} > \frac{\sigma^{j=0,2}(11s \rightarrow 21s)}{\sigma^{j=0}(11s \rightarrow 21s)} \qquad 3.6.1a$$

$$\frac{\sigma^{j=0,2}(11s \rightarrow 22a)}{\sigma^{j=0}(11s \rightarrow 22a)} > \frac{\sigma^{j=0,2}(11s \rightarrow 22s)}{\sigma^{j=0}(11s \rightarrow 22s)} \qquad 3.6.1b$$

$$\frac{\sigma^{j=0,2}(21s \rightarrow 22a)}{\sigma^{j=0}(21s \rightarrow 22a)} > \frac{\sigma^{j=0,2}(21s \rightarrow 22s)}{\sigma^{j=0}(21s \rightarrow 22s)} \qquad 3.6.1c$$

To study these trends systematically, a far larger calculation would be needed at a series of collision energies, but it appears that in every case the symmetry changing collision is most effected by the inclusion of ($j_2 = 2$) states in the H_2 basis set. In particular, for case (a) above it is the dipole allowed transition that has

3.11a: Basis convergence wrt NH_3 basis

Calculations were done at an energy of $60cm^{-1}$, using an ortho-H_2 ($j_2 = 1$ only) basis, and the first four partial waves. Cross-sections are given in units of $10^{-16}cm^2$.

Transition	NH_3 basis			
$jk\epsilon \rightarrow j'k'\epsilon'$	B8	B10	B14	B16
11+ → 11+	10.4	10.4	10.4	10.4
11+ → 11−	0.9	0.8	0.9	0.9
11+ → 21+	1.4	1.5	1.5	1.5
11+ → 21−	1.3	1.2	1.2	1.2
11+ → 22+	0.3	0.3	0.4	0.4
11+ → 22−	0.3	0.3	0.3	0.3
21+ → 21+	30.1	29.0	29.9	29.8
21+ → 21−	2.7	2.5	2.5	2.6
21+ → 22+	0.7	0.9	0.9	1.0
21+ → 22−	1.1	1.1	1.1	1.1
22+ → 22+	20.0	19.8	19.7	19.5
22+ → 22−	3.6	3.3	3.3	3.3

3.11b: Basis convergence, wrt H_2 basis

Calculations were done at an energy of $60cm^{-1}$, using a para-NH_3 basis consisting of the energetically lowest ten rotational states, and the first three partial waves. Cross-sections are given in units of $10^{-16}cm^2$.

Transition	H_2 basis			
$jk\epsilon \rightarrow j'k'\epsilon'$	$j_2 = 1$	$j_2 = 1,3$	$j_2 = 0$	$j_2 = 0,2$
$11+ \rightarrow 11+$	5.34	5.42	7.11	5.77
$11+ \rightarrow 11-$	0.52	0.44	0.56	1.13
$11+ \rightarrow 21+$	0.71	0.69	0.51	1.29
$11+ \rightarrow 21-$	0.64	0.69	0.14	0.23
$11+ \rightarrow 22+$	0.15	0.15	0.006	0.063
$11+ \rightarrow 22-$	0.15	0.16	0.37	0.25
$21+ \rightarrow 21+$	14.37	14.51	20.96	13.96
$21+ \rightarrow 21-$	1.32	1.26	0.28	0.45
$21+ \rightarrow 22+$	0.29	0.32	0.44	0.61
$21+ \rightarrow 22-$	0.55	0.57	0.07	0.46
$22+ \rightarrow 22+$	9.46	9.44	11.62	8.04
$22+ \rightarrow 22-$	1.65	1.56	0.92	2.77

3.12: Para-NH_3 results

Inelastic cross-sections (in units of 10^{-16}cm^2) at a relative collision energy of 60cm^{-1}, using the SCF+EK potential. Cross-sections for transitions from the $\epsilon = -1$ state can be obtained from the relation:

$$\sigma(jk+ \rightarrow j'k'\pm) = \sigma(jk- \rightarrow j'k'\mp)$$

Transition	ortho-H_2	para-H_2	
$jk\epsilon \rightarrow j'k'\epsilon'$	$j_2 = 1$	$j_2 = 0$	$j_2 = 0, 2$
$11+ \rightarrow 11-$	28.4	7.18	20.5
$11+ \rightarrow 21+$	12.6	4.15	14.3
$11+ \rightarrow 21-$	9.97	1.67	2.81
$11+ \rightarrow 22+$	1.74	0.0457	0.229
$11+ \rightarrow 22-$	1.70	2.86	2.72
$21+ \rightarrow 21-$	23.8	4.67	19.8
$21+ \rightarrow 22+$	3.59	2.93	3.76
$21+ \rightarrow 22-$	4.55	0.411	1.59
$22+ \rightarrow 22-$	44.2	15.2	48.1

increased the most, supporting the hypothesis that it is indeed indirect transitions involving dipole – quadrupole type interactions that are responsible for the change in behaviour.

Ortho-H_2 versus Para-H_2

Once again it is clear that the ortho-H_2 cross-sections are in general larger than the corresponding para-H_2 results. This is true for all but the $jk\epsilon = (11+ \rightarrow 22-)$ cross-section if only $(j_2 = 0)$ is included in the hydrogen basis set, but if $(j_2 = 2)$ is included it is no longer true for the dipole allowed transition, $jk\epsilon = (21+ \rightarrow 11+)$.

Comparing the results in more detail, the para-NH_3 analogue of the $(00+ \rightarrow j3\pm)$ propensity rules can be seen. We have that:

$$\text{CME} \sim (1 + \epsilon\epsilon'(-1)^{\lambda+\lambda_2+j_1+j_1'+\mu}) \qquad 3.6.2$$

In the case of the $(11+ \rightarrow 22\pm)$ transition we have for para-H_2:

$$\begin{aligned} j_2 = j_2' = 0 \quad &\Rightarrow \quad \lambda_2 = 0 \\ j_1 = 1, j_1' = 2 \quad &\Rightarrow \quad \lambda_1 = 1, 2, 3 \\ &\qquad \text{only} \quad \lambda_1 = 3 \quad \text{allowed} \end{aligned} \qquad 3.6.3$$

thus we have:

$$\text{CME} \sim (1 + \epsilon\epsilon'(-1)^{3+3+3}) \qquad 3.6.4$$

which is identically zero if $\epsilon = \epsilon'$.

With ortho-H_2 the additional terms in the potential contribute to a non-zero coupling matrix element for this transition.

3.7 Summary

In this chapter, the results of the first fully quantal close coupling calculations on rotationally inelastic collisions of NH_3 with $(j > 0)$ H_2 have been reported. The consequences of including $(j > 0)$ states in the hydrogen basis set are summarised below:

- Cross-sections for rotational excitation of both para and ortho-NH_3 in collisions with ground state ortho-H_2 are qualitatively different from those for collisions with ground state para-H_2.

- In particular, the transitions that are 'forbidden' by symmetry for collisions with ground state para-H_2 are allowed in collisions with rotationally excited ($j > 0$) H_2.

- In calculations of rotational excitation in collisions with ground state para-Hydrogen it is necessary to include ($j = 2$) in the para-H_2 basis set to obtain converged results, however, it is not so important to include the ($j = 3$) state in an ortho-H_2 basis set where ($j = 1$) and ($j = 3$) H_2 might be expected to behave similarly as collision partners.

- The change in propensities for collisions with ortho-H_2 can explain, at least in part, the discrepancies between theory and experiment for rotationally inelastic collision of ortho-NH_3 with H_2.

Previous semi-classical coupled states calculations (Billing and Diercksen, 1988) and other quantal coupled states calculations (Ebel et al, 1990) have failed to predict the change in propensities discussed above, but this can be explained by the fact that the potential expansion used in their calculations (Billing and Diercksen, 1985) does not include the potential terms that are directly responsible for the different behaviour found in collisions with rotationally excited H_2.

A possible implication of the change in behaviour of the cross-sections for ($j > 0$) H_2 will be discussed in the following chapter.

Chapter IV

An Application : The jk = 33 Maser

4.1 Introduction

Ammonia is widely observed in the interstellar medium through a range of transitions in the infrared, microwave and radio frequencies (eg Ho and Townes, 1983). In particular, the $\Delta j = 0, \Delta k = 0$ inversion transitions, which fall in the microwave region of the spectrum, have been particularly well documented, and the observations can provide valuable information on the physical conditions within a cloud.

Walmsley and Ungerechts (1983) showed how observations of the para-NH_3 inversion transitions could be used to obtain an estimate of the kinetic temperature, T, within a cloud by solving the relevant statistical equilibrium calculations, to derive a relationship between the relative level populations for para-NH_3 and the local kinetic temperature. The ammonia thermometer was recalibrated by Danby et al (1988) using quantal NH_3 - H_2 calculations, and was shown to give good agreement with results obtained from CO observations.

For ortho-NH_3, the possibility of collisional pumping leading to population inversion in the ($jk\epsilon = 33\pm$) doublet was first mentioned in the same paper of Walmsley and Ungerechts (1983). They calculated the NH_3 level populations under typical molecular cloud conditions. Their calculations showed population inversion in the 33 inversion doublet for a narrow range of densities. Observationally Guilloteau et al (1983) made a tentative identification of maser emission in the 33 inversion doublet towards the continuum source DR21. Their deduction was based on observations of the (1,1),(2,2) and (3,3) inversion transitions. Assuming that the ortho:para-NH_3 ratio was the same in the area of the (1,1) and (2,2) absorption as in the area of the (3,3) emission line lead to the conclusion that the excitation temperature (section 4.2) across the 33 doublet was greater than 100K, or even negative (implying population inversion). They explained the anomaly

using the collisional rates of Green, concluding collisional excitation could produce the observed excitation temperatures.

Johnston et al (1989) published results confirming the existence of (jk=33) maser emission in $^{15}NH_3$ towards NGC7538-IRS1 where the kinetic temperature in the core of the NH_3 region was believed to be $\geq$ 170K, with a molecular hydrogen density of $n_{H_2} \sim 5 \times 10^7 cm^{-3}$. They discussed both the collisional pumping scheme of Walmsley and Ungerechts (1983) and alternative schemes involving transfer of population to vibrationally excited NH_3 levels (Mauersberger et al, 1988). The latter was suggested by Mauersberger et al to explain masers in non-metastable states and in reality there are probably a number of mechanisms leading to inversion depending on the local conditions.

Previous work has used the calculated ground state para-H_2 collisional rates, however, the ortho:para ratio is not known. It is thought that H_2 is probably formed in excited rotational states on grains resulting in a 3:1 ortho:para ratio. The ortho:para ratio may vary with time (Flower and Watt 1984) through proton exchange reactions of the form:

$$\begin{aligned} H_2(ortho) + H^+ &\leftrightarrow H_2(para) + H^+ + 170.5K \\ H_2(ortho) + H_3^+ &\leftrightarrow H_2(para) + H_3^+ + 170.5K \end{aligned} \qquad 4.1.1$$

with a rate of $\approx 2.2 \times 10^{-10} cm^3 s^{-1}$. Thus the ortho:para-$H_2$ ratio would fall from the initial value of 3:1 to the thermodynamic equilibrium value given by:

$$\frac{n(o-H_2)}{n(p-H_2)} = 9 \times \exp\left(\frac{-170.5}{T}\right) \qquad 4.1.2$$

The factor or nine in the equation is correct if all the ortho and para-hydrogen molecules are in their respective ground states, and comes from the statistical weight factor $(2I+1)(2j+1)$, where I is the nuclear spin. In this chapter the effect of including ortho-H_2 collisions is investigated using a simple model calculation.

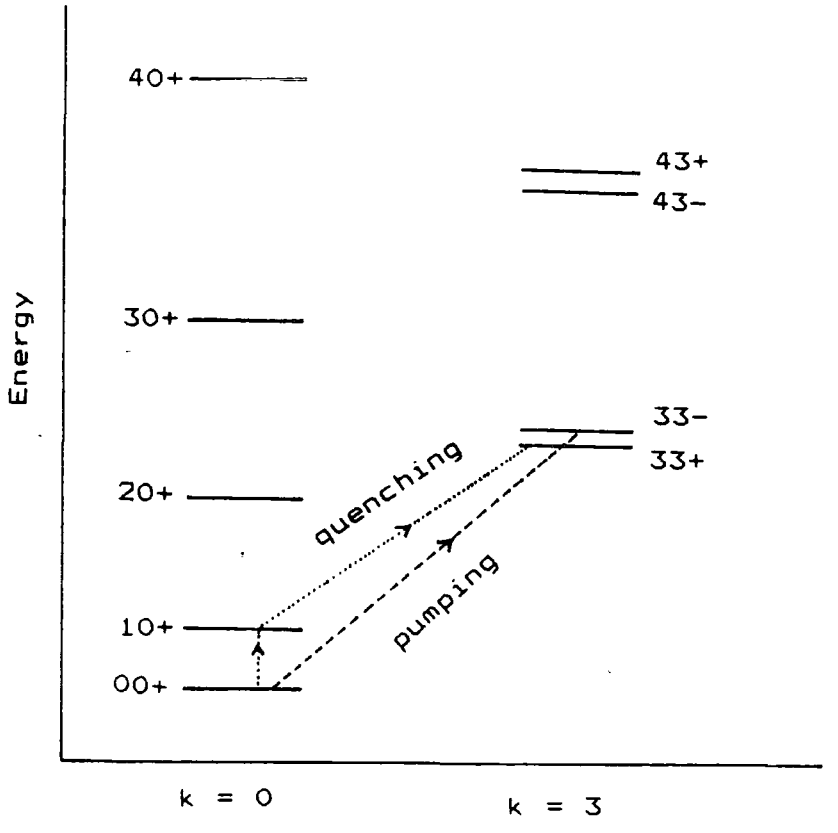

Figure 4.1: Rotational energy levels of ortho-NH_3
and the proposed collisional pumping mechanism

4.2 Theory

A necessary condition for $(jk = 33)$ maser emission is population inversion in the 33 doublet. A schematic energy level diagram for the first few rotational states of ortho-NH_3 is given in figure 4.1. In general, both radiative and collisional transitions between the levels occur, with the relative importance of the two being determined by the local molecular hydrogen density. However, transitions between the k-ladders are almost entirely due to collisional processes.

The simple model for producing population inversion in the metastable 33 doublet that was proposed by Walmsley and Ungerechts (1983) was based on the NH_3 - He collisional rates of Green (1982). In the temperatures applicable to dark interstellar clouds most of the NH_3 molecules will be in their rotational ground

state, at least for moderate molecular Hydrogen densities. Collisions between ground state ortho-NH_3 and ground state para-H_2 preferentially excite the $\epsilon = -1$ (upper) component of the 33 doublet leading to population inversion in that doublet. Maser emission can then follow. As the H_2 density increases the maser will be quenched by the increasing population in the non-metastable rotational states.

To investigate how this scheme is effected if ortho-H_2 is included, a model for the level population is needed. For a cloud in statistical equilibrium the number of transitions into a state i per unit time must be equal to the number of transitions out of state i per unit time. If molecular formation and destruction effects and any convective effects are neglected, and if only collisional and radiative excitations and de-excitations are considered, then, denoting the population density in level i by n_i/cm^3 we have, at some point in the cloud, (eg Spitzer 1978)

$$\begin{aligned}\frac{dn_j}{dt} &= -n_j\left(\sum_k(n_c\alpha_{jk}+B_{jk}U_\nu)+\sum_{k<j}A_{jk}\right)\\ &\quad+\sum_k n_k\left(n_c\alpha_{kj}+B_{kj}U_\nu\right)+\sum_{k>j}n_kA_{kj} \qquad 4.2.1\\ &= 0\,.\end{aligned}$$

Here A_{ij}, B_{ij} are the Einstein probability coefficients for spontaneous and induced emission (absorption) respectively, and α_{ij} is the collisional rate for transitions from state i to j. The number density of the collision partners is n_c ($= n_{H_2}$ here), and U_ν is the local radiant energy density at the frequency, ν_{ij}, of the transition. U_ν can be obtained from a consideration of the transfer of radiation within the cloud.

In general, the statistical equilibrium equations and the equations of radiative transfer have to be solved simultaneously. The size of U_ν depends on how readily the emitted photons can escape from the cloud. If the probability of reabsorption is relatively high emitted photons can become trapped within the cloud decreasing the radiant energy density.

A simplifying assumption that is often used is to assume that there is a large velocity gradient within a cloud (eg de Jong et al (1975)). Under these conditions

a photon travelling a distance greater than $l \simeq \frac{v_t}{dV/dr}$, where V is a typical large scale velocity and v_t is the thermal velocity, can escape because photons cannot be absorbed by molecules more than a Doppler width away. This simplifies the physics considerably and expressions for U_ν can be obtained for various cloud models allowing the equation to be solved in the radiative trapping case.

In the limit where all photons escape, U_ν is just the black body radiation field and under these conditions $B_{ij}U_\nu << n_c(r)\alpha_{ij}$ for a typical n_{H_2} of $10^5 \mathrm{cm}^{-3}$, and the induced emission (absorption) terms can be neglected for $T \lesssim 10\mathrm{K}$.

With an appropriate approximation for the radiative transfer term, the equilibrium system including N rotational levels leads to $N-1$ linearly independent equations which can be solved to give the ratio of the level populations.

A useful quantity in discussing the level populations is that of the excitation temperature, $T_{ex}(ij)$, defined by:

$$\frac{n_i}{n_j} = \exp\left(\frac{-h\nu_{ij}}{k_B T_{ex}(ij)}\right) \qquad 4.2.2$$

where ν is the frequency of the transition $i \rightarrow j$, h is Plancks constant and k_B is Boltzmanns constant. If the level populations have their local thermodynamic equilibrium values, T_{ex} is just the kinetic temperature. This condition is reached in the limit of high density, where $n_c\alpha_{ij}/A_{ij} >> 1$. The excitation temperature is related to the observable quantity, the brightness temperature, T_b, by:

$$T_b = (1 - \exp(-\tau_\nu))\, T_{ex} + \exp(-\tau_\nu)\, T_{bg} \qquad 4.2.3$$

where τ_ν is the optical depth at the frequency ν, and T_{bg} is the temperature of the background radiation. τ_ν can be deduced from the observations.

4.3 Collisional and Radiative Rates

The necessary molecular constants required for solving the statistical equilibrium equations are the radiative and collisional rates.

The radiative rates can be calculated from:

$$A_{if} = \frac{64\pi^4 \nu_{if}^3}{2hc^3} |\mu_{if}|^2 \qquad 4.3.1$$

where c denotes the velocity of light and $|\mu_{if}|^2$ is the square of the dipole matrix element, $\mu_{if} = \int \psi_i^* \mu \psi_f d\tau$, where μ is the molecular dipole moment. For a symmetric top molecule the non-vanishing $|\mu_{if}|^2$ are (Townes and Schawlow, 1955):

$$\begin{aligned}
\Delta j = +1, \Delta k = 0: \quad & |\mu_{if}|^2 = \mu^2 \frac{(j+1)^2 - k^2}{(j+1)(2j+1)} \\
\Delta j = +0, \Delta k = 0: \quad & |\mu_{if}|^2 = \mu^2 \frac{k^2}{j(j+1)} \\
\Delta j = -1, \Delta k = 0: \quad & |\mu_{if}|^2 = \mu^2 \frac{j^2 - k^2}{j(2j+1)}
\end{aligned} \qquad 4.3.2$$

Here we are assuming that the very slow $\Delta k = 3$ transitions (Oka et al, 1971) can be ignored. The radiative rates were calculated from the above equations with $\mu = 0.589 au$ (Diercksen and Sadlej, 1986).

The collisional rates are more problematical due to the variation of the collisional cross sections with energy. In the general case the collisional rates are obtained from the cross-sections by averaging over a Maxwellian velocity distribution (eg Spitzer 1978):

$$\alpha_{if}(T) = \int_0^\infty \sigma_{if}(v) v^3 \exp\left(-\frac{m_1 m_2 v^2}{2(m_1+m_2) k_B T}\right) dv \qquad 4.3.3$$

where v is the velocity corresponding to the collision energy, E, and m_1, m_2 are the masses of the collision partners.

Although, for a Maxwellian velocity distribution, the maximum contribution from $\sigma_{if}(E)$ ($\equiv \sigma_{if}(v)$) is that when $E = k_B T$, the contribution from $E \neq k_B T$ can be non-negligible, especially as the cross-sections may be increasing with Energy.

However, with results available at a single collision energy only, an *ad hoc* method of obtaining rates from cross-sections must be found. Danby et al (1986) have published a full set of rates for the rotational excitation of NH_3 in collisions

with para ($j = 0$) H_2, using essentially the same potential as was used here (SCF+EK). It was therefore decided to scale the new cross-sections (obtained with the SCF+EK potential) to the published rates using the expression:

$$\alpha^{j\geq 0}(T) = \alpha^{j=0}(T) \times \frac{\sigma^{j\geq 0}(E)}{\sigma^{j=0}(E)} \qquad 4.3.4$$

where $\alpha^{j=0}(T)$ are the rates of Danby et al (1986) at some temperature, T, $\alpha^{j\geq 0}(T)$ are the 'new' scaled rates at the same temperature, $\sigma^{j=0}(E)$ are the cross-sections computed for ($j = 0$) collisions in the present work and $\sigma^{j\geq 0}(E)$ are the cross-sections computed for ($j = 1$) and ($j = 0, 2$) H_2 collisions.

Implicit in this scaling method is the assumption that $\sigma^{j\geq 0}(E)$ varies in the same way with energy as $\sigma^{j=0}(E)$, at least in the region of interest. Whilst this may be a reasonable assumption for most transitions, it is unlikely to be true for the ($jk\epsilon = 00+ \rightarrow 33+$) transition. As discussed in chapter 3, this transition proceeds only by indirect couplings when the collision partner is ground-state para-H_2, but is coupled directly for collisions with ground state ortho-H_2. For this reason the ortho-H_2 ($00+ \rightarrow 33+$) cross-section was scaled to the ground state para-H_2 ($00+ \rightarrow 33-$) rates. The scaled rates for a temperature of 50K are given in table 4.1.

It should be bourne in mind that, for collisions at interstellar temperatures ($\approx$ 30K), the principal contributions to the collisional rates come from low energy collisions. Such collisions tend to sample long range forces, and it is expected that it is in the large R region that the interactions between ground-state para-H_2 and NH_3 differ most from the interactions between ground-state ortho-H_2 and NH_3.

4.1: Scaled rates at 50 Kelvin

Rates are given in units of cm^3s^{-1}. Numbers in parenthesis are powers of ten.

$jk\epsilon \rightarrow j'k'\epsilon'$	Danby et al	scaled ($j = 0, 2$)	scaled ($j = 1$)
00+ → 10+	0.76(-10)	0.188(- 9)	0.272(- 9)
00+ → 20+	0.94(-11)	0.746(-11)	0.353(-10)
00+ → 33+	0.34(-12)	0.134(-12)	0.657(-11)
00+ → 33−	0.12(-10)	0.101(-10)	0.381(-11)
00+ → 30+	0.85(-12)	0.516(-12)	0.642(-12)
10+ → 20+	0.29(-10)	0.726(-10)	0.824(-10)
10+ → 33+	0.15(-10)	0.122(-10)	0.725(-11)
10+ → 33−	0.14(-11)	0.240(-11)	0.122(-10)
10+ → 30+	0.96(-12)	0.955(-12)	0.263(-11)
20+ → 33+	0.67(-11)	0.624(-11)	0.139(-10)
20+ → 33−	0.21(-10)	0.195(-10)	0.211(-10)
20+ → 30+	0.14(-10)	0.193(-10)	0.162(-10)
33+ → 33−	0.13(- 9)	0.296(- 9)	0.346(- 9)
33+ → 30+	0.81(-11)	0.493(-11)	0.107(-10)
33− → 30+	0.38(-11)	0.429(-11)	0.130(-10)

Rates for de-excitation may be obtained from the detailed balance relation:

$$g_i \alpha_{i \rightarrow j}(T) = g_j \alpha_{j \rightarrow i}(T) \exp\left(-\frac{(E_j - E_i)}{k_B T}\right)$$

4.4 Level Population Calculations

In their 1983 paper, Walmsley and Ungerechts solved the statistical equilibrium calculations using a total of 38 ortho-NH_3 levels with the collisional rates of Green (1982). In addition they included the effects of radiative trapping using a large velocity gradient approximation. They noted however, that the role played by radiative trapping in exchange between k ladders was relatively unimportant, as k changing transitions are largely driven by collisions. In the case of the excitation temperature between the $jk = 33$ inversion doublet it is the difference between the collisional rates for $(j0+ \leftarrow 33+)$ and the A_{33} Einstein coefficient that is the critical parameter.

Schilke (1989) has performed similar multilevel statistical equilibrium calculations using the para (j=0) H_2 rates of Danby et al (1986). In addition he performed similar calculations scaling the $(00+ \rightarrow 33+)$ rates to the experimental results of Seelemann et al (1988). The latter calculation then contained some of the features found when ortho-H_2 is included in the calculation.

These calculations all showed population inversion in the 33 doublet, characterised by negative $T_{ex}(33)$. This behaviour was found in a range of densities, $n_{H_2} = 10^4 \rightarrow 10^5$, but Schilke found that the extent of the population inversion was markedly reduced when the theoretical collisional rates were modified by the experimental results as described above.

These calculations are all, however, essentially considering only excitation with ground state para-H_2. Walmsley and Ungerechts (1983) discuss the possible effect of ignoring collisions with ortho-H_2, but they suggest that collisions with rotationally excited H_2 might enhance the dipole allowed transitions, whilst leaving the k changing transitions, which are dependent on short range forces, largely unchanged. However, it was shown in chapter three that, whilst this is generally true for transitions driven by similar terms in the potential, it is *not* true for transitions such as the $(00+ \rightarrow 33+)$ transition which are forbidden by symmetry selection rules when the collision partner is ground-state para-H_2, but allowed for collisions with ground-state ortho-H_2.

Using the approximate rates obtained in the previous section we are now in a position to get some idea of how the level populations might change for an arbitrary ortho:para-H_2 ratio.

Given that reliable cross-sections have only been calculated at one energy that is below the threshold of levels with $j \geq 4$, and given the *ad hoc* nature of the rate scaling procedure, a large scale statistical equilibrium calculation of the type described above, would not be justified. However, a qualitative estimate of the behaviour could be obtained using a reduced statistical equilibrium calculation, and restricting detailed examination of the results to the regions in which they might be expected to be valid.

It was decided to perform the calculations using only the first six rotational levels for which the scaled rates could be obtained, ignoring any radiative effects. This is clearly only an approximate model, but it will be shown (figure 4.2) that it reproduces the main features of the more complete calculations when the same rates are used.

The statistical equilibrium calculations are obtained by equating the rates of transitions into a given rotational level, $jk\epsilon$, with the rate of transitions out of the level, thus:

$$n_j \quad \left\{ \sum_k \alpha_{jk}(T) + \sum_{k<j} \frac{A_{jk}}{n_{H_2}} \right\} = \left\{ \sum_k n_k \alpha_{kj}(T) + \sum_{k>j} n_k \frac{A_{kj}}{n_{H_2}} \right\} \qquad 4.4.1$$

Here we are assuming collisions with collision partners other than molecular hydrogen are negligible.

It can be seen from this equation that radiative transitions dominate for low n_{H_2}, whilst collisions dominate at high n_{H_2}. The quantities α_{kj} and α_{jk} are related by detailed balance:

$$g_j \alpha_{jk}(T) = g_k \alpha_{kj}(T) \exp\left(-\frac{(E_k - E_j)}{k_B T} \right) \qquad 4.4.2$$

where g_i is the statistical weight of level i, and E_i is its energy. Thus if radiative transitions are negligible, local thermodynamic equilibrium level populations are reached:

$$\frac{n_k}{n_j} = \frac{g_k}{g_j} \exp\left(-\frac{(E_k - E_j)}{k_B T}\right) \qquad 4.4.3$$

Dividing the set of equations 4.4.1 by the population density in level 1, n_1, gives $N - 1$ coupled equations in the $N - 1$ unknowns, here $N = 5$ and the five unknowns are $n_{jk\epsilon}/n_{00+}$, ($jk\epsilon = 10+, 20+, 30+, 33+$ and $33-$). In the current work these equations were solved using the NAG routine F04JAF. The 0.7962cm^{-1} energy splitting between the $33\pm$ levels, which had previously been ignored, was introduced explicitly.

Thus results for n_{33-}/n_{33+} and the excitation temperature, $T_{ex}(33)$, could be obtained as a function of kinetic temperature, molecular hydrogen density or ortho:para-H_2 ratio.

4.5 Discussion

4.5.1 Variation of $T_{ex}(33)$ with density.

Figure 4.2 shows the results of a calculation of the 33 excitation temperature as a function of the molecular hydrogen density at a kinetic temperature of 50K. Here the results are given using the scaled ($j = 1$) and ($j = 0, 2$) rates for ortho:para-H_2 ratios of 0,1,2 and 3. In addition, results are given using the ($j = 0$) H_2 rates of Danby et al, in the same six level model calculation, for comparison with the results obtained by Schilke using the same rates in a full (multilevel including the effects of radiative trapping) calculation. The latter comparison provides some measure of the adequacy of the model calculations being performed here. In particular, it can be seen that the model calculation fails to reproduce the behaviour of the more complete calculation above $n_{H_2} \approx 5 \times 10^5\text{cm}^{-3}$. At higher densities, levels with higher j become appreciably populated, and the influence of the higher rotational levels, ignored here, causes the system to reach local thermodynamic equilibrium populations sooner. However, at the lower molecular hydrogen densities, the qualitative behaviour seems to be well reproduced.

Figure 4.2a

The variation of $T_{ex}(33)$ with n_{H_2} with varying ortho:para-H_2 ratios. (Triangles: pure para-H_2, squares: ortho:para ratio of one, crosses: ortho:para ratio of two, circles: ortho:para ratio of three).

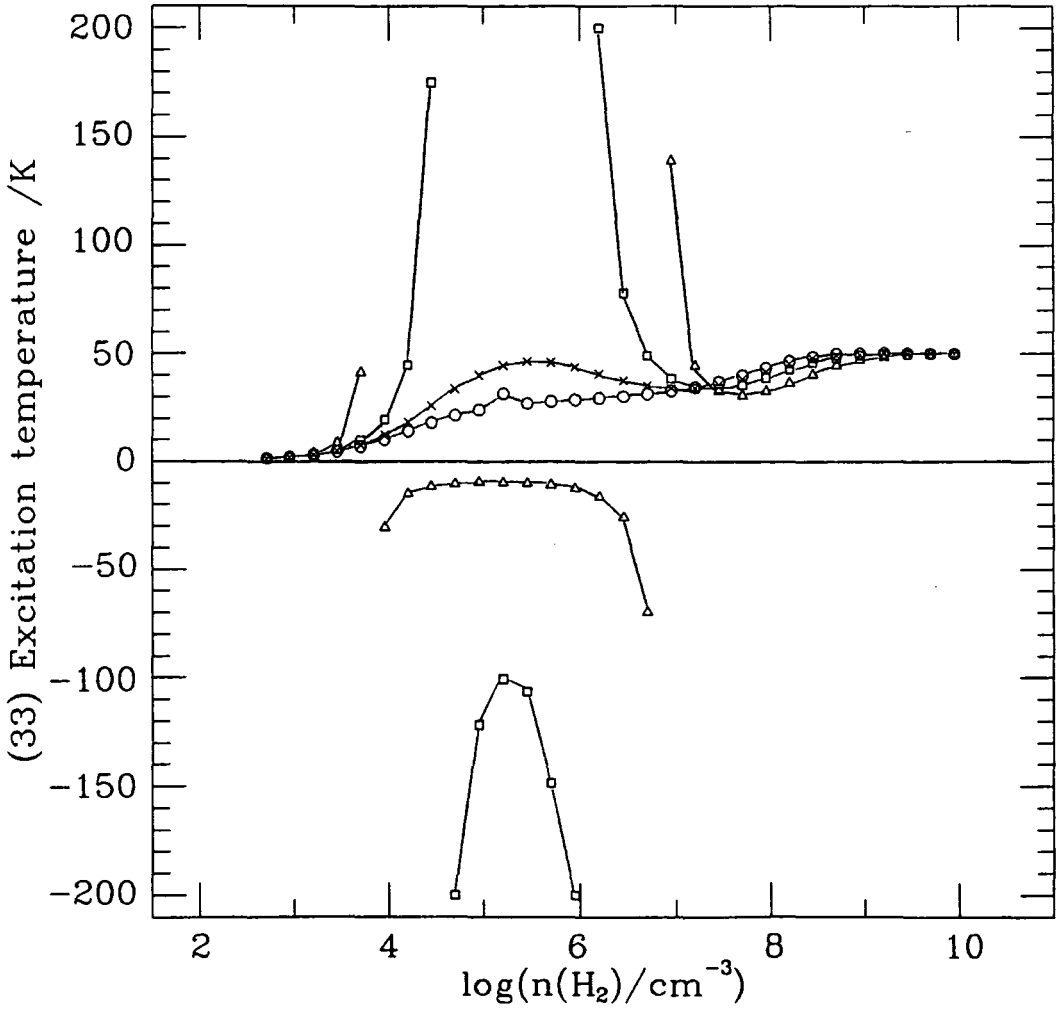

Figure 4.2b

The variation of $T_{ex}(33)$ with n_{H_2} for pure para-H_2 from the model calculation with $(j_2 = 0, 2)$ rates (squares), with the $(j_2 = 0)$ rates of Danby et al (crosses) and the results of the more complete calculation of Schilke (1989) with the same $(j_2 = 0)$ rates (solid line).

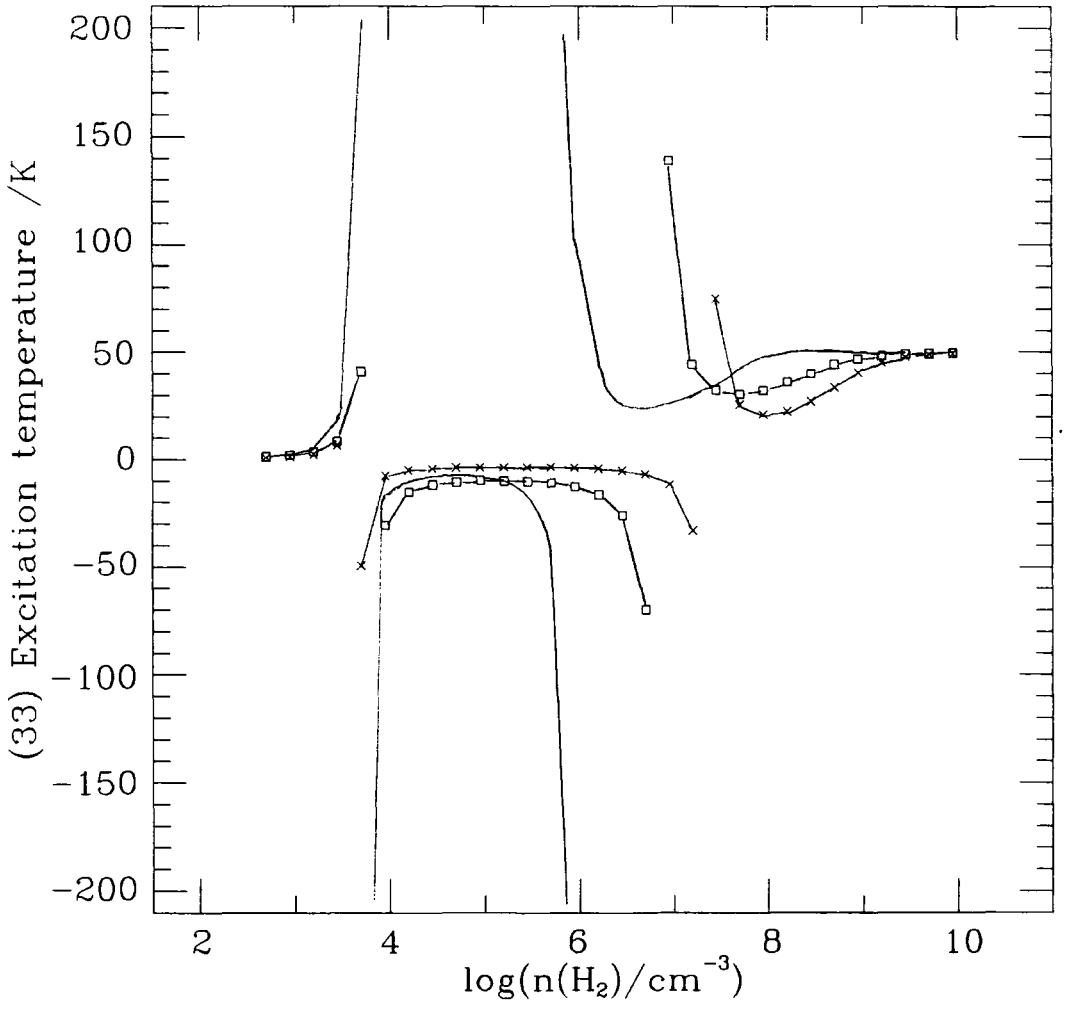

Figure 4.3a

The variation of $\ln\left(\frac{n_{33-}}{n_{33+}}\right)$ with ortho:para-H_2 ratio for a density of $n_{H_2} = 5 \times 10^4 \mathrm{cm}^{-3}$.

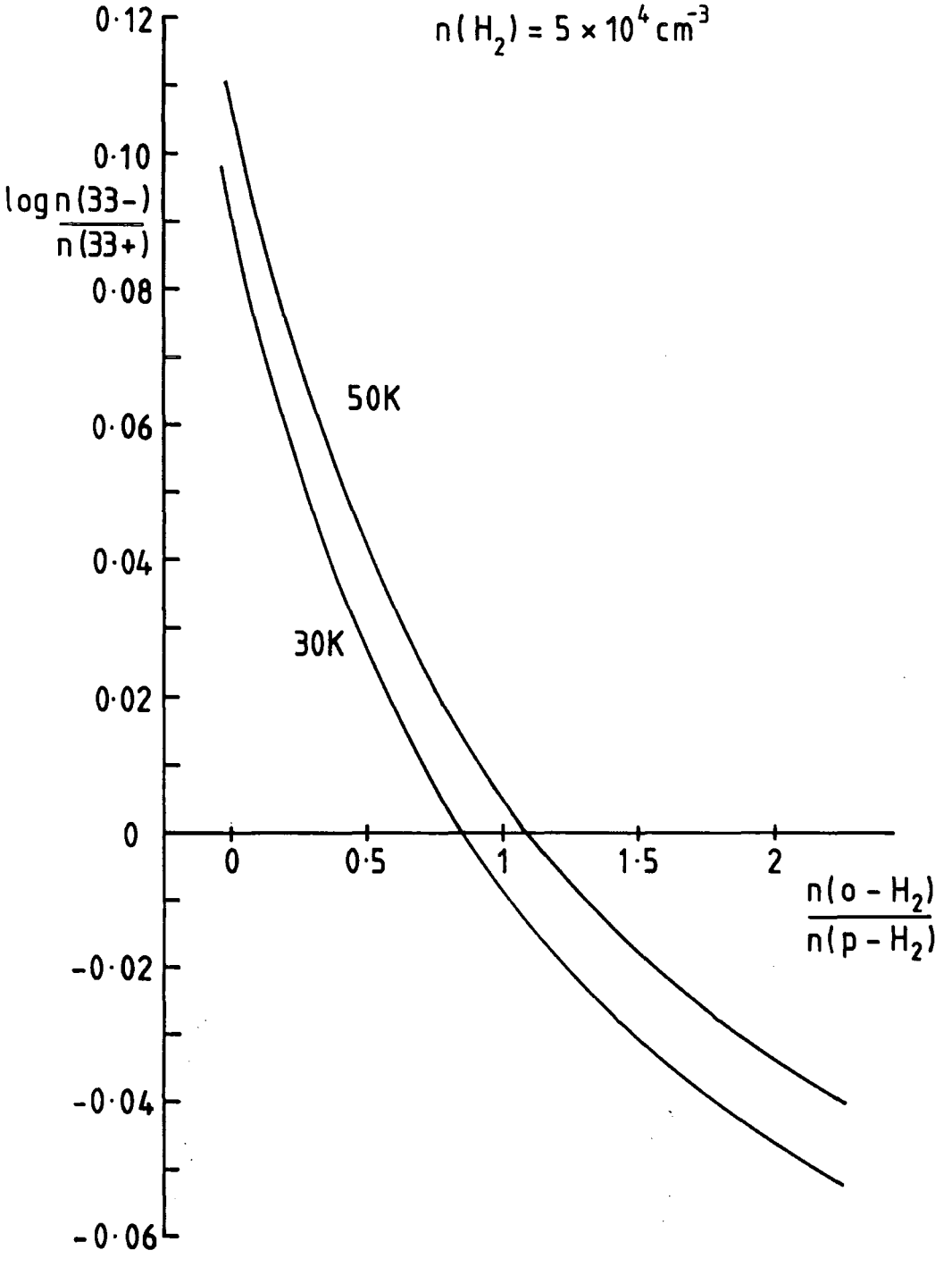

Figure 4.3b

The variation of $\ln\left(\frac{n_{33-}}{n_{33+}}\right)$ with ortho:para-H_2 ratio for a density of $n_{H_2} = 5 \times 10^5 \mathrm{cm}^{-3}$.

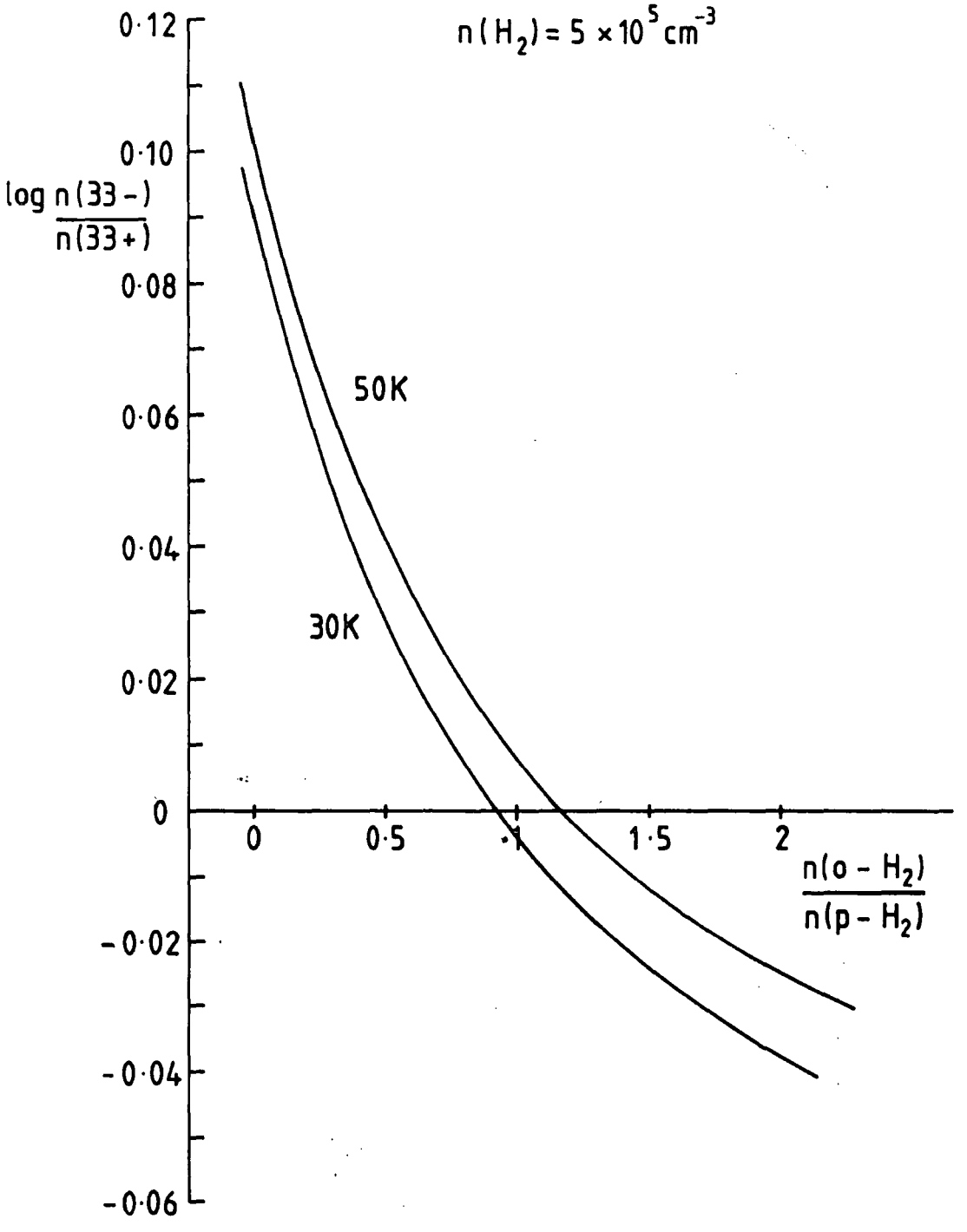

From the figure that it can be seen that there is no population inversion for ortho:para-H_2 ratios greater than unity. This conclusion should be relatively independent of the simplicity of the model used. The *probable* effect of a more complex model would be to reduce n_{33-}/n_{33+}.

4.5.2 Variation of n_{33-}/n_{33+} with ortho:para-H_2 ratio

Given that the levels are expected to be formed with an ortho:para-H_2 ratio of 3:1 which is gradually depleted with time it is instructive to investigate the variation of the ratio of the population in the 33− level to the population in the 33+ level with the ortho:para-H_2 ratio for a given kinetic temperature.

The results of two such calculations, for $T = 30$K and $T = 50$K, with $n_{H_2} = 5 \times 10^4$ and $5 \times 10^5 \mathrm{cm}^{-3}$, are shown in figure 4.3. As expected, the value of $\log(n_{33-}/n_{33+})$ falls off rapidly with increasing ortho:para-H_2 ratio. In both cases, population inversion is only found for values of ortho:para-H_2 ratios less than about unity. Thus, if the 33 maser is indeed caused by collisional pumping, the efficiency of the pumping is heavily dependent on the local ortho:para-H_2 ratio, and through the variation of the ortho:para-H_2 ratio with time, it is also dependent on the age of the cloud (Flower et al, 1990).

To investigate this further requires solving a model for the chemical composition of the cloud to derive the variation of the ortho:para-H_2 ratio with time. This can be done by solving the statistical equilibrium equations for the various molecular species, which, under stationary state conditions, take the form:

$$\frac{d}{dt}(n_{mol}) = \text{rate of production of } mol - \text{rate of destruction of } mol \qquad 4.5.1$$

where the rate for the production / destruction process $A + B \rightarrow C + D$ is given by the product of n_A, n_B and the rate coefficient for the process. The change in the ortho:para-H_2 ratio with time is obtained in a similar way from:

$$\begin{aligned}\frac{d}{dt}n_{para\,H_2} = &\frac{\text{rate of production of } H_2}{4} + n_{ortho\,H_2}\,\alpha(o \rightarrow p) \\ &- n_{para\,H_2}\,\alpha(p \rightarrow o) - n_{para H_2} \times (\text{rate of destruction of } H_2)\end{aligned} \qquad 4.5.2a$$

$$n_{ortho\,H_2} = n_{H_2} - n_{para\,H_2} \qquad 4.5.2b$$

The evolution of the molecular abundances with time is extracted by solving the equations for a large number of molecular formation and destruction processes.

Using a reaction network of $\sim$ 400 chemical reactions (Pineau des Forets et al, 1990) plus the spin changing reactions (eqn 4.1.1), the equations can be solved using the MHD computer code (Heck et al, 1990).

Calculations at a grain temperature of 30K and a density of $n_{H_2} = 5 \times 10^4$ with non-ionized initial conditions, gave an ortho:para-H_2 ratio that dropped sharply from around 3:1 to very much less than 1, passing through unity at around 10^6 years (Flower and Watt, 1984, Flower et al, 1990).

The models here presented are very simple, but in principle observations of the 33 maser could yield information on the ortho:para-H_2 ratio in a cloud, if estimates of the density were available and more reliable NH_3 - ortho-H_2 rates could be established. The latter would probably need coupled state calculations, once the validity of the coupled state approximation for this system had been checked. Meanwhile, a preliminary investigation using data from the source NGC 7538 has been performed by Schilke (Flower et al, 1990).

Chapter V

Rotational Excitation of OH in collisions with ortho and para-Hydrogen

5.1 Introduction

The electronic ground state of the astrophysically important OH molecule is a $^2\Pi$ state, with rotational levels labelled by half integer angular momentum. In the notation of Hunds coupling case (a) the rotational states are split by the spin orbit interaction into two rotational ladders labelled by $\Omega = 1/2$ and $\Omega = 3/2$, and these rotational states are further split into Λ doublets. Because of the complex nature of the rotational coupling in OH, collisions with other molecules lead to an unequal excitation of the Λ doublets in collisions, and this preferential excitation has been widely investigated as a possible pumping mechanism for the observed OH masers.

Pumping by collisions with H_2 was proposed by Gwinn et al (1973), and early work on OH – H_2 collisions suggested that collisional pumping could lead to population inversion in the $^2\Pi_{3/2}$ rotational ladder (Bertojo et al, 1976, Dixon and Field, 1979, Dewangan and Flower, 1981, 1983). Although this was subsequently discounted when phase errors were corrected (Alexander and Dagdigian, 1984, Dixon et al, 1985), collisional pumping may be responsible for masers in the $^2\Pi_{1/2}$ states (Andresen, Haüsler, Lülf and Kegel, 1984), and under some conditions collisional pumping could lead indirectly to inversion in the $j = 3/2, \Omega = 3/2$ ground state, via a scheme involving the infra-red relaxation of $\Omega = 1/2$ states (Andresen, 1986).

Rotational transitions of OH have been observed in relatively dense regions of the interstellar gas and it is likely that the major collision partner in such regions is molecular hydrogen. Previous theoretical calculations of OH – H_2 collisions have looked at collisions with ground state para-H_2 only, and in view of the change in behaviour found in NH_3 – H_2 collisions when ($j > 0$) H_2 is used as the collision

partner, it is interesting to investigate how the propensity rules found in OH - H_2 collisions change when a similar substitution is made. In addition, the available experimental data (Andresen, Haüsler and Lülf, 1984) is for collisions of OH with normal H_2, and a more complete treatment of the rotational structure of the H_2 molecule is needed to fully compare experimental and theoretical results.

The rotational wavefunction of $X^2\Pi$ OH can be expanded as a linear combination of rotation matrices and, as such, the algebra needed to treat OH - H_2 collisions is structurally the same as that required for linear rotor - asymmetric top collisions. However, the collision systems are not identical and it is not clear how the propensity rules will change if rotationally excited Hydrogen molecules are included in the H_2 basis set.

In this chapter, the treatment of linear rotor - symmetric top molecules, introduced in chapter two, is extended to treat OH - H_2 collisions, and the results are presented at 190cm^{-1} and at 680cm^{-1} for comparison with the experimental cross-beam measurements (Andresen et al, 1984)

5.2 The OH molecule

5.2.1 Angular momentum coupling

OH, with three π electrons in it s valence shell, has a non-zero electronic angular momentum about the internuclear axis. The ground state of the OH molecule is designated $X^2\Pi$ in standard spectroscopic notation ($\Lambda = 1$, where Λ is the component of the electronic orbital angular momentum, **L**, along the internuclear axis). It has three electrons in the valence shell one of which is unpaired, giving a total electronic spin angular momentum, **S**, of 1/2. The spin angular momentum couples to the orbital and nuclear rotational angular momentum to form a resultant, **j**, the total molecular angular momentum (ignoring nuclear spin).

The correct form of angular momentum coupling for the OH molecule is intermediate between Hunds coupling cases (a) and (b). Hunds coupling cases are described in standard texts (Herzberg, 1950, Townes and Schawlow, 1955), but the relevant cases are reviewed here.

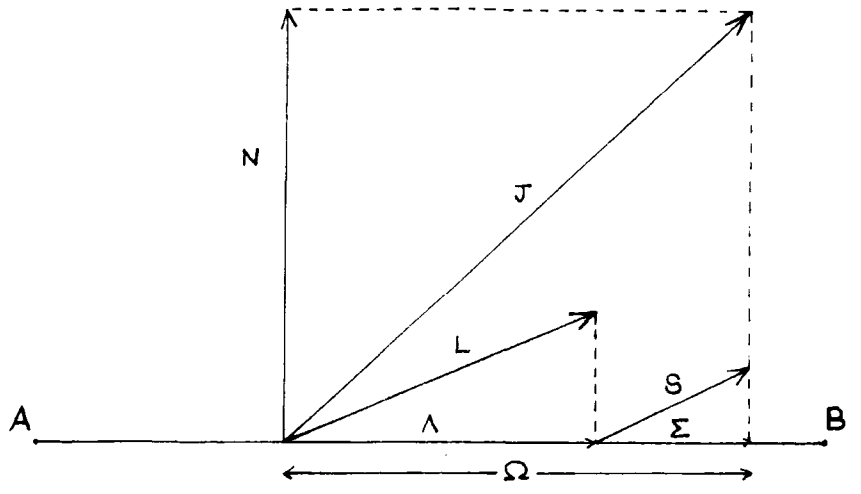

Figure 5.1: Hunds coupling case (a)

Hunds coupling case (a)

The case (a) limit (figure 5.1) is approached at low total angular momentum where the magnitude of the spin orbit coupling is greater than the coupling between the spin, **S**, and the nuclear rotation, **N**. (I.e. when $|A\Lambda| >> BJ$, where A is the spin orbit constant and B is the rotational constant.)

In Hunds coupling case (a) the interaction of the orbital angular momentum, **L**, and the electronic spin, **S**, with the nuclear rotation, **N**, is assumed to be weak. The orbital angular momentum is strongly coupled to the internuclear axis, and its projection on this axis, Λ, is well defined. **S** is also strongly coupled to the axis (via its interaction with **L** through spin-orbit coupling) and its projection, Σ, is also a good quantum number, as is the quantity $\Omega = |\Sigma + \Lambda|$. The case (a) limit is approached for the OH molecule at low total angular momentum where the magnitude of the spin orbit coupling is greater than the coupling between **S** and **N**.

The total angular momentum is formed by vector addition of Ω and the nuclear rotational angular momentum:

$$\mathbf{j} = \mathbf{\Omega} + \mathbf{N} \qquad 5.2.1$$

where here **j** includes both spin and rotational angular momentum.

For OH, $\Sigma = \pm 1/2$ and $\Lambda = \pm 1$, giving $\Omega = \pm 1/2, \pm 3/2$. This results in a separation of the energy levels into two Ω ladders labelled by $^2\Pi_{1/2}$ and $^2\Pi_{3/2}$, with an energy given by:

$$E_{rot} = B(j(j+1) - \Omega^2 + S(S+1) - \Sigma^2) \qquad 5.2.2$$

(Lefebvre-Brion and Field, 1986).

The quantity Ω has the same relation to **j** as k has to **j** in the symmetric top coupling, and the wavefunction for case (a) molecules can be expressed as a linear sum of products of a wavefunction embedding the vibrational and electronic motion, and a rotational eigenfunction:

$$|j\Omega m\rangle|v\Lambda S\Sigma\rangle \qquad 5.2.3$$

where

$$|j\Omega m\rangle = \left(\frac{2j+1}{8\pi}\right)^{1/2} D^j_{\Omega m}(\alpha\beta\gamma) \qquad 5.2.4$$

where v is the vibrational quantum number and (α, β, γ) are the Euler angles (Edmonds 1960).

Suppressing the index S, and treating the OH as a rigid rotor, the parity adapted wavefunction for OH can be written as:

$$\begin{aligned} |jm\Omega\epsilon\rangle &= 2^{-1/2}(|jm\Omega\rangle|\Lambda = 1, \Sigma = \Omega - \Lambda\rangle \\ &\quad + \epsilon|jm - \Omega\rangle|\Lambda = -1, \Sigma = -\Omega - \Lambda\rangle) \\ &= \psi^{(a)}_{\Omega}(J) \end{aligned} \qquad 5.2.5$$

where $\epsilon = \pm 1$ and from henceforth, $\Omega \equiv |\Omega|$ (Alexander 1982). A spectroscopic notation that is often employed is to use the notation '**f**' to refer to the $\epsilon = +1$ states and '**e**' to refer to the $\epsilon = -1$ states. The quantity ϵ is related to the parity, p, of the state by (Alexander and Dagdigian, 1984):

$$p = \epsilon\,(-1)^{j-s}. \qquad 5.2.6$$

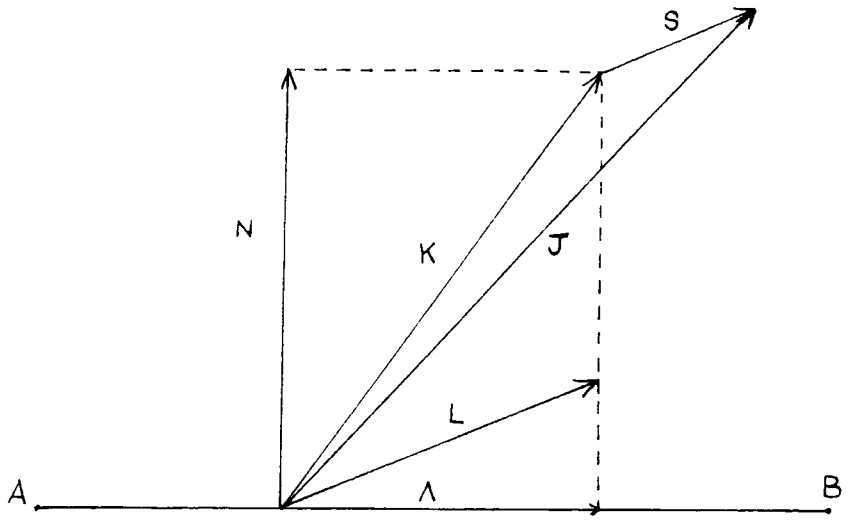

Figure 5.2: Hunds coupling case (b)

Hunds coupling case (b)

At high values of j, the nuclear rotation increases to the point where **S** is only weakly coupled to the internuclear axis. In this limit $BJ >> |A\Lambda|$, and Hunds case (b) is approached (figure 5.2). In Hunds case (b) **L** and **N** couple to give the total angular momentum neglecting spin, **K**,

$$\mathbf{K} = \mathbf{L} + \mathbf{N} \qquad 5.2.7$$

The total angular momentum, **j**, is then the resultant of **K** and **S**,

$$\mathbf{j} = \mathbf{K} + \mathbf{S} \qquad 5.2.8$$

where each level for a given K consists of $2S + 1(= 2)$ components.

Intermediate coupling

In reality the 'correct' coupling case for OH lies between case (a) and (b) (Dousmanis et al, 1955, Bertojo et al, 1976), the case (b) limit being approached as j increases. It is usual to express the intermediate coupling wavefunction as a linear combination of case a wavefunctions, (Dousmanis et al, 1955, Lefebvre-Brion and

Field, 1986). In the notation applicable to case (a) the intermediate wavefunction can be written:

$$\Psi_{3/2}(j) = a_j \psi^{(a)}_{3/2}(j) - b_j \psi^{(a)}_{1/2}(j)$$
$$\Psi_{1/2}(j) = b_j \psi^{(a)}_{3/2}(j) + a_j \psi^{(a)}_{1/2}(j) \qquad 5.2.9a$$

where:

$$a_j = \left[\frac{X - (\lambda - 2)}{2X}\right]^{1/2} \qquad b_j = \left[\frac{X + (\lambda - 2)}{2X}\right]^{1/2} \qquad 5.2.9b$$

$$X = \left[4(j + 1/2)^2 + \lambda(\lambda - 4)\right]^{1/2}$$
$$\lambda = \frac{A}{B} \qquad 5.2.9c$$

here λ is the ratio of the spin orbit constant, A, to the rotational constant, B. Case (a) is regained in the limit ($\lambda \rightarrow \infty$), and the case (b) wavefunctions are obtained as ($\lambda \rightarrow 0$). Thus departures from the case (a) limit manifest themselves as a mixing of the $\Omega = 1/2$ and $\Omega = 3/2$ states.

The value of λ used in the work reported here is $\lambda = -7.501$ (Poynter and Beaudet, 1968). Schinke and Andresen (1984) used a value of $\lambda = -7.44$ (Dieke and Crosswhite, 1961) in their coupled states calculations.

5.2.2 Lambda Doubling

In addition to the splitting of the energy levels of different j and $|\Omega|$, the levels are further split by Λ doubling. The physical cause of the splitting is the interaction of the nuclear rotational angular momentum with the electronic orbital angular momentum which splits the otherwise degenerate $\epsilon = \pm 1$ levels by around 0.55cm^{-1}, the magnitude of the splitting increasing with j. The splitting is much smaller than the separation of the energy levels and is ignored in the collisional calculation, but it is the preferential excitation of one of the components of the Λ doublets, with respect to the other, that leads to the population inversion or anti-inversion that has caused so much interest. For pure case (a) coupling both components of the Λ doublets are equally populated, the preferential excitation is a direct result of the departure from the case (a) ideal.

Figure 5.3: Ordering of the OH rotational energy levels

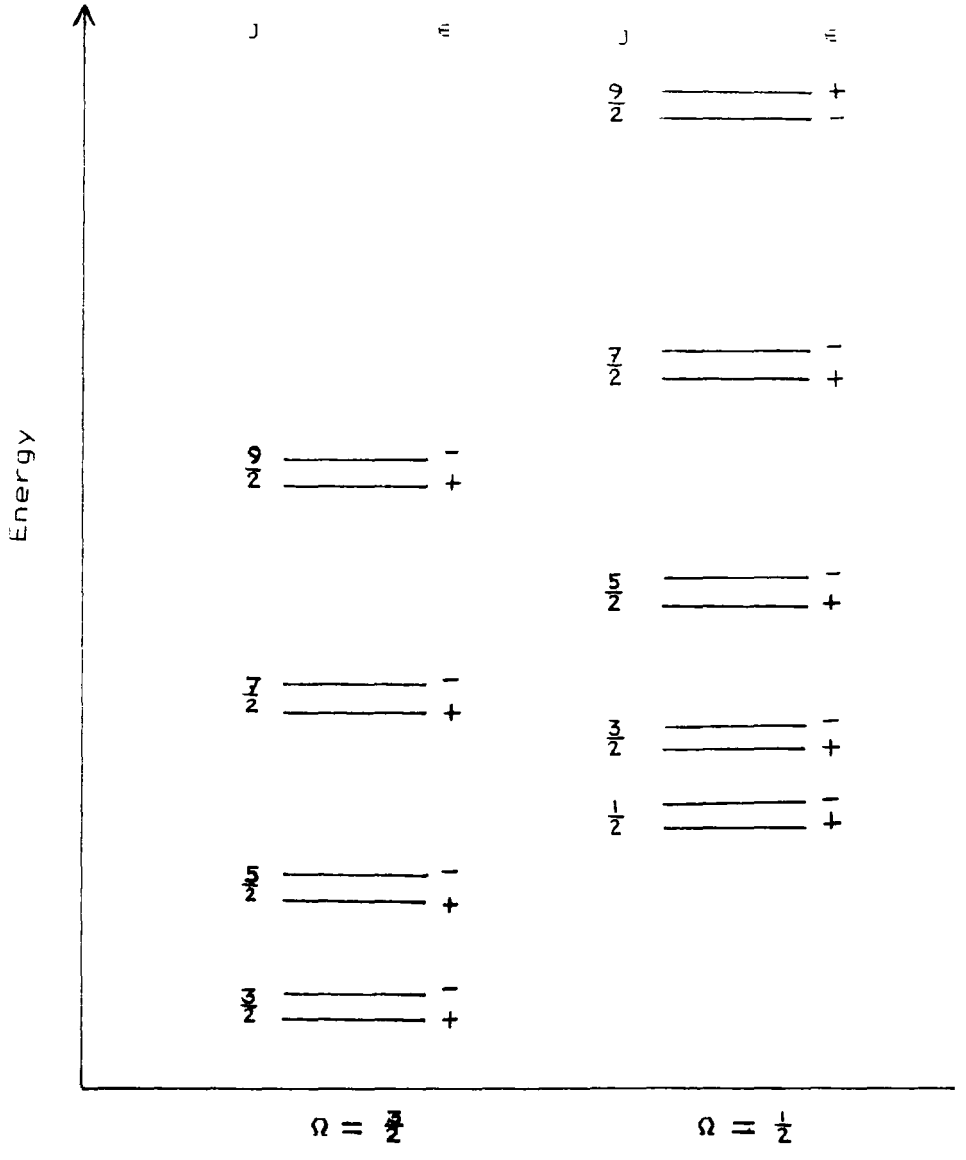

Note that in the $\Omega = 1/2$ ladder (using the nomenclature applicable to Hunds case (a)), the ordering of the ϵ levels reverses for $j \geq 9/2$ as the case (b) limit is approached.

5.2.3 Energy Level Ordering

In order to interpret the results of collisional calculations, the energetic ordering of the Λ doublets is important, and has been much discussed (Alexander and Dagdigian 1984). The ordering of the rotational levels, using the nomenclature of Hunds coupling case (a), is shown in figure 5.3, with the splitting of the Λ doublets greatly exaggerated. At high j values where the coupling approximates to Hunds case (b), the $\epsilon = +1$ (**e**) levels are higher than the $\epsilon = -1$ (**f**) levels for the $\Omega = 1/2$ ladder, and vice versa for the $\Omega = 3/2$ ladder. As j decreases the case (a) limit is approached, and the ordering of the Λ-doublets in the $\Omega = 1/2$ ladder reverses. For values of j of 7/2 or less, the $\epsilon = -1$ (**f**) level is higher than the $\epsilon = +1$ (**e**) level for both the $\Omega = 1/2$ and the $\Omega = 3/2$ ladder.

Alexander and Dagdigian (1984) have shown that, in so far as the levels tend towards case (b), the **e** level in the $^2\Pi_{3/2}$ ladder, and the **f** level in the $^2\Pi_{1/2}$ ladder are symmetric with respect to reflection in the plane of rotation of the molecule, whilst the other two states are antisymmetric.

5.3 The Story So Far

There have been a number of theoretical treatments of the excitation of OH in low energy collisions with H_2 molecules and, to date, they have exclusively treated collisions with para-H_2 constrained to its rotational ground state.

The first work on OH - H_2 collisions was the semi-quantitative treatment of Bertojo et al (1976), who treated the collision as occurring either along the V(A′) potential surface or the V(A″) surface, with the latter leading to a higher cross-section. They interpreted the preferential excitation of the Λ doublets in terms of the change in moment of inertia caused by the finite mass of the electrons. Although the argument was not correct (Alexander and Dagdigian, 1984), they correctly predicted anti-inversion in the $\Omega = 3/2$ ladder. The treatment of OH - spherical perturber type collisions in the case (a) limit has been discussed in detail by Alexander (1982, 1985) and close coupled calculations of OH - ground state para-H_2 in the case (b) limit using the potential of Kochanski and Flower (1981) have been reported by Dewangan and Flower (1981).

The CC equations for the intermediate coupling case can be formulated using either case (b) wavefunctions (cf. Dixon and Field, 1979), or case (a) wavefunctions. For the work reported here the nomenclature of Hunds case (a) coupling has been used, and the formulation of the equations with case (a) wavefunctions has been discussed by Dewangan and Flower (1983), Schinke and Andresen (1984) and Corey and Alexander (1988). The extent to which one level will be excited in preference to the other is governed by the amount by which the coupling deviates from pure case (a) coupling, and by the signs and relative magnitudes of the $\mu = 2$ terms in the potential expansion (equation 5.4.5). In particular it has been found that collisions with ground state para-H_2 have a tendency to invert doublets in the $\Omega = 1/2$ ladder (for $j \leq 7/2$) and anti-invert doublets in the $\Omega = 3/2$ ladder (Schinke and Andresen, 1984, Dewangan and Flower, 1985, Corey and Alexander, 1988). There was initially some confusion over phase factors which lead to the opposite conclusion in earlier work, but this has since been resolved (Alexander and Dagdigian, 1984, Andresen, Haüsler and Lülf, 1984, Dixon, Field and Zare, 1985, Dewangan and Flower, 1985).

The most complete experimental information on the system comes from the cross-beam measurements of Andresen, Haüsler and Lülf (1984). They studied inelastic collisions between the molecules in a rotationally cold OH beam, in which essentially all OH was in the $^2\Pi_{3/2}, j = 3/2$ ground state, and the H_2 molecules from a pulsed nozzle beam, at a collision energy of approximately 680cm^{-1}. The final level population of the beam was probed by laser induced fluorescence, and results were interpreted as relative integral cross-sections.

The results were presented as summed and averaged cross-sections (Schinke and Andresen, 1984) defined by:

$$\sigma(j_1 = 3/2, \Omega = 3/2 \rightarrow j_1'\Omega') = \frac{1}{2}\sum_{\epsilon\epsilon'}\sigma(j_1 = 3/2, \Omega = 3/2, \epsilon \rightarrow j_1'\Omega'\epsilon') \qquad 5.3.1$$

For $\Omega' = \Omega = 3/2$ transitions the experimental results showed cross-sections falling off rapidly with increasing Δj, whilst for $\Omega' \neq \Omega$ transitions the decrease was much slower. The large difference between $\Delta j = 1$ and $\Delta j = 2$ transitions for the former case was explained by the polar nature of the OH molecule.

In addition, Andresen et al (1984) also investigated the extent of preferential excitation of the Λ doublet substates by defining the quantity $\sigma^{\pm}/\sigma^{\mp}$ where:

$$\sigma^{\pm}(j_1'\Omega') = \frac{1}{2}\sum_{\epsilon}\sigma(j_1 = 3/2, \Omega = 3/2, \epsilon \rightarrow j_1'\Omega'\epsilon' = \pm) \qquad 5.3.2$$

Their results showed anti-inversion in the $\Omega = 3/2$ manifold ($\sigma^+ > \sigma^-$) and inversion in the $\Omega = 1/2$ manifold ($\sigma^- > \sigma^+$).

In order to compare with the experimental results, Schinke and Andresen (1984) performed calculations at the approximate experimental energy of 680cm^{-1}. They used the *ab initio* potential of Kochanski and Flower (1981), and employed the coupled states approximation (section 2.3). Their results showed qualitative agreement with the experiment concerning the Λ doublet populations, but the calculations predicted a much stronger preference for one of the Λ doublets than was found experimentally, especially for the $\Omega' = \Omega = 3/2$ transitions. They suggested that the discrepancy could be caused by an over estimation of the $\mu = 2$ term in the potential of Kochanski and Flower.

Dewangan et al (1986) performed close coupled calculations of the same system but used a potential in which the $\mu = 2$ term was smaller than the 'true' value by a factor of two. When comparing the average of their results at 556cm^{-1} and 834cm^{-1} with the experimental results they found better quantitative agreement with the experiment than was found for the calculations of Schinke and Andresen which used the larger $\mu = 2$ term. In particular, the quantity σ^+/σ^- gave much better agreement with experiment for transitions within the $\Omega = 3/2$ ladder, although the calculations still over estimated the extent of population inversion for transitions to the $\Omega = 1/2$ ladder.

In view of the fact that an erroneous value of the v_{22} term gave a better quantitative agreement with experiment (Dewangan et al 1986), subsequent calculations to determine the rate coefficients at low (interstellar) energies (Dewangan, Flower and Alexander, 1987) used a $v_{\lambda\mu} = v_{22}$ coefficient scaled by a factor of one half. This 'doctored' potential was also used by Corey and Alexander (1988) in a study of collision induced transitions between the hyperfine levels.

Following the results of the NH_3 - H_2 ($j > 0$) calculations which showed significant changes in the propensities towards certain transitions when rotationally excited H_2 replaced ($j = 0$) H_2 as the collision partner, it is interesting to extend this work to see how the OH - H_2 propensity rules are affected by inclusion of rotationally excited H_2, and whether the inclusion of ortho-H_2 can improve the agreement between theory and experiment.

5.4 Extension to OH - H_2 (j > 0)

5.4.1 Rotational Wavefunction

The rotational eigenfunctions for the OH in the intermediate coupling regime were given by equation 5.2.9a as:

$$\begin{aligned}\Psi_{\Omega=3/2}(j) &= a_j\psi^{(a)}_{\Omega=3/2}(j) - b_j\psi^{(a)}_{\Omega=1/2}(j)\\ \Psi_{\Omega=1/2}(j) &= a_j\psi^{(a)}_{\Omega=1/2}(j) + b_j\psi^{(a)}_{\Omega=3/2}(j)\end{aligned} \qquad 5.4.1$$

with a_j and b_j given by equation 5.2.9b. The case (a) rotational eigenfunctions are related to the primitive symmetric top functions $|j\Omega m\rangle$ by:

$$\psi^{(a)}_{\Omega}(j) = 2^{-1/2}(|j\Omega m\rangle|\Lambda\Sigma\rangle + \epsilon|j - \Omega m\rangle| - \Lambda - \Sigma\rangle) \qquad 5.4.2$$

Like the asymmetric top eigenfunctions (section 2.6.7), the intermediate coupling case eigenfunctions are linear combinations of primitive symmetric top eigenfunctions, and the coupling matrix elements are best evaluated using the $|j\Omega m\rangle$ from which the true coupling matrix elements may be formed by a linear combination of the simple coupling matrix elements.

The eigenfunctions of total angular momentum (excluding the electronic component) can then be formed as before from:

$$|j_1\Omega j_2 j_{12} l; JM\rangle = \sum_{\substack{m_1 m_2\\ m_{12} m_l}} C^{j_1\ j_2\ j_{12}}_{m_1 m_2 m_{12}} C^{j_{12}\ l\ J}_{m_{12} m_l M} |j_1\Omega m_1\rangle|j_2 m_2\rangle|lm\rangle \qquad 5.4.3$$

where the subscript (1) refers to the OH molecule and the subscript (2) to the H_2 molecule.

5.4.2 Potential Expansion

The body fixed potential expansion for OH - ground state para-H_2 can be written as:

$$V(R,\theta') = \sum_{\lambda\mu} v_{\lambda\mu}(R) D^{\lambda}_{\mu 0}(0,\theta',0) \qquad 5.4.4$$

This is of the same form as that used in the discussion of the atom - symmetric top problem except that now the potential expansion is independent of the angle, ψ'_1, which, in the case of OH, relates to the orientation of the electronic wavefunction about the internuclear axis. Thus the body fixed and molecule fixed frames are defined in such a way that the molecule fixed y'' and body fixed y' axes coincide, and the $x''z''$ and $x'z'$ planes are parallel.

The form of equation 5.4.4 was derived for the general case of a $^2\Pi$ molecule in collision with a spherical perturber by Alexander (1985), and it is readily extended to give the potential expansion for linear rotor - OH collisions:

$$V(R,\theta'_1,\theta'_2,\phi'_2) = \sum_{\substack{\lambda_1,\lambda_2 \\ \mu\nu}} v_{\lambda_1\mu\lambda_2\nu}(R) D^{\lambda_1}_{\mu\nu}(0,\theta'_1,0) Y^{\lambda_2}_{-\nu}(\theta'_2,\phi'_2) \qquad 5.4.5$$

The Euler angles appearing in equation 5.4.5 define a rotation taking the body fixed frame into the internal molecule fixed frame.

It is convenient to rewrite equation 5.4.5 by expressing the rotation matrix and spherical harmonics as products of reduced rotation matrices and exponential functions (cf eq. 2.6.15). Summing over the positive values of μ and ν only this gives:

$$\begin{aligned} V(R,\theta'_1,\theta'_2,\phi'_2) = & \sum_{\substack{\lambda_1\lambda_2 \\ \mu\geq 0,\nu\geq 0}} \frac{1}{(1+\delta_{\mu 0})(1+\delta_{\nu 0})} \left(\frac{2\lambda_2+1}{4\pi}\right)^{1/2} \\ & \times \left(v_{\lambda_1\mu\lambda_2\nu}(R) d^{\lambda_1}_{\mu\nu}(\theta'_1) d^{\lambda_2}_{0-\nu}(\theta'_2) e^{-i\nu\phi'_2} + v_{\lambda_1\mu\lambda_2-\nu}(R) d^{\lambda_1}_{\mu-\nu}(\theta'_1) d^{\lambda_2}_{0\nu}(\theta'_2) e^{i\nu\phi'_2}\right. \\ & \left. + v_{\lambda_1-\mu\lambda_2\nu}(R) d^{\lambda_1}_{-\mu\nu}(\theta'_1) d^{\lambda_2}_{0-\nu}(\theta'_2) e^{-i\nu\phi'_2} + v_{\lambda_1-\mu\lambda_2-\nu}(R) d^{\lambda_1}_{-\mu-\nu}(\theta'_1) d^{\lambda_2}_{0\nu}(\theta'_2) e^{i\nu\phi'_2}\right) \end{aligned} \qquad 5.4.6$$

For even μ we have the relationships:

$$\begin{aligned} v_{\lambda_1\mu\lambda_2\nu}(R) &= v_{\lambda_1-\mu\lambda_2-\nu}(R) \\ d^{\lambda}_{\mu\nu}(\theta) &= (-1)^{\nu} d^{\lambda}_{-\mu-\nu}(\theta) \\ Y^{\lambda}_{\nu}(\theta,\phi) &= (-1)^{\nu} Y^{\lambda *}_{-\nu}(\theta,\phi) \end{aligned} \qquad 5.4.7$$

using these, equation 5.4.6 can be rewritten as:

$$V(R,\theta_1',\theta_2',\phi_2') = \sum_{\substack{\lambda_1\lambda_2\nu \\ \mu\geq 0}} \left(\frac{2\lambda_2+1}{4\pi}\right)^{1/2} \frac{v_{\lambda_1\mu\lambda_2\nu}(R)}{(1+\delta_{\mu 0})} d^{\lambda_1}_{\mu\nu}(\theta_1') d^{\lambda_2}_{0-\nu}(\theta_2') \cos(\nu\phi_2') \quad 5.4.8a$$

or alternatively:

$$V(R,\theta_1',\theta_2',\phi_2') = \sum_{\substack{\lambda_1\lambda_2\mu \\ \nu\geq 0}} \left(\frac{2\lambda_2+1}{4\pi}\right)^{1/2} \frac{v_{\lambda_1\mu\lambda_2\nu}(R)}{(1+\delta_{\nu 0})} d^{\lambda_1}_{\mu\nu}(\theta_1') d^{\lambda_2}_{0-\nu}(\theta_2') \cos(\nu\phi_2') \quad 5.4.8b$$

Further use will be made of the above expressions in subsection 5.5.2.

5.4.3 The Coupling Matrix Elements

Combining the rotational wavefunction (eqn 5.4.2 and 5.4.3) and the space fixed potential expansion (eq 5.4.5), the coupling matrix elements required for solving the close coupled equations are a linear combination of functions of the form:

$$\begin{aligned} &\sum_{m's} C^{j_1\ j_2\ j_{12}}_{m_1 m_2 m_{12}} C^{j_{12}\ l\ J}_{m_{12} m_l M} C^{j_1'\ j_2'\ j_{12}'}_{m_1' m_2' m_{12}'} C^{j_{12}'\ l'\ J}_{m_{12}' m_l' M} \\ &\quad \times \langle l'm'|\langle j_2'm_2'|\langle j_1'\Omega'm_1'|\langle \Lambda'\Sigma'|V|\Lambda\Sigma\rangle|j_1\Omega m_1\rangle|j_2m_2\rangle|lm\rangle \end{aligned} \qquad 5.4.9$$

The potential cannot couple states of different Σ, being spin independent, and the innermost term becomes:

$$\langle \Lambda'\Sigma'|V|\Lambda\Sigma\rangle = \delta_{\Sigma\Sigma'}\,\delta_{\mu(\Lambda'-\Lambda)} \sum_{\substack{\lambda_1\lambda_2 \\ \mu\nu}} v_{\lambda_1\mu\lambda_2\nu} D^{\lambda_1}_{\mu\nu}(0,\theta_1',0) Y^{\lambda_2}_{-\nu}(\theta_2',\phi_2') \qquad 5.4.10$$

The possible Ω transitions are thus limited to the following eight:

	Ω	Ω'	μ	Ω	Ω'	μ
$\Sigma = +1/2$	-1/2	-1/2	0	3/2	-1/2	-2
	3/2	3/2	0	-1/2	3/2	2
$\Sigma = -1/2$	1/2	1/2	0	-3/2	1/2	2
	-3/2	-3/2	0	1/2	-3/2	-2

The selection rules reflected in equation 5.4.10 limit the possible values of μ to $0, \pm 2$.

The expression for the coupling matrix element for case (a) coupling is then the same as that given by equation 2.6.36, with the added restrictions on the value of μ:

$$\begin{aligned}\langle j_1' j_2' j_{12}' l' \Omega' \epsilon'; JM|V|j_1 j_2 j_{12} l \Omega \epsilon; JM\rangle = \sum_{\lambda_1 \lambda_2 \lambda} \frac{(-1)^{j_2'+j_1'-j_{12}-J-\Omega'}}{8\pi} \\ \times (1 - \epsilon\epsilon'(-1)^{j_1+j_1'+\lambda+\lambda_2})((2j_1+1)(2j_2+1)(2j_{12}+1)(2l+1) \\ \times (2j_1'+1)(2j_2'+1)(2j_{12}'+1)(2l'+1)(2\lambda_2+1)(2\lambda+1)^2)^{1/2} \\ \times \left[\begin{pmatrix} j_1' & \lambda_1 & j_1 \\ -\Omega' & 0 & \Omega \end{pmatrix} \delta_{\Omega\Omega'}\, v_{\lambda_1\lambda_2\lambda 0} + \epsilon \begin{pmatrix} j_1' & \lambda_1 & j_1 \\ -\Omega' & 2 & -\Omega \end{pmatrix} (1 - \delta_{\Omega\Omega'})\, v_{\lambda_1\lambda_2\lambda 2}\right] \\ \begin{pmatrix} j_2' & \lambda_2 & j_2 \\ 0 & 0 & 0 \end{pmatrix} \begin{pmatrix} l' & \lambda & l \\ 0 & 0 & 0 \end{pmatrix} \begin{Bmatrix} \lambda & j_{12} & j_{12}' \\ J & l' & l \end{Bmatrix} \begin{Bmatrix} j_{12} & j_2 & j_1 \\ j_{12}' & j_2' & j_1' \\ \lambda & \lambda_2 & \lambda_1 \end{Bmatrix}\end{aligned} \qquad 5.4.11$$

The minus sign in the parity factor is a consequence of the fact that Ω is now half integer.

It was shown in chapter two that the coupling matrix element vanishes unless:

$$\epsilon\epsilon'(-1)^{j_1-j_2-l+j_1'-j_2'-l'-2\Omega'+\mu} = (+1) \qquad 5.4.12$$

In the current case $2\Omega'$ is always odd, and μ is always even so this condition reduces to:

$$\epsilon(-1)^{j_1-j_2-l} = -\epsilon'(-1)^{-j_1'+j_2'+l'} \qquad 5.4.13$$

In addition we now have that $(-1)^{S+S'} = (-1)$ where S is the electronic spin of the OH molecule and $S = S' = 1/2$. Thus the condition for a non-vanishing coupling matrix element becomes:

$$\epsilon(-1)^{j_1-j_2-l+S} = \epsilon'(-1)^{j_1'-j_2'-l'+S'} \qquad 5.4.14$$

The two non-interacting parity blocks can be solved separately.

The coupling matrix element, equation 5.4.11 was derived using Hunds case (a) wavefunctions but, as discussed in section 5.2, the correct angular momentum coupling scheme for the OH molecule is intermediate between Hunds cases (a) and (b). Using the notation $\langle\Omega'|V_0|\Omega\rangle$ to refer to the terms in the case (a) coupling matrix element with $\mu = 0$, coupling Ω and Ω', $\epsilon\langle\Omega'|V_2|\Omega\rangle$ to refer to the terms with $\mu = 2$, and introducing $\tilde{\Omega}_1, \tilde{\Omega}_2$ where $\tilde{\Omega}_{1(2)} \neq \Omega_{1(2)}$, the coupling matrix element in the intermediate coupling regime becomes:

$$\begin{aligned} &a_j a_j'\langle\Omega'|V_0|\Omega\rangle + (-1)b_j b_j'\langle\tilde{\Omega}'|V_0|\tilde{\Omega}\rangle \\ &+\epsilon(-1)^{\Omega'+1/2}a_j b_j'\langle\Omega'|V_2|\tilde{\Omega}\rangle + \epsilon(-1)^{\Omega+1/2}b_j a_j'\langle\tilde{\Omega}'|V_2|\Omega\rangle \end{aligned} \qquad 5.4.15a$$

when $\Omega = \Omega'$ and:

$$\begin{aligned} &\epsilon a_j a_j'\langle\Omega'|V_2|\Omega\rangle + (-1)\epsilon b_j b_j'\langle\tilde{\Omega}'|V_2|\tilde{\Omega}\rangle \\ &+(-1)^{\Omega'+1/2}a_j b_j'\langle\Omega'|V_0|\tilde{\Omega}\rangle + (-1)^{\Omega+1/2}b_j a_j'\langle\tilde{\Omega}'|V_0|\Omega\rangle \end{aligned} \qquad 5.4.15b$$

when $\Omega \neq \Omega'$.

The magnitude of the intermediate case coupling matrix element (eq 5.4.15) is dependant on the sign of ϵ, which leads to the unequal excitation of the Λ doublets.

5.5 Interaction Potential

5.5.1 Details of the Potential Used

The interaction potential used in the present study is the OH – H_2 potential energy surface of Kochanski and Flower (1981). The potential data is available at a

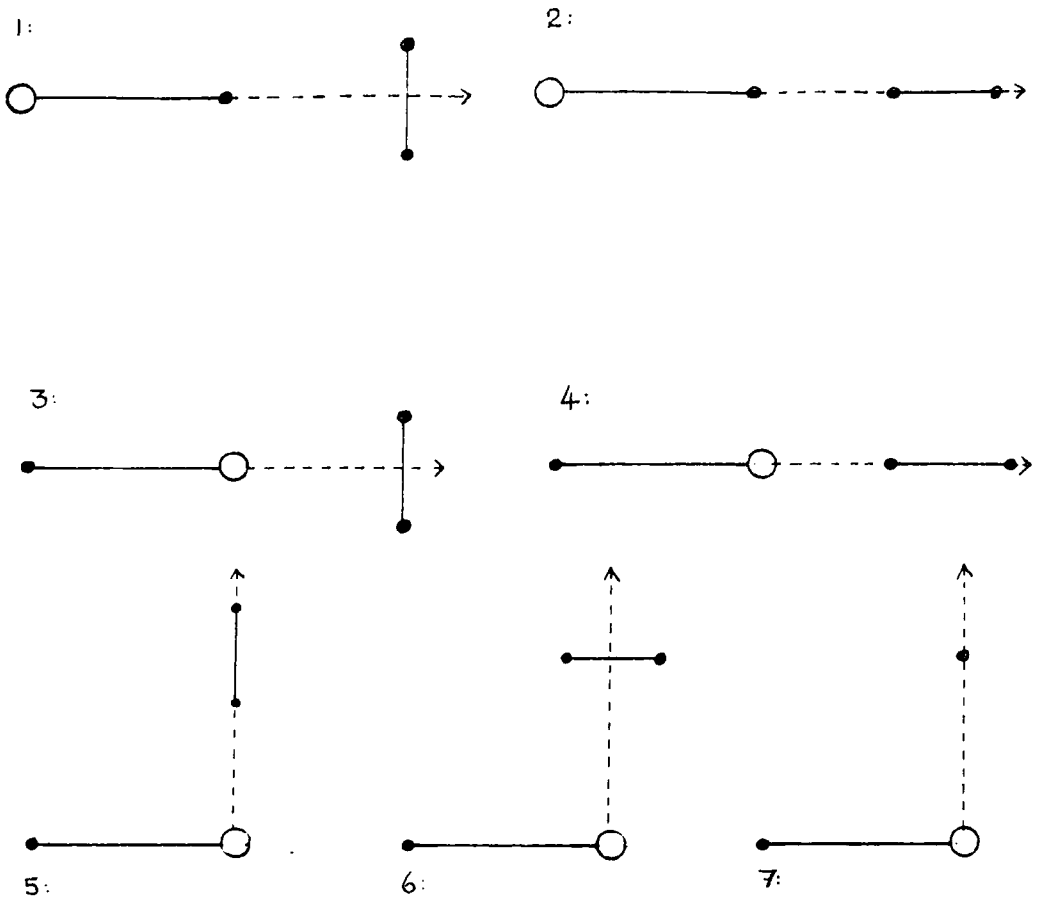

Figure 5.4: Geometries at which potential data was available

total of seven geometries, detailed in figure 5.4. The symmetry of the two collinear geometries correspond to the point group C_{∞}, whilst the remaining five correspond to the point group C_s, and give rise to two distinct potential curves, V(A′) and V(A″). The V(A′) surface is the least repulsive surface. It is symmetric with respect to reflection in the $x'z'$ plane, and corresponds to the surface with the unpaired π electronic wave function preferentially parallel to the $x'z'$ plane. The V(A″) surface is antisymmetric, and corresponds to the unpaired π electronic wave function lying perpendicular to the $x'z'$ plane.

The twelve separate potential energy curves that result, enable twelve $v_{\lambda_1\mu\lambda_2\nu}$ coefficients to be found, however only eleven are independent:

v_{0000}	$v_{2022} = v_{202-2}$
v_{1000}	v_{2200}
v_{2000}	v_{2210}
v_{0020}	v_{2220}
v_{1020}	v_{2222}
v_{2020}	v_{222-2} .

There are insufficient geometries to allow the $\nu = 1$ terms in the expansion to be evaluated, thus terms allowing the projection of the molecules rotational angular momentum on the intermolecular axis to change by ± 1 are omitted. The physical significance of this omission was discussed in chapter three.

5.5.2 Relationship between V(A′), V(A″) and the potential coefficients

To utilize the *ab initio* potential data, a relationship between the V(A′) and V(A″) surfaces and the potential expansion must be found.

In the OH molecule fixed frame the z''-axis is defined as lying along the internuclear axis, but the orientation of the x'' and y'' axes depend on the convention used. With the Euler angles used in equation 5.4.5 the OH molecule fixed $x''z''$ plane coincides with the body fixed $x'z'$ plane. Following Alexander (1985), a relationship between the body fixed v coefficients and the V(A′), V(A″) potential surfaces can be obtained by considering definite symmetry molecular electronic wavefunctions of the form:

$$|\bar{\Lambda}\eta\rangle = 2^{-1/2}(|\bar{\Lambda}\rangle + \eta|-\bar{\Lambda}\rangle) \qquad 5.5.1$$

where here $\bar{\Lambda} = |\Lambda|$, and $\eta = \pm 1$. When $\eta = +1$ this is antisymmetric with respect to reflection in the xz plane, when $\eta = -1$ it is symmetric (Alexander and Dagdigian, 1984).

The matrix elements of the interaction potential (eq 5.4.5) in the $|\bar{\Lambda}\eta\rangle$ basis can be written:

$$\langle\bar{\Lambda}'\eta'|V|\bar{\Lambda}\eta\rangle = \frac{1}{2}(\langle\bar{\Lambda}'| + \eta'\langle -\bar{\Lambda}'|) \sum_{\substack{\lambda_1\lambda_2 \\ \mu\nu}} v_{\lambda_1\mu\lambda_2\nu}(R) D^{\lambda_1}_{\mu\nu}(0,\theta_1',0) Y^{\lambda_2}_{-\nu}(\theta_2',\phi_2') \\ (|\bar{\Lambda}\rangle + \eta|-\bar{\Lambda}\rangle) \qquad 5.5.2$$

Using equation 5.4.10 we have that:

$$\langle\Lambda'|V|\Lambda\rangle = \sum_{\lambda_1\lambda_2\nu} v_{\lambda_2(\Lambda'-\Lambda)\lambda_2\nu}(R) D^{\lambda_1}_{(\Lambda'-\Lambda)\nu}(0,\theta_1',0) Y^{\lambda_2}_{-\nu}(\theta_2',\phi_2') \\ \equiv F_{\Lambda'-\Lambda} \qquad 5.5.3$$

In the case of a $^2\Pi$ molecule, $|\Lambda| = 1$, thus:

$$\langle\bar{\Lambda}'\eta'|V|\bar{\Lambda}\eta\rangle = \frac{F_0}{2} + \eta\eta'\frac{F_0}{2} + \frac{\eta}{2}(F_2 + \eta\eta' F_{-2}) \qquad 5.5.4$$

Adding $\langle\bar{\Lambda}+|V|\bar{\Lambda}+\rangle$ to $\langle\bar{\Lambda}-|V|\bar{\Lambda}-\rangle$, and using equation 5.4.8a to rewrite F_0 we have:

$$1/2(\langle\bar{\Lambda}+|V|\bar{\Lambda}+\rangle + \langle\bar{\Lambda}-|V|\bar{\Lambda}-\rangle) \\ = \sum_{\lambda_1\lambda_2\nu}\left(\frac{2\lambda_2+1}{4\pi}\right)^{1/2} \frac{v_{\lambda_1 0\lambda_2\nu}(R)}{2} d^{\lambda_1}_{0\nu}(\theta_1') d^{\lambda_2}_{0-\nu}(\theta_2')(e^{i\nu\phi_2'} + e^{-i\nu\phi_2'}) \qquad 5.5.5$$

Subtracting $\langle\bar{\Lambda}-|V|\bar{\Lambda}-\rangle$ from $\langle\bar{\Lambda}+|V|\bar{\Lambda}+\rangle$, and using equation 5.4.8b gives:

$$1/2(\langle\bar{\Lambda}+|V|\bar{\Lambda}+\rangle - \langle\bar{\Lambda}-|V|\bar{\Lambda}-\rangle) \\ = \sum_{\lambda_1\lambda_2\nu}\left(\frac{2\lambda_2+1}{4\pi}\right)^{1/2} \frac{v_{\lambda_1 2\lambda_2\nu}(R)}{2} d^{\lambda_1}_{2\nu}(\theta_1') d^{\lambda_2}_{0-\nu}(\theta_2')(e^{i\nu\phi_2'} + e^{-i\nu\phi_2'}) \qquad 5.5.6$$

The $|\bar{\Lambda}+\rangle$ states are antisymmetric under reflection in the $x'z'$ plane and the $|\bar{\Lambda}-\rangle$ are symmetric so one can identify:

$$\langle\bar{\Lambda}+|V|\bar{\Lambda}+\rangle \equiv \mathrm{V(A'')} \\ \langle\bar{\Lambda}-|V|\bar{\Lambda}-\rangle \equiv \mathrm{V(A')} \qquad 5.5.7$$

Explicitly, for the coefficients $\lambda_1 = 0, 1, 2$, $\lambda_2 = 0, 2$, and $\nu = 0, 2$ this gives:

$$1/2(\mathrm{V(A'')} + \mathrm{V(A')}) = \sum_{\lambda_1=0}^{2} \left[\frac{v_{\lambda_1 000}}{2\pi^{1/2}} + \left(\frac{5}{16\pi}\right)^{1/2} v_{\lambda_1 020}(3\cos^2\theta_2' - 1) \right] d^0_{00}(\theta_1') + \left(\frac{15}{32\pi}\right)^{1/2} v_{2022}\, 2\sin^2\theta_2'\, \cos(2\phi_2')\, d^2_{02}(\theta_1') \qquad 5.5.8a$$

where $\phi_2' = 0, \pi/2$, and:

$$1/2(\mathrm{V(A'')} - \mathrm{V(A')}) = \left[\frac{v_{2200}}{2\pi^{1/2}} + \left(\frac{5}{16\pi}\right)^{1/2} v_{2220}(3\cos^2\theta_2' - 1) \right] d^2_{20}(\theta_1') + \left(\frac{15}{32\pi}\right)^{1/2} v_{2222}\, 2\sin^2\theta_2'\, \cos(2\phi_2')\, d^2_{22}(\theta_1') + \left(\frac{15}{32\pi}\right)^{1/2} v_{222-2}\, 2\sin^2\theta_2'\, \cos(2\phi_2')\, d^2_{2-2}(\theta_1') \qquad 5.5.8b$$

From henceforth the potential expansion coefficients obtained in this way will be referred to as the 'true' potential.

5.5.3 The 'doctored' potential

For the OH – ground state para-H_2 collision system Dewangan, Flower and Danby (1986) found that better agreement with the experimental data was obtained using a $\mu = 2$ term smaller by a factor of two than that which would be obtained using the above argument. Subsequent calculations on the OH ground state para-H_2 collision problem used this 'doctored' potential. The smaller $\mu = 2$ term was originally obtained by expanding the OH – spherical perturber potential in the form:

$$V(R, \theta_1', \psi_1') = \sum_{\lambda\mu} v_{\lambda\mu}(R) Y^{\lambda}_{\mu}(\theta_1', \psi_1') \qquad 5.5.9$$

This differs from that derived by Alexander (1985) in that the angle describing the orientation of the OH electronic wavefunction, ψ_1', is explicitly included (Dewangan et al, 1986). To relate equation 5.5.9 to the V(A') and V(A'') potential surfaces, the V(A') surface is identified with $\psi_1' = \pi/2$, and the V(A'') surface is identified with $\psi_1' = 0$ expansion.

Whilst this does not correctly represent the system (Dewangan et al, 1987), the smaller $\mu = 2$ terms that resulted from this treatment gave better agreement with the experimental data than did the 'true' $\mu = 2$ terms.

For a full comparison with previous results both the 'doctored' potential and the true potential were used in the present calculation, and for consistency, the derivation of the 'doctored' potential for the OH – linear rotor case is given here.

The OH – linear rotor equivalent of equation 5.5.9 is:

$$V(R,\theta_1',\psi_1',\theta_2',\phi_2') = \sum_{\substack{\lambda_1\lambda_2\\ \mu\nu}} v_{\lambda_1\mu\lambda_2\nu}(R) D^{\lambda_1}_{\mu\nu}(0,\theta_1',\psi_1') Y^{\lambda_2}_{-\nu}(\theta_2',\phi_2'). \qquad 5.5.10$$

Making the identification

$$\mathrm{V(A'')} \equiv \psi_1' = 0 \qquad \mathrm{V(A')} \equiv \psi_1' = \pi/2 \qquad 5.5.11$$

we can write:

$$\begin{aligned} \mathrm{V(A'')}(R,\theta_1',\theta_2',\phi_2') &= \sum_{\substack{\lambda_1\lambda_2\\ \mu\nu}} v_{\lambda_1\mu\lambda_2\nu}(R) D^{\lambda_1}_{\mu\nu}(0,\theta_1',0) Y^{\lambda_2}_{-\nu}(\theta_2',\phi_2') \\ \mathrm{V(A')}(R,\theta_1',\theta_2',\phi_2') &= \sum_{\substack{\lambda_1\lambda_2\\ \mu\nu}} v_{\lambda_1\mu\lambda_2\nu}(R) D^{\lambda_1}_{\mu\nu}(0,\theta_1',\pi/2) Y^{\lambda_2}_{-\nu}(\theta_2',\phi_2') \end{aligned} \qquad 5.5.12$$

From the definition of the rotation matrices (equation 2.6.6),

$$\begin{aligned} D^{\lambda_1}_{0\nu}(0,\theta_1,\pi/2) &= D^{\lambda_1}_{0\nu}(0,\theta_1,0) \\ D^{\lambda_1}_{2\nu}(0,\theta_1,\pi/2) &= -D^{\lambda_1}_{2\nu}(0,\theta_1,0) \end{aligned} \qquad 5.5.13$$

Substituting 5.5.13 into 5.5.12 gives:

$$\begin{aligned} \begin{Bmatrix} \mathrm{V(A'')} \\ \mathrm{V(A')} \end{Bmatrix} = & \sum_{\lambda_1\lambda_2\nu} v_{\lambda_1 0\lambda_2\nu}(R) D^{\lambda_1}_{0\nu}(0,\theta_1',0) Y^{\lambda_2}_{-\nu}(\theta_2',\phi_2') \\ & \pm \sum_{\lambda_1\lambda_2\nu} [v_{\lambda_1 2\lambda_2\nu}(R) D^{\lambda_1}_{2\nu}(0,\theta_1',0) Y^{\lambda_2}_{-\nu}(\theta_2',\phi_2') \\ & + v_{\lambda_1 2\lambda_2 -\nu}(R) D^{\lambda_1}_{2-\nu}(0,\theta_1',0) Y^{\lambda_2}_{+\nu}(\theta_2',\phi_2')] \end{aligned} \qquad 5.5.14$$

where we have made use of the relationships summarized by equation 5.4.7. Here the upper sign refers to V(A″) and the lower sign to V(A′). Adding V(A″) and V(A′) gives the same result as equation 5.5.5 but subtracting gives:

$$1/2(\mathrm{V(A'')} - \mathrm{V(A')}) = \sum_{\lambda_1\lambda_2\nu} v_{\lambda_1 2\lambda_2\nu}(R) \left(\frac{2\lambda_2+1}{4\pi}\right)^{1/2} d^{\lambda_1}_{2\nu}(\theta'_1) d^{\lambda_2}_{0-\nu}(\theta'_2)\, 2\cos(\nu\phi'_2) \qquad 5.5.15$$

Thus when this derivation is used *all* the $\mu = 2$ terms are smaller by a factor of two.

5.5.4 Fitting of the potential surface

The method used for interpolation and fitting of both the SCF and dispersion energy surfaces was basically the same as that discussed for the NH_3 - H_2 collision so the method will only be described in outline here.

The potential data points were given at intermolecular distances of 4 to 10au, in steps of 0.5au, with an additional long range dispersion data point at 80au. The analytical form of the long range electrostatic terms included in the SCF fitting procedure, were taken from the paper of Kochanski and Flower (1981) and include terms proportional to $\mu_{(1)}\Theta_{zz(2)}/R^4$, $\Theta_{zz(1)}\Theta_{(2)}/R^5$ and $(\Theta_{xx} - \Theta_{yy})_{(1)}\Theta_{(2)}/R^5$, where $\mu_{(1)}$ is the dipole moment of the OH molecule, $(\Theta_{xx}, \Theta_{yy}, \Theta_{zz})_{(1)}$ are the diagonal elements of the OH quadrupole moments, and $\Theta_{(2)}$ is the H_2 quadrupole moment. Values of $\mu_{(1)} = 0.87$, $(\Theta_{xx} - \Theta_{yy})_{(1)} = 1.37$, $\Theta_{zz(1)} = 1.20$ and $\Theta_{(2)} = 0.42$ atomic units were used (Kochanski and Flower, 1981). Again we note that, in contrast to NH_3 - H_2 collisions this does not include the $\nu = 1$ terms.

The dispersion surface was fitted using an expansion of the form given by equation 3.4.6, but including fourteen terms, and fitting using the NAG routine F04JAF.

The potential expansion coefficients were calculated by fitting the average of the two potential surfaces, V(A″) and V(A′), and half the difference to functions of the form given by equations 5.5.8 or 5.5.15. For the collinear geometries the two potential surfaces are degenerate, and only the average is non-zero.

The angular functions appearing in equation 5.5.8 are given in table 5.1. In the first case, for 1/2(V(A″)+V(A′)), there are seven equations for seven unknowns, but when the difference of the two potential surfaces is taken there are five available pieces of information for only four unknowns.

5.1: Numerical value of the Angular Functions

coefficient	Configuration						
$\lambda_1\mu\lambda_2\nu$	1	2	3	4	5	6	7
0 0 0 0	0.282	0.282	0.282	0.282	0.282	0.282	0.282
1 0 0 0	-0.282	-0.282	0.282	0.282	0.000	0.000	0.000
2 0 0 0	0.282	0.282	0.282	0.282	-0.141	-0.141	-0.141
0 0 2 0	-0.315	0.631	-0.315	0.631	0.000	0.000	0.000
1 0 2 0	0.315	-0.631	-0.315	0.631	-0.316	0.158	0.158
2 0 2 0	-0.315	0.631	-0.315	0.631	-0.316	0.158	0.158
2 0 2 2	0.000	0.000	0.000	0.000	0.000	0.473	-0.473
2 2 0 0	0.000		0.000		0.173	0.173	0.173
2 2 2 0	0.000		0.000		0.387	-0.193	-0.193
2 2 2 2	0.000		0.387		0.000	0.097	-0.097
2 2 2-2	0.387		0.000		0.000	0.097	-0.097
divide the $\mu = 2$ terms by two for the 'doctored' potential							

To evaluate the potential expansion coefficients, the simultaneous equations were solved using the NAG routine F04JAF and a final check on the adequacy of the potential fit was carried out by reversing the process, using the calculated potential coefficients to regain the potential surfaces. The results for two of the configurations, 2 and 7′, are given in table 5.2a and b. The agreement between the data and fit is clearly better for configuration 2, which used only the V(A″)+V(A′)

fit, than for configuration 7'which makes use of the V(A'')−V(A') fit. However, the latter is not necessarily less accurate, and may give a closer representation of the true potential as extra information is available.

5.2(a) and (b):SCF fits for configurations 2 and 7' (long range)

configuration 2				configuration 7'			
R	fit	data	$E_{induction}$	R	fit	data	$E_{induction}$
8.0	2.760	2.760		8.0	-0.223	-0.256	
8.5	2.138	2.138		8.5	-0.142	-0.153	
9.0	1.756	1.756		9.0	-0.066	-0.088	-0.107
9.5	1.466	1.466		9.5	-0.040	-0.054	
10.0	1.237	1.237	1.399	10.0	-0.022	-0.035	-0.063
15.0	0.256		0.256	15.0	-0.527		
20.0	0.078		0.078	20.0	-0.001		-0.002

The body fixed potential coefficients were converted into their space fixed form using the conversion 2.6.27, and the calculated potential coefficients are given in appendix E.

5.6 Low Energy Calculation ($190cm^{-1}$)

5.6.1 Integration of the coupled equations

The rotational constant of the OH molecule in its ground state is $B_0 = 18.52cm^{-1}$ (Poynter and Beaudet, 1968). This compares to $B_0 = 9.94cm^{-1}$ for the NH_3 molecule (Green, 1976), thus the OH molecule, with wider spaced energy levels, is more amenable to a full close coupled treatment than is the NH_3 molecule. However, for collisions with a linear rotor molecule it is still a sizeable calculation.

The energies of the first few rotational levels can be calculated using the formula (Bertojo et al, (1976)):

$$E_{rot} = B_0 \left\{ \left(j(j+1) - \frac{3}{4} \right) \pm \frac{X}{2} \right\} \qquad 5.6.1$$

where the '+' sign gives the $\Omega = 1/2$ state and the '$-$' sign gives the $\Omega = 3/2$ state. X is given by equation 5.2.9c.

With $B_0 = 18.52$ and $\lambda = -7.501$ the energies in inverse centimetres relative to the ground state are:

j	$E_{\Omega=1/2}$	$E_{\Omega=3/2}$
1/2	126.06	
3/2	187.28	0.0
5/2	288.63	83.85
7/2	429.39	202.37
9/2	608.94	356.18

A collision energy of 190.0cm^{-1} was chosen for the calculations.

Once again, the problem of basis set size has to be considered. For the OH basis, basis set convergence tests were done using basis sets consisting of the energetically lower 12, 14 and 16 rotational levels, and a fourth basis set of 14 levels with the $(9/2, 1/2, \pm)$ states replaced by the $(7/2, 3/2, \pm)$ states. The results of the tests are shown in table 5.3, a B16 basis set was chosen for the full calculation.

For collisions with ortho-H_2 a basis set consisting of only the $(j = 1)$ level was employed on the H_2 molecule. The rationale for this being that the studies of rotational excitation of the NH_3 molecule reported in chapter three suggested that the results were not significantly altered if the $(j_2 = 3)$ level was included in the basis set.

For collisions with para-H_2 a number of approaches were used. Initially, to draw a clean comparison between the ortho-H_2 results and those that would be obtained by treating the Hydrogen molecules as spherically symmetric collision partners, a $(j_2 = 0)$ only basis set was used. These calculations were supplemented

5.3: OH basis convergence tests

Basis set convergence tests at an energy of 190cm^{-1}, using the first two partial waves ($J_{tot} = 1/2, 3/2$), and a ($j = 0$) only basis set on the H_2 .

Transition	Basis Set				
$j\epsilon \rightarrow j'\epsilon'$	B10	B12	B14	B14a	B16
$\Omega = \Omega' = 3/2$					
$3/2+ \rightarrow 3/2-$	0.12	0.12	0.12	0.12	0.13
$3/2+ \rightarrow 5/2+$	0.20	0.20	0.21	0.20	0.21
$3/2+ \rightarrow 5/2-$	0.02	0.02	0.02	0.02	0.02
$3/2- \rightarrow 5/2+$	0.07	0.07	0.07	0.07	0.07
$3/2- \rightarrow 5/2-$	0.17	0.18	0.18	0.18	0.18
$5/2+ \rightarrow 5/2-$	0.02	0.02	0.01	0.02	0.02
$\Omega = \Omega' = 1/2$					
$1/2+ \rightarrow 1/2-$	0.02	0.03	0.03	0.04	0.04
$1/2+ \rightarrow 3/2+$	0.37	0.33	0.33	0.34	0.34
$1/2+ \rightarrow 3/2-$	0.09	0.10	0.10	0.10	0.10
$1/2- \rightarrow 3/2+$	0.03	0.02	0.02	0.02	0.02
$1/2- \rightarrow 3/2-$	0.33	0.27	0.27	0.28	0.28
$3/2+ \rightarrow 3/2-$	3.40	4.23	4.19	4.08	4.03

continued overleaf...

table 5.3 continued: Ω changing transitions

Transition	Basis Set				
$j\epsilon \rightarrow j'\epsilon'$	B10	B12	B14	B14a	B16
$\Omega = 3/2, \Omega' = 1/2$					
$3/2+ \rightarrow 1/2+$	0.001	0.001	0.001	0.001	0.001
$3/2+ \rightarrow 1/2-$	0.046	0.050	0.049	0.051	0.050
$3/2+ \rightarrow 3/2+$	0.023	0.027	0.027	0.028	0.028
$3/2+ \rightarrow 3/2-$	0.047	0.040	0.044	0.047	0.047
$3/2- \rightarrow 1/2+$	0.035	0.040	0.041	0.040	0.041
$3/2- \rightarrow 1/2-$	0.010	0.013	0.012	0.012	0.012
$3/2- \rightarrow 3/2+$	0.016	0.021	0.021	0.021	0.021
$3/2- \rightarrow 3/2-$	0.045	0.054	0.053	0.055	0.055
$5/2+ \rightarrow 1/2+$	0.017	0.019	0.021	0.019	0.021
$5/2+ \rightarrow 1/2-$	0.019	0.022	0.024	0.023	0.024
$5/2+ \rightarrow 3/2+$	0.006	0.008	0.008	0.007	0.007
$5/2+ \rightarrow 3/2-$	0.042	0.045	0.046	0.049	0.049
$5/2- \rightarrow 1/2+$	0.008	0.010	0.011	0.011	0.010
$5/2- \rightarrow 1/2-$	0.010	0.014	0.015	0.015	0.015
$5/2- \rightarrow 3/2+$	0.060	0.064	0.067	0.067	0.070
$5/2- \rightarrow 3/2-$	0.015	0.013	0.014	0.014	0.015

by calculations with a more complete ($j_2 = 0, 2$) hydrogen basis set. In addition, calculations were performed with a ($j_2 = 2$) only basis set. The implicit assumption made is then that the ($j_2 = 2$) rotational state of H_2 is not significantly coupled to the other para-H_2 rotational states at the collision energy used. This is an equivalent assumption to that implicit in the use of a ($j_2 = 0$) only basis set.

The calculations with the ($j_2 = 0$) and ($j_2 = 1$) hydrogen basis sets were performed using both the 'true' potential expansion obtained by fitting the potential to a potential expansion of the form given by equation 5.4.5, and the 'doctored' potential, obtained by fitting the potential an expansion of the form of equation 5.5.10, in which the $\mu = 2$ terms are smaller by a factor of two. For the large basis set para-H_2 collision and the ($j_2 = 2$) collision only the 'true' potential was used.

The coupled equations were integrated with the Manolopoulos integrator using the MOLSCAT computer code (Hutson and Green, 1986). The alterations that were necessary to treat the OH - H_2 collision are detailed in appendix C. In particular, it was necessary to adapt MOLSCAT to deal with half integral angular momentum. The alterations were checked at every stage both by comparing para ($j = 0$) H_2 results with those of Dewangan and Flower (1983), and by comparing results for a model system with integer angular momentum and pure case (a) coupling with results obtained using the symmetric top - linear rotor program which it then resembles.

The ortho-H_2 and ground state para-H_2 calculations were performed on the Amdahl 5860 at Durham. Typical times per partial wave were 308 cpu seconds for para-H_2 and 4900 cpu seconds for *one of the two non-interacting symmetry blocks* for ortho-H_2. A maximum of 300000 eight byte words of storage were required for the ortho-H_2 collisions. The remaining para-H_2 calculations were integrated on the CRAY XMP at Rutherford where typical CPU times per partial wave were 1000 CPU seconds for the $j_2 = 0, 2$ calculation.

5.4:Inelastic cross-sections at 190cm^{-1}

Cross-sections (in units of 10^{-16}cm^2) for both potential surfaces.

Transition	'true' potential				'doctored' potential	
$j\epsilon \rightarrow j'\epsilon'$	$(j_2 = 0)$	$(j_2 = 0, 2)$	$(j_2 = 2)$	$(j_2 = 1)$	$(j_2 = 0)$	$(j_2 = 1)$
$\Omega = \Omega' = 3/2$						
$3/2+ \rightarrow 3/2-$	10.6	12.1	21.4	22.9	9.93	23.5
$3/2+ \rightarrow 5/2+$	3.91	4.26	7.95	7.08	3.19	6.70
$3/2+ \rightarrow 5/2-$	1.58	1.16	5.22	4.36	1.08	3.82
$3/2- \rightarrow 5/2+$	4.56	2.56	5.96	5.21	2.18	4.10
$3/2- \rightarrow 5/2-$	3.34	3.74	7.38	7.07	3.00	6.64
$5/2+ \rightarrow 5/2-$	7.99	8.29	18.9	23.0	7.06	24.0
$\Omega = \Omega' = 1/2$						
$1/2+ \rightarrow 1/2-$	10.6	10.3	18.8	22.7	12.3	14.4
$1/2+ \rightarrow 3/2+$	0.450	1.01	1.55	1.48	0.731	2.53
$1/2+ \rightarrow 3/2-$	0.198	0.237	1.39	1.00	0.204	1.77
$1/2- \rightarrow 3/2+$	0.0651	0.335	1.14	0.980	0.0431	1.65
$1/2- \rightarrow 3/2-$	0.284	0.647	1.56	1.54	0.602	2.49
$3/2+ \rightarrow 3/2-$	2.19	5.63	27.8	35.7	7.98	43.0

continued overleaf...

table 5.4 continued :Inelastic cross-sections at 190cm^{-1} for Ω changing transitions.

Transition	'true' potential				'doctored' potential	
$j\epsilon \rightarrow j'\epsilon'$	$j_2 = 0$	$j_2 = 0, 2$	$j_2 = 2$	$j_2 = 1$	$j_2 = 0$	$j_2 = 1$
$\Omega = 3/2, \Omega' = 1/2$						
$3/2+ \rightarrow 1/2+$	0.296	0.230	1.37	1.20	0.272	0.595
$3/2+ \rightarrow 1/2-$	2.32	1.98	2.14	1.94	0.975	0.956
$3/2+ \rightarrow 3/2+$	0.268	0.268	0.251	0.179	0.0865	0.0814
$3/2+ \rightarrow 3/2-$	0.324	0.447	0.212	0.242	0.135	0.126
$3/2- \rightarrow 1/2+$	2.38	2.12	2.07	1.97	0.749	0.874
$3/2- \rightarrow 1/2-$	0.439	0.527	1.30	1.24	0.273	0.677
$3/2- \rightarrow 3/2+$	0.184	0.305	0.169	0.220	0.0591	0.127
$3/2- \rightarrow 3/2-$	0.399	0.375	0.237	0.241	0.177	0.136
$5/2+ \rightarrow 1/2+$	1.11	0.956	1.33	1.31	0.400	0.625
$5/2+ \rightarrow 1/2-$	0.927	0.804	1.28	1.37	0.359	0.685
$5/2+ \rightarrow 3/2+$	0.0252	0.119	0.209	0.249	0.0311	0.142
$5/2+ \rightarrow 3/2-$	0.360	0.559	0.318	0.432	0.144	0.201
$5/2- \rightarrow 1/2+$	0.739	0.747	1.38	1.26	0.413	0.603
$5/2- \rightarrow 1/2-$	0.868	1.01	1.60	1.74	0.377	0.867
$5/2- \rightarrow 3/2+$	0.745	0.807	0.463	0.522	0.201	0.201
$5/2- \rightarrow 3/2-$	0.0816	0.172	0.301	0.316	0.0389	0.348

5.5: σ^+, σ^- and their ratio, R, for all results.

σ^+, σ^- and their ratio, R = $\sigma^{max}/\sigma^{min}$, for all results. For each Hydrogen basis set the first entry was obtained with the 'true' potential and the second with the 'doctored' potential.

j_1', Ω'	$j_2 = 1$			$j_2 = 0$			$j_2 = 0, 2$		
	σ^+	σ^-	R	σ^+	σ^-	R	σ^+	σ^-	R
1/2, 1/2	1.59	1.59	1.00	1.34	1.18	1.26	1.18	1.26	1.07
	0.74	0.82	1.11	0.51	0.63	1.22			
1/2, 3/2	.20	.25	1.22	.23	.36	1.60	.29	.41	1.43
	.11	.13	1.26	.08	.16	2.14			
5/2, 3/2	6.15	5.70	1.08	4.23	2.46	1.72	3.41	2.45	1.39
	5.40	5.25	1.03	2.69	2.04	1.32			

5.6.2 Discussion

In order to study the trends in behaviour, it is useful to discuss the quantity σ^+/σ^- (or σ^-/σ^+ for interladder transitions) as defined by equation 5.3.2. Table 5.5 gives the values of σ^+, σ^- and their ratio for all the rotational levels accessible at 190cm^{-1}. The table gives some indication of the strength of the preferential excitation of the Λ doublets for each set of results.

We first briefly compare the results obtained with the 'doctored' potential with those obtained using the 'true' potential. It is clear from table 5.5 that for both ($j_2 = 1$) and ($j_2 = 0$) collisions, the propensities toward preferential excitation of one or other of the Λ doublets are greater with the 'doctored' potential for $\Omega \neq \Omega'$ transitions, and greater with the 'true' potential for $\Omega = \Omega'$ transitions. This is to be expected in view of the fact that the $\mu = 2$ terms in the potential expansion

act as the interference terms for $\Omega = \Omega'$ transitions, whilst they directly drive the $\Omega \neq \Omega'$ transitions. In the latter the $\mu = 0$ terms act as interference terms, and these are *relatively* larger in the 'doctored' potential. In previous OH – para-H_2 collisions (Dewangan, Flower and Danby, 1986) the 'doctored' potential was found to give better agreement with experimental results than the 'true' potential and it is noteworthy that when the 'doctored' potential was used it was the $\Omega = \Omega'$ transitions that showed improved agreement with the experiment.

We now compare results obtained with different H_2 basis sets.

Para (j = 0) H_2 versus Ortho (j = 1) H_2

As might be expected, the cross-sections for ortho-H_2 transitions are in general larger than the corresponding para-H_2 cross-sections at least for $\Omega = \Omega'$ transitions.

From table 5.5. it can be seen that the overall effect of replacing ground state para-H_2 by ground state ortho-H_2 as the collision partner is to reduce the strength of the propensities leading to preferential excitation of the Λ doublets. This is a consequence of the additional number of terms contributing to the coupling matrix element sum for each transition, leading to a reduction in the propensities. In particular, the potential matrix now contains terms allowing the projection of j_1 on the intermolecular axis to change. As this is principally a damping effect caused by the increased number of terms contributing to the coupling matrix element sum, it is independent of the relative magnitudes of the $\mu = 0$ and $\mu = 2$ terms, and decreases the propensities for both Ω changing and Ω conserving transitions.

A more direct comparison between the ortho and para-H_2 collisions can be made by considering the ratio of the cross-sections obtained with a ($j_2 = 1$) calculation to cross-sections for the same transition with a ($j_2 = 0$) calculation. Such a comparison is made in table 5.6, and it can be seen that the ortho-H_2 cross-sections are consistently larger than the ground state para-H_2 cross-sections.

For the $\Omega \neq \Omega'$ transitions the cross-sections tend to be of a similar magnitude for both ortho and para-H_2 collisions however some qualitative differences in behaviour are evident. In particular, cross-sections for the transitions ($j_1 \Omega \epsilon = j \, \frac{3}{2} \pm \rightarrow (j \pm 1) \, \frac{1}{2} \pm$) are consistently larger for ortho-H_2 collisions than for para-H_2 collisions. This is analogous to the strong propensity rules noted for NH_3–para-H_2

5.6: Comparison between results with different hydrogen basis sets

Transition	$\sigma(j=1)/\sigma(j=0)$		$\sigma(j=0,2)/\sigma(j=0)$
$j\epsilon \rightarrow j'\epsilon'$	'true' potential	'doctored' potential	'true' potential
	$\Omega = \Omega' = 3/2$		
$3/2+ \rightarrow 3/2-$	2.15	2.37	1.14
$3/2+ \rightarrow 5/2+$	1.81	2.10	1.09
$3/2+ \rightarrow 5/2-$	2.76	3.54	0.73
$3/2- \rightarrow 5/2+$	1.14	1.88	0.85
$3/2- \rightarrow 5/2-$	2.12	2.21	1.00
$5/2+ \rightarrow 5/2-$	2.87	3.40	1.38
	$\Omega = \Omega' = 1/2$		
$1/2+ \rightarrow 1/2-$	2.14	1.17	0.97
$1/2+ \rightarrow 3/2+$	3.29	3.46	2.24
$1/2+ \rightarrow 3/2-$	5.05	8.68	1.19
$1/2- \rightarrow 3/2+$	15.1	38.3	5.15
$1/2- \rightarrow 3/2-$	5.22	4.14	2.28
$3/2+ \rightarrow 3/2-$	16.3	5.39	2.57

continued overleaf...

table 5.6 continued: Comparison between results with different hydrogen basis sets for Ω changing transitions.

Transition	$\sigma(j=1)/\sigma(j=0)$		$\sigma(j=0,2)/\sigma(j=0)$
$j\epsilon \rightarrow j'\epsilon'$	'true' potential	'doctored' potential	'true' potential
	$\Omega = 3/2, \Omega' = 1/2$		
$3/2+ \rightarrow 1/2+$	4.05	2.19	0.777
$3/2+ \rightarrow 1/2-$	0.836	0.981	0.853
$3/2+ \rightarrow 3/2+$	0.668	0.941	1.00
$3/2+ \rightarrow 3/2-$	0.747	0.933	1.38
$3/2- \rightarrow 1/2+$	0.828	1.17	0.891
$3/2- \rightarrow 1/2-$	2.82	2.48	1.20
$3/2- \rightarrow 3/2+$	1.20	2.14	1.66
$3/2- \rightarrow 3/2-$	0.604	0.768	0.940
$5/2+ \rightarrow 1/2+$	1.18	1.56	0.861
$5/2+ \rightarrow 1/2-$	1.48	1.91	0.867
$5/2+ \rightarrow 3/2+$	9.88	4.57	4.72
$5/2+ \rightarrow 3/2-$	1.20	1.39	1.55
$5/2- \rightarrow 1/2+$	1.71	1.46	1.01
$5/2- \rightarrow 1/2-$	2.00	2.30	1.16
$5/2- \rightarrow 3/2+$	0.701	1.00	1.08
$5/2- \rightarrow 3/2-$	3.87	8.95	2.11

collisions (sections 3.5.2 and 3.6.2), but the effect is heavily damped here by the mixing of the $\Omega = 3/2$ and $\Omega = 1/2$ states.

For interladder transitions the *major* contribution to the coupling matrix element comes from the $\mu = 2$ terms. The parity factor in the coupling matrix element is:

$$p = (1 - \epsilon\epsilon'(-1)^{j_1+j_1'+\lambda}) \qquad 5.6.3$$

For $\Delta j = 1$ transition, $(j_1 + j_1')$ is always an even integer. From the 3-j symbols, $\lambda = \lambda_1$, and:

$$\begin{aligned} \lambda_1 &= |j_1 - j_1'| \ldots (j_1 + j_1') \\ &= 1, 2, \ldots, (j_1 + j_1' - 1), (j_1 + j_1') \end{aligned} \qquad 5.6.4$$

For $\mu = 2$ terms, $\lambda_1 \geq 2$. With the potential employed here, $\lambda_1 \leq 2$ only terms are present, and the parity factor vanishes if $\epsilon = \epsilon'$. With ortho-H_2 as the collision partner, however, λ may take all values between $\lambda_1 - 2$ and $\lambda_1 + 2$, and the parity factor no longer vanishes for all terms in the sum. A more complete potential including terms with $\lambda_1 > 2$ would, presumably, reduce this difference. It should be noted here that this does not directly affect the mechanism of preferential excitation of the lambda doublets as it effects transitions to the $\epsilon = \pm 1$ levels equally.

Para (j = 0) H_2 basis set versus Para (j = 0, 2) H_2 basis set

The ratio $\sigma(j = 0, 2)/\sigma(j = 0)$ is given in table 5.6 for the 'true' potential only. It is evident that the coupling between the $(j_2 = 0)$ and $(j_2 = 2)$ states is important. However, the change in cross-sections found for this collision is less than the corresponding change found for NH_3 – H_2 collisions where the dipole allowed transitions were appreciably enhanced. In contrast, with a few exceptions, the tendency is for the cross-sections to be of a similar magnitude. However, we note that, once again, the propensity towards preferential excitation of the Λ doublets is damped by the inclusion of the $j_2 = 2$ states in the H_2 basis set.

($j_2 = 2$) versus ($j_2 = 0$) and ($j_2 = 1$)

The use of a ($j_2 = 2$) only basis gives the cross-section for rotational excitation of OH in collisions with rotationally excited ($j_2 = 2$) hydrogen molecules. This information cannot be obtained by using a ($j_2 = 0, 2$) basis set at this energy because H_2 and OH are treated equally and ($j_2 = 2$) is a closed channel. However, it should be remembered that the use of this basis assumes that coupling between the ($j_2 = 0$) and ($j_2 = 2$) channels can be neglected.

From table 5.4 it can be seen that the cross-section for collisions with ($j_2 = 2$) H_2 are quantitatively very similar to those obtained for collisions with ($j_2 = 1$) H_2 as might be expected given that similar terms in the potential expansion are contributing.

Thus it would seem that an assumption that ($j_2 > 0$) H_2 behaves in the same way as ($j = 1$) H_2 as a collision partner could be justified at least in so far as the coupling to other H_2 rotational states can be neglected. However, in reality there will be coupling with the $j_2 = 0$ state as was seen from the comparison of results obtained with a ($j = 0$) and ($j = 0, 2$) hydrogen basis set. How this would effect the cross-sections is not easy to say.

In conclusion, the low energy results appear to suggest that the ($j = 0$) para-H_2 basis set is the 'worst case' basis set leading to the strongest preferential excitation of the Λ doublets. As more potential terms contribute to the coupling the propensities are increasingly damped.

Finally...

An additional calculation for para-H_2 was performed at 192.3cm^{-1} to compare against the results of Dewangan and Flower (1983). The calculations here are essentially the same apart from differences in the fitting of the potential surface and the different integrators used. The results of this calculation are given in table 5.7. It can be seen that, when compared with the 192.3cm^{-1} calculation the 190cm^{-1} cross-section for the $(3/2, 3/2+ \rightarrow 1/2, 1/2+)$ transition is much larger than its value at the sightly higher energy. To a lesser extent this is also true for the $(3/2, 3/2+ \rightarrow 5/2, 3/2-)$ and the $(5/2, 3/2- \rightarrow 1/2, 1/2+)$ cross-section. The difference can be attributed to a resonance phenomenon occurring for partial waves with total angular momentum in the range ($J_{tot} = 11/2$) to ($J_{tot} = 15/2$). This comparison serves as a useful reminder of the perils of placing too much weight on conclusions drawn from just one calculation, especially at low energies where resonances might be lurking.

5.7: Comparison with calculations at 192.5cm^{-1}

Transition	Present Work		Dewangan and Flower (1983)
$j\epsilon \rightarrow j'\epsilon'$	190cm^{-1}	192.5cm^{-1}	192.5cm^{-1}
$\Omega = \Omega' = 3/2$			
$3/2+ \rightarrow 3/2-$	9.93	9.73	9.80
$3/2+ \rightarrow 5/2+$	3.19	2.89	2.86
$3/2+ \rightarrow 5/2-$	1.08	0.561	0.550
$3/2- \rightarrow 5/2+$	2.18	1.91	1.93
$3/2- \rightarrow 5/2-$	3.00	2.74	2.78
$5/2+ \rightarrow 5/2-$	7.06	6.46	6.61
$\Omega = \Omega' = 1/2$			
$1/2+ \rightarrow 1/2-$	12.26	11.7	11.7
$1/2+ \rightarrow 3/2+$	0.731	0.797	0.642
$1/2+ \rightarrow 3/2-$	0.204	0.200	0.176
$1/2- \rightarrow 3/2+$	0.0431	0.0396	0.0445
$1/2- \rightarrow 3/2-$	0.602	0.659	0.526
$3/2+ \rightarrow 3/2-$	7.98	4.53	5.28

continued overleaf...

table 5.7 continued: Comparison with calculations at 192.5cm^{-1} for Ω changing transitions.

Transition	Present Work		Dewangan and Flower
$j\epsilon \rightarrow j'\epsilon'$	190cm^{-1}	192.5cm^{-1}	192.5cm^{-1}
$\Omega = 3/2, \Omega' = 1/2$			
$3/2+ \rightarrow 1/2+$	0.272	0.0815	0.0817
$3/2+ \rightarrow 1/2-$	0.975	0.765	0.777
$3/2+ \rightarrow 3/2+$	0.0865	0.0987	0.0975
$3/2+ \rightarrow 3/2-$	0.135	0.151	0.148
$3/2- \rightarrow 1/2+$	0.749	0.585	0.600
$3/2- \rightarrow 1/2-$	0.273	0.221	0.218
$3/2- \rightarrow 3/2+$	0.0591	0.0607	0.0601
$3/2- \rightarrow 3/2-$	0.177	0.208	0.209
$5/2+ \rightarrow 1/2+$	0.400	0.397	0.403
$5/2+ \rightarrow 1/2-$	0.359	0.288	0.282
$5/2+ \rightarrow 3/2+$	0.0311	0.0255	0.0233
$5/2+ \rightarrow 3/2-$	0.144	0.188	0.189
$5/2- \rightarrow 1/2+$	0.413	0.159	0.161
$5/2- \rightarrow 1/2-$	0.377	0.271	0.266
$5/2- \rightarrow 3/2+$	0.201	0.273	0.276
$5/2- \rightarrow 3/2-$	0.0389	0.0563	0.0589

5.7 Experimental Energy (680 cm^{-1})

5.7.1 Motivation

The experimental results of Andresen et al (1984) have already been reviewed in section 5.3. In their paper they gave experimental results for the summed and averaged cross-sections for transitions from the rotational ground state defined as:

$$\sigma(j_1 = 3/2, \Omega = 3/2 \rightarrow j_1'\Omega') = \frac{1}{2}\sum_{\epsilon\epsilon'}\sigma(j_1 = 3/2, \Omega = 3/2, \epsilon \rightarrow j_1'\Omega'\epsilon') \qquad 5.7.1$$

and in addition, gave results for the quantity σ^+/σ^- where $\sigma^\pm$ is defined as:

$$\sigma^\pm(j_1'\Omega') = \frac{1}{2}\sum_{\epsilon}\sigma(j_1 = 3/2, \Omega = 3/2, \epsilon \rightarrow j_1'\Omega'\epsilon' = \pm) \qquad 5.7.2$$

Theoretical coupled states results of Schinke and Andresen gave cross-sections for rotational excitation of OH in collisions with ground state para-H_2 that seriously over estimated the extent to which the Λ doublets were preferentially excited. They suggested that the discrepancy could be explained if the potential of Kochanski and Flower over estimated the value of the v_{22} (or v_{2022}) coefficient. This hypothesis was supported by the comparison made by Dewangan, Flower and Danby (1986) who used the 'doctored' potential in which the offending coefficient is reduced by a factor of two.

However, the experiment was performed using normal hydrogen at room temperature where approximately three quarters of the hydrogen molecules are ortho-H_2 molecules. In view of the reduction in propensity shown by the 190cm^{-1} results when ortho-H_2 ($j = 1$) is the collision partner, it is interesting to repeat the calculation at 680cm^{-1} using the 'true' potential to give a direct comparison with the experiment.

5.7.2 Basis set

At 680cm^{-1} the first twenty rotational levels of OH are energetically accessible. These include levels up to $j = 9/2$ in the $\Omega = 1/2$ ladder and $j = 11/2$ in the $\Omega = 3/2$ ladder. In addition the first excited states of both ortho and para-H_2

are available. Clearly a close-coupled calculation fully converged with respect to OH and H_2 basis sets would be very large and a certain amount of economy is needed. For a comparison with experiment only cross-sections for transitions out of the ground state are required, and as lower j transitions converge faster with respect to basis set size, a smaller basis set can be used than would otherwise be required. Basis set convergence tests were carried out with basis sets consisting of the energetically lowest 20, 24, 26 and 28 rotational states using ground state para-H_2 as the collision partner, and including the first three partial waves ($J_{tot} = 1/2 \rightarrow 5/2$). The results of these tests are given in table 5.8. A basis consisting of the lowest 24 levels (a B24 basis) was chosen for the calculations.

For both ortho and para-H_2 collisions only the lowest rotational state was included in the H_2 basis. Whilst this can be justified for ortho-H_2 where the inclusion of additional rotational states in the basis does not introduce extra couplings, it is less adequate for para-H_2 collisions. However, the purpose of the calculation is to compare with an experiment performed at room temperature. Normal H_2 has a 3:1 ortho-H_2:para-H_2 ratio, so the results were weighted in a 3:1 ($j = 1$):($j = 0$) ratio. With this weighting the comparison will be largely dominated by the ortho-H_2 collision rates, and the precise behaviour of the para-H_2 collision rates will be less critical.

5.7.3 Integration of the Coupled Equations

The para-H_2 ($j = 0$) equations were integrated on the Amdahl at Durham, whilst the CRAY XMP at Rutherford was used for the ortho-H_2 ($j = 1$) calculations. Integration of the ortho-H_2 equations typically took 1850 CPU seconds per partial wave on the CRAY.

To economise on computing time, the calculations were performed for every other partial wave ($J_{tot} = 1/2, 5/2, 9/2...$). At higher energies the cross-sections are more slowly varying with total angular momentum, and the likelihood of sharp resonances is much reduced. Comparisons of the results using alternate partial waves with results of the same calculation performed at every sixth partial wave imply that the cross-sections should be adequately represented by the former.

5.8: 680cm^{-1}basis convergence tests

Basis set convergence tests for OH basis at 680cm^{-1}, with a ($j = 0$) basis set for the H_2 molecule, and including first three partial waves ($J_{tot} = 1/2$ to $5/2$).

$j, \epsilon \rightarrow j'\epsilon'$	B20	B24	B26	B28
$\Omega = \Omega' = 3/2$				
$3/2+ \rightarrow 3/2+$	0.56	0.57	0.56	0.56
$3/2+ \rightarrow 3/2-$	0.010	0.013	0.013	0.013
$3/2+ \rightarrow 5/2+$	0.076	0.070	0.070	0.069
$3/2+ \rightarrow 5/2-$	0.017	0.018	0.018	0.018
$3/2+ \rightarrow 7/2+$	0.0078	0.0056	0.0058	0.0057
$3/2+ \rightarrow 7/2-$	0.0028	0.0035	0.0033	0.0034
$3/2+ \rightarrow 9/2+$	0.052	0.057	0.059	0.059
$3/2+ \rightarrow 9/2-$	0.0029	0.0023	0.0022	0.0027
$3/2+ \rightarrow 11/2+$	0.011	0.011	0.013	0.013
$3/2+ \rightarrow 11/2-$	0.0003	0.0005	0.0005	0.0006
$3/2- \rightarrow 3/2-$	0.56	0.55	0.55	0.55
$3/2- \rightarrow 5/2+$	0.033	0.030	0.031	0.031
$3/2- \rightarrow 5/2-$	0.022	0.026	0.025	0.026
$3/2- \rightarrow 7/2+$	0.076	0.076	0.077	0.076
$3/2- \rightarrow 7/2-$	0.011	0.011	0.011	0.011
$3/2- \rightarrow 9/2+$	0.015	0.019	0.017	0.017
$3/2- \rightarrow 9/2-$	0.016	0.016	0.016	0.017
$3/2- \rightarrow 11/2+$	0.0058	0.0091	0.010	0.010
$3/2- \rightarrow 11/2-$	0.0017	0.0022	0.0022	0.0023

continued overleaf...

table 5.8 continued: 680cm^{-1} basis convergence tests for Ω changing transitions ($\Omega = 3/2, \Omega' = 1/2$)

$j\epsilon \rightarrow j'\epsilon'$	B20	B24	B26	B28
$\Omega = 3/2, \Omega' = 1/2$				
$3/2+ \rightarrow 1/2+$	0.0012	0.0012	0.0011	0.0012
$3/2+ \rightarrow 1/2-$	0.013	0.011	0.010	0.0098
$3/2+ \rightarrow 3/2+$	0.022	0.019	0.018	0.018
$3/2+ \rightarrow 3/2-$	0.052	0.049	0.048	0.047
$3/2+ \rightarrow 5/2+$	0.037	0.036	0.035	0.036
$3/2+ \rightarrow 5/2-$	0.013	0.010	0.010	0.011
$3/2+ \rightarrow 7/2+$	0.0050	0.0046	0.0047	0.0048
$3/2+ \rightarrow 7/2-$	0.039	0.044	0.044	0.045
$3/2+ \rightarrow 9/2+$	0.00082	0.0012	0.0013	0.0013
$3/2+ \rightarrow 9/2-$	0.0073	0.0074	0.0074	0.0086
$3/2- \rightarrow 1/2+$	0.021	0.019	0.018	0.018
$3/2- \rightarrow 1/2-$	0.00061	0.00093	0.00096	0.00083
$3/2- \rightarrow 3/2+$	0.047	0.044	0.044	0.043
$3/2- \rightarrow 3/2-$	0.012	0.012	0.012	0.011
$3/2- \rightarrow 5/2+$	0.0078	0.0080	0.0076	0.0076
$3/2- \rightarrow 5/2-$	0.069	0.067	0.067	0.067
$3/2- \rightarrow 7/2+$	0.0096	0.0098	0.0098	0.010
$3/2- \rightarrow 7/2-$	0.013	0.016	0.016	0.015
$3/2- \rightarrow 9/2+$	0.00091	0.0011	0.0011	0.0012
$3/2- \rightarrow 9/2-$	0.0055	0.0071	0.0071	0.0081

The results of these calculations are shown in table 5.9. Partial waves up to a total angular momentum of 89/2 were included in the calculation. At this point all the relevant inelastic cross-sections were judged to be converged with respect to the number of partial waves.

5.7.4 Discussion of results

The experimental results (Andresen, Haüsler and Lülf, 1984, Schinke and Andresen, 1984) for the transitions ($j = 3/2, \Omega = 3/2, \epsilon = \pm 1 \rightarrow j', \Omega', \epsilon'$) are given in the form of graphs showing the variation of σ^+/σ^- (for $\Omega' = 1/2$) or σ^-/σ^+ (for $\Omega' = 3/2$) with j', where $\sigma^\pm$ is defined by equation 5.7.1, and the variation of the summed and averaged cross-sections (equation 5.7.2) with j'. For ease of comparison the same format is used here.

Variation of the summed and averaged cross-section with j'

The numerical results of the summed and averaged cross-sections for each ($j'\Omega'$) are given in table 5.10 for both the results of the present calculation and the earlier results of Schinke and Andresen. The latter employed the same potential as here, but used the coupled states approximation to integrate the equations, with a larger basis set consisting of the 32 rotational states up to $j_1 = 15/2$ in both the $\Omega = 3/2$ and $\Omega = 1/2$ manifolds.

For comparison with the experiment all results are normalised to coincide with the para-H_2 value for the ($j\Omega = 3/2, 3/2 \rightarrow 5/2, 3/2$) cross-section. The result of the comparison is shown in figure 5.5. The 3:1 ($j = 1$):($j = 0$) results show remarkably good agreement with the experimental results for the $\Omega' = 3/2$ transitions. The agreement is less good at low j' for the $\Omega' = 1/2$ transitions, but in view of the uncertainties in the potential it is still satisfactory, and is certainly better on the whole than the para ($j = 0$) H_2 results.

5.9: Inelastic Cross-Sections at 680cm^{-1}

Cross-sections in units of 10^{-16}cm^{+2} are quoted for transitions out of the OH rotational ground state for both ortho and para-H_2 collisions. For the ortho-H_2 collisions results are given with calculations using alternate partial waves (Jstep= 2) and every sixth partial wave (Jstep= 6). The final column shows the results of Schinke and Andresen, 1984.

transition	ortho ($j = 1$) H_2		para ($j = 0$) H_2	
$j\epsilon \rightarrow j'\epsilon'$	Jstep= 2	Jstep= 6	Jstep= 2	CS calc., 84
$\Omega = 3/2, \Omega' = 3/2$				
$3/2+ \rightarrow 5/2+$	5.71	5.69	4.61	4.72
$3/2+ \rightarrow 5/2-$	2.40	2.38	0.551	0.47
$3/2+ \rightarrow 7/2+$	1.52	1.50	0.873	0.94
$3/2+ \rightarrow 7/2-$	0.892	0.882	0.404	0.27
$3/2+ \rightarrow 9/2+$	0.856	0.832	1.28	1.43
$3/2+ \rightarrow 9/2-$	0.177	0.168	0.0357	0.04
$3/2+ \rightarrow 11/2+$	0.159	0.153	0.104	0.19
$3/2+ \rightarrow 11/2-$	0.043	0.040	0.0074	0.05
$3/2- \rightarrow 5/2+$	3.51	3.47	2.35	2.46
$3/2- \rightarrow 5/2-$	5.03	5.04	2.44	2.15
$3/2- \rightarrow 7/2+$	1.97	1.93	3.08	3.36
$3/2- \rightarrow 7/2-$	1.19	1.18	0.332	0.21
$3/2- \rightarrow 9/2+$	0.608	0.590	0.219	0.32
$3/2- \rightarrow 9/2-$	0.224	0.221	0.247	0.16
$3/2- \rightarrow 11/2+$	0.153	0.145	0.137	0.13
$3/2- \rightarrow 11/2-$	0.0596	0.0579	0.0195	0.02

continued overleaf...

Table 5.9 continued: Inelastic Cross-Sections at $680cm^{-1}$ for Ω changing transitions out of the $j\Omega = 3/2, 3/2$ rotational ground state (in units of $10^{-16}cm^2$).

transition	ortho ($j = 1$) H_2		para ($j = 0$) H_2	
$j\epsilon - j'\epsilon'$	Jstep= 2	Jstep= 6	Jstep= 2	CS calc., 84
$\Omega = 3/2, \Omega' = 1/2$				
$3/2+ \rightarrow 1/2+$	0.790	0.767	0.0690	0.08
$3/2+ \rightarrow 1/2-$	1.71	1.68	2.30	2.26
$3/2+ \rightarrow 3/2+$	1.40	1.40	1.75	1.46
$3/2+ \rightarrow 3/2-$	1.30	1.31	1.76	1.71
$3/2+ \rightarrow 5/2+$	0.680	0.666	0.828	1.02
$3/2+ \rightarrow 5/2-$	0.856	0.844	0.626	0.46
$3/2+ \rightarrow 7/2+$	1.33	1.28	0.0525	0.12
$3/2+ \rightarrow 7/2-$	0.466	0.453	0.852	0.60
$3/2+ \rightarrow 9/2+$	0.0172	0.0163	0.0136	0.01
$3/2+ \rightarrow 9/2-$	0.0564	0.0524	0.0591	0.05
$3/2- \rightarrow 1/2+$	1.62	1.59	2.43	2.12
$3/2- \rightarrow 1/2-$	0.788	0.772	0.0729	0.01
$3/2- \rightarrow 3/2+$	1.17	1.17	1.15	1.31
$3/2- \rightarrow 3/2-$	1.65	1.65	2.03	2.00
$3/2- \rightarrow 5/2+$	0.532	0.531	0.327	0.26
$3/2- \rightarrow 5/2-$	1.03	1.00	2.06	1.92
$3/2- \rightarrow 7/2+$	1.62	1.58	0.161	0.20
$3/2- \rightarrow 7/2-$	0.254	0.247	0.173	0.21
$3/2- \rightarrow 9/2+$	0.0163	0.0151	0.00864	0.02
$3/2- \rightarrow 9/2-$	0.0598	0.0572	0.0879	0.01

5.10: Summed and Averaged Cross-Sections

The summed and averaged cross-sections are defined by equation 5.7.1, and are given here in units of 10^{-16}cm^2.

$j'\Omega'$	ortho-H_2	para-H_2	Schinke and Andresen, 1984
5/2, 3/2	8.29	4.98	4.91
7/2, 3/2	2.79	2.34	2.39
9/2, 3/2	0.93	0.89	0.97
11/2, 3/2	0.21	0.13	0.20
1/2, 1/2	2.45	2.44	2.24
3/2, 1/2	2.76	3.35	3.24
5/2, 1/2	1.55	1.92	1.80
7/2, 1/2	0.51	0.62	0.56
9/2, 1/2	0.075	0.085	0.04

Figure 5.5

Comparison with experiment: The summed and averaged cross-sections

Computed and measured values of the Λ doublet summed and averaged cross-sections (equation 5.7.1) normalised at $\sigma(3/2, 3/2 \rightarrow 5/2, 3/2)$. (Circles: The measurements of Andresen et al, $\times$'s: the computed values with para-H_2 ($j_2 = 0$), $+$'s: the computed values for normal H_2 (3:1 ortho:para-H_2 ratio)).

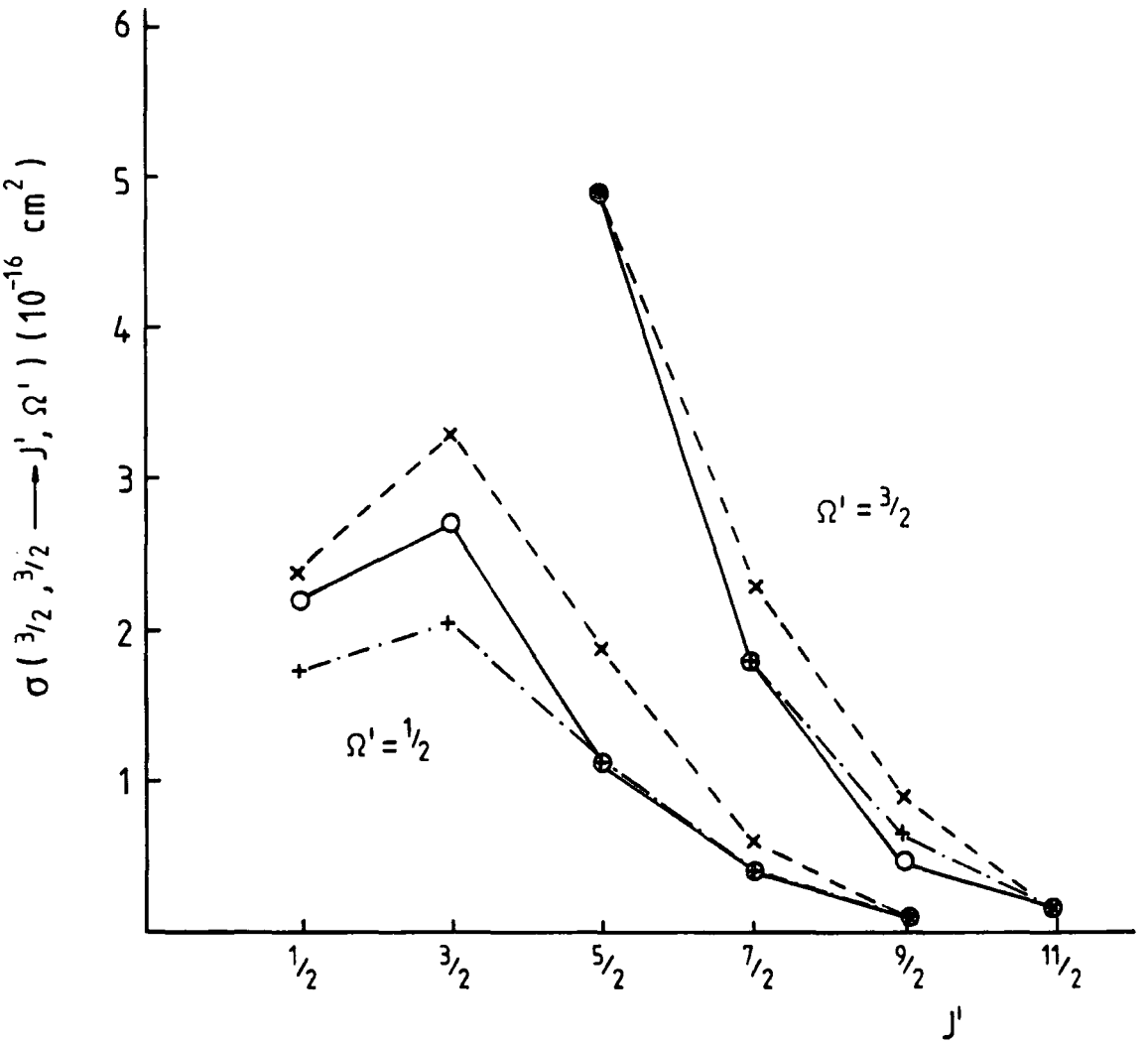

Variation of $\sigma^{\pm}/\sigma^{\mp}$ with j'

The numerical values of $\sigma^{\pm}$ are shown in table 5.11. For transitions within the $\Omega = 3/2$ ladder σ^{+} is larger than σ^{-}, whereas the reverse is true for transitions between the $\Omega = 3/2$ and $\Omega = 1/2$ ladders. The comparison with the experimental results is shown in figure 5.6. The agreement with experiment is again very encouraging. The $\Omega \neq \Omega'$ calculations give a $\sigma^{\pm}/\sigma^{\mp}$ that rises too quickly with increasing j' but for $\Omega = \Omega'$, the calculations give much better agreement with experiment than pure ground state para-H_2 results which grossly over estimate the propensity for preferential excitation of the Λ doublets.

5.11: $\sigma^{\pm}/\sigma^{\mp}$ at 680cm^{-1}

Ratios of cross-sections, $\sigma^{\pm}$ (cf equation 5.7.2) weighted 3:1 for excitation by ortho ($j = 1$), and para ($j = 0$) H_2. The measured values are taken from Andresen et al (1984).

$j'\Omega'$	σ^{+}/σ^{-}	σ^{-}/σ^{+}	Measured
5/2, 3/2	1.4		1.0±0.1
7/2, 3/2	2.1		1.4
9/2, 3/2	4.0		2.6
11/2, 3/2	3.5		4.6±1.2
1/2, 1/2		1.0	1.1±0.2
3/2, 1/2		1.2	
5/2, 1/2		1.7	1.6
7/2, 1/2		2.9	1.8
9/2, 1/2		3.4	2.0±0.5

Figure 5.6
Comparison with experiment: $\sigma^{\pm}/\sigma^{\mp}$

Computed and measured values of the ratio $\sigma^{\pm}/\sigma^{\mp}$ defined by equation 5.7.2. (Crosses: the measurements of Andresen et al, open squares: the computed values with para-H_2 ($j_2 = 0$), coloured squares: the computed values for normal H_2 (3:1 ortho:para-H_2 ratio)). The dashed lines are for $\Omega = 3/2, \Omega' = 3/2$ transitions, the solid lines are for $\Omega = 3/2, \Omega' = 1/2$ transitions.

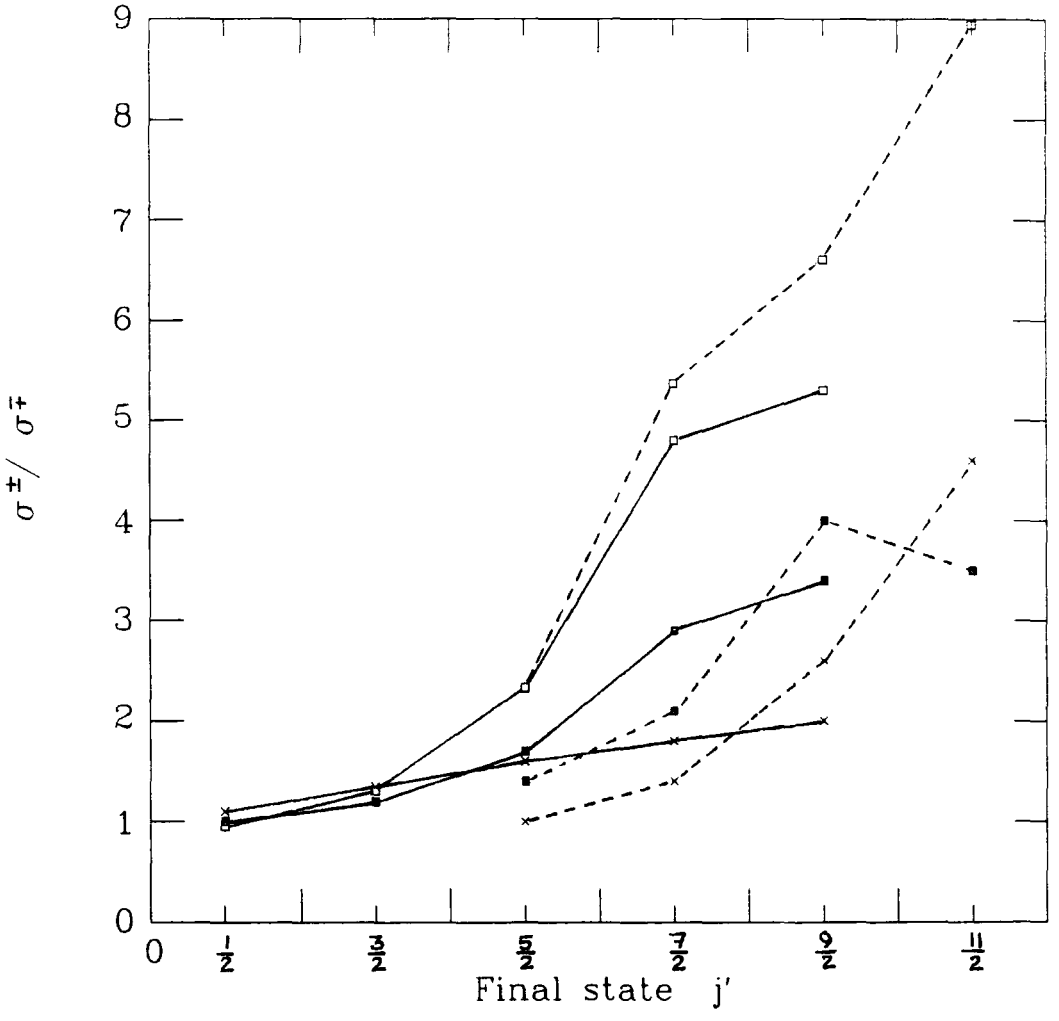

5.8 Summary

The calculations reported here are the first quantal calculations to include the rotational structure of the H_2 molecule in the OH - H_2 collision calculation. The principal conclusions are

- collisions with rotationally excited H_2 lead to reduced propensities for preferential excitation of the Λ doublets when compared to collisions with ground state para-H_2
- Agreement between the experimental and theoretical results can be improved by the treatment of the rotational structure of the hydrogen molecule neglected in earlier calculations.

Chapter VI

Summary and Conclusion

In this thesis the results of an investigation into the effect of including the rotational structure of the hydrogen molecule in the quantal calculation for NH_3 - H_2 and OH - H_2 collisions have been reported. These are the first full close coupled calculations to include rotationally excited H_2 molecules for both NH_3 and OH collisions, although there have been some limited coupled states calculations for NH_3 - H_2 (Billing et al, 1987, 1988, Ebel et al, 1990).

The results of both NH_3 - H_2 and OH - H_2 collisions calculations suggest that the introduction of the ($j > 0$) H_2 levels can have a qualitative effect on the collisional propensities governing the transitions. The effects can be divided into two types.

Firstly, there are the changes, seen for NH_3 - H_2 collisions, where transitions that are 'forbidden' for ground state para-H_2 collisions are allowed, and even preferred, when ortho-H_2 is the collision partner.

These changes are a direct result of the 'symmeterization' of the symmetric top, (or OH), wavefunction that leads to the parity factor,

$$p = (1 + \epsilon\epsilon'(-1)^{j_1+j_1'-2k'+\lambda+\lambda_2+\mu}) \qquad 6.1$$

appearing in the coupling matrix element (equation 2.6.44). Such changes are potential independent in so far as they can be qualitatively deduced from the algebra alone, and are *relatively* uneffected by the finer details of the potential surface used for the calculation. The fact that the transitions are allowed in collisions with ($j > 0$) H_2 is a result of the presence of the $\nu > 0$ terms in the potential expansion (equation 2.6.14), which, in the limit of the coupled states approximation, allow the projection of the NH_3 or OH angular momentum on the intermolecular axis to change. Transitions suppressed by the parity factor for collisions with ($j = 0$) H_2

but allowed for collisions with rotationally excited H_2 were present for NH_3 - H_2 collisions and included the transitions:

$$\begin{aligned} &(00+ \rightarrow j3+) \\ &(00+ \rightarrow j6-) \\ &(11\pm \rightarrow 22\pm). \end{aligned} \qquad 6.2$$

The changes were not predicted by the semi-classical treatment of Billing et al (1987, 1988) and the associated quantal treatment of Ebel et al (1990) but this can be attributed to the absence of the $\nu > 0$ terms in the form of potential expansion used (equation 3.5.9).

Secondly there are the changes linked to the limitations imposed on the coupling matrix elements by the 3-j symbols:

$$\begin{pmatrix} l' & \lambda & l \\ 0 & 0 & 0 \end{pmatrix} \begin{pmatrix} j_2' & \lambda_2 & j_2 \\ 0 & 0 & 0 \end{pmatrix} \begin{pmatrix} j_1' & \lambda_1 & j_1 \\ -k' & \mu & k \end{pmatrix} \qquad 6.3$$

These are present regardless of whether the molecular wavefunction has been 'symmeterized', and are linked to the constraints imposed by the angular terms present in the potential expansion, and the conservation of angular momentum.

For molecule - H_2 collisions, $\lambda_2 = 0$ only is allowed if ($j_2 = j_2' = 0$), but if ($j > 0$) H_2 is included in the hydrogen molecule basis set, $\lambda_2 > 0$ terms are permitted. The additional couplings that result lead to the increased cross-sections for dipole allowed transitions in NH_3 - H_2 collisions (and also for HCl - H_2 collisions (Green, 1977)). The damping of the propensities towards preferential excitation of the Λ doublets found for OH - H_2 collisions is also attributable to this cause. The effect of the additional terms on the cross-sections is harder to predict qualitatively from the algebra alone, although they may be predicted by physical arguments, and the changes are more dependent on the precise potential used.

It might be noted here that approximating normal H_2 cross-sections by a ($j = 0$) H_2 only calculation appears to be a better approximation for OH - H_2 collisions than for NH_3 - H_2 collisions. For the former, the changes in the cross-sections are 'type two' changes, and collisional propensities are in the same sense, if slightly

damped. For the latter, both 'type one' and 'type two' changes are evident, and the cross-sections show a qualitatively different behaviour in collisions with ortho and para-H_2.

In addition to the qualitative changes in the collision cross-sections found when a ($j > 0$) H_2 basis replaced a ($j = 0$) H_2 basis, the results of the calculations also showed that the cross-sections can be quantitatively changed by the inclusion of the ($j = 2$) H_2 state in a ground state para-H_2 collision calculation. For NH_3 - H_2 collisions it was found that this was less true when ($j = 3$) H_2 was included in a ground state ortho-H_2 collision calculation, and it was tentatively suggested that this may be due to the fact that ($j = 2$) H_2 and ($j = 0$) H_2 collisions lead to a qualitatively different behaviour, for the reasons outlined above, whilst ($j = 1$) H_2 and ($j = 3$) H_2 might be expected to behave similarly. At any rate, it is clear that para-H_2 cross-sections obtained with a ($j = 0$) H_2 basis set should be treated with some caution, although the inaccuracy is probably no greater than that introduced by uncertainties in the interaction potential.

The changes in propensities found when ortho-H_2 is included in the collision calculation could have consequences in the field of astrophysics where inelastic molecular collision rates are used in interpreting observations, and one such possible application was discussed in chapter three. In addition these changes can help explain discrepancies between experimental and theoretical data for both NH_3 - H_2 and OH - H_2 collisions. Comparison between theory and experiment involves a certain amount of averaging and normalisation, so such comparisons are perhaps less sensitive to the features of the potential surface than they are to the effects of changes in the algebra pertaining to the collision.

The calculations presented in this thesis constitute preliminary investigation of the effect of including rotationally excited H_2 in the basis set. Calculations have been performed at only a single low energy in each case, with additional limited calculations at the experimental energies of 605cm^{-1} for ortho-NH_3 and 680cm^{-1} for OH. To extend this work, and produce the astrophysical rate coefficients, calculations at a large range of energies are needed. Such calculations would be computationally expensive, but would be feasible if the coupled states approximation was used, once the accuracy of the coupled states approximation for these

collisions had been checked numerically. From the algebra there does not appear to be any reason why full CS calculations should not satisfactorily reproduce the close coupled cross-sections.

In conclusion, the results of the calculations show that the inclusion of rotationally excited H_2 does have an effect on the collisional cross-sections, and whilst the effect is most marked for NH_3 – H_2 collisions, it is also appreciable for OH – H_2 collision calculations. The changes can help explain discrepancies between theory and experiment and could have interesting astrophysical consequences. However, further study of the latter must await calculations at a wider range of energies.

Bibliography

Abramowitz M. and Stegun I.A. (1965) "Handbook of Mathematical Functions", New York: Dover Publications.

Alexander M.H. (1982) *J.Chem.Phys* **76** 5974

Alexander M.H. (1985) *Chemical Physics* **92** 337

Alexander M.H. and Dagdigian, P.(1984) *J.Chem.Phys* **80** 4325

Allison A.C. (1988) *Adv.Atom.Mol.Physics* **25** 323

Andresen P., Haüsler D. and Lülf, H.W. (1984) *J.Chem.Phys* **81** 571

Andresen P., Haüsler D., Lülf H.W. and Kegel W.H. (1984) *Astron.Astrophys* **138** L17

Andresen P. (1986) *Astron.Astrophys* **154** 42

Arthurs A.M. and Dalgarno A. (1960) *Proc.R.Soc.London* **A256** 540

Bertojo M., Cheung A.C. and Townes C.H. (1976) *Astrophys.J* **208** 914

Billing G.D. (1975) *Chem.Phys.Lett* **30** 391

Billing G.D. (1976) *J.Chem.Phys* **65** 1

Billing G.D. and Poulsen L. (1984) *J.Chem.Phys* **81** 3866

Billing G.D., Poulsen L. and Diercksen G.H.F. (1985) *Chemical Physics* **98** 397

Billing G.D. and Diercksen G.H.F. (1985) *Chem.Phys.Lett* **121** 94

Billing G.D. and Diercksen G.H.F. (1986) *Chemical Physics* **105** 145

Billing G.D. and Diercksen G.H.F. (1987) *Chemical Physics* **118** 161

Billing G.D. and Diercksen G.H.F. (1988) *Chemical Physics* **124** 77

Blatt J.M. and Biedenharn L.L. (1952) *Rev.Mod.Phys* **258**

Brechignac Ph., Picard-Bersellini A., Charneau, R. and Launay J.M. (1980) *Chemical Physics* **53** 165

Broquier M., Picard-Bersellini A. (1985) *Chem.Phys.Lett* **121** 437

Broquier M., Picard-Bersellini A. and Hall J. (1987) *Chem.Phys.Lett* **136** 531

Broquier M., Picard-Bersellini A. (1988) *J.Chem.Phys* **88** 1551

Buck U. (1988) In "Atomic and Molecular Beam Methods" vol.1, Ed. G.Scoles, Oxford University Press, pp 449 and pp 525

Buckingham A.D. (1967) *Adv.Chem.Phys* **12** 107

Buckingham A.D. (1978) In "Intermolecular Interactions: from diatomics to biopolymers" Ed. B.Pullman, J.Wiley and Sons, pp 1

Cheung A.C., Rank D.M., Townes C.H., Thornton D.D. and Welch W.J. (1968) *Phys.Rev.Lett.* **21** 1701

Child M.S. (1976) In "Dynamics of Molecular Collisions" part B, Ed. W.Miller, Plenum Press, pp 171

Choi B.H., Poe R.T. and Tang K.T. (1977) *Chem.Phys.Lett* **48** 237

Corey G.C. and Alexander M.H. (1988) *J.Chem.Phys* **88** 6931

Dagdigian P.J. (1988) In "Atomic and Molecular Beam Methods" vol. 1, Ed. G.Scoles, Oxford University Press, pp567

Daly P.W. and Oka T. (1970) *J.Chem.Phys* **53** 3272

Danby G., Flower D.R., Kochanski E., Kurdi L., Valiron P. and Diercksen G.H.F. (1986) *J.Phys.B:At.Mol.Physics* **19** 2891

Danby G., Flower D.R., Valiron P., Kochanski E., Kurdi L. and Diercksen G.H.F. (1987) *J.Phys.B:At.Mol.Physics* **20** 1039

Danby G., Flower D.R., Valiron P., Schilke P, and Walmsley C.M. 1988 *Mon. Not.Royal.Astron.Soc* **235** 229

Danby G. and Valiron P. (1989) *Chem.Phys.Lett* **163** 75

Davis S.L. and Boggs J.E. (1978) *J.Chem.Phys* **69** 2355

de Jong T, Chu Shih-I. and Dalgarno A. (1975) *Astrophys.J* **199** 69

Dewangan D.P. and Flower D.R.(1981) *J.Phys.B:At.Mol.Phys* **14** 2179

Dewangan D.P. and Flower D.R.(1981) *J.Phys.B:At.Mol.Phys* **14** L425

Dewangan D.P. and Flower D.R.(1983) *J.Phys.B:At.Mol.Phys* **16** 2157

Dewangan D.P. and Flower D.R.(1985) *J.Phys.B:At.Mol.Phys* **18** L137

Dewangan D.P., Flower D.R. and Danby G. (1986) *J.Phys.B:At.Mol.Phys* **19** L747

Dewangan D.P., Flower D.R. and Alexander M.H. (1987) *Mon.Not.Royal. Astron.Soc.* **226** 505

Dickinson A.S. and Richards D. (1982) *Adv.At.Mol.Phys* **18** 161

Dieke G.H. and Crosswhite M.W. (1961) *J.Quant.Spectr.Rad.Transfer* **2** 97

Diercksen G.H.F. and Sadlej A.J. (1986) *Molec.Physics* **57** 509

Dixon R.N. and Field D. (1979) *Proc.Royal.Soc.London* **A368** 99

Dixon R.N., Field D. and Zare R.N. (1985) *Chem.Phys.Lett* **122** 310

Dousmanis G.C., Sanders T.M. and Townes C.H. (1955) *Phys.Review* **100** 1735

Eastes W. and Secrest D. (1972) *J.Chem.Phys* **56** 640

Ebel G., Krohne K., Meyer H., Buck U., Schinke R., Seelemann T., Andresen P., Schleipen J., Ter Meulen J.J. and Diercksen G.H.F. (1990) preprint

Edmonds A.R. (1960) "Angular Momentum in Quantum Mechanics", Princeton, New York.

Fabris A.R. and Oka T. (1972) *J.Chem.Phys* **56** 3168

Flower D.R., Launay J.M., Kochanski E., Prissette J. (1979) *Chemical Physics* **37** 355

Flower D.R. and Watt G.D. (1984) *Mon.Not.Royal.Astron.Soc.* **209** 25

Flower D.R., Offer A. and Schilke P. (1990) *Mon.Not.Royal.Astron.Soc.* **224** 4P

Garrison B.J., Lester W.A. and Miller W.H. (1976) *J.Chem.Phys* **65** 2193

Garrison B.J. and Lester W.A. (1977) *J.Chem.Phys* **66** 531

Green S. (1975) *J.Chem.Phys* **62** 2271

Green S. (1976) *J.Chem.Phys.* **64** 3463

Green S. (1977) *Chem.Phys.Lett.* **47** 119

Green S. (1979) *J.Chem.Phys.* **70** 816

Green S. (1980) *J.Chem.Phys.* **73** 2740

Green S. (1982) Referenced by Walmsley and Ungerechts, 1983

Green S. and Thaddeus P. (1976) *Astrophys.J.* **205** 766

Guilloteau S., Wilson T.L., Martin R.N., Batrla W. and Pauls T.A. (1983) *Astron.Astrophys.* **124** 322

Gwinn W.D., Turner B.E., Goss W.M., Blackman G.L. (1973) *Astrophys.J.* **179** 789

Heck L., Flower D.R. and Pineau des Forets G. (1990) *Comput.Phys.Commun.* **58** 169

Hehre W.J., Radom L., Schleyer P.v.R. and Pople J.A. (1986) "Ab Initio Molecular Orbital Theory", J.Wiley and Sons.

Herzberg G. (1950) "The Spectra of Diatomic Molecules", Van Nostrand

Ho P.T.P. and Townes C.H. (1983) *Ann.Rev.Astron.Astrophys* **21** 239

Hutson J.M. and Green S. (1986) MOLSCAT computer code, version 9, CCP6 (Daresbury Laboratory:UKSERC)

Johnson B.R. (1973) *J.Comput.Phys* **13** 445

Johnston K.J., Stolovy S.R., Wilson T.L., Henkel C. and Mauersberger R. (1989) *Astrophys.J.* **343** l41

Karl G., Poll J.L. and Wolniewicz L. (1975) *Canad.J.Phys.* **53** 1781

Klaasen D.B.M., Reijnders J.M.H., Ter Meulen J.J. and Dynamus A. (1982) *J.Chem.Phys* **77** 4972

Klaasen D.B.M., Ter Meulen J.J. and Dynamus A. (1983) *J.Chem.Phys* **78** 767

Kochanski E. and Flower D.R. (1981) *Chemical Physics* **57** 217

Kolos W. and Wolniewicz L. (1967) *J.Chem.Phys.* **46** 1426

Kreek H., Ellis and Marcus K.A. (1975) *J.Chem.Phys.* **62** 913

Launay J.M. (1976) *J.Phys.B:Atom.Mol.Phys.* **9** 1823

Leavitt R.P. (1980) *J.Chem.Phys.* **72** 3472

Lefebvre-Brion H. and Field R.W. (1986) "Perturbations in the Spectra of Rotating Diatomic Molecules", Academic Press

Lester W.A. (1971) *Methods.Comput.Phys* **10** 211

Lester W.A. (1976) In "Dynamics of Molecular Collisions", Ed. W.Miller, Plenum Press, pp 1

Manolopoulos D.E. (1986) *J.Chem.Phys.* **85** 6425

Mauersberger R., Henkel C. and Wilson T.L. (1987) *Astron.Astrophys.* **173** 352

Mauersberger R., Wilson T.L. and Henkel C. (1988) *Astron.Astrophys.* **201** 123

McGuire P. and Kouri D.J. (1974) *J.Chem.Phys.* **60** 2488

Miller W. (1971) *J.Chem.Phys.* **54** 5386

Miller W. (1974) *Adv.Chem.Phys.* **25** 69

Miller W. (1975) *Adv.Chem.Phys.* **30** 77

Oka T., Shimuzu T. and Watson J.K.G. (1971) *Astrophys.J.Lett.* **165** L15

Oka T. (1973) *Adv.Atom.Molec.Phys.* **9** 127

Pack R.T. (1974) *J.Chem.Phys.* **60** 633

Pineau des Forets G., Roueff E. and Flower D.R. (1989) *Mon.Not.Royal. Astron.Soc* **244** 268

Poynter R.L. and Beaudet R.A. (1968) *Phys.Rev.Lett.* **21** 305

Rabitz H. (1976) In "Dynamics of Molecular Collisions", part a, Ed. W.Miller, Plenum Press, pp 33

Roothaan C.J. (1951) *Rev.Modern.Phys* **23** 69

Schilke P. (1989) Diplomarbeit, Universität Bonn.

Schinke R. and Andresen P. (1984) *J.Chem.Phys* **81** 5644

Secrest D. (1979) In "Atom–Molecule Collision Theory: A Guide for the Experimentalist", Ed. R.B.Bernstein, Plenum Press, pp 265

Secrest D. (1983) In "Molecular Collision Dynamics",
Ed. J.M.Bowman, Springer Verlag, Berlin, Heidelberg, N.Y. pp 7

Seelemann P., Andresen J., Schleipen B., Beyer J.J. and Ter Meulen J.J. (1988) *Chemical Physics* **126** 27

Spitzer L. (1978) "Physical Processes in the Interstellar Medium", J.Wiley and Sons.

Stone A.J. and Tough R.J.A. (1984) *Chem.Phys.Lett.* **110** 123

Takano T. (1986) *Astrophys.J.* **303** 349

Takayanagi K. (1965) *Adv.Atom.Molec.Phys.* **1** 149

Thomas L.D., Alexander M.H., Johnson B.R., Lester W.A., Light J.C., McLenithan K.D., Parker G.A., Redmon M.J., Schmalz T.G., Secrest D. and Walker R.B. (1981) *J.Comput.Phys* **41** 407

Toennies J.P. (1976) *Ann.Rev.Phys.Chem.* **27** 225

Townes C.H. and Schawlow A.L. (1955) "Microwave Spectroscopy", McGraw Hill.

Valiron P. (1988) Private Communication

Walmsley C.M. and Ungerechts H. (1983) *Astron.Astrophys.* **122** 164

Walmsley C.M. (1987) In "Physical Processes in Interstellar Clouds", Ed. G.E.Morfill and M.Scholer, D.Reidel, pp 161

Appendix A

The Relationship between the S-matrix and the Integral Cross-Sections

The close coupled equations may be written;

$$\left[\frac{d^2}{dR^2} - \frac{l'(l'+1)}{R^2} + \kappa_{\alpha'}^2\right] G_{\gamma'}^{J\gamma}(R) = 2\mu \sum_{\gamma''} \langle \gamma' | V | \gamma'' \rangle G_{\gamma''}^{J\gamma} \qquad A1$$

where $\gamma \equiv (j_1, j_2, j_{12}, k_1, k_2, l)$ and $\alpha \equiv (j_1, j_2, k_1, k_2)$.

In the limit $V \rightarrow 0$ the general solution to equation A1 can be written as a linear sum of spherical Bessel functions of the first and second kind ($j_l(\kappa R)$ and $n_l(\kappa R)$),

$$G_{\gamma'}^{J\gamma}(R) \rightarrow \delta_{\gamma\gamma'} \quad \kappa_\alpha^{1/2} R \left\{ A_\gamma^J j_l(\kappa_\alpha R) + B_\gamma^J n_l(\kappa_\alpha R) \right\} \qquad A2$$

In equation A1, $G_{\gamma'}^{J\gamma}(R)$ is the radial part of the wavefunction, and is related to the full wavefunction, Ψ by:

$$\Psi_\gamma^{JM}(\mathbf{R}, \hat{\Omega}_1, \hat{\Omega}_2) = \sum_{\gamma'} \frac{G_{\gamma'}^{J\gamma}(R)}{R} Z_{\gamma'}^{JM}(\hat{R}, \hat{\Omega}_1, \hat{\Omega}_2) \qquad A3$$

where $Z_{\gamma'}^{JM}(\hat{R}, \hat{\Omega}_1, \hat{\Omega}_2)$ is given by equation 2.2.3.

The asymptotic behaviour of the spherical Bessel functions as $R \rightarrow \infty$ is given by:

$$\begin{aligned} j_l(\kappa R) &\rightarrow (\kappa R)^{-1} \sin(\kappa R - l\pi/2) \\ &= (\kappa R)^{-1} \left(\frac{\exp(i(\kappa R - l\pi/2)) - \exp(-i(\kappa R - l\pi/2))}{2i} \right) \\ n_l(\kappa R) &\rightarrow -(\kappa R)^{-1} \cos(\kappa R - l\pi/2) \\ &= -(\kappa R)^{-1} \left(\frac{\exp(i(\kappa R - l\pi/2)) + \exp(-i(\kappa R - l\pi/2))}{2} \right) \end{aligned} \qquad A4$$

Substituting A4 into A2 yields the asymptotic solution:

$$G^{J\gamma}_{\gamma'}(R) \rightarrow \delta_{\gamma\gamma'}\kappa_\alpha^{-1/2}\left\{a^J_\gamma \exp(-i(\kappa_\alpha R - l\pi/2)) - b^J_\gamma \exp(i(\kappa_\alpha R - l\pi/2))\right\} \qquad A5$$

where:

$$a^J_\gamma = -\left[\frac{A^J_\gamma + iB^J_\gamma}{2i}\right] \qquad b^J_\gamma = \left[\frac{-A^J_\gamma + iB^J_\gamma}{2i}\right] \qquad A6$$

Here a^J_γ is the amplitude of an incoming spherical wave, and b^J_γ is the amplitude of an outgoing wave. The Scattering matrix is defined by (Lester, 1976):

$$b^J_{\gamma'} = \sum_\gamma S^J_{\gamma\rightarrow\gamma'} a^J_\gamma. \qquad A7$$

With this definition of the scattering matrix, the solution to the CC equations as $R \rightarrow \infty$ can be written (Takayanagi, 1965):

$$G^{J\gamma}_{\gamma'}(R) \rightarrow \frac{a^J_\gamma}{\kappa^{1/2}_{\alpha'}}\left\{\exp(-i(\kappa_\alpha R - l\pi/2))\delta_{\gamma\gamma'} - \exp(i(\kappa_{\alpha'}R - l'\pi/2))S^J_{\gamma\rightarrow\gamma'}\right\}. \qquad A8$$

The relationship between the S-matrix elements, $S^J_{\gamma\rightarrow\gamma'}$, and the scattering amplitude, $f_{\alpha m_1 m_2\rightarrow\alpha' m_1' m_2'}(\hat{R})$, can be derived by expressing the full wavefunction, Ψ^{JM}_γ, in terms of an incoming (incident) plane wave in channel γ, and an outgoing (scattered) spherical wave thus as $R \rightarrow \infty$:

$$\begin{aligned}\Psi^{JM}_\gamma \rightarrow\ & \exp(i\mathbf{k}_\alpha.\mathbf{R})\ \chi^{j_1}_{k_1 m_1}(\hat{\Omega}_1)\chi^{j_2}_{k_2 m_2}(\hat{\Omega}_2) \\ & + \sum_{\alpha' m_1' m_2'} \frac{f_{\alpha m_1 m_2\rightarrow\alpha' m_1' m_2'}(\hat{R})}{R} \exp(i\kappa_{\alpha'}R)\ \chi^{j_1'}_{k_1' m_1'}(\hat{\Omega}_1)\chi^{j_2'}_{k_2' m_2'}(\hat{\Omega}_2)\end{aligned} \qquad A9$$

where $\chi^j_{km}(\hat{\Omega})$ are the molecular rotational eigenfunctions.

The first term on the right hand side of equation A9 can be expanded in a standard plane wave expansion:

$$\begin{aligned}\exp(i\mathbf{k}_\alpha.\mathbf{R}) \rightarrow & \sum_l (2l+1)^{1/2}(-i^{l+1})\left(\frac{\pi^{1/2}}{\kappa_\alpha R}\right) Y^l_0(\hat{R}) \\ & \times (\exp(i(\kappa_\alpha R - l\pi/2)) - \exp(-i(\kappa_\alpha R - l\pi/2)))\end{aligned} \qquad A10$$

Using the transformation :

$$\chi^{j_1}_{k_1 m_1}(\hat{\Omega}_1)\chi^{j_2}_{k_2 m_2}(\hat{\Omega}_2)Y^l_0(\hat{R}) = \sum_{JM}\sum_{j_{12}} C^{j_1\ j_2\ j_{12}}_{m_1 m_2 M} C^{j_{12} l\ J}_{M\ 0 M} Z^{JM}_\gamma(R,\hat{\Omega}_1,\hat{\Omega}_2), \qquad A11$$

we obtain in the limit $R \to \infty$:

$$\begin{aligned}\Psi^{JM}_\gamma(\mathbf{R},\hat{\Omega}_1,\hat{\Omega}_2) \to & \sum_{JM}\sum_{j_{12}l}(-i^{l+1})\frac{(2l+1)^{1/2}}{\kappa_\alpha R}\pi^{1/2} \\ & \times C^{j_1\ j_2\ j_{12}}_{m_1 m_2 M} C^{j_{12} l\ J}_{M\ 0 M} Z^{JM}_\gamma(\hat{R},\hat{\Omega}_1,\hat{\Omega}_2) \\ & \times (\exp(i(\kappa_\alpha R - l\pi/2)) - \exp(-i(\kappa_\alpha R - l\pi/2))) \\ & + \sum_{\alpha' m_1' m_2'} \frac{f_{\alpha m_1 m_2 \to \alpha' m_1' m_2'}(\hat{R})}{R}\exp(i\kappa_{\alpha'} R) \\ & \times \chi^{j_1'}_{k_1' m_1'}(\hat{\Omega}_1)\chi^{j_2'}_{k_2' m_2'}(\hat{\Omega}_2)\end{aligned} \qquad A12$$

Equating the coefficients of the incoming and outgoing waves in equation A11 with those in the asymptotic form of the wavefunction given by equations A3 and A8, we have:

$$a^J_\gamma = \left(\frac{\pi}{\kappa_\alpha}\right)^{1/2} i^{l+1}\, C^{j_1\ j_2\ j_{12}}_{m_1 m_2 M}\, C^{j_{12} l\ J}_{M\ 0 M}\,(2l+1)^{1/2} \qquad A13$$

and:

$$\begin{aligned}f_{\alpha m_1 m_2 \to \alpha' m_1' m_2'}(\hat{R}) = & \sum_J \sum_{j_{12} j_{12}' l l'} \left(\frac{\pi}{\kappa_\alpha \kappa_{\alpha'}}\right)^{1/2} i^{l-l'+1}(2l+1)^{1/2} \\ & \times C^{j_1\ j_2\ j_{12}}_{m_1 m_2 M} C^{j_{12} l\ J}_{M\ 0 M} C^{j_1'\ j_2'\ j_{12}'}_{m_1' m_2' M} C^{j_{12}'\ l'\ J}_{m_{12}' m_l' M} \\ & \times Y^{l'}_{m_l'}(\hat{R})(\delta_{\gamma\gamma'} - S^J_{\gamma\to\gamma'})\end{aligned} \qquad A14$$

The differential cross-section is obtained from the scattering amplitude through (Lester, 1976):

$$\begin{aligned}\frac{d}{d\hat{R}}\sigma(\alpha m_1 m_2 \to \alpha' m_1' m_2'|\hat{R}) &= \frac{\text{scattered flux}}{\text{incident flux}} \\ &= \frac{\kappa_{\alpha'}}{\kappa_\alpha}|f_{\alpha m_1 m_2 \to \alpha' m_1' m_2'}(\hat{R})|^2\end{aligned} \qquad A15$$

For most applications the cross-sections are averaged over the initial $(2j_1 + 1)$ $\times(2j_2 + 1)$ possible values of m_1, m_2, and summed over the final values :

$$d\sigma(\alpha \rightarrow \alpha'|\hat{R}) = \frac{1}{(2j_1+1)(2j_2+1)} \sum_{m_1' m_2'} d\sigma(\alpha m_1 m_2 \rightarrow \alpha' m_1' m_2'|\hat{R}). \qquad A16$$

The integral cross-sections are obtained by integrating over all angles, $\hat{R}$, to give (Takayanagi, 1965):

$$\sigma(\alpha \rightarrow \alpha') = \sum_J \sigma^J(\alpha \rightarrow \alpha') = \frac{\pi}{(2j_1+1)(2j_2+1)\kappa_\alpha^2} \sum_J \sum_{j_{12} j_{12}' l l'} (2J+1)|T^J_{\gamma\gamma'}|^2 \qquad A17$$

where the $\sigma^J(\alpha \rightarrow \alpha')$ are the partial cross-sections, and the matrix, $\mathbf{T}$, is the transmission matrix defined by:

$$\mathbf{T^J} = \mathbf{I} - \mathbf{S^J} \qquad A18$$

To avoid the use of complex algebra, in practice the $R \rightarrow \infty$ boundary condition that is often used in place of equation A8 takes the form:

$$G^{J\gamma}_{\gamma'} \rightarrow = \kappa_{\alpha'}^{-1/2}(\sin(\kappa_\alpha R - l\pi/2)\delta_{\gamma\gamma'} + K^J_{\gamma\gamma'}\cos(\kappa_{\alpha'} R - l'\pi/2)) \qquad A19$$

where $\mathbf{K}$ is the reactance matrix related to the scattering matrix by:

$$\mathbf{S^J} = (\mathbf{I} + i\mathbf{K^J})(\mathbf{I} - i\mathbf{K^J})^{-1} \qquad A20$$

Appendix B

Modifications to Molscat for NH_3–H_2 collisions

The program MOLSCAT (Hutson and Green, 1986) provides template subroutines BAS9IN and CPL9 that facilitate the addition of an extra collision type (labelled ITYPE= 9). In the case of NH_3–H_2 collisions the extension is fairly straight forward, and the additional subroutines used are given below.

```
      SUBROUTINE BAS9IN(PRTP,IBOUND)
      IMPLICIT DOUBLE PRECISION (A-H,O-Z)
      CHARACTER*8 PRTP(4),QNAME(10)
      LOGICAL LEVIN,EIN,LCNT
      DIMENSION ROTI(10),ELEVEL(200),JLEVEL(400)
      DIMENSION JLEV(1),VL(1),IV(1),J(1),L(1),CENT(1),LAM(1)
      DIMENSION WT(2),ALPHAE(2),BE(2),DE(2),A(2),B(2),C(2)
      EQUIVALENCE (ROTI(1),BE(1),A(1)),(ROTI(3),ALPHAE(1),B(1)),
     1           (ROTI(5),DE(1),C(1)),(JMIN,J1MIN),(JMAX,J1MAX),
     2           (JSTEP,J1STEP)
      COMMON/CMBASE/ROTI,ELEVEL,EMAX,WT,SPNUC,JMIN,JMAX,J2MIN,
     1           J2MAX,JSTEP,J2STEP,NLEVEL,JLEVEL,IDENT
C
      IF (IDENT.GT.0.OR.IBOUND.GT.0) STOP ' IDENT/IBOUND > 0 '
C
      PRTP(1) =  ' SYMMETR'
      PRTP(2) =  'IC TOP -'
      PRTP(3) =  ' LINEAR '
      PRTP(4) =  'ROTOR.  '
      RETURN
```

Entry 'SET9' sets up the arrays JLEVEL, ELEVEL (if these are not given as input data) and JLEV. The latter holds the channel indices, $j_1, j_2, k, \epsilon, j_{12}$ and

I where I labels the channel. The ELEVEL array contains the energies of the rotational levels which may be calculated from equation 2.6.8, and the JLEVEL array contains the indices, j_1, j_2, k and $\epsilon(= (-1)^{IP})$ for each level included in the basis set.

```
      ENTRY SET9(LEVIN,EIN,NLEV,JLEV,NQN,QNAME,MXPAR,NLABV)
C     Number of indices to describe each term in potnl expansion
C     i.e. NLABV(9)
      NLABV = 4
C     Format statements:
 310  FORMAT('SYM.TOP LEVELS COMP. FROM J1MIN=',I3,', J1MAX=',
     1  I3,', J1STEP=',I2/' LINEAR ROTOR LEVELS COMPUTED'
     2  ' FROM J2MIN =',I3,', J2MAX =',I3,', J2STEP =',I2)
 603  FORMAT('0 SYM. TOP ENERGY LEVELS COMPUTED USING '
     1  ROTL CONSTS:',12X,'  A = B =',F12.4,',  C =',F12.4)
 631  FORMAT('0 ENERGY LEVELS TAKEN FROM (ELEVEL) INPUT')
 632  FORMAT('0 ROTL LEVELS TAKEN FROM JLEVEL INPUT NLEVEL='
     1  ,I3)
 633  FORMAT('0 LINEAR ROTOR ENERGY LEVELS CALCULATED'
     1  FROM B(E)=',F12.6)
 634  FORMAT(27X,' CORRECTED FOR ALPHA(E) = ',F10.6)
 635  FORMAT(27X,' CORRECTED FOR D(E) = ',F12.8)
C     Set QNAME values:
      QNAME(1) = '    J1  '
      QNAME(2) = '    J2  '
      QNAME(3) = '     K  '
      QNAME(4) = '  PRTY '
      QNAME(5) = '    J12  '
      MXPAR = 2
      NQN = 6
C
```

```
      IF(.NOT.LEVIN) THEN
        WRITE(6,310)J1MIN,J1MAX,J1STEP,J2MIN,J2MAX,J2STEP
        J1MIN = MAXO(J1MIN,0)
        J1MAX = MAXO(J1MIN,J1MAX)
        J1STEP = MAXO(J1STEP,1)
        J2MIN = MAXO(J2MIN,0)
        J2MAX = MAXO(J2MIN,J2MAX)
        J2STEP = MAXO(J2STEP,1)
        NLEVEL=0
        I = 0
        DO 910 JJ1 = J1MIN,J1MAX,J1STEP
        DO 910 JJ2 = J2MIN,J2MAX,J2STEP
        DO 910 KVAL= 0,JJ1
               IMP = 1
               IF (KVAL.EQ.0) IMP = 0
        DO 910  IP = IMP,0,-1
           JLEVEL(I+1) = JJ1
           JLEVEL(I+2) = JJ2
           JLEVEL(I+3) = KVAL
           JLEVEL(I+4) = IP
           I = I + 4
           NLEVEL = NLEVEL + 1
 910    CONTINUE
      ELSE
        WRITE(6,632)NLEVEL
      END IF
C
      JMIN = IABS(JLEVEL(1) - JLEVEL(2))
      JMAX = JMIN
```

```
C     Sort out in the same way as for SET3
      NLEV = 0
      DO 920 I=1,NLEVEL
         JJ1 = JLEVEL(4*I-3)
         JJ2 = JLEVEL(4*I-2)
         DO 920 J12 = IABS(JJ1-JJ2),(JJ1+JJ2)
            JLEV(6*NLEV+1) = JJ1
            JLEV(6*NLEV+2) = JJ2
            JLEV(6*NLEV+3) = JLEVEL(4*I-1)
            JLEV(6*NLEV+4) = JLEVEL(4*I)
            JLEV(6*NLEV+5) = J12
            JLEV(6*NLEV+6) = I
            NLEV = NLEV + 1
            JMIN = MINO(JMIN,J12)
            JMAX = MAXO(JMAX,J12)
 920  CONTINUE
C     Rearrange to the proper order
      JK = 6*NLEV
      DO 930 I = 1,NLEV
        DO 930 IB = 0,5
          JLEV(JK+(IB*NLEV)+I) = JLEV(6*I-(5-IB))
 930  CONTINUE
C     Copy back
      DO 940 I = 1,JK
        JLEV(I) = JLEV(JK+I)
 940  CONTINUE
C     Set ELEVEL values:
      IF (.NOT.EIN) THEN
         WRITE(6,603) B(1),C(1)
```

```
          WRITE(6,633) BE(2)
          IF (ALPHAE(2).NE.0.D0) WRITE(6,634) ALPHAE(2)
          IF (DE(2).NE.0.D0) WRITE(6,635) DE(2)
          DO 950 I = 1,NLEVEL
            FJ1 = DFLOAT(JLEVEL(4*I-3))
            FJ2 = DFLOAT(JLEVEL(4*I-2))
            FK  = DFLOAT(JLEVEL(4*I-1))
C           Symmetric top characterized by A(1)=B(1),C(1)
C           Linear rotor by A(2)=BE,B(2)=ALPHAE,C(2)=DE
            ELEVEL(I) = ((BE(2)-ALPHAE(2)*0.5D0)*FJ2*(FJ2+1))
     1                 -  DE(2) * FJ2 * FJ2    +
     2                 B(1)*(FJ1*(FJ1+1)) + (C(1)-B(1))*FK*FK
 950      CONTINUE
        ELSE
            WRITE(6,631)
        END IF
        RETURN
```

Entry BASE9 sets the range of orbital angular momenta, l, for a given calculation $l_{\min} = J - j_{12}, l_{\max} = J + j_{12}$, and splits the calculation into two non-interacting parity blocks (cf equation 2.6.28).

```
        ENTRY BASE9(LCNT,N,JTOT,ICODE,JLEV,NLEV,NQN,J,L)
C
        N=0
        IPAR=ICODE-2*(ICODE/2)
        IEXCH=(ICODE+1)/2
 8002   LMAX=JTOT+JMAX
        LMIN=JTOT-JMAX
        IF (LMIN.GE.0)  GO TO 4101
        LMIN=JMIN-JTOT
```

```
      IF (LMIN.LT.0)  LMIN=0
 4101 DO 4201 LI=LMIN,LMAX
      JK=IABS(JTOT-LI)
      JTOP=JTOT+LI
      DO 4201 I=1,NLEV
C
 9009 JI=JLEV(4*NLEV+I)
      LPJ=JLEV(I)+JLEV(NLEV+I)+JLEV(2*NLEV+I)+
     1    JLEV(3*NLEV+I)+LI+JTOT
C
      IF ( (LPJ-2*(LPJ/2)) .NE. IPAR) GO TO 4201
      IF (JI.LT.JK .OR. JI.GT.JTOP)  GO TO 4201
      N=N+1
      IF (LCNT) GO TO 4201
      J(N)=I
      L(N)=LI
 4201 CONTINUE
      RETURN
```

Entry DEGEN9 gives the degeneracy factor $((2j_1+1)(2j_2+1))^{-1}$ that appears in equation 2.2.12.

```
      ENTRY DEGEN9(J1,J2,RESULT)
      JI1 = JLEVEL(4*J1-3)
      JI2 = JLEVEL(4*J1-2)
      RESULT = DBLE((2*JI1+1)*(2*JI2+1))
      RETURN
      END
```

Subroutine CPL9 provides returns an array containing the values of the *individual* terms in the coupling matrix element sum:

$$\langle j_1' k' j_2' j_{12}' \epsilon'; JM | V_{\lambda_1 \lambda_2 \lambda_\mu} | j_1 k j_2 j_{12} \epsilon; JM \rangle$$

The linear rotor – symmetric top routine given here closely follows the atom – symmetric top routine (ITYPE=5) implemented in the MOLSCAT computer code.

```
      SUBROUTINE CPL9(N,ICODE,NPOTL,LAM,MXLAM,NLEV,JLEV,J,L,
     1 JTOT,VL,IV,CENT,IBOUND,IEXCH,IPRINT)
      IMPLICIT DOUBLE PRECISION (A-H,O-Z)
      DIMENSION LAM(1),JLEV(NLEV,2),J(1),L(1)
      DIMENSION VL(1),IV(1)
      DATA EPS/1.D-10/
C
      SQRTHF=SQRT(.5DO)
C     loop over lambda1,lambda2,lambda and mu:
      DO 1519 LL = 1,MXLAM
        NNZ = 0
        I = LL
        LM1 = LAM(4*LL-3)
        LM2 = LAM(4*LL-2)
        LM  = LAM(4*LL-1)
        MU  = LAM(4*LL)
C     loop over j1,j2,k,j12 and epsilon:
        DO 1529 ICOL = 1,N
           J1 = JLEV(J(ICOL),1)
           J2 = JLEV(J(ICOL),2)
            K = JLEV(J(ICOL),3)
          IS1 = JLEV(J(ICOL),4)
```

```
          J12 = JLEV(J(ICOL),5)
C     loop over j1',j2',k',j12' and epsilon':
          DO 1529 IROW = 1,ICOL
             J1P = JLEV(J(IROW),1)
             J2P = JLEV(J(IROW),2)
              KP = JLEV(J(IROW),3)
             IS2 = JLEV(J(IROW),4)
             J12P= JLEV(J(IROW),5)
             IV(I) = LL
             VL(I) = 0.D0
C     PARFCT is the parity factor in the symmetry adapted CME.
             PARFCT=(1.D0+PARITY(J1+J1P+LM+LM2+MU+IS1+IS2))/2.0
             IF (PARFCT.GE.EPS) THEN
                IF (K.EQ.0)  PARFCT=PARFCT*SQRTHF
                IF (KP.EQ.0) PARFCT=PARFCT*SQRTHF
                KDIF = KP - K
                IF (IABS(KDIF).EQ.MU) THEN
                  WPAR = 1.D0
                  IF (KDIF.LT.0) WPAR = PARITY(MU+LM+LM1+LM2)
                  VL(I) = VL(I) + WPAR * PARFCT *
     1            FLRST(J1,K,J2,J12,L(ICOL),J1P,KP,J2P,J12P,
     2                  L(IROW),LM1,LM2,LM,KDIF,JTOT)
                END IF
                KSUM = K + KP
                IF (IABS(KSUM).EQ.MU) THEN
                  VL(I) =  VL(I) + PARFCT * PARITY(IS1) *
     1            FLRST(J1,-K,J2,J12,L(ICOL),J1P,KP,J2P,J12P,
     2                  L(IROW),LM1,LM2,LM,KSUM,JTOT)
                END IF
```

```
                IF (VL(I).NE.0.D0) NNZ = NNZ + 1
              END IF
C     End of loops over angular momentum indices:
 1529   I = I + NPOTL
        IF (NNZ.EQ.0) WRITE (6,612) JTOT,LL
  612   FORMAT(' *** FOR JTOT=',I4,', ALL COUPLING COEFFS.'
     1         'ARE ZERO FOR POTNL SYMMETRY ',I4,' * * * ')
C     End of loop over lambda1,lambda2,lambda,mu:
 1519 CONTINUE
      RETURN
      END
```

The angular functions appearing in the coupling matrix element (eqn 2.6.36) are calculated by a call to the function FLRST which utilizes the MOLSCAT functions THRJ, THREEJ, SIXJ and NINEJ to calculate the relevant 3-j, 6-j and 9-j functions.

```
      FUNCTION FLRST(J1,K,J2,J12,L,J1P,KP,J2P,J12P,LP,
     1               LAM1,LAM2,LAM,MU,JTOT)
      IMPLICIT DOUBLE PRECISION (A-H,O-Z)
      DOUBLE PRECISION NINEJ
      F(J)=DFLOAT(2*J+1)
      PI=3.14159265358979323846433
      FACTOR=DSQRT(F(J1)*F(J1P)*F(J2)*F(J2P)*F(J12)*F(J12P)*
     1             F(L)*F(LP)*F(LAM)*F(LAM)*F(LAM2))
C     If K1-K2+MU does not equal zero then COUPLE=0
      IF ((K-KP+MU).NE.0) THEN
        CAR=0.D0
      ELSE
        C1=((-1.D0)**(J1P+J2P+KP-J12-JTOT))*FACTOR/(4.D0*PI)
        C2=THREEJ(L,LP,LAM)*THREEJ(J2,J2P,LAM2)
```

```
      C3=THRJ(DFLOAT(J1),DFLOAT(J1P),DFLOAT(LAM1),
     1              DFLOAT(K),DFLOAT(-KP),DFLOAT(MU))
      C4=SIXJ(LP,L,J12P,J12,LAM,JTOT)
      C5=NINEJ(J12,J2,J1,J12P,J2P,J1P,LAM,LAM2,LAM1)
      CAR=C1*C2*C3*C4*C5
    END IF
    FLRST=CAR
    RETURN
    END
```

Appendix C

Modifications to Molscat for OH–H_2 collisions

For the case of OH–H_2 collisions the modifictaion was made more complex by the fact that j_1, Ω, j_{12} and the total angular momentum, J are all half integer. The problem can be largely overcome by carrying $2 \times j_1$ (or j_2, j_{12}, Ω, l or J) in the integer arrays, JLEV and JLEVEL. However, some of the MOLSCAT routines assume that the j's are integral. In particular care must be taken with the 3-j, 6-j, and 9-j routines, and with the output routine where the value of $(2J_{tot} + 1)$ is required.

```
C                    OH-H2 case.
C
C     As j1,j12,Omega, and Jtot are now half integer
C     values stored in integer array jlevel,jlev are
C     twice the real value.
C
C
      SUBROUTINE BAS9IN(PRTP,IBOUND)
      IMPLICIT DOUBLE PRECISION (A-H,O-Z)
      CHARACTER*8 PRTP(4),QNAME(10)
      LOGICAL LEVIN,EIN,LCNT
      DIMENSION ROTI(10),ELEVEL(200),JLEVEL(400)
      DIMENSION JLEV(1),VL(1),IV(1),J(1),L(1),CENT(1),LAM(1)
      DIMENSION WT(2),ALPHAE(2),BE(2),DE(2),A(2),B(2),C(2)
      EQUIVALENCE (ROTI(1),BE(1),A(1)),(ROTI(3),ALPHAE(1),B(1)),
     1        (ROTI(5),DE(1),C(1)),(JMIN,J1MIN),(JMAX,J1MAX),
     2        (JSTEP,J1STEP)
      COMMON/CMBASE/ROTI,ELEVEL,EMAX,WT,SPNUC,JMIN,JMAX,J2MIN,
     1        J2MAX,JSTEP,J2STEP,NLEVEL,JLEVEL,IDENT
```

```
      IF (IDENT.GT.0.OR.IBOUND.GT.0) STOP ' IDENT/IBOUND > 0 '
C
      PRTP(1) =  ' OH MOLE'
      PRTP(2) =  'CULE AND'
      PRTP(3) =  ' LINEAR '
      PRTP(4) =  'ROTOR.  '
      RETURN
C
C       ********************************************
C
      ENTRY SET9(LEVIN,EIN,NLEV,JLEV,NQN,QNAME,MXPAR,NLABV)
C
C     No. of indices to describe each term in potnl expansion:
C                                                 i.e. NLABV(9)
      NLABV = 4
C
C     Format statements:
C
 310  FORMAT('0 OH LEVELS COMPUTED FROM J1MIN =',I3,'/2,J1MAX=',
     1       I3,'/2, J1STEP=',I2/' LINEAR ROTOR LEVELS COMP. '
     2       'FROM J2MIN =',I3,', J2MAX =',I3,', J2STEP =',I2)
 603  FORMAT('0 OH ENERGY LEVELS COMPUTED USING ROTL CONST:'/
     1       12X,'   B =',F12.4)
 631  FORMAT('0 ENERGY LEVELS TAKEN FROM (ELEVEL) INPUT')
 632  FORMAT('0 ROTL LEVELS TAKEN FROM (JLEVEL) INPUT...NLEVEL='
     1        ,I3)
 633  FORMAT(' LINEAR ROTOR ENERGY LEVELS CALC. FROM B(E)=',
     1       F12.6)
 634  FORMAT(27X,' CORRECTED FOR ALPHA(E) = ',F10.6)
```

```
 635  FORMAT(27X,' CORRECTED FOR D(E) = ',F12.8)
C
C     Warning message:
C
      WRITE(6,6999)
 6999 FORMAT( '      1          '2 x j1,j2,k C
C     Set QNAME values:
C
      QNAME(1) = '  2xJ1   '
      QNAME(2) = '  2xJ2   '
      QNAME(3) = '  2xOM   '
      QNAME(4) = '   PRTY '
      QNAME(5) = '  2xJ12   '
      MXPAR = 2
      NQN = 6
C
      IF(.NOT.LEVIN) THEN
        WRITE(6,310)J1MIN,J1MAX,J1STEP,J2MIN,J2MAX,J2STEP
        J1MIN = MAXO(J1MIN,0)
        J1MAX = MAXO(J1MIN,J1MAX)
        J1STEP = MAXO(J1STEP,1)
        J2MIN = MAXO(J2MIN,0)
        J2MAX = MAXO(J2MIN,J2MAX)
        J2STEP = MAXO(J2STEP,1)
        NLEVEL=0
        I = 0
        DO 910 JJ1 = J1MIN,J1MAX,(J1STEP*2)
        DO 910 JJ2 = J2MIN,J2MAX,(J2STEP*2)
        DO 910 KVAL= 0,JJ1,2
```

```
              IMP = 1
              IF (KVAL.EQ.0) IMP = 0
        DO 910  IP = IMP,0,-1
C
C          All J levels = 2 x their real value :
C
           JLEVEL(I+1) = JJ1
           JLEVEL(I+2) = JJ2
           JLEVEL(I+3) = KVAL
           JLEVEL(I+4) = IP
           I = I + 4
           NLEVEL = NLEVEL + 1
 910    CONTINUE
      ELSE
        WRITE(6,632)NLEVEL
      END IF
C
      JMIN = IABS(JLEVEL(1) - JLEVEL(2))
      JMAX = JMIN
C
C     Sort out in the same way as for SET3
C
      NLEV = 0
      DO 920 I=1,NLEVEL
         JJ1 = JLEVEL(4*I-3)
         JJ2 = JLEVEL(4*I-2)
         DO 920 J12 = IABS(JJ1-JJ2),(JJ1+JJ2),2
C
C           All j values 2 x their real values:
```

```
C
            JLEV(6*NLEV+1) = JJ1
            JLEV(6*NLEV+2) = JJ2
            JLEV(6*NLEV+3) = JLEVEL(4*I-1)
            JLEV(6*NLEV+4) = JLEVEL(4*I)
            JLEV(6*NLEV+5) = J12
            JLEV(6*NLEV+6) = I
            NLEV = NLEV + 1
            JMIN = MINO(JMIN,J12)
            JMAX = MAXO(JMAX,J12)
 920  CONTINUE
C
C     Rearrange to proper order
C
      JK = 6*NLEV
      DO 930 I = 1,NLEV
        DO 930 IB = 0,5
          JLEV(JK+(IB*NLEV)+I) = JLEV(6*I-(5-IB))
 930  CONTINUE
C
C     Copy back
C
      DO 940 I = 1,JK
        JLEV(I) = JLEV(JK+I)
 940  CONTINUE
C
C     Set ELEVEL values:
C     These were just used when checking the program,
C     final Energy levels were read in from the input data
```

```
C
      IF (.NOT.EIN) THEN
         WRITE(6,603) B(1)
         WRITE(6,633) BE(2)
         IF (ALPHAE(2).NE.0.D0) WRITE(6,634) ALPHAE(2)
         IF (DE(2).NE.0.D0) WRITE(6,635) DE(2)
         DO 950 I = 1,NLEVEL
           FJ1 = DFLOAT(JLEVEL(4*I-3))/2.D0
           FJ2 = DFLOAT(JLEVEL(4*I-2))/2.D0
           OM  = DFLOAT(JLEVEL(4*I-1))/2.D0
C
C          OH characterised by B(1)(J(J+1) - OMEGA x OMEGA )
C          to first order.
C          Linear rotor by A(2)=BE,B(2)=ALPHAE,C(2)=DE
C
           ELEVEL(I) = ((BE(2)-ALPHAE(2)*0.5D0)*FJ2*(FJ2+1)) -
     1                   DE(2) * FJ2 * FJ2    +
     2                B(1)*(FJ1*(FJ1+1) - OM * OM )
 950     CONTINUE
      ELSE
          WRITE(6,631)
      END IF
      RETURN
C
C       ***********************************************
C
      ENTRY BASE9(LCNT,N,JTOT,ICODE,JLEV,NLEV,NQN,J,L)
C
      N=0
```

```
      IPAR=ICODE-2*(ICODE/2)
      IEXCH=(ICODE+1)/2
C
C     L values will be 2 x true L values
C
 8002 LMAX=JTOT+JMAX
      LMIN=JTOT-JMAX
      IF (LMIN.GE.0)  GO TO 4101
      LMIN=JMIN-JTOT
      IF (LMIN.LT.0)  LMIN=0
 4101 DO 4201 LI=LMIN,LMAX,2
      JK=IABS(JTOT-LI)
      JTOP=JTOT+LI
      DO 4201 I=1,NLEV
C
 9009 JI=JLEV(4*NLEV+I)
C
C     parity blocks...cf equation 5.4.14
C     LPJ ≡ j1 + 2 * Omega + j2 + l + Jtot + IS1
C
      LPJ=(JLEV(I) + JLEV(NLEV+I) + JTOT + LI) / 2
     1                +JLEV(3*NLEV+I) + JLEV(2*NLEV+I)
C
      IF ( (LPJ-2*(LPJ/2)) .NE. IPAR) GO TO 4201
      IF (JI.LT.JK .OR. JI.GT.JTOP)  GO TO 4201
      N=N+1
      IF (LCNT) GO TO 4201
      J(N)=I
      L(N)=LI/2
```

```
      IF (LI .NE.(L(N)*2))STOP 'ERROR IN L(I)'
 4201 CONTINUE
      RETURN
C
C         ****************************************
C
      ENTRY DEGEN9(J1,J2,RESULT)
C
C     Degeneracy factor:
C
      JI1 = JLEVEL(4*J1-3)
      JI2 = JLEVEL(4*J1-2)
C
C     Degen factor = (2j1+1)(2j2+1)
C     ...but j's are 2× real values:
C     (2*JTOT + 1 ) problem dealt with in OH.OUTPUT
C
      RESULT = DBLE((JI1+1)*(JI2+1))
      RETURN
      END
```

CPL9 returns the individual elements in the coupling matrix element sum (equation 5.4.15). The coefficients X (equation 5.2.9c) are returned from the function XCOE, and the angular functions are returned from the function FOHH2.

```
      SUBROUTINE CPL9(N,ICODE,NPOTL,LAM,MXLAM,NLEV,JLEV,J,L,
     1 JTOT,VL,IV,CENT,IBOUND,IEXCH,IPRINT)
      IMPLICIT DOUBLE PRECISION (A-H,O-Z)
      DIMENSION LAM(1),JLEV(NLEV,2),J(1),L(1)
      DIMENSION VL(1),IV(1)
      DATA EPS/1.D-10/
```

```
C
C     Statement function to convert J array values to real j
C
      G(I)=DFLOAT( I )/2.D0
C
      SQRTHF=DSQRT(.5D0)
      XJTOT  = G( JTOT )
C
      DO 1519 LL = 1,MXLAM
        NNZ = 0
        I = LL
        LM1 = LAM(4*LL-3)
        LM2 = LAM(4*LL-2)
        LM  = LAM(4*LL-1)
        MU  = LAM(4*LL)
C
C       Loop over initial state...
C
        DO 1529 ICOL = 1,N
          L0 = L(ICOL)
          J1 = JLEV(J(ICOL),1)
          J2 = JLEV(J(ICOL),2)
         IOM = JLEV(J(ICOL),3)
         IS1 = JLEV(J(ICOL),4)
         J12 = JLEV(J(ICOL),5)
         XJ1 = G(J1)
C
C        Loop over final state:
C
```

```
            DO 1529 IROW = 1,ICOL
               LP = L(IROW)
              J1P = JLEV(J(IROW),1)
              J2P = JLEV(J(IROW),2)
             IOMP = JLEV(J(IROW),3)
              IS2 = JLEV(J(IROW),4)
              J12P= JLEV(J(IROW),5)
              XJ1P= G(J1P)
C
C   Initialize VL array:
C
               IV(I) = LL
               VL(I) = 0.DO
C
C       Parity factor: ...Note minus sign for OH-H2 problem
C                           enters from the 2xOmega power of one.
C
               IPWR = (J1 + J1P + 2 * IOMP )/2
               PARFCT=(1.DO + PARITY(IPWR+LM+LM2+IS1+IS2))/2.DO
               IF (PARFCT.GE.EPS) THEN
C
C       Now sum over omega...
C
                DO 2222 KOM = 1,3,2
                   OM = DFLOAT(KOM) / 2.DO
                DO 2224 KOMP = 1,3,2
                   OMP = DFLOAT(KOMP) / 2.DO
C
C       Values of A_j, B_j, A'_j and B'_j returned from
```

```
C       function as XCOE
C
                  XCOEF = XCOE(J1P,IOMP,KOMP)*XCOE(J1,IOM,KOM)
C
C       Note for OH... mu = 0 terms have Omega = Omega' only
C                              hence, kom - komp only here.
C                       mu = 2 terms have Omega <> Omega' only.
C
                  IF (MU.EQ.0 .AND. IABS(KOM-KOMP).EQ.0) THEN
                      F1 = FOHH2(J1,KOM,J2,J12,L0,J1P,KOMP,J2P,
     1                         J12P,LP,LM1,LM2,LM,0,JTOT,LL)
                  ELSE IF(MU.EQ.2.AND.IABS(KOM+KOMP).EQ.4) THEN
                      F1 = FOHH2(J1,-KOM,J2,J12,L0,J1P,KOMP,J2P,
     1                         J12P,LP,LM1,LM2,LM,2,JTOT,LL)
                      F1 = F1 * PARITY(IS1)
                  ELSE
                      F1 = 0.D0
                  END IF
                  VL(I) = VL(I) + PARFCT * F1 * XCOEF
C
C        End of summation over omega's
C
 2224           CONTINUE
 2222           CONTINUE
              END IF
C
              IF (VL(I).NE.0.D0) NNZ = NNZ + 1
 1529       I = I + NPOTL
            IF (NNZ.EQ.0) WRITE (6,612) JTOT,LL
```

```
  612       FORMAT('*** FOR JTOT =',I4,'/ 2 ,ALL COUPLING',
     1         'COEFFS. = 0 FOR LAMBDA INDEX ',I4,' *** ')
 1519    CONTINUE
         RETURN
         END
```

The routines DSIXJ and DNINEJ that are called from the function FOHH2, are modified versions of the MOLSCAT routines SIXJ and NINEJ, modified to accept real arguments. The subroutine DNINEJ calls DJ9J, a modified version of J9J that does not assume that the angular momentum indices are integer.

```
      FUNCTION FOHH2(J1,K,J2,J12,L,J1P,KP,J2P,J12P,LP,
     1                LAM1,LAM2,LAM,MU,JTOT,LL)
C
C     WORKS OUT COUPLING MATRIX ELEMENTS
C
      IMPLICIT DOUBLE PRECISION (A-H,O-Z)
      DOUBLE PRECISION NINEJ
      F(J)=DFLOAT(2*J+1)
      H(J)=DFLOAT(  J+1)
      G(J)=DFLOAT(J)/2.DO
      PI=3.14159265358979323846433
      EPS=0.1D-5
      FACTOR=DSQRT(H(J1)*H(J1P)*H(J2)*H(J2P)*H(J12)*H(J12P)*
     1             F(L)*F(LP)*F(LAM)*F(LAM)*F(LAM2))
C
C     if K1-K2+MU does not equal zero then COUPLE=0
C
      IF ((K-KP+(2 * MU)).NE.0) THEN
        CAR=0.DO
        PRINT*,'LL =',LL,'   WHAT AM I DOING HERE ??? '
```

```
      ELSE
        C1=((-1.D0)**((J1P+J2P-KP-J12-JTOT)/2))*FACTOR/(4.D0*PI)
        C2=THREEJ(L,LP,LAM)*THREEJ(J2/2,J2P/2,LAM2)
        C3=THRJ(G(J1),G(J1P),DFLOAT(LAM1),
     1              G(K),G(-KP),DFLOAT(MU))
        C4=DSIXJ(DFLOAT(LP),DFLOAT(L),G(J12P),
     1             G(J12),DFLOAT(LAM),G(JTOT))
        C5=DNINEJ( DFLOAT(LAM),DFLOAT(LAM2),DFLOAT(LAM1),
     1             G(J12),G(J2),G(J1),G(J12P),G(J2P),G(J1P))
        CAR=C1*C2*C3*C4*C5
      END IF
      FOHH2=CAR
      RETURN
      END
C
C   ************************************************************
C
      FUNCTION DSIXJ(XJ1,XJ2,XJ5,XJ4,XJ3,XJ6)
      IMPLICIT DOUBLE PRECISION(A-H,O-Z)
      DIMENSION XJ6J(200)
C
      CALL J6J(XJ2,XJ3,XJ4,XJ5,XJ6,IVAL,XJ1MIN,XJ6J)
C
      IND= 1 + (INT(2.D0*XJ1+0.1D0)-INT(2.D0*XJ1MIN +0.1D0))/2
      DSIXJ = 0.D0
      IF (IND.GE.1.AND.IND.LE.IVAL) DSIXJ = XJ6J(IND)
      RETURN
      END
C
```

```
C   ************************************************************
C
      FUNCTION DNINEJ(X1,Y1,Z1,X2,Y2,Z2,X3,Y3,Z3)
      IMPLICIT DOUBLE PRECISION(A-H,O-Z)
      DIMENSION XJ9J(200)
C
      CALL DJ9J( X1,Y1,X2,Y2,Z2,X3,Y3,Z3,IVAL,Z1MIN,XJ9J)
C
      IND= 1 + (INT(2.DO*Z1+0.1DO)-INT(2.DO*Z1MIN+0.1DO))/2
      DNINEJ = 0.DO
      IF (IND.GE.1.AND.IND.LE.IVAL) DNINEJ = XJ9J(IND)
      RETURN
      END
```

Note that the 9-j J9J routine implemented in MOLSCAT also needs slight editing (giving DJ9J here), as it too assumes that the j's are integer.

The value of the coefficient X defined by equation 5.2.9c is returned from the function XCOE:

```
      FUNCTION XCOE(J,IOM,K)
      IMPLICIT REAL*8 (A-H,O-Z)
      DATA TWO/ 2.DO /, EPS / 1.D-05 /
      DATA RATIO / -7.501DO /
C
C
      CONST = RATIO * (RATIO - 4.DO)
      FJ = DFLOAT(J)/2.DO
      OMEGA = DFLOAT(IOM)/2.DO
      FK = DFLOAT(K)/2.DO
C
C
```

```
      FJPH = FJ + 0.5D0
      X = DSQRT( 4.D0 * FJPH * FJPH + CONST )
C
C     Case where omega ≠ k
C
      IF (DABS(OMEGA-FK) .GT. EPS) THEN
           SJJ = X - TWO + RATIO
           IF (DABS(SJJ) .LE. EPS) THEN
                SJ = 0.D0
           ELSE
                SJ = DSQRT( SJJ / ( TWO * X ) )
           END IF
           IF (OMEGA .LT. 1.45D0 ) THEN
                SJ = -SJ
           END IF
C
C     Case where omega = k
C
      ELSE
           SJJ = X + TWO - RATIO
           IF (DABS(SJJ) .LE. EPS) THEN
                SJ = 0.D0
           ELSE
                SJ = DSQRT( SJJ / (TWO * X) )
           END IF
      END IF
      XCOE = SJ
      RETURN
      END
```

Appendix D

NH_3–H_2 space fixed potential coefficients

SCF+EK potential

The potential coefficients are given in units of cm^{-1} at selected intermolecular distances.

$v_{\lambda_1\lambda_2\lambda\mu}$	$4.0a_0$	$4.4a_0$	$4.8a_0$	$5.2a_0$	$5.6a_0$	$6.0a_0$
v_{0000}	74375.063	35458.883	15531.074	6102.250	1868.738	101.099
v_{0220}	2277.437	960.354	328.689	63.867	-35.759	-65.194
v_{1010}	-12876.395	-6505.680	-3193.224	-1549.452	-743.686	-352.559
v_{1210}	5201.809	3095.042	1999.412	1369.350	968.332	702.750
v_{1230}	-1085.176	-587.739	-331.537	-200.823	-133.704	-95.386
v_{2020}	-9440.414	-3863.168	-1397.266	-393.042	-27.858	76.349
v_{2200}	-12481.793	-7027.191	-4249.199	-2716.202	-1795.615	-1217.265
v_{2220}	3530.340	1946.488	1177.016	754.112	496.607	333.364
v_{2240}	-788.225	-432.854	-244.559	-143.989	-93.725	-66.623
v_{3030}	11566.574	5637.688	2671.778	1231.759	539.902	213.904
v_{3033}	-13711.836	-6717.406	-3202.722	-1493.427	-670.110	-280.143
v_{3210}	4391.113	2058.423	967.816	481.053	264.249	159.906
v_{3213}	-1248.817	-564.430	-292.702	-168.427	-102.755	-64.341
v_{3223}	-311.300	-151.175	-65.977	-28.116	-13.538	-7.849
v_{3230}	-1723.172	-772.251	-365.723	-186.368	-102.442	-59.658
v_{3233}	945.640	404.399	196.634	106.244	60.196	34.101
v_{3243}	675.135	328.211	153.048	73.541	39.491	23.966
v_{3250}	548.021	224.040	139.268	99.017	65.896	40.333
v_{3253}	-2732.359	-1318.324	-679.583	-377.888	-222.745	-136.367
v_{4040}	326.792	68.746	-7.673	-23.819	-22.188	-16.847
v_{4043}	4936.992	2264.956	1031.896	467.076	205.707	83.900
v_{4220}	671.510	278.174	144.695	85.288	49.114	25.953
v_{4223}	1384.184	577.783	263.203	132.982	73.902	43.474
v_{4233}	-1008.150	-491.983	-246.550	-130.937	-74.337	-44.832

$v_{\lambda_1\lambda_2\lambda\mu}$	$4.0a_0$	$4.4a_0$	$4.8a_0$	$5.2a_0$	$5.6a_0$	$6.0a_0$
v_{4240}	-125.366	-52.044	-29.423	-19.546	-12.715	-7.721
v_{4243}	-724.527	-283.380	-122.070	-60.242	-33.761	-20.133
v_{4253}	1082.667	521.373	261.314	139.917	80.361	49.158
v_{4260}	-125.512	-18.159	0.673	3.254	5.099	6.284
v_{4263}	1341.479	592.365	279.557	144.734	81.753	48.624
v_{5050}	-1975.918	-773.190	-312.659	-129.665	-52.523	-18.751
v_{5053}	212.687	82.074	32.552	11.681	2.441	-1.573
v_{5230}	-1890.052	-756.101	-319.972	-146.921	-75.430	-42.965
v_{5233}	733.951	347.601	164.992	82.553	45.208	26.791
v_{5243}	861.468	395.086	181.372	88.160	47.382	27.805
v_{5250}	553.688	197.335	79.639	36.877	19.089	10.500
v_{5253}	-213.597	-96.378	-46.512	-25.178	-15.418	-10.237
v_{5263}	-833.166	-385.332	-174.589	-83.160	-44.232	-26.051
v_{5270}	9.920	26.598	10.575	-0.451	-3.121	-2.021
v_{5273}	-326.874	-166.328	-80.963	-41.533	-24.043	-15.666
v_{6060}	562.150	187.093	61.760	20.930	7.315	2.333
v_{6063}	-1009.280	-345.546	-121.582	-44.950	-17.246	-6.439
v_{6066}	1065.404	376.473	134.679	49.519	18.771	6.923
v_{6240}	340.419	98.271	28.638	8.231	1.075	-1.876
v_{6243}	-1153.609	-453.644	-185.688	-82.793	-41.430	-22.735
v_{6246}	1110.423	405.223	154.655	65.868	31.812	16.275
v_{6253}	-175.510	-93.255	-48.177	-25.913	-15.012	-9.179
v_{6256}	-56.709	-24.046	-9.952	-4.458	-2.424	-1.418
v_{6260}	-154.827	-40.411	-10.828	-3.160	-0.606	0.498
v_{6263}	241.965	71.420	17.311	2.995	0.444	0.401
v_{6266}	-339.055	-108.237	-37.427	-15.015	-7.022	-3.559
v_{6273}	183.185	100.196	49.464	25.762	15.451	10.287
v_{6276}	-135.130	-51.360	-20.888	-9.452	-4.607	-2.170
v_{6280}	224.175	82.328	32.716	15.176	8.642	5.749
v_{6283}	-87.242	-6.976	3.510	2.761	1.926	1.559
v_{6286}	99.492	34.462	7.406	-0.903	-1.294	0.068

$v_{\lambda_1\lambda_2\lambda\mu}$	$6.4a_0$	$6.8a_0$	$7.2a_0$	$7.6a_0$	$8.0a_0$	$8.4a_0$
v_{0000}	-538.047	-686.900	-643.288	-539.561	-430.563	-335.925
v_{0220}	-66.270	-56.426	-44.247	-33.293	-24.623	-18.221
v_{1010}	-166.299	-79.980	-41.105	-23.792	-15.750	-11.560
v_{1210}	528.114	405.668	316.396	252.365	206.337	171.347
v_{1230}	-68.699	-51.630	-40.970	-33.072	-26.494	-21.292
v_{2020}	84.394	63.624	40.066	21.696	9.710	3.002
v_{2200}	-853.815	-615.641	-453.230	-342.200	-265.521	-209.935
v_{2220}	231.212	165.616	121.993	92.184	71.243	56.074
v_{2240}	-46.780	-34.064	-26.397	-20.805	-16.092	-12.302
v_{3030}	67.090	6.371	-15.116	-19.618	-17.677	-14.096
v_{3033}	-102.731	-27.671	0.412	8.739	9.732	8.343
v_{3210}	100.542	64.828	43.103	30.459	23.182	18.282
v_{3213}	-40.535	-26.040	-17.235	-12.092	-9.067	-6.980
v_{3223}	-4.456	-2.385	-1.326	-0.849	-0.645	-0.535
v_{3230}	-35.584	-21.685	-13.620	-9.085	-6.556	-4.974
v_{3233}	19.094	11.021	6.865	4.675	3.407	2.595
v_{3243}	14.876	9.226	5.809	3.875	2.817	2.144
v_{3250}	25.009	16.045	10.402	6.841	4.622	3.221
v_{3253}	-86.472	-56.960	-38.899	-27.803	-20.811	-15.983
v_{4040}	-11.831	-7.960	-5.400	-3.815	-2.805	-2.129
v_{4043}	27.689	3.715	-5.144	-7.007	-6.067	-4.572
v_{4220}	14.159	8.798	6.136	4.053	2.255	1.171
v_{4223}	25.747	15.345	9.158	5.620	3.718	2.615
v_{4233}	-28.391	-18.616	-12.655	-9.014	-6.696	-5.106

$v_{\lambda_1\lambda_2\lambda\mu}$	$6.4a_0$	$6.8a_0$	$7.2a_0$	$7.6a_0$	$8.0a_0$	$8.4a_0$
v_{4240}	-4.796	-3.114	-2.050	-1.294	-0.746	-0.407
v_{4243}	-11.820	-6.825	-3.863	-2.287	-1.545	-1.130
v_{4253}	31.677	21.122	14.505	10.446	7.894	6.108
v_{4260}	5.109	3.183	1.633	0.798	0.471	0.279
v_{4263}	29.237	17.746	10.844	6.948	4.847	3.542
v_{5050}	-4.430	1.023	2.643	2.487	1.762	1.147
v_{5053}	-3.044	-3.212	-2.845	-2.287	-1.695	-1.172
v_{5230}	-24.886	-14.647	-9.045	-5.816	-3.848	-2.633
v_{5233}	16.222	9.917	6.117	3.985	2.871	2.214
v_{5243}	16.742	10.329	6.550	4.362	3.123	2.335
v_{5250}	5.742	3.152	1.773	1.090	0.772	0.588
v_{5253}	-6.944	-4.694	-3.135	-2.155	-1.599	-1.259
v_{5263}	-15.734	-9.578	-5.837	-3.797	-2.790	-2.153
v_{5270}	-1.377	-1.067	-0.708	-0.549	-0.530	-0.473
v_{5273}	-10.765	-7.601	-5.451	-4.113	-3.275	-2.600
v_{6060}	0.277	-0.561	-0.796	-0.657	-0.413	-0.252
v_{6063}	-1.974	-0.147	0.571	0.600	0.339	0.144
v_{6066}	1.782	-0.246	-0.943	-0.923	-0.595	-0.330
v_{6240}	-2.601	-2.314	-1.759	-1.344	-1.127	-0.967
v_{6243}	-12.924	-7.582	-4.503	-2.810	-1.955	-1.438
v_{6246}	8.435	4.741	2.817	1.671	1.010	0.650
v_{6253}	-5.702	-3.677	-2.444	-1.683	-1.233	-0.942
v_{6256}	-0.678	-0.362	-0.308	-0.223	-0.096	-0.023
v_{6260}	0.814	0.694	0.431	0.249	0.183	0.159
v_{6263}	0.378	0.169	-0.100	-0.107	0.060	0.153
v_{6266}	-1.810	-0.952	-0.484	-0.249	-0.166	-0.133
v_{6273}	6.984	4.852	3.400	2.478	1.935	1.546
v_{6276}	-0.946	-0.529	-0.433	-0.295	-0.118	-0.012
v_{6280}	3.894	2.575	1.720	1.276	1.052	0.870
v_{6283}	1.184	0.847	0.523	0.316	0.253	0.230
v_{6286}	0.405	0.136	-0.156	-0.140	0.043	0.135

$v_{\lambda_1\lambda_2\lambda\mu}$	$9.0a_0$	$10.0a_0$	$15.0a_0$	$20.0a_0$	$25.0a_0$	$35.0a_0$
v_{0000}	-228.113	-120.253	-8.974	-1.483	-0.363	-0.042
v_{0220}	-11.753	-5.816	-0.242	-0.033	-0.008	-0.001
v_{1010}	-7.699	-3.601	0.156	0.035	0.009	0.001
v_{1210}	128.904	76.785	7.616	2.246	0.957	0.254
v_{1230}	-16.802	-14.337	-6.052	-1.985	-0.793	-0.204
v_{2020}	-0.832	-1.047	0.111	0.018	0.004	0.001
v_{2200}	-147.211	-77.207	-1.825	-0.236	-0.138	-0.033
v_{2220}	39.635	21.978	1.110	0.213	0.086	0.018
v_{2240}	-9.267	-8.360	-3.797	-0.969	-0.296	-0.053
v_{3030}	-9.219	-4.117	-0.019	0.003	0.001	0.000
v_{3033}	5.525	2.249	0.042	0.007	0.002	0.000
v_{3210}	12.085	4.940	0.502	0.088	0.008	-0.000
v_{3213}	-4.461	-1.725	-0.103	-0.045	-0.009	-0.000
v_{3223}	-0.331	0.011	-0.020	-0.024	-0.005	-0.000
v_{3230}	-3.212	-1.347	-0.140	-0.025	-0.003	-0.000
v_{3233}	1.741	0.857	0.046	0.014	0.003	0.000
v_{3243}	1.282	0.264	0.014	0.026	0.005	-0.000
v_{3250}	2.025	1.013	-0.266	-0.049	-0.004	0.000
v_{3253}	-10.566	-4.781	0.021	0.021	0.004	0.000
v_{4040}	-1.443	-0.731	-0.042	-0.011	-0.003	-0.000
v_{4043}	-2.864	-1.345	0.055	0.015	0.003	0.000
v_{4220}	0.780	1.037	-0.098	-0.084	-0.015	-0.000
v_{4223}	1.484	0.380	-0.074	-0.018	-0.002	0.000
v_{4233}	-3.383	-1.577	-0.048	-0.019	-0.004	0.000

$v_{\lambda_1\lambda_2\lambda\mu}$	$9.0a_0$	$10.0a_0$	$15.0a_0$	$20.0a_0$	$25.0a_0$	$35.0a_0$
v_{4240}	-0.200	-0.164	0.027	0.019	0.003	0.000
v_{4243}	-0.644	-0.129	0.013	0.003	0.000	-0.000
v_{4253}	4.053	1.810	0.042	0.019	0.003	-0.000
v_{4260}	-0.025	-0.388	0.055	0.050	0.009	0.000
v_{4263}	2.129	0.774	0.074	0.017	0.002	0.000
v_{5050}	0.675	0.362	-0.026	-0.007	-0.002	-0.000
v_{5053}	-0.614	-0.144	0.033	0.004	0.001	0.000
v_{5230}	-1.571	-0.743	-0.344	-0.107	-0.016	-0.000
v_{5233}	1.469	0.621	0.020	0.013	0.003	0.000
v_{5243}	1.432	0.461	-0.001	0.001	-0.001	-0.000
v_{5250}	0.376	0.164	0.087	0.025	0.005	0.000
v_{5253}	-0.866	-0.394	0.000	-0.000	0.000	0.000
v_{5263}	-1.277	-0.262	0.008	-0.001	0.001	0.000
v_{5270}	-0.287	-0.063	0.177	0.062	0.008	-0.000
v_{5273}	-1.651	-0.538	0.024	-0.004	-0.001	0.000
v_{6060}	-0.196	-0.197	-0.018	-0.004	-0.001	-0.000
v_{6063}	0.117	0.239	0.039	0.005	0.001	0.000
v_{6066}	-0.203	-0.205	0.000	-0.000	-0.001	-0.000
v_{6240}	-0.676	-0.204	0.016	-0.008	-0.000	0.000
v_{6243}	-0.786	-0.065	0.087	0.025	0.005	0.000
v_{6246}	0.363	0.121	-0.180	-0.063	-0.011	-0.000
v_{6253}	-0.610	-0.235	0.041	0.013	0.002	0.000
v_{6256}	-0.027	-0.061	-0.015	-0.007	-0.001	-0.000
v_{6260}	0.108	0.019	0.001	0.002	0.000	-0.000
v_{6263}	0.058	-0.155	-0.028	-0.006	-0.001	-0.000
v_{6266}	-0.081	-0.010	0.026	0.010	0.002	0.000
v_{6273}	1.013	0.366	-0.054	-0.016	-0.003	-0.000
v_{6276}	-0.027	-0.129	0.011	0.008	0.002	0.000
v_{6280}	0.553	0.128	-0.019	0.004	-0.000	-0.000
v_{6283}	0.135	-0.032	-0.042	-0.016	-0.003	-0.000
v_{6286}	0.040	-0.131	0.131	0.045	0.008	0.000

SCF+MBPT potential

The potential coefficients are given in unit of cm^{-1}at selected intermolecular distances.

$v_{\lambda_1\lambda_2\lambda\mu}$	$4.0a_0$	$4.4a_0$	$4.8a_0$	$5.2a_0$	$5.6a_0$	$6.0a_0$
v_{0000}	78615.188	37400.164	16720.395	6701.949	2088.711	123.946
v_{0220}	2834.602	1213.932	495.008	154.530	2.429	-56.162
v_{1010}	-12305.445	-6052.965	-3034.048	-1493.101	-708.292	-317.791
v_{1210}	4832.926	2774.621	1841.841	1285.220	911.782	657.911
v_{1230}	-789.410	-330.831	-205.200	-133.369	-88.363	-59.435
v_{2020}	-7587.293	-2532.885	-577.814	96.550	265.527	254.658
v_{2200}	-12375.191	-6862.793	-4193.422	-2705.043	-1792.906	-1212.014
v_{2220}	3166.391	1739.052	1064.450	698.393	470.059	319.979
v_{2240}	-603.340	-295.163	-180.266	-117.293	-81.819	-59.408
v_{3030}	11404.188	5412.234	2608.800	1219.002	530.654	199.890
v_{3033}	-13505.785	-6399.422	-3113.534	-1476.023	-657.118	-259.237
v_{3210}	4376.551	2018.802	974.714	496.596	274.526	164.051
v_{3213}	-1022.986	-352.728	-214.699	-142.392	-89.908	-53.512
v_{3223}	-302.492	-107.054	-54.518	-25.918	-11.530	-5.032
v_{3230}	-1584.496	-693.981	-329.847	-171.700	-97.130	-58.106
v_{3233}	842.580	338.086	171.169	101.338	62.222	36.881
v_{3243}	679.287	349.010	158.449	74.577	40.438	25.294
v_{3250}	499.177	180.405	132.090	102.591	69.569	41.990
v_{3253}	-2586.044	-1190.207	-632.069	-363.102	-216.776	-131.655
v_{4040}	-165.502	-358.327	-247.771	-146.209	-85.958	-54.037
v_{4043}	5115.793	2382.152	1126.913	529.174	241.558	103.517
v_{4220}	510.602	149.904	76.225	56.217	39.445	24.031
v_{4223}	1316.036	555.906	256.225	129.057	70.534	40.548
v_{4233}	-945.458	-429.681	-220.291	-119.643	-68.100	-40.626

$v_{\lambda_1\lambda_2\lambda\mu}$	$4.0a_0$	$4.4a_0$	$4.8a_0$	$5.2a_0$	$5.6a_0$	$6.0a_0$
v_{4240}	-28.038	26.650	13.049	-2.698	-8.677	-8.549
v_{4243}	-768.421	-343.363	-150.444	-72.905	-40.143	-23.824
v_{4253}	1118.030	556.516	276.127	146.288	83.879	51.530
v_{4260}	-247.364	-115.556	-51.427	-18.587	-1.796	5.299
v_{4263}	1309.947	593.066	281.961	145.309	81.188	47.696
v_{5050}	-2183.285	-889.899	-385.974	-175.597	-80.829	-35.968
v_{5053}	202.002	71.916	24.630	6.679	-0.365	-3.029
v_{5230}	-2053.895	-837.928	-360.981	-168.131	-86.738	-49.113
v_{5233}	653.292	303.851	140.121	68.381	37.112	22.121
v_{5243}	868.969	399.320	183.854	89.590	48.193	28.261
v_{5250}	598.160	216.114	87.013	40.024	20.621	11.316
v_{5253}	-318.459	-156.630	-80.513	-44.386	-26.407	-16.646
v_{5263}	-828.448	-382.669	-173.028	-82.261	-43.722	-25.764
v_{5270}	-110.189	-32.714	-18.751	-15.488	-11.109	-6.361
v_{5273}	-361.159	-184.264	-91.208	-47.403	-27.393	-17.585
v_{6060}	605.171	216.049	79.554	30.951	12.651	5.067
v_{6063}	-1075.684	-388.273	-148.458	-60.725	-26.089	-11.260
v_{6066}	1135.972	420.662	163.228	67.075	29.185	12.977
v_{6240}	355.591	105.523	32.334	10.064	1.939	-1.498
v_{6243}	-1133.838	-443.441	-180.764	-80.290	-40.048	-21.911
v_{6246}	1154.587	428.245	167.118	72.589	35.414	18.200
v_{6253}	-111.332	-56.783	-27.255	-13.915	-8.084	-5.123
v_{6256}	-69.637	-30.335	-12.605	-5.517	-2.831	-1.567
v_{6260}	-156.023	-40.918	-11.668	-3.875	-1.075	0.227
v_{6263}	326.727	115.344	40.653	15.478	7.168	4.063
v_{6266}	-336.532	-107.268	-37.648	-15.495	-7.427	-3.832
v_{6273}	226.634	124.888	63.628	33.885	20.141	13.033
v_{6276}	-143.883	-55.618	-22.684	-10.169	-4.883	-2.271
v_{6280}	235.384	87.675	35.539	16.626	9.347	6.069
v_{6283}	-87.141	-6.956	3.160	2.480	1.799	1.542
v_{6286}	131.111	51.003	16.486	4.054	1.387	1.511

$v_{\lambda_1\lambda_2\lambda\mu}$	$6.4a_0$	$6.8a_0$	$7.2a_0$	$7.6a_0$	$8.0a_0$	$8.4a_0$
v_{0000}	-596.990	-766.946	-717.204	-597.814	-471.950	-362.608
v_{0220}	-70.622	-65.369	-53.525	-41.176	-30.641	-22.463
v_{1010}	-131.163	-47.012	-12.166	0.429	3.868	3.975
v_{1210}	490.430	373.876	289.906	230.594	188.639	157.069
v_{1230}	-38.484	-26.140	-19.731	-15.616	-12.304	-9.844
v_{2020}	194.689	133.097	84.594	50.702	28.886	15.850
v_{2200}	-844.886	-604.486	-441.402	-330.763	-255.056	-200.687
v_{2220}	223.062	159.241	116.098	86.419	65.613	50.679
v_{2240}	-40.600	-27.929	-20.252	-14.837	-10.483	-7.171
v_{3030}	50.572	-9.611	-28.820	-30.464	-25.761	-19.814
v_{3033}	-77.188	-2.140	23.096	27.464	24.439	19.477
v_{3210}	100.809	63.281	41.021	28.489	21.584	17.113
v_{3213}	-29.997	-16.264	-8.759	-5.134	-3.583	-2.792
v_{3223}	-1.618	-0.163	0.048	-0.283	-0.731	-1.091
v_{3230}	-35.358	-21.803	-13.730	-9.091	-6.457	-4.797
v_{3233}	20.569	10.916	5.514	2.522	0.833	-0.124
v_{3243}	16.213	10.273	6.457	4.141	2.776	1.881
v_{3250}	25.079	15.289	9.369	5.834	3.774	2.569
v_{3253}	-81.520	-51.926	-34.159	-23.600	-17.236	-13.029
v_{4040}	-37.369	-28.199	-22.831	-19.334	-16.708	-14.530
v_{4043}	38.485	10.096	-0.841	-3.645	-3.138	-1.876
v_{4220}	14.457	9.105	5.787	3.016	0.705	-0.687
v_{4223}	23.428	13.671	8.058	4.977	3.411	2.543
v_{4233}	-25.436	-16.663	-11.522	-8.521	-6.669	-5.396

$v_{\lambda_1\lambda_2\lambda\mu}$	$6.4a_0$	$6.8a_0$	$7.2a_0$	$7.6a_0$	$8.0a_0$	$8.4a_0$
v_{4240}	-6.655	-4.510	-2.600	-1.063	0.063	0.770
v_{4243}	-14.084	-8.165	-4.551	-2.511	-1.449	-0.827
v_{4253}	33.343	22.224	15.144	10.724	7.909	5.945
v_{4260}	5.730	3.700	1.548	0.106	-0.673	-1.141
v_{4263}	28.345	17.034	10.330	6.606	4.636	3.426
v_{5050}	-14.803	-5.172	-1.016	0.363	0.563	0.504
v_{5053}	-3.752	-3.535	-2.983	-2.342	-1.719	-1.187
v_{5230}	-28.246	-16.458	-9.980	-6.253	-4.002	-2.630
v_{5233}	13.483	8.274	5.103	3.339	2.444	1.921
v_{5243}	16.999	10.474	6.633	4.409	3.150	2.352
v_{5250}	6.174	3.351	1.822	1.044	0.669	0.453
v_{5253}	-10.768	-7.032	-4.603	-3.102	-2.225	-1.684
v_{5263}	-15.573	-9.487	-5.785	-3.768	-2.772	-2.142
v_{5270}	-3.746	-2.337	-1.353	-0.837	-0.614	-0.445
v_{5273}	-11.878	-8.259	-5.853	-4.367	-3.443	-2.716
v_{6060}	1.636	0.098	-0.483	-0.506	-0.335	-0.203
v_{6063}	-4.560	-1.521	-0.158	0.209	0.122	0.015
v_{6066}	5.267	1.751	0.200	-0.268	-0.220	-0.113
v_{6240}	-2.454	-2.271	-1.759	-1.357	-1.141	-0.978
v_{6243}	-12.404	-7.242	-4.275	-2.656	-1.850	-1.368
v_{6246}	9.465	5.295	3.117	1.837	1.104	0.706
v_{6253}	-3.282	-2.201	-1.520	-1.088	-0.840	-0.674
v_{6256}	-0.729	-0.377	-0.311	-0.224	-0.097	-0.024
v_{6260}	0.670	0.622	0.397	0.233	0.175	0.154
v_{6263}	2.403	1.310	0.559	0.286	0.303	0.309
v_{6266}	-1.976	-1.048	-0.537	-0.277	-0.180	-0.139
v_{6273}	8.622	5.852	4.026	2.881	2.201	1.727
v_{6276}	-0.980	-0.539	-0.436	-0.296	-0.118	-0.013
v_{6280}	4.025	2.618	1.726	1.269	1.043	0.863
v_{6283}	1.221	0.903	0.577	0.362	0.288	0.254
v_{6286}	1.181	0.553	0.071	-0.015	0.114	0.177

$v_{\lambda_1\lambda_2\lambda\mu}$	$9.0a_0$	$10.0a_0$	$15.0a_0$	$20.0a_0$	$25.0a_0$	$35.0a_0$
v_{0000}	-238.578	-116.738	-4.360	-0.247	0.004	0.008
v_{0220}	-13.903	-5.993	0.256	0.109	0.035	0.005
v_{1010}	2.941	1.807	0.205	-0.018	-0.014	-0.003
v_{1210}	118.641	70.893	7.143	2.183	0.945	0.253
v_{1230}	-8.572	-9.613	-5.673	-1.935	-0.783	-0.203
v_{2020}	6.371	1.833	0.141	0.009	0.001	-0.000
v_{2200}	-139.822	-72.379	-1.263	-0.141	-0.116	-0.030
v_{2220}	34.770	18.189	0.382	0.056	0.043	0.012
v_{2240}	-4.936	-5.275	-3.319	-0.874	-0.271	-0.050
v_{3030}	-12.275	-4.690	0.503	0.157	0.048	0.007
v_{3033}	12.463	4.954	-0.390	-0.149	-0.049	-0.007
v_{3210}	11.477	4.909	0.677	0.138	0.023	0.002
v_{3213}	-1.797	-0.616	-0.234	-0.096	-0.026	-0.003
v_{3223}	-1.295	-1.120	-0.365	-0.106	-0.028	-0.003
v_{3230}	-2.972	-1.101	-0.079	-0.012	0.001	0.000
v_{3233}	-0.879	-1.255	-0.352	-0.069	-0.019	-0.003
v_{3243}	0.828	-0.269	-0.149	-0.013	-0.006	-0.001
v_{3250}	1.643	0.923	-0.195	-0.027	0.002	0.001
v_{3253}	-8.421	-3.584	0.073	0.020	0.002	-0.000
v_{4040}	-11.740	-8.042	-1.221	-0.251	-0.066	-0.008
v_{4043}	-0.417	0.679	0.530	0.124	0.034	0.004
v_{4220}	-1.233	-0.775	-0.508	-0.175	-0.040	-0.004
v_{4223}	1.619	0.635	0.017	0.004	0.004	0.001
v_{4233}	-3.939	-2.240	-0.249	-0.067	-0.017	-0.002

$v_{\lambda_1\lambda_2\lambda\mu}$	$9.0a_0$	$10.0a_0$	$15.0a_0$	$20.0a_0$	$25.0a_0$	$35.0a_0$
v_{4240}	1.225	1.211	0.360	0.094	0.024	0.003
v_{4243}	-0.178	0.382	0.159	0.038	0.010	0.001
v_{4253}	3.740	1.436	-0.071	-0.008	-0.004	-0.001
v_{4260}	-1.597	-1.826	-0.275	-0.023	-0.012	-0.002
v_{4263}	2.103	0.810	0.095	0.022	0.004	0.000
v_{5050}	0.473	0.417	0.010	0.000	0.000	0.000
v_{5053}	-0.631	-0.170	0.020	0.001	0.000	0.000
v_{5230}	-1.460	-0.598	-0.309	-0.099	-0.014	-0.000
v_{5233}	1.291	0.529	0.007	0.010	0.002	-0.000
v_{5243}	1.441	0.465	-0.001	0.001	-0.001	-0.000
v_{5250}	0.225	0.026	0.055	0.018	0.003	0.000
v_{5253}	-1.116	-0.509	-0.009	-0.002	-0.000	0.000
v_{5263}	-1.272	-0.259	0.009	-0.001	0.001	0.000
v_{5270}	-0.181	0.063	0.207	0.068	0.010	0.000
v_{5273}	-1.723	-0.578	0.017	-0.006	-0.001	0.000
v_{6060}	-0.159	-0.159	-0.002	0.000	0.000	0.000
v_{6063}	0.046	0.193	0.023	0.000	0.000	-0.000
v_{6066}	-0.107	-0.177	0.005	0.001	0.000	0.000
v_{6240}	-0.680	-0.201	0.019	-0.007	-0.000	0.000
v_{6243}	-0.748	-0.053	0.084	0.024	0.005	0.000
v_{6246}	0.393	0.137	-0.176	-0.061	-0.011	-0.000
v_{6253}	-0.451	-0.159	0.048	0.014	0.002	0.000
v_{6256}	-0.029	-0.063	-0.015	-0.007	-0.001	-0.000
v_{6260}	0.103	0.013	-0.002	0.001	-0.000	-0.000
v_{6263}	0.148	-0.111	-0.020	-0.004	-0.001	-0.000
v_{6266}	-0.083	-0.011	0.025	0.009	0.002	0.000
v_{6273}	1.120	0.418	-0.049	-0.015	-0.003	-0.000
v_{6276}	-0.028	-0.131	0.011	0.008	0.002	0.000
v_{6280}	0.551	0.132	-0.016	0.005	0.000	-0.000
v_{6283}	0.148	-0.030	-0.045	-0.017	-0.003	-0.000
v_{6286}	0.062	-0.119	0.135	0.046	0.008	0.000

Appendix E

OH-H_2 space fixed potential coefficients

Listed below are the potential coefficients (in units of cm^{-1}) at selected intermolecular distances. To obtain the coefficients for the 'doctored' potential divide the $\mu = 2$ terms by two.

$v_{\lambda_1\lambda_2\lambda\mu}$	$4.0a_0$	$4.5a_0$	$5.0a_0$	$5.5a_0$	$6.0a_0$	$6.5a_0$
v_{0000}	36940.867	11987.973	2886.357	-117.835	-881.374	-886.353
v_{0220}	2061.999	592.895	125.009	-8.199	-36.292	-36.884
v_{1010}	18875.215	6627.762	2141.568	480.843	-64.220	-184.136
v_{1210}	-5689.590	-2483.585	-1273.895	-737.067	-466.906	-315.309
v_{1230}	4561.824	1991.298	1021.387	590.968	374.357	252.810
v_{2020}	11716.332	4075.677	1349.012	353.410	13.171	-79.523
v_{2022}	8060.168	3313.802	1283.388	442.927	113.066	-1.767
v_{2200}	4520.785	1851.037	897.058	492.934	298.451	192.735
v_{2202}	-2470.259	-1413.341	-857.481	-541.588	-353.263	-236.124
v_{2212}	-241.851	-107.633	-48.059	-19.795	-6.999	-1.818
v_{2220}	-2268.848	-894.208	-412.828	-217.129	-126.676	-79.040
v_{2222}	295.106	243.957	182.099	132.285	96.039	69.323
v_{2232}	-79.164	-35.231	-15.731	-6.480	-2.291	-0.595
v_{2240}	2354.956	949.749	451.719	244.170	145.840	93.029
v_{2242}	-893.199	-542.335	-343.241	-223.989	-150.165	-102.509

$v_{\lambda_1\lambda_2\lambda\mu}$	$7.0a_0$	$7.5a_0$	$8.0a_0$	$8.5a_0$	$9.0a_0$	$9.5a_0$
v_{0000}	-689.036	-479.301	-314.188	-202.708	-128.714	-84.405
v_{0220}	-30.293	-22.409	-15.167	-9.196	-6.109	-3.538
v_{1010}	-173.017	-132.849	-92.702	-61.041	-37.314	-21.285
v_{1210}	-222.894	-162.577	-120.767	-91.813	-71.491	-56.500
v_{1230}	178.713	130.352	96.829	73.614	57.320	45.301
v_{2020}	-88.694	-74.594	-54.868	-36.666	-23.291	-14.529
v_{2022}	-29.332	-26.284	-16.596	-7.050	-4.600	-2.254
v_{2200}	129.057	86.451	59.269	40.556	31.164	22.580
v_{2202}	-159.963	-108.879	-74.457	-51.718	-37.174	-27.619
v_{2212}	-0.083	0.372	0.408	0.253	0.222	0.140
v_{2220}	-50.650	-33.694	-22.523	-15.646	-10.515	-8.068
v_{2222}	49.216	33.897	22.785	16.367	10.686	7.739
v_{2232}	-0.027	0.122	0.134	0.083	0.073	0.046
v_{2240}	61.345	40.995	27.865	19.165	14.098	10.402
v_{2242}	-70.384	-48.073	-32.710	-22.945	-16.043	-11.836

$v_{\lambda_1\lambda_2\lambda\mu}$	$10.0a_0$	$15.0a_0$	$20.0a_0$	$25.0a_0$	$30.0a_0$	$40.0a_0$
v_{0000}	-55.098	-3.554	-0.214	0.073	0.066	0.024
v_{0220}	-2.329	-0.071	0.024	0.018	0.010	0.003
v_{1010}	-11.583	-0.184	0.113	0.074	0.040	0.012
v_{1210}	-45.476	-9.661	-3.069	-1.260	-0.608	-0.193
v_{1230}	36.462	7.746	2.461	1.010	0.488	0.155
v_{2020}	-8.447	-0.210	0.024	0.025	0.015	0.005
v_{2022}	-1.209	0.086	0.074	0.036	0.017	0.005
v_{2200}	17.870	2.842	0.686	0.228	0.092	0.022
v_{2202}	-20.992	-2.656	-0.614	-0.197	-0.078	-0.018
v_{2212}	0.123	0.017	0.009	0.004	0.002	0.000
v_{2220}	-5.860	-0.775	-0.183	-0.061	-0.025	-0.006
v_{2222}	5.824	0.703	0.160	0.051	0.020	0.005
v_{2232}	0.040	0.006	0.003	0.001	0.001	0.000
v_{2240}	8.014	1.209	0.290	0.096	0.039	0.009
v_{2242}	-8.972	-1.121	-0.258	-0.083	-0.033	-0.008